APPLICATIONS AND FUNDAMENTAL CHARACTERIZATION OF OPEN AIR AND ACOUSTIC-DRIVEN IONIZATION METHODS FOR MASS SPECTROMETRY

A Dissertation
Presented to
The Academic Faculty

by

Christina Young Hampton

In Partial Fulfillment
of the Requirements for the Degree
Doctor of Philosophy in the
School of Chemistry & Biochemistry

Georgia Institute of Technology

August 2009

APPLICATIONS AND FUNDAMENTAL CHARACTERIZATION OF OPEN AIR AND ACOUSTIC-DRIVEN IONIZATION METHODS FOR MASS SPECTROMETRY

Approved by:

Dr. Facundo M. Fernández, Advisor
School of Chemistry & Biochemistry
Georgia Institute of Technology

Dr. Alfred H. Merrill, Jr.
School of Biology
Georgia Institute of Technology

Dr. Lawrence A. Bottomley
School of Chemistry & Biochemistry
Georgia Institute of Technology

Dr. Thomas M. Orlando
School of Chemistry & Biochemistry
Georgia Institute of Technology

Dr. Wendy L. Kelly
School of Chemistry & Biochemistry
Georgia Institute of Technology

Dr. M. Cameron Sullards
School of Chemistry & Biochemistry
Georgia Institute of Technology

Date Approved: May 28th, 2009

You cannot hope to build a better world without improving the individuals. To that end, each of us must work for his own improvement, and at the same time share a general responsibility for all humanity, our particular duty being to aid those to whom we think we can be most useful.

— Marie Sklodowska Curie, 1937[1]

This is dedicated to…

my father, Charles, for showing me how to reason and be patient,
my mother, Ok Sun, for showing me how to persevere and be self-reliant,
and my sister, Michele, for showing me how to laugh and be forgiving.

Thank you for your unconditional love, support and faith.

ACKNOWLEDGEMENTS

A lot can happen in five years… During my time here at Georgia Tech, I've learned a great deal, not only about mass spectrometry and science but also about myself, thanks to the wonderful people around me. First and foremost, I wish to thank my family for loving and supporting me throughout this journey… I know that they haven't always understood the decisions that I've made, but they've stood by me, offered me their wisdom, and cheered me up every time I broke another chip. They have been a blessing to my throughout my life. Thank you also to Michele Dagenais, Haley Jessup, and Jennifer Thackeray. You have been the best friends anyone could ever ask for! Thank you also to my friend and undergraduate research advisor, Dr. Steven R. Emory, who inspired my love of research and encouraged me to pursue a graduate degree in chemistry.

I also wish to thank my other family – the awesome Fernández research group here at Georgia Tech. You are all such wonderful, considerate people and I couldn't have asked for a better graduate student experience... Thank you all for being such good (lifelong) friends... So, listed in order of when I met you...

Thank you, Facundo, for accepting me into your group and being so patient with me. I joke all the time that I don't know how you've put up with me for so long but I really mean it. I know that I can be tricky to work with and I'm very grateful that you've supported me for so long and believed in me when I didn't. There really aren't enough words for me to express how truly grateful I am for the guidance you've given me these

last few years (at least in my vocabulary, you've probably got enough in yours to find the words!). So all I can do is say, thank you, thank you, thank you...

Thank you Arti, for making me laugh and being such a great friend to me. Thank you also for keeping me grounded (mentally and emotionally... unfortunately, not physically as I just shocked myself while writing this...) and stopping me whenever I got out of control with the number of experiments that I wanted to do. You have definitely helped me to gain perspective about what's important and I will always be grateful to you for that. I've also thoroughly enjoyed making fun of you (and laughing when you get me back) during these last five years, I'll always remember the times we've shared.

Thank you also to Mark for brightening my day with your cheery disposition. (It'll be okay... just keep breathing and everything will eventually work out in the end.) Seriously though, I really learned a lot from you and I'm very happy to have you as a friend. Carrie, I am constantly amazed by how you manage to juggle working full time, being in grad school and having two babies... Thank you for teaching me the importance of being efficient and prioritizing! Leonard, you are the coolest guy I've ever known. I've never met anyone as patient and as level-headed as you. If you do run for president, I'll vote for you. Manshui, you are the funniest storyteller I've ever met and also the kindest. Being around you always cheers me up. Glenn, you will definitely be famous some day... I'm not sure what you'll be famous for but it's coming. I've very much enjoyed our conversations on life, science, and the random weirdness of grad school and I'm grateful to you for sharing your insights (and hilarious sarcastic remarks) with me. If you run for president, I'll vote for you too (I'm not sure what I'll do if you and Leonard run at the same time, though! Perhaps, I'll have to find a way to vote twice!) Jose, I'm not sure why

it is that every time I say something to you that I think is funny, it comes out wrong... Thank you for laughing with me after I realize what I said. Courtney, I can't believe that I've only known you for a year! It feels like we've been friends forever. You really are just like a mini-me. (Except for the fact that you're taller, look completely different from me, drive better, and are so much more creative than me... we're exactly alike!) I'm very happy that I've gotten to know you this past year and I'm certain that you will always be a part of my life. Dana, you certainly had me fooled... When I met you, you seemed so sweet and thoughtful and now I know that you're also secretly very mischievous! Thank you for being so nice, friendly, and funny! Your sense of humor is really infectious! Thank you, Asiri, for being so much fun to be around. I've learned a lot from your example and I'm grateful to have you as a friend. Last, but not least, thank you to our undergrad researchers... Joe Caramore, Kristin Johnson, Horace Leung, David Rizzo, Catherine Silvestri, and our high schooler, Felicia Yang.

Thank you also to my extended family - everyone in the School of Chemistry and Biochemistry here at GA Tech. A special thank you goes to Irene Anestis-Richard, Kane Barker, Otonye Braide, Elizabeth Cowan, Hyungie Doo, Justyna Wiedemair, and Christina Young (Hooray for Christina Y.^{2}!) for being such great friends. Thank you also to my friends... Jabulani Barber, James Bradshaw, Karen Goeders, James Goeders, Hillary Huttenhower, Yuliya Luzinova, Nicole Marotta, Jong-Seok Moon. Jenny Raynor, and Vonda Sheppard. Thank you to the faculty... Dr. Bridgette Barry, Dr. Bill Baron, Dr. Toby Block, Dr. Leigh Bottomley, Dr. Robert Braga, Dr. Richard F. Browner, Dr. Jiri Janata, Dr. Christina Kranz, Dr. Joseph Perry and Dr. Cameron J. Tyson. A special thank you to the faculty who agreed to be my mentors as part of my committee... Dr. Larry

Bottomley, Dr. Wendy Kelly, Dr. Alfred Merrill, Dr. Thomas Orlando, and Dr. Cameron Sullards.

Thank you to the wonderful GA Tech staff including... Richard Bedell and Jose Fonts (for fixing the mass specs and helping me everytime I come to you frazzled because something doesn't work!), Sam Mize (for building all of these wonderful toys for us!), Selina Tinsley and Kourtnie Robins (our awesome administrative assistants), Thomas Westbrook and Adrian Padron (our IT specialists), Mark Smith, Scott, Maxwell, Lee, and Billy (and everyone else in Facilities Area 2 who have helped us modify our lab space to work for us and not against us), and Kevin and Jason (our friendly neighborhood VWR stockroom specialists).

I would also like to thank all of the brilliant collaborators I've had the opportunity to work with...AMUSE: Dr. F. Levent Degertekin, Dr. Andrei G. Fedorov, Thomas P. Forbes, J. Mark Meacham, and Mark J. Varady... DART forensics: Dr. Paul N. Newton, Dr. Chip Cody... Ovarian Cancer Metabolomics: Dr. Alex Gray, Dr. John McDonald, Wei Guan, L. DeEtte Walker, and Benedict Benigno... AK-295: Dr. Jonathan Glass, Dr. James Powers, Seneshaw Asress, and Asli Ovat... I'd also like to thank Dr. Charlene Bayer and Dr. Victor de Jesus from GTRI for allowing me to use their mass spec, Dr. Charles L. Liotta and Dr. Charles A. Eckerts from GT Chemistry for providing me with switchable solvent, Dr. David Muddiman and Brent Dixon from North Carolina State University for their insightful comments about the AMUSE project.

Finally, my apologies to anyone that I may have inadvertently left off this list... It's been a long five years with very little sleep and I'm looking forward to taking a nap before I begin my next adventure!

TABLE OF CONTENTS

LIST OF TABLES

LIST OF FIGURES

LIST OF SYMBOLS

‰	"per mil" (parts per thousand)
2^3S_1	Helium metastable atom excited to the triplet state
Δm	mass accuracy (in millimass units)
ΔH_f	Heat of formation
D[3,2]	Sauter mean diameter
<E>	Mean internal energy
E_0	Critical energy (minimum energy needed by an ion to overcome the dissociation energy barrier and form product ions.)
E_{app}	Appearance energy (minimum energy needed to observe an ion.)
He^*	Helium metastable atom
$Int_{Precursor}$	Intensity of the precursor ion peak in a mass spectrum.
$Int_{Product}$	Intensity of the production ion peak in a mass spectrum.
m/z	mass-to-charge ratio
P(E)	Internal energy distribution
Py	Pyridine
Py^+R	Benzylpyridinium cation
R^+	Benzyl cation
S/N	Signal-to-noise ratio
θ	Contact angle
t_R	Retention Time
V_{DC}	Applied DC voltage

V_{PP}	Peak-to-peak voltage
V_{RMS}	Root-mean-square voltage

LIST OF ABBREVIATIONS

-pESI	Negative Ion Mode Pneumatically-Assisted Electrospray Ionization
+pESI	Positive Ion Mode Pneumatically-Assisted Electrospray Ionization
12-fold CV	12-Fold Cross Validation
52-20 Split	52-20 Split Validation
AAS	Atomic Absorption Spectroscopy
Abu	4-Aminobutyric Acid
ACT	Artemisinin Derivative Combination Therapy
ADME	Adsorption, Distribution, Metabolism, Excretion
AGC	Automatic Gain Control
AI	Active Ingredient
AK-295	Benzyloxycarbonyl-leucine-4-aminobutyric acid-CONH-$(CH_2)_3$-4-morpholinyl
AMUSE	Array of Micromachined UltraSonic Electrosprays
AP	Atmospheric Pressure
APCI	Atmospheric Pressure Chemical Ionization
API	Atmospheric Pressure Interface
APIE	Atmospheric Pressure Ion Evaporation
AP LD/CI	Atmospheric Pressure Laser Desorption/Chemical Ionization
AP-MALDI	Atmospheric Pressure Matrix-Assisted Laser Desorption/Ionization
APTDI	Atmospheric Pressure Thermal Desorption/Ionization

ASAP	Atmospheric Pressure Solids Analysis Probe
BBB	Blood Brain Barrier
CA125	Cancer Antigen 125
CE	Capillary Electrophoresis
CI	Chemical Ionization
CID	Collision Induced Dissociation
CSI	Cold Spray Ionization
DAPCI	Desorption Atmospheric Pressure Chemical Ionization
DAPPI	Desorption Atmospheric Pressure Photoionization
DART	Direct Analysis in Real Time
DBDI	Dielectric Barrier Discharge Ionization
DC	Direct Current
DC-AMUSE	AMUSE Operating Mode (Applied $V_{DC} > 0$)
DDA	Dodecylamine
DESI	Desorption Electrospray Ionization
DeSSI	Desorption ElectroSonic Spray Ionization
DOF	Degrees of Freedom
EASI	Easy Ambient Sonicspray Ionization
EESI	Extractive Electrospray Ionization
EHD	Electrohydrodynamic Ionization
EI	Electron Ionization
ELDI	Electrospray-Assisted Laser Desorption/Ionization
ESI	Electrospray Ionization

ESSI	ElectroSonic Spray Ionization
FAB	Fast Atom Bombardment
FAPA	Flowing Atmospheric Pressure AfterGlow
FD	Field Desorption
FD-ESI	Fused Droplet – Electrospray Ionization
FDA	Food and Drug Administration
FI	Field Ionization
FWHM	Full-Width Half-Maximum
GA	Genetic Algorithm
GC	Gas Chromatography
GD	Glow Discharge
Guilin	Guilin Pharmaceutical Company, Ltd.
HMDB	Human Metabolome Database
HNP	Heated Nebulizer Probe
HPLC	High Performance Liquid Chromatography
IE	Internal Energy
INTERPOL	International Criminal Police Organization
IRB	Institutional Review Board
IR-LADESI	Infrared Laser-Assisted Desorption Electrospray Ionization
ISTD	Internal Standard
IT	Ion Trap
KEGG	Kyoto Encyclopedia of Genes and Genomes Database
KOH	Potassium Hydroxide

LAESI	Laser-Assisted Electrospray Ionization
Laos	Lao People's Democratic Republic (PDR)
LC	Liquid Chromatography
Leu	Leucine
LIAD/ESI	Laser-Induced Acoustic Desorption Electrospray Ionization
LiT	Linear Ion Trap
LM	Lipid Maps
LOOCV	Leave-One-Out Cross Validation
LTP	Low Temperature Plasma
μESI	Microelectrospray Ionization
MALDESI	Matrix-Assisted Laser Desorption Electrospray Ionization
MALDI	Matrix-Assisted Laser Desorption/Ionization
MDMA	Methylenedioxymethamphetamine (Ecstasy)
MEMS	MicroElectroMechanical Systems
Metlin	Metlin Scripps Center of Mass Spectrometry Metabolite Database
Microchip ESI	Microfabricated ESI-type Ionization Techniques
MID	Metlin Identification Number
MMCD	Madison Metabolomics Consortium Database
MPS	Ministry of Public Security
MS	Mass Spectrometry
MS/MS	Tandem Mass Spectrometry
NaTFA	Sodium Trifluoroacetate
ND	Not Detected

ND-EESI	Neutral Desorption Extractive Electrospray Ionization
nESI	Nanoelectrospray Ionization
NMR	Nuclear Magnetic Resonance
NQ	Not Quantifiable
Nva	Norvaline
NWL	Normal Within Limits
OTS	n-Octadecyltrichlorosilane
P. falciparum	*Plasmodium falciparum*
PADI	Plasma-Assisted Desorption Ionization
PCA	Principal Component Analysis
PD	Plasma Desorption
PDMS	Polydimethylcyclosiloxane
PECVD	Plasma-enhanced Chemical Vapor Deposition
PEEK	Poly-ether-ether-ketone
PEG	Polyethylene glycol
pESI	Pneumatically-assisted (nebulizer-assisted) ESI
PI	Photoionization
PLSDA	Partial Least Squares Discriminant Analysis
PTFE	Polytetrafluoroethylene
PZT	Lead Zirconate Titanate ($Pb[Zr_xTi_{1-x}]O_3$, Piezoelectric Transducer)
Q-IMS-TOF	Quadrupole Ion Mobility Time-of-Flight
QiT	Quadrupole Ion Trap
QiT-FT	Quadrupole Ion Trap-Fourier Transform

QqQ	Triple Quadrupole
Q-TOF	Quadrupole Time-of-Flight
PC	Glycerophosphocholine
PE	Glycerophospholipid
RADIO	Radiofrequency-Assisted Desorption/Ionization
RF	Radiofrequency
RFE	Recursive Feature Elimination
RF-only AMUSE	AMUSE Operating Mode (0 V_{DC} Applied)
RIE	Reactive Ion Etch
RSD	Relative Standard Deviation
SE	Southeast
SELDI	Surface-Enhanced Laser Desorption/Ionization
SI	Spark Ionization
Si_3N_4	Silicon Nitride
SIMS	Secondary Ion Mass spectrometry
SRM	Selected Reaction Monitoring
SSI	Sonic Spray Ionization
SVM	Support Vector Machines
SY	Survival Yield
TI	Thermal Ionization
TIC	Total Ion Chromatograms
TL	Tube Lens Offset Voltage (a.k.a. Capillary-Skimmer Potential)
TLC	Thin-Layer Chromatography

TOF	Time-of-Flight
TR	Trypaflavine
TS	Thermospray
UA-EESI	Ultrasonically-Assisted Extractive Electrospray Ionization
UA-ESI	Ultrasonically-Assisted ESI
UPLC	Ultraperformance Liquid Chromatography
USP	United States Pharmacopeia
UV	Ultraviolet
WHO	World Health Organization
WPRO	Western Pacific Regional Office
XRD	X-ray Diffraction
YGGFL	Leucine Enkephalin
Z	Benzyloxycarbonyl
ZLAK-3001	Benzyloxycarbonyl-leucine-4-aminobutyric acid-CONH-$(CH_2)_3$-adenine
ZLAK-3002	Benzyloxycarbonyl-leucine-4-aminobutyric acid-CONH-$(CH_2)_3$-N-(1-methyl)piperazine
ZLAK-3005	Benzyloxycarbonyl-leucine-phenylalanine-CONH-$(CH_2)_3$-N-$(CH_3)_2$
ZLAK-74	Benzyloxycarbonyl-leucine-norvaline-CONH-$(CH_2)_3$-4-morpholinyl

SUMMARY

One of the most fundamental challenges in analytical mass spectrometry (MS) is the efficient conversion of neutral molecules into *intact* gas-phase ions. In this thesis, I investigate the capabilities of various new and established ionization techniques including (a) the Array of Micromachined UltraSonic Electrosprays (AMUSE), (b) Direct Analysis in Real Time (DART) and (c) Electrospray Ionization (ESI) for bioanalytical and biomedical analysis purposes.

The AMUSE is a MicroElectroMechanical System (MEMS)-based device that was created as an alternative, and more sensitive approach for ion generation in an array format. In the AMUSE, the processes of droplet formation and DC droplet charging are separated allowing ionization of liquid samples using low charging voltages and a wide variety of solvents. Our analytical characterization work with the AMUSE showed that ion generation with this device was indeed possible, and that incorporation of a Venturi device increased signal stability and sensitivity due to enhanced droplet desolvation and increased ion transfer efficiency. A detailed investigation to determine the optimal source parameters for ionization of aqueous solutions of model compounds including reserpine, leucine enkephalin and cytochrome C was carried out and it was found that ionization was possible even without the application of a DC charging potential. Subsequent experiments using the thermometer ion method to characterize the AMUSE from a more fundamental point of view, showed that AMUSE ions are lower in internal energy than ESI ions, opening interesting possibilities for the mass spectrometric study of labile species. Furthermore, it was found that it was possible to manipulate the internal energy

of the ion population by varying the parameters that most strongly affect desolvation and focusing.

Our studies with DART were directed at investigating its analytical potential. DART was applied to the identification of active ingredients (AIs) in low quality combination medicines that are used for the treatment of fever, the first clinical symptom that is observed for malaria. As these drugs are commonly sold in regions of the world (particularly Southeast Asia) where drug resistant malaria is endemic, their use may engender increased resistance against the few remaining effective antimalarials. The analytical utility of DART was further extended to the screening of counterfeit pharmaceuticals to determine their chemical composition and to aid in a collaborative forensic investigation aimed at identifying the sources of these fakes.

CHAPTER 1. TOWARDS SOFTER AND HIGHER-THROUGHPUT IONIZATION TECHNIQUES

1.1. Abstract

This chapter describes some of the advantages and limitations of established ionization methods and introduces two ionization techniques that attempt to improve the performance of previous approaches to ion generation. The chapter begins with an overview of early ionization techniques that operated under vacuum and then describes the gradual shift towards techniques capable of operating at atmospheric pressure (AP). A review of AP spray-based ionization techniques leading to the development of chip-based ion sources is presented followed by a review of the explosive new trend towards developing ionization techniques that operate under ambient conditions.

1.2. Early Ionization Techniques – Ionization Under Vacuum

The efficient conversion of neutral molecules into low-internal energy gas-phase ions is one of the most fundamental challenges in mass spectrometry (MS).[2, 3] The most traditional mass spectrometers combine an ionization source with a mass analyzer and detector all operating under medium or high vacuum. Ionization in these early instruments was typically accomplished using either electron ionization (EI) or chemical ionization (CI). EI, introduced in 1918 by Dempster, is a "hard" ionization method that produces fragmentation spectra from ions generated by collisions between gas-phase analyte molecules and energetic electrons (70 eV).[4] CI, developed by Munson and Field in 1966, is a "softer" ionization techniques that provides complementary information

about the analyte of interest.[5] In CI, intact molecular ions are generated via low-energy (~5–10 eV) collisions between gas-phase analyte molecules and reactive ions produced from the preferential ionization of reagent gas molecules (i.e. methane) during EI. This preferential ionization can be attributed to the large excess of reagent gas in the ion source, which increases the probability of hard collisions occurring between the reagent gas and energetic electrons, and leads to the formation of an excess of reactive ions. These reactant ions then interact with the less abundant gaseous analyte molecules to form analyte ions. Despite the analytical utility of EI and CI, which enabled the creation of massive spectral databases allowing routine identification of compounds by comparing experimental fragmentation spectra with reference spectra (EI) and allowed for the facile determination of a compound's molecular weight from relatively simple spectra (CI), these techniques are limited to the analysis of volatile compounds which are stable in the gas phase (i.e. low molecular weight organic compounds).

Since the introduction of EI, a plethora of other ionization techniques has been introduced to extend the capability of MS to non-volatile, thermally labile compounds of higher molecular weight. These ionization techniques differ in the types and phases of analyte molecules that can be probed and also differ in the methods by which analyte desorption and ionization occur. In thermal ionization (TI, 1923),[6, 7] sample coated onto a metal ribbon is thermally desorbed and ionized via electron transfer from the analyte to the metal while in secondary ion mass spectrometry (SIMS, 1931),[8] a surface is bombarded by a primary ion beam causing the ejection of secondary ions from the sample surface. In spark ionization (SI, 1936),[9] a high-voltage arc between two electrodes ionizes analyte incorporated into the tips of the electrodes while in field ionization (FI,

1954),[10] ionization occurs via the removal of electrons from analyte vapors introduced into a high electric field. In photoionization (PI, 1956),[11, 12] absorption of incident photons causes the emission of ions from a solid sample while in field desorption (FD, 1969),[13] analyte coated onto a metal emitter is heated and exposed to a high potential causing desorption and ionization of low-vapor pressure compounds. In glow discharge (GD, 1971),[14] a discharge gas causes sputtering of analyte from a cathode and ionization occurs via electron transfer or Penning ionization while in electrohydrodynamic ionization (EHD, 1972),[15] an interaction between a strong electrostatic field and liquid at the end of a capillary causes the liquid to form a sharp point at which field ionization occurs. In plasma desorption (PD, 1974),[16] ions are generated from a sample deposited on foil by the bombardment by beta particles while in fast atom bombardment (FAB, 1981),[17] analyte is mixed with a liquid matrix (such as glycerol) which prevents sample damage as ions are sputtered from the surface due to bombardment by a beam of energetic atoms (i.e. argon). Table 1.1 lists these techniques in chronological order according to when they were first reported and describes the operating principles, analytical figures of merit, and some of the advantages and disadvantages for each.[18-25]

Table 1.1. List of vacuum ionization techniques, in chronological order.

Technique (Year)	Energy Deposition Method	Ionization Process	Upper Mass Limit	Sensitivity	Notes	Refs.
EI (1918)	Collision with Energetic e^-	e^- Transfer	2 000 u	femtomole	+ Produces reproducible fragment spectra. + Provides structural information. - Sample must be volatile. - Induces thermal decomposition.	4, 18
TI (1923)	Thermal Desorption from Metal	e^- Transfer	400	picogram	+ Produces simple spectra. + Stable ion beam. - Limited to volatile compounds. - Limited to low mass compounds.	6-7, 22
SIMS (1931)	Bombardment with Low-energy Particles (Xe^+, Cs^+; keV)	Energy Transfer	12 000 u	ppm	+ Sensitive analysis of organic compounds. + Allows imaging and depth profiling. - Ion beam induces chemical changes. - Exhibits mass-dependent ion yields.	8, 18
SI (1936)	Evaporation / Ionization by Spark Plasma	e^- Transfer	300 u	ppb	+ Useful for analytes of any state. + High sensitivity analyses. - Difficult sample preparation. - Limited to low-mass compounds.	9, 19
FI (1954)	Field Ionization	e^- Transfer	1 000 u	ppm	+ Allows observation of molecular ions. + Useful for volatile organic compounds. - Source is subject to arcing and is fragile. - Compound dependent sensitivity.	10, 20
PI (1956)	Ion Emission by Absorption of High-energy Photons	Photoelectron Transfer	500u	micrograms	+ Amenable to analysis of labile compounds. - Complex source setup and operation. - Not amenable to direct analysis of solids.	11-12, 21
CI (1966)	Low-energy Collisions with Reactive Ions	Protonation / Reactive Ion Transfer	2 000 u	picomole	+ Produces simple spectra containing $M^{+\cdot}$. + Operates in positive or negative ion mode. - Limited to volatiles species. - Source is subject to electrical discharge.	5, 18
FD (1969)	Field Evaporation from Metal Emitter	e^- Transfer / Protonation / Cationization	10 000 u	picograms	+ Useful for volatile & nonvolatile compounds. + Produces simple spectra containing $M^{+\cdot}$. - Fragile emitter. - Relatively slow analysis.	13, 20
GD (1971)	Sputtered Neutral Ionized by GD Plasma	Penning / e^- Transfer	300 u	ppb	+ Sensitive method for analysis of solids. + Useful for elemental analysis. - Limited to low-mass analyses. - Low sample throughput.	14, 22
EHD (1973)	Electrostatic Ionization	Protonation / Cationization / Deprotonation / Halide Attachment	4 000 u	nanomole	+ Useful for volatile & nonvolatile compounds. + Self-replenishing analyte (external pump). - Generally uses low vapor pressure solvent. - Signal shows high analyte dependence.	15, 23
PD (1974)	Bombardment with High-energy Beta Particles (^{252}Cf; MeV)	Energy Transfer	45 000 u	nanograms	+ Useful for detection of large molecules. + Useful for nonvolatile & labile compounds. - Difficult sample preparation. - Exhibits poor peak resolution.	16, 24
FAB (1981)	Bombardment of Analyte/Matrix by Atoms/Neutrals (Ar; keV)	Protonation / Deprotonation	24 000 u	nanomole	+ Useful for detection of large molecules. + Useful for nonvolatile & labile compounds. - Exhibits significant chemical background. - Produces solvent-ion clusters.	17, 25

All of these techniques are amenable to the analysis of non-volatile compounds to some degree. However, TI is limited to the ionization of compounds having low ionization potentials (primarily inorganic compounds). SIMS provides sensitive analysis of organic compounds and is becoming increasingly popular today in imaging mode, however, the energetic primary ion beam can cause changes in the chemical composition of the sample and the upper mass limit of the technique is 12,000 Da, showing mass-dependent ion yields.[26] SI can be used to analyze samples in any state but produces a large number of fragment ions and ions having a large distribution of kinetic energy; thus, it was typically coupled to expensive, high resolution mass analyzers such as double-focusing magnetic sector mass analyzers. Both FI and FD produce simple spectra from volatile compounds generally containing the intact molecular ion and FD can be applied to the analysis of non-volatiles species. However, both techniques are limited by the presence of arcing in the source and exhibit compound-dependent sensitivity. PI can be used to analyze thermally labile organic compounds but is difficult to operate and is not amenable to the direct analysis of solids. However, PI can be considered a precursor to modern laser desorption-based techniques such as matrix-assisted laser desorption/ionization (MALDI, 1988),[27, 28] which differs from PI primarily in the use of an organic acid as a matrix which greatly enhances desorption and ionization of analyte molecules. Although MALDI, along with electrospray ionization (ESI) [29-31] an atmospheric-pressure (AP) spray-based technique that is described in more detail below, has revolutionized the field of MS by allowing the soft ionization of large biomolecules, the utility of MALDI at lower mass ranges is somewhat hindered by intense chemical background due to the crystalline matrix. GD provides sensitive analysis of solid surfaces

and is particularly useful for elemental analyses but is only useful at low mass ranges and exhibits a low sample throughput. EHD, a progenitor of modern spray-based ionization techniques such as ESI, has been applied to the analysis of non-volatile, polar compounds but requires a volatile solvent having a high conductivity, incorporation of a stabilizer such as glycerol, high needle voltages (8-13 kV) and very low flow rates (<10 μL min^{-1}). PD, FAB and a variant of FAB known as continuous-flow FAB (CF-FAB)[32] have been successfully applied to the analysis of high mass (up to 45 kDa), non-volatile compounds,[33] however, spectra obtained using these techniques typically show significant chemical background.

Although some of these techniques, specifically, EI, CI, MALDI, FAB, and SIMS, are still routinely used for MS analyses, all of these ionization methods share one distinct limitation – in their early versions all had to be operated under vacuum. As such, operation of mass spectrometers was limited to one ion source at a time if vacuum was to be preserved. It is also clear from a review of the literature that none of the previously-described ionization techniques can be considered universal in terms of the kinds of compounds that can be analyzed. Furthermore, these techniques, with the exception of CF-FAB and EHD, are not easily applied to on-line or continuous flow analyses, as would be preferred for coupling MS with chromatographic techniques. To that end, a paradigm shift towards the development of AP ionization sources, including an AP version of MALDI (AP-MALDI),[34] progressively occurred allowing for modularity in the design of modern mass spectrometers, enabling the performance of complementary analyses using different ionization techniques with a single mass analyzer, and facilitating the coupling between MS and liquid chromatography (LC) and capillary

electrophoresis (CE). Development of these ionization techniques is described in detail in section 1.3.

A more recent theme in ion generation technology development is the progressive trend towards ambient ionization techniques[35, 36] which are capable of directly interrogating samples of odd shapes in their native state, without sample preparation. The development of new ambient ionization sources has skyrocketed in recent years catalyzed by the introduction of desorption electrospray ionization (DESI) by Cooks and coworkers[37] and direct analysis in real time (DART) by Cody and coworkers[38] and leading to the development of twenty-two new ionization techniques (as of May 2009) since 2004. These devices, which are capable of conducting direct analysis (i.e. probing the surfaces of solid or liquid samples directly), are ideal for use in high-throughput screening experiments which are described in section 1.4.

1.3. Atmospheric Pressure Ionization Techniques

AP ionization sources are characterized by operation at atmospheric pressure outside of the vacuum system of the mass spectrometer. Typically, these apparati are coupled to mass analyzers via an interface that provides differential pumping to aid in ion transmission as ions are transported through a pressure reduction on the order of 10^5-10^{12} Torr. One of the central motivations for the development of AP ionization techniques was to find a means of coupling LC with MS. Prior to the 1980's, gas chromatography (GC)-MS was well developed and routinely enabled the analysis of low molecular weight compounds via EI or CI ionization. However, LC-MS was thought to be impossible due to the large flow rates used with LC at that time (1-3 mL min^{-1}) and the need to vaporize

the LC effluent prior to MS analysis to prevent overloading of the vacuum system.[39, 40] Despite these challenges, there was considerable interest in using MS as a detector for LC separations to provide improved resolution of overlapping components in the chromatograms obtained from nonspecific detectors, such as UV-Vis, which were largely prevalent at the time. Successful merging of these analytical techniques was ultimately accomplished by the development of AP ionization sources that now routinely enable the generation of gas-phase ions from neutral molecules emanating from a liquid stream.

The first reported bioanalytical LC-MS coupling was by Horning and coworkers in 1974 who introduced atmospheric pressure chemical ionization (APCI) as an interface for LC-MS.[41, 42] In APCI, a mixture of solvent and analyte is vaporized using a heated nebulizer and is ionized through ion/molecule reactions with reagent ions present in the area surrounding a corona discharge needle. Due to the use of heat, analytes are subject to thermal degradation, thus, APCI is not considered suitable for the analysis of thermally labile species. In addition, APCI has been shown to preferentially ionize low-mass (<1200 u) nonpolar compounds.

In 1979, Thomson et al. introduced AP Ion Evaporation (APIE), which used a pneumatic nebulizer to create a spray of droplets that were ionized by being placed in close proximity to an electrode held at 3.5 kV.[43] Using this technique, Thomson and coworkers were able to obtain mass spectra for 30 cations and anions from salts such as NaCl and some small drugs but their work was limited to small molecules due to the low mass range of the mass analyzer they used. Because no heat was used, solvent-ion clusters were also commonly observed in their experiments. In 1983, Thomson and coworkers introduced the Heated Nebulizer Probe (HNP), which used a pneumatic

nebulizer to create a stream of droplets sprayed from a heated metal capillary.[44] In this technique, ionization occurred as desolvated droplets passed near a corona discharge needle. This technique was fundamentally the same as APCI, differing primarily in probe design and the method by which heat was used to desolvate the droplets, and produced APCI-type spectra while suffering from the same limitations as conventional APCI experiments.

This strategy of decoupling aerosol generation from ionization was also used by Willoughby and Browner who introduced the Monodisperse Aerosol Generator Interface for Chromatography (MAGIC) in 1984.[45] In MAGIC, highly uniformly-sized droplets (12 – 20 μm diameter) are formed from a liquid effluent (0.1-0.5 mL min^{-1}) flowing orthogonal to a nebulizing gas stream. The droplet stream is desolvated in a heated, AP desolvating chamber and the volatilized sample is ionized externally using EI. Despite the clear advantage of using this probe, namely the ability to couple it to most types of mass spectrometers and ionization sources, the relatively complicated setup hindered widespread acceptance of MAGIC.

At the same time, Vestal and coworkers introduced Thermospray (TS), a technique in which aqueous mobile phase was vaporized as it passed through a stainless steel capillary located in a heated ion source.[46] Unlike the previously-mentioned techniques, no external field or charging was used to induce ionization. Rather, this apparatus took advantage of the statistical partitioning of charges within the droplet population, which included some positively charged droplets and an equal number of negatively charged droplets in the overall neutral bulk distribution. However, a discharge needle was commonly integrated into the apparatus to allow for the generation of APCI-

type spectra when operation in thermospray mode produced insufficient signal. Vestal et al. used TS to analyze peptides and drugs but the technique suffered from poor interday reproducibility and analyte ion intensities exhibited a strong dependence on variations in the sample flow rate and composition.[46]

Despite the success of these techniques, the coupling of LC with MS did not become routine until the introduction of ESI as an ionization method for biomolecular MS analysis by Fenn and coworkers[30, 31, 47] and Aleksandrov and coworkers[48] in the early 1980's as discussed in the following section.

1.3.1. ESI-Based Ionization Techniques

The usefulness of ESI for MS analysis was first demonstrated by Dole and coworkers in 1968 who used it to produce charged gas-phase polystyrene ions[29] by passing solution through a hypodermic needle held at -10 kV. The analytical utility of ESI was further extended in 1984 by Fenn and coworkers who characterized the behavior of a slightly modified ESI ion source,[30] later demonstrating the ability to analyze proteins having molecular weights up to 180,000 Da in 1989.[31] A schematic showing the basic principle of a conventional ESI analysis is shown in Figure 1.1.

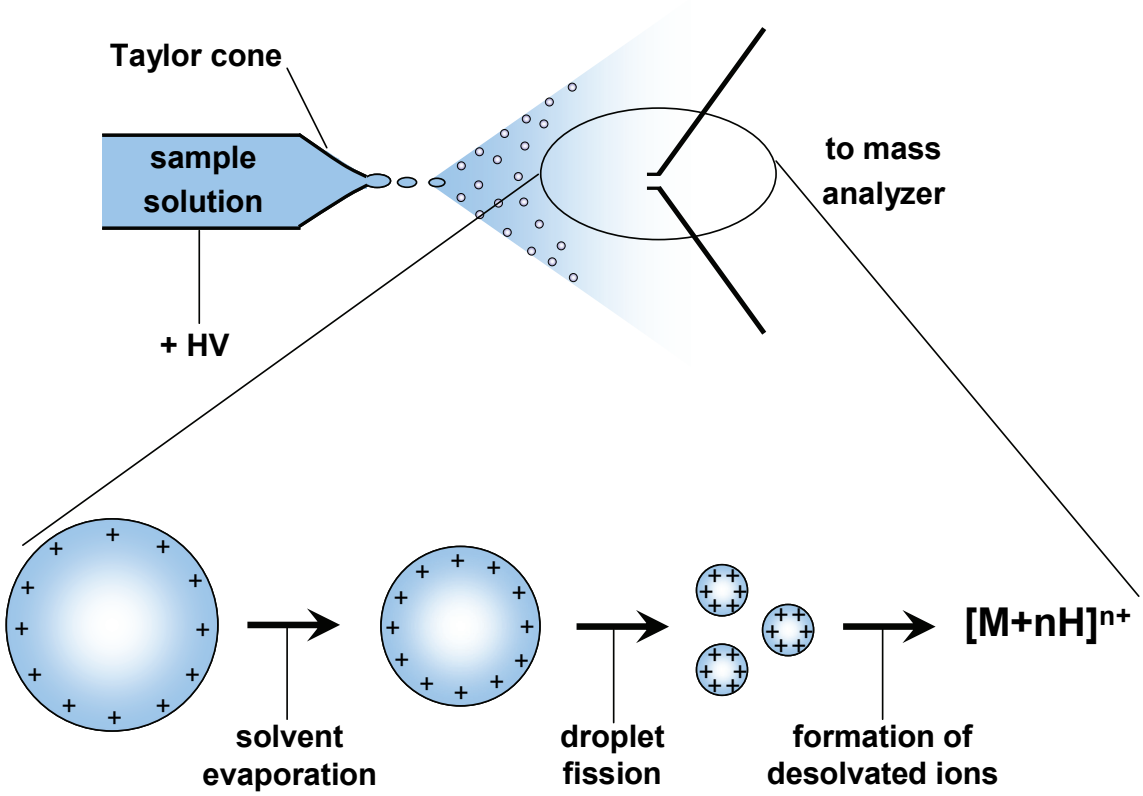

Figure 1.1. ESI Schematic. Charged droplets are ejected from a metal capillary. Solvent evaporates until droplet fission occurs leading to the formation of desolvated ions. (Adapted from Gaskell, et al.[49])

In conventional ESI, a potential is applied to the exterior of a capillary inducing charge separation in the solution flowing through. Charge builds up at the tip of the capillary forming a Taylor cone and causing the forcible ejection of a charged droplet. Due to the application of a concurrent flow of nitrogen (N_2) through the evacuated chamber in Dole's apparatus or a countercurrent N_2 flow in Fenn's apparatus, solvent evaporates from the droplet as it transits through the evacuated chamber until the droplet reaches the Rayleigh limit and undergoes Coulombic explosion to form desolvated ions.[50] Early on it was recognized that spray stability and desolvation varied widely in conventional ESI experiments, thus a variant of ESI, pneumatically-assisted ESI (pESI),

was introduced by Henion and coworkers.[51] This ionization source (Fig. 1.2) was later trademarked by PE/Sciex (Perkin Elmer, Concord, Ontario, Canada) and is currently the most widely used ESI-based ion source today.

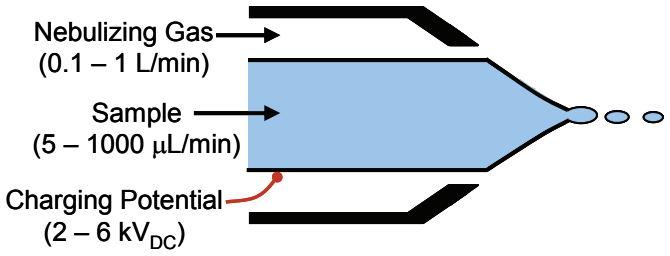

Figure 1.2. Schematic of pESI technique. Average droplet diameter is 5 – 12 μm.[51]

In ESI, desolvated ions are formed via one of two proposed models: (1) the charged residue model[29] which proposes that electrospray droplets repeatedly evaporate and explode as the charge on the surface exceeds the Rayleigh limit forming successively smaller droplets containing a portion of the charge and ultimately leading to ions and (2) the ion evaporation model[52] which proposes that ions are ejected directly out of the droplet due to the high electric field strength on the surface. It has been observed that the charged residue model appears to dominate when analyzing high mass compounds (> 3300 u) while the ion evaporation model dominates when analyzing low mass compounds, however, ESI mechanisms are still the subject of active discussion.[53] Despite this ongoing debate, it is clear that the power of ESI lies in its ability to generate and make amenable to analysis ions from non-volatile compounds spanning a large mass range, which can be attributed to the tendency to create multiply-charged species, and its flow-through nature allowing facile coupling to LC and other liquid phase separation

techniques. However, ESI does suffer from some limitations that are inherent to the electrospray process itself.

One of the limitations of Taylor cone liquid atomization is that the high voltage required for effective ionization sets a minimum to the distance between the sprayer and other instrument components that can be used for operation without electrical discharges. This minimum distance limits the efficiency with which highly-charged droplets can be collected and transmitted into the mass spectrometer via the AP interface. These high voltages can also cause an increase in background signal due to the increased rate of solvent oxidation[54] and because of possible ionization of volatile contaminants present in the laboratory air[55]. In addition, the Taylor cone behavior is highly influenced by the surface tension of the sprayed solution, and thus, improvement of signal stability is generally achieved by addition of organic solvents. However, these solvents may modify the native conformation of the solutes thus distorting, to an unknown extent, the correlation between solution-phase and gas-phase conformations,[56-58] important in techniques such as ion mobility-MS. Also the variable purity of organic solvents can introduce contaminants into the spray causing degradation of the signal.[59] In addition, conventional pESI requires the use of high flow rates (5-2000 μL min^{-1}) due to the relatively large internal diameter of the metal capillary through which the sample flows[49] causing the consumption of large amounts of sample.

Moreover, in scenarios where analytes with largely disparate concentrations are present in the sprayed solution, the intrinsic limitation in the total current that can be supported by Taylor cone electrospray can seriously limit dynamic range, and concomitantly, the relative peak intensities (ion suppression effect).[60-62] Furthermore, it is

well-known that variations in gas phase acidity and basicity,[63, 64] as well as differences in hydrophobicity,[65] can significantly affect the ionization efficiency of some analytes by ESI, which preferentially ionizes hydrophobic analytes having high proton affinities (for positive mode ESI). Finally, the throughput of conventional ESI is limited by ion source geometry, as most commercial sources are limited to containing only one or two sprayers.

Some of these limitations have been overcome by the introduction of (microelectrospray ionization) μESI[66] and (nanoelectrospray ionization) nESI,[67-69] which aim to reduce ion suppression effects in ESI and improve signal intensities by reducing the initial droplet size which increases droplet charge density. Ultrasonically-assisted electrospray (UA-ESI),[70, 71] which aims to increase the range of mobile phase compositions amenable to spray-based ionization techniques and also to reduce ion suppression has also been reported. Despite the improvements offered by these approaches, these still suffer from limited throughput, poor reproducibility (in the case of pulled nESI capillaries) and cross-contamination. Conversion of these techniques into chip-based format by making use of miniaturized devices[72-76] was attempted to further improve their figures of merit.

1.3.2. Miniaturized Ion Sources

Ionization using the nESI format is one of the preferred techniques for proteomic workflows. Typically, nESI (Fig. 1.3) is conducted using pulled or tapered glass capillaries, to which charging voltages between 900 V_{DC} and 1500 V_{DC} are applied, resulting in sensitivities that are 10–100 times greater than that of conventional ESI.[69]

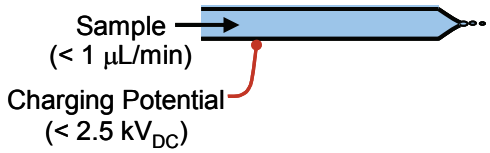

Figure 1.3. Schematic of nESI technique. Average droplet diameter is < 200 nm.[67, 68]

A wider linear dynamic range (10^2 increase in upper concentration limit) has also been observed in nESI and is attributed to the higher charge density of nESI droplets. The higher charge density allows for a reduction in charge competition between analytes in mixtures making more charge available to each analyte and causing a concomitant reduction in ion suppression effects.[62] nESI is particularly amenable to miniaturization and spray nozzles with internal diameters of a few microns have been successfully fabricated with techniques normally used for the manufacturing of semiconductor microchips.[77] Microfabricated nanospray (microchip ESI) devices offer a number of advantages for mass spectrometric analysis, including reduced sample consumption and cross-contamination, improved sprayer reproducibility, high-throughput and automation capabilities, and the potential for integration with on-chip solid-phase extraction, and chromatographic or electrophoretic separations.[78, 79]

To date, reported miniaturized nanospray infusion devices fall into four main categories: (1) devices using fused silica capillary emitters attached to a chip,[80-91] (2) devices using a microchannel exiting the edge of a wafer,[92-105] (3) monolithic devices using etched ESI tips,[61, 106-118] and (4) integrated miniaturized nESI devices comprising enrichment columns, reverse-phase separation channels and micromachined nanospray emitters.[73, 119-123] Although all of these devices have been shown to successfully generate gas-phase ions from small sample volumes (nL–μL), they still rely on the generation of a

Taylor cone for liquid atomization, which can only be overcome via the use of a fundamentally different approach to the ionization process.

1.3.3. Ultrasonic Electrospray Ion Sources - Decoupling Droplet Formation and Droplet Charging

To overcome some of the innate limitations of Taylor cone electrospray mass spectrometry, several reports on the use of acoustic liquid ejection for ESI purposes have been reported. Unlike droplet ejection in conventional ESI which relies on charge repulsion to force ejection of liquid from a capillary, acoustic liquid ejection, which is commonly used in inkjet printing technology,[124, 125] relies on the use of an ultrasonic pulse to focus acoustic energy on a portion of the liquid sample, forcing the ejection of a droplet from the liquid surface. In 1994, Banks et al. introduced UA-ESI, which uses a piezoelectric transducer to produce a continuous droplet stream by Rayleigh vibrational breakup of a liquid jet (Fig. 1.4).[70, 71]

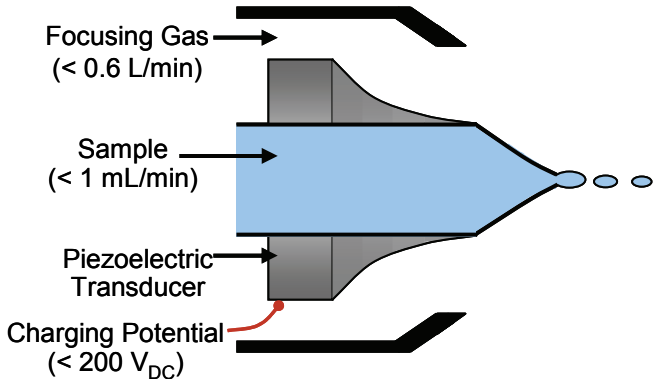

Figure 1.4. Schematic of UA-ESI technique. Average droplet diameter is 10 – 20 μm.[70]

The underlying motivation for this approach was to decouple the spray formation and ionization processes. This enables efficient and stable ionization of analytes from solutions containing little or no volatile solvents. However, the proposed UA-ESI device suffered from instabilities due to temperature variations that affected the resonant frequency needed for optimum ejection.

Shiea et al. also recognized the potential of ultrasonic nebulization and coupled an ultrasonic nebulizer to an array of seven electrospray nozzles to which a charging voltage of 4000 V_{DC} was applied, showing the feasibility of generating multiply charged protein ions.[126] Smith et al. later utilized drop-on-demand technology in conjunction with ESI, with charging voltages of up to 4900 V_{DC} to sensitively ionize insulin samples dissolved in 1:1 methanol/water, 1% acetic acid.[74] In this approach, a single droplet is released from the end of a capillary because of a rapid pressure pulse generated by a radially-contracting piezoelectric element. Droplet bursts or continuous trains are ejected from this capillary by application of a corresponding pulse burst or sine wave to the cylindrical piezoelectric actuator surrounding the electrospray capillary. In a related experiment, Murray et al. demonstrated the feasibility of performing MALDI-MS on aerosol particles derived from discrete droplets produced using a piezoelectric dispenser.[127] More recently, Muddiman and coworkers used RF actuation to cause desorption of analyte (ubiquitin and a peptide, brain natriuretic peptide-32) from a quartz crystal microbalance. These analytes were ionized via interaction with an ESI spray, demonstrating the utility of this technique for the analysis of biomolecules.[128]

1.3.4. Overcoming Challenges in AP Ion Generation – AMUSE Ionization

To overcome some of the limitations inherent to current spray-based technologies, we demonstrated the successful generation of ions from a MEMS device first conceptualized by Fedorov and coworkers,[129] the Array of Micromachined UltraSonic Electrosprays (AMUSE). This ion generation technique is based on the concept of decoupling the processes of droplet formation and droplet charging by acoustically driving the ejection of droplets using the mechanical oscillations of a piezoelectric crystal and charging the droplets via the application of an additional DC potential of only a few hundred volts to the sample reservoir.[76, 130-135] Part I (Chapter 2-4) of this thesis describes our advances made towards the development of the AMUSE as a stable ion source for analytical mass spectrometry and its applications, as well as our efforts to characterize and reduce the internal energy deposition of AP ionization techniques in general. Chapter 2 presents efforts to couple the AMUSE with MS and characterize the device by comparing results for the analysis of standard compounds, including a drug, peptide and protein, to results obtained by ESI and nESI.[76, 133] Chapter 3 describes extensive experiments to measure and modulate the internal energy deposited on ions by both ESI and AMUSE[135] while Chapter 4 describes our proof-of-principle efforts to couple LC to a quadrupole ion trap LC-MS detector via AMUSE.

1.4. Ambient Ionization Techniques

The revolution in time-of-flight (TOF) instrumentation following technological advances in reflectron technology, collisional cooling, orthogonal ion acceleration and analog-to-digital data acquisition,[136] as well as the introduction of novel mass analyzers

such as linear ion traps[137] and the Orbitrap,[138, 139] and the development of new hybrid instruments such as the quadrupole ion trap-fourier transform (QiT-FT),[140] linear ion trap-Orbitrap (LiT-Orbitrap),[141] and quadrupole-ion mobility-time-of-flight (Q-IMS-TOF)[142] mass spectrometers has put exquisitely powerful mass analysis tools in the mass spectrometrist's fingertips, enabling the simultaneous non-targeted detection, identification and quantitation of hundreds of analytes. This has translated the performance bottleneck to the front end of the mass spectrometer. The need to dissolve, extract and/or filter the sample prior to analysis and for placing it under vacuum constrain the type and shape of materials that can be investigated. The recent introduction of ionization techniques that operate under ambient conditions aims to address these limitations and has further expanded the toolbox of analytical methodologies available for drug discovery, metabolomics, forensics, and quality control applications by enabling the rapid screening of chemical systems of medium complexity[35] with sample throughputs of up to 45 samples min^{-1}.[143]

Ambient ionization sources are characterized by operating at AP, and by being able to probe the surface of samples of any size, shape and texture/morphology. Ions are created outside of the instrument, in the open air. Whereas in conventional mass spectrometric experiments the sample is generally dissolved prior to analysis, in ambient MS the sample is interrogated in its native state, accelerating the analytical pipeline, preserving spatial chemical information, avoiding dilution, and maximizing sensitivity. The breadth of the new field of ambient MS is reflected by the explosive appearance of a multitude of new ionization approaches, spearheaded by DESI,[37] and soon followed by DART.[38] These new ionization techniques can be separated into five categories based on

their respective desorption mechanisms and include techniques exhibiting desorption due to the action of a spray or jet, laser, heat, gas, or resonance.

Ionization techniques utilizing spray- or jet-based desorption include DESI, easy ambient sonicspray ionization (EASI, formerly known as desorption electrosonic spray ionization (DeSSI)),[144] and fused droplet ESI (FD-ESI),[145] while techniques that rely on laser-assisted desorption include electrospray-assisted laser desorption ionization (ELDI),[146] matrix-assisted laser desorption electrospray ionization (MALDESI),[147] laser ablation-electrospray ionization (LAESI),[148] infrared laser-assisted desorption ESI (IR-LADESI),[149] AP-laser desorption/chemical ionization (AP-LD/CI)[150] and laser-induced acoustic desorption/ESI (LIAD/ESI).[151] Ambient ionization techniques that use thermal desorption include DART, atmospheric pressure thermal desorption/ionization (APTDI),[152] atmospheric-pressure solids analysis probe (ASAP),[153] desorption atmospheric pressure chemical ionization (DAPCI),[154] desorption atmospheric pressure photoionization (DAPPI),[155] plasma-assisted desorption/ionization (PADI),[156] and low temperature plasma (LTP).[157] Ambient techniques that rely on desorption via gas flow include extractive electrospray ionization (EESI),[158, 159] neutral desorption sampling extractive electrospray ionization (ND-EESI),[160] dielectric barrier discharge ionization (DBDI),[161] and flowing atmospheric pressure afterflow (FAPA).[162] Finally, techniques relying on ultrasonic desorption include ultrasonically-assisted EESI (UA-EESI),[163] and radio frequency acoustic desorption/ionization (RADIO).[128]

1.4.1. Spray- or Jet-Based Ambient Ionization Techniques: DESI, EASI, and FD-ESI.

DESI was first introduced by the Cooks group in 2004[37] and uses a pneumatically-assisted high-velocity electrospray jet that is directed onto the surface of a sample to bring about analyte desorption. Following desorption the analyte is "picked-up" by impacting droplets and subsequently ionized via either the ion evaporation or charge residue mechanism.[164, 165] Recently, computational fluid dynamics simulations have confirmed this "droplet pick-up mechanism" showing that the DESI process contains three consecutive stages: 1) the formation of a thin liquid film on the sample surface, 2) extraction of solid-phase analytes into this thin film, and 3) collision of primary droplets with this thin film, producing secondary droplets which take up part of the analyte-containing liquid.[166]

Like DESI, the EASI ionization process also uses a high velocity spray to probe the sample, but in EASI, no voltage is applied to the sprayed solution. It is believed that droplet charging in EASI occurs as a result of statistical fluctuations of the charge spatial distributions within the sprayed droplets.[167, 168] It has also been speculated that desorption and ionization in this technique, which has been shown to be useful for the direct analysis of pharmaceuticals,[144] probably follow the DESI mechanisms described above.

One particularly interesting and somewhat unexplored DESI aspect is its "reactive" mode, which allows for specific chemical reactions to occur via introduction of various reagents into the DESI spray solution.[169-171] Cooks and coworkers were the first to demonstrate the potential of reactive DESI for the rapid, sensitive detection of explosives from a wide variety of surfaces by selective adduction with chloride, trifluoroacetate and methoxide anions introduced into the DESI spray.[169] In reactive

DESI, the mass spectrometric detection of specific products formed as a result of these in-situ chemical reactions can be used to increase the selectivity of the technique and may also provide increased sensitivity as in some cases, the chemical species produced are better able to survive transport through the mass spectrometer's ion optics.[171]

In FD-ESI, a pneumatic nebulizer is used to create a sample aerosol which is carried to the tip of a capillary where the neutral sample aerosols fuse with charged methanol droplets generated by electrospraying an acidified methanol solution.[172] This ionization technique has been shown to provide high quality mass spectra from biological samples such as myoglobin prepared in Tris buffer and containing detergent, as the solubility of the unwanted components can be decreased by changing the electrospraying solvent.[145]

1.4.2. Laser-Assisted Desorption/Ionization Techniques: ELDI, MALDESI, LAESI, IR-LADESI, AP-LD/CI, and LIAD/ESI.

Laser-assisted desorption/ionization techniques include techniques combining laser desorption with ESI (ELDI, MALDESI, LAESI, and IR-LADESI) or with corona discharge ionization (AP-LD/CI). Shiea et al. used ELDI coupled to a Q-TOF to directly detect the active ingredient (AI) in drugs using UV irradiation to desorb methaqualone from a tablet followed by ESI.[146] MALDESI, which Muddiman et al. coupled to FT-ICR to obtain high resolution spectra from peptides and proteins, is similar to ELDI but uses an organic acid matrix to improve ion signal.[147] LAESI,[148] which was introduced by Vertes, et al., and IR-LADESI,[149] which was introduced by Rezenom, et al., both use a mid-IR laser to irradiate water-rich samples, causing desorption of analyte from the

surface. However, the sources used by Vertes and Rezenom have different geometries whereby the laser source in LAESI is orthogonal to the sample surface while the laser in IR-LADESI is oriented 45º with respect to the sample surface. In the latter, lower pulse energies were also used which resulted in both ablation and desorption of surface neutrals.[149] In AP-LD/CI, a laser pulse is used to desorb intact neutral molecules that then undergo chemical ionization via interaction with reactive ions produced by the corona discharge. Preliminary experiments comparing the results of these experiments using model compounds with those by AP-IR-MALDI yielded a 150-fold increase in signal intensity, indicating the benefit of incorporating multiple ionization processes into techniques that include desorption steps that produce a large number of neutral species.[150]

In LIAD/ESI, a sample solution deposited on a metal foil is irradiated with a pulsed laser that creates acoustic waves that propagate through the foil and enable desorption of the sample from the foil. Following desorption, ionization via interaction with the charged ESI solution occurs. One unique feature of LIAD desorption is that there is little excitation of intramolecular vibrational states, thus a wide variety of molecules can be desorbed as intact neutral species.[151]

1.4.3. Heat-Assisted Ambient Ionization Techniques: DART, APTDI, ASAP, DAPCI, DAPPI, PADI, and LTP.

In DART, which was first introduced in 2005 by Cody et al., a stream of heated helium gas flows past a glow discharge region within the source leading to the production of metastable helium atoms of 19.8 eV.[38] When analyte-containing samples are placed in the region between the DART ionization source and the mass spectrometer inlet, analyte

is desorbed, or possibly sputtered, from the surface and ionization is accomplished via one of the mechanisms described in detail in section 5.3.1.[38, 173, 174]

In addition to DART, several other discharge-based ambient ionization techniques have been reported in the literature. The first report of APTDI was by Cooks and coworkers in 2006 who observed that heating organic and inorganic salts led to the production of reagent ions that generated analyte ions via proton transfer similar to what occurs in CI.[152] In ASAP, a solid sample probe is introduced directly into the corona discharge region of an enclosed APCI ion source via a custom built sample port.[153] The heated gas stream from an APCI probe desorbs the analytes, which are ionized by interaction with the corona discharge plasma. ASAP has been applied to a variety of analytical problems, including the analysis of biological tissue, pharmaceuticals, polymers, currency,[153] and inhibitors of the ergosterol pathway.[175]

DAPCI was originally implemented using toluene as the reagent gas flowing through the annular gas flow of a modified DESI sprayer in which the spray capillary was replaced by a sharp stainless steel tip.[154] Unlike DESI, DAPCI has been shown to be effective at ionizing compounds of moderate to low polarity.[176] In DAPCI, the sample is directly introduced into the corona discharge region generated between a sharp needle and the capillary inlet of a mass spectrometer. Qiao et al. recently demonstrated the feasibility of using ambient air as the CI reagent in DAPCI.[177]

In DAPPI, a heated jet of vaporized solvent is directed towards the surface of a sample causing thermal desorption of analyte(s) which is then ionized by photons emitted by a photoionization lamp (10 eV photons). Unlike the previously described techniques, DAPPI is well-suited to the analysis of polar, non-polar and neutral compounds. Thus,

DAPPI can provide complementary information to what would be obtained via other ambient methods.[155, 178]

A related method, PADI[156] has also been recently reported and is carried out by generating a non-thermal RF plasma into which the sample is placed directly, as in ASAP and DAPCI. In the LTP, helium (0.5 L min^{-1}) flowing through a plasma generated by a small probe is directed at the surface of a sample. In these experiments, the sample is heated to provide thermal desorption and ionization most likely occurs via the same mechanisms as those described for DART. This ionization technique has been successfully applied to the detection and quantitation of melamine in milk powder and whole milk.[179]

1.4.4. Gas-Assisted Ambient Ionization Techniques: EESI, ND-EESI, DBDI, and FAPA.

EESI, introduced by the Cooks group in 2006, uses a gas stream to desorb compounds from a solid or liquid surface generating a neutral aerosol mixture that is subsequently ionized by interactions with an electrospray solution.[158] Zenobi et al. recently demonstrated the rapid profiling of complex biological samples such as frozen meat, vegetation and human skin samples using ND-EESI[160] on a hybrid quadrupole-time-of-flight (Q-TOF) mass spectrometer. Mass accuracies of 10 ppm or better with detection limits as low as 10 femtograms histamine/cm^2 were achieved using this ionization technique with an analysis speed of 1-2 s.

Zhang et al. reported DBDI in 2007[161] which was employed for the direct analysis of hexahydro-1,3,5-trinitro-1,3,5-triazine (RDX), 2,4,6-trinitrotoluene (TNT), and

pentaerythritol tetranitrate (PETN) from explosives-contaminated surfaces, and for amino acids. In DBDI, a needle–plate electrical discharge generates energetic species, such as electrons, and these species launch desorption and ionization of the analyte from a solid surface used as a dielectric barrier, where the sample is deposited. In negative ion mode, DBDI was observed to form the typical $[TNT]^-$, $[TNT-H]^-$, $[RDX+NO_2]^-$, $[PETN+ONO_2]^-$, and $[RDX+ONO_2]^-$ anions. For amino acids in positive ion mode, the $[M+H]^+$ protonated molecules were observed.[161]

FAPA, which was recently reported by Hieftje and coworkers,[180-182] uses a beam of energetic helium metastable species to create a high flux of reagent ions such as protonated water clusters, nitrogen dimer ions and oxygen ions. In this source, gas-assisted analyte desorption likely occurs while ionization most likely follows CI mechanisms.[162]

1.4.5. Ultrasonically-Assisted Desorption/Ionization Techniques: UA-EESI, RADIO.

Ultrasonic desorption can generally be achieved using a piezoelectric transducer. In UA-EESI, a small droplet of sample (~3 μL) is deposited on an ultrasonic transducer and nebulized. The neutral sample aerosol then undergoes extraction via interaction with a droplet stream from an ESI sprayer. This method has been successfully applied to the detection of melamine in various food matrices including raw milk, wheat gluten, and milk powder.[163] RADIO was recently reported by Dixon et al. and utilizes acoustic desorption of a sample deposited on a quartz crystal microbalance electrode prior to RF actuation. Ionization occurs via interaction with a continuous ESI stream flowing directly above the electrode and oriented towards the mass spectrometer inlet. Using this method,

MS signal for several model compounds, such as melittin and ubiquitin, was obtained, demonstrating the potential of ultrasonically-assisted desorption as an alternative desorption method for the analysis of large molecules.[128]

Of the new ambient ionization techniques described above, DART and DESI seem to have experienced the most commercial success and have been applied to a variety of problems including the direct (i.e. without sample preparation) screening of solid pharmaceutical samples[176, 183] counterfeit drugs,[184-189] writing inks,[190] ink photoinitiators in food,[191] pathogenic bacteria,[192, 193] flavors and fragrances,[194] analytes separated by high performance thin layer chromatography,[195] biological fluids,[196] food contaminants,[197, 198] insects,[199] and nonpolar compounds not accessible using other techniques.[173] Several other applications have been posted as on-line application notes but without the benefit of the peer-review process.[200] The majority of these applications have focused on screening samples without requiring any preparation or chromatographic separation, which can be followed by a more comprehensive LC-MS examination, if necessary.[183, 189] In this two-tiered approach, samples are first screened in a high-throughput fashion to establish an estimate of their complexity, analyte concentration range, the presence of unknowns and authenticity. Samples of interest selected during the high-throughput screening step are then subjected to more comprehensive, but time- and resource-consuming, LC-MS analysis for in-depth chemical characterization.

Part II of my thesis describes the application of DART for the screening analysis of pharmaceutical agents as well as an exploration of the importance of various DART parameters on sample throughput. Chapter 5 presents the application of DART to the screening of the chemical composition of low quality antimalarial drugs in an effort to

identify the contents of these pharmaceuticals, to estimate their effect on the increasing prevalence of drug-resistant strains,[183] and to determine the realistic sample throughput of this technique.[189] Chapter 6 presents results for the first application of DART to the screening of counterfeit drug samples that mimic the vital antimalarial artesunate,[201-203] the consumption of which has led to the death of many patients.[204-206] This technique will also be compared to DESI ionization in the same context.

1.5. Conclusion

Advancements in the development of new ion generation approaches continue to revolutionize the field of MS. Progress towards the development of AP ionization techniques in μESI and nESI formats as well as miniaturization of these sources has alleviated some of the challenges inherent to the electrospray process, but improvements are still possible. The introduction of a new approach to ion generation in array format for mass spectrometry, AMUSE, attempts to circumvent these limitations by producing ions using a method that decouples the processes of droplet formation and droplet charging. Recently introduced ambient ionization techniques and a detailed description of the DART ion source are also presented to provide a framework for the discussion of the applications and the effects of DART parameters included in the following chapters.

PART I: ADVANCES IN ATMOSPHERIC PRESSURE IONIZATION TECHNIQUES

CHAPTER 2. ANALYTICAL PERFORMANCE OF A VENTURI-ASSISTED AMUSE

2.1. Abstract

Analytical characterization of the AMUSE ion source performed using model compounds is presented in this chapter. The basic concept of the technique is described followed by a brief explanation of methods for improving ion transmission efficiency. In this work, a Venturi device is coupled to the AMUSE to increase desolvation, droplet focusing, and signal stability. Three model compounds, a drug, a peptide, and a protein, are analyzed under a variety of conditions to determine the effects of the Venturi gas flow rate and temperature, DC charging potential, solvent composition, and nozzle diameter, which are described in more detail below.

2.2. AMUSE Ionization – Concept and Challenges

The AMUSE ionization source was invented by Fedorov and Degertekin for high throughput, multiplexed MS[129] and first demonstrated on a MS system jointly by the Fedorov, Degertekin, and Fernández groups.[76] AMUSE intends to overcome the limitations of conventional microchip ESI based on Taylor cone liquid atomization by acoustically driving the ejection of droplets, thus offering the potential for high-throughput, on-demand, multiplexed and inexpensive mass spectrometric analysis with minimum sample consumption.

2.2.1. AMUSE Concept

The AMUSE is a fundamentally different type of ion generation device consisting of three major components: 1) a piezoelectric transducer that creates ultrasonic waves at one of the resonant frequencies of the sample-filled device, 2) an array of pyramidally-shaped nozzles micromachined on a silicon wafer, and 3) a spacer which prevents contact between the array and transducer ensuring the transfer of acoustic energy to the sample (Fig. 2.1).

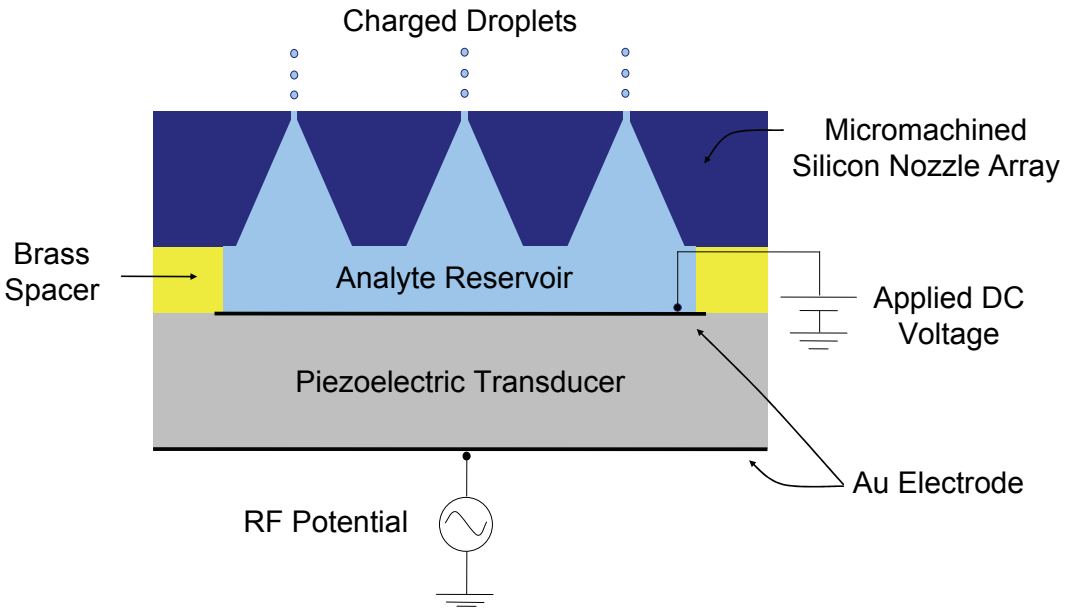

Figure 2.1. Schematic of the AMUSE ion source.

Droplet ejection is driven by the application of a RF potential to the piezoelectric transducer causing resonance within the device and generating a high pressure gradient at the apices of the nozzle pyramids. This resonance forces the periodic ejection of multiple droplet streams from the device. Droplet charging can be accomplished via a DC potential applied to the interior electrode of the piezoelectric transducer. With this device,

the processes of droplet formation and droplet charging are separated; hence, the limitations of conventional electrospray-type ionization techniques, including the need for high charging potentials and the addition of organic solvent to decrease surface tension, can be avoided.

2.2.2. AMUSE Nozzle Array Fabrication

Fabrication of the 20x20 5-μm-nozzle (1st generation) array was first described by Meacham and coworkers in 2004.[130] Fabrication of these 1st generation devices can be broken down into two major steps: 1) the creation of pyramidally-shaped nozzles and 2) the opening of orifices at the apices of these pyramidal cavities. Each of these steps can be further separated into several individual processing steps, which are shown in Figure 2.2. As this fabrication protocol has been described in detail elsewhere,[130-132] only a brief explanation of the method will be provided here. The fabrication process begins with the removal of organic contaminants from a 4"-diameter, 500-μm thick wafer of (100) silicon via immersion in a Piranha solution (4:1 sulfuric acid:hydrogen peroxide v:v) and is followed by the deposition of 1 μm of silicon nitride (Si_3N_4) using plasma-enhanced chemical vapor deposition (PECVD). Photolithography followed by reactive ion etching (RIE) is used to create the base pattern of the device. The pyramidally-shaped nozzles are wet etched using potassium hydroxide (KOH) until the apex of the pyramid extends through the entire wafer thickness. Photolithography followed by RIE is then used to open the orifices and the photoresist is removed from the surface.

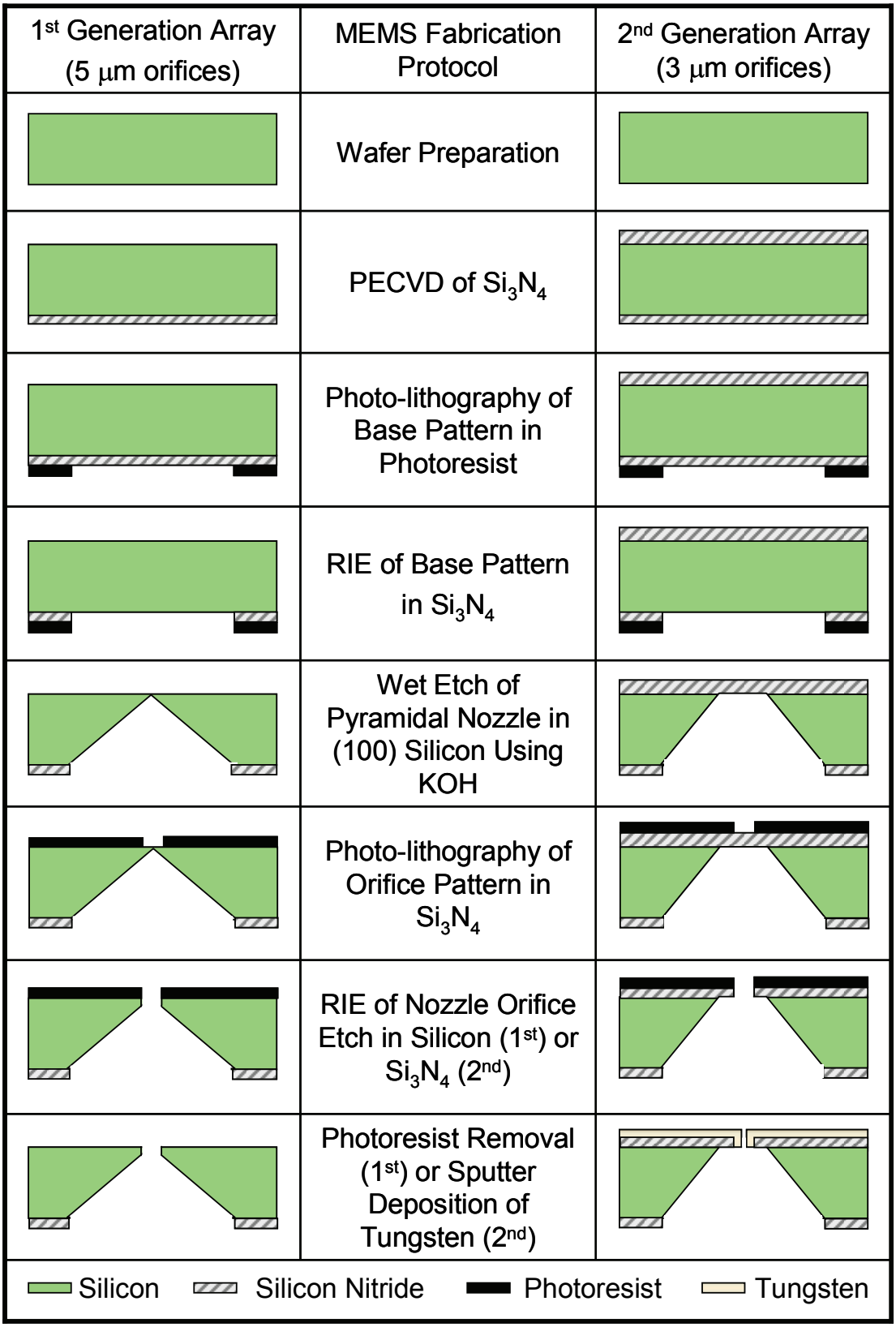

Figure 2.2. Workflow for fabrication of 1st and 2nd generation AMUSE nozzle arrays.

Due to the difficulty of aligning the orifices with the apices of the pyramidal cavities, the fabrication process was modified to enable more facile and reproducible array fabrication and was used to generate a 20 x 20 array of 3-μm nozzles (2nd generation).[132] In this workflow, silicon nitride is deposited on both sides of the cleaned wafer and the base pattern is generated as described above. KOH is used to etch through the silicon forming a large orifice that is capped by the additional silicon nitride layer. RIE is used to etch the orifice through the Si_3N_4 membrane layer and tungsten is sputter-coated on top to further strengthen this layer. Due to the tungsten deposition, the diameter of the orifice diameter decreases from 5 μm to 3 μm as the tungsten coats the walls of the orifice opening.

2.2.3. Improving Ion Transmission of AP Ion Sources

One challenge commonly faced during AP ion generation is the low ion transfer efficiency, reported as the ratio of the detected ion current in the analyzer vs. the total ion current, from the source to the ion optics via the spectrometer's AP interface (API) with estimated losses of up to 99.9% for ESI,[207] 99% for nESI,[208] and 99.2% for AP-MALDI.[209] To mitigate this difficulty, several solutions have been proposed including air amplifiers (also known as Venturi devices),[168, 210] flared inlet capillaries,[211, 212] flared inlet capillaries coupled to Venturi devices,[213] and ion funnels.[214, 215]

Initial, proof-of-principle experiments performed by Aderogba, et al. using the AMUSE on a TOF mass spectrometer (Jeol JMS-100TLC (AccuTOF™), Peabody MA) demonstrated the ability of this device to generate ions from small test compounds.[76] However, inconsistent droplet/ion transmission and limited desolvation hindered further

practical use of the AMUSE ion source in that particular instrumental configuration (Fig. 2.3). This is due to the relatively short distance between the AMUSE and the MS inlet (~5 mm), which limits the time for adequate desolvation, and to the small inlet aperture size (400 μm), which reduces the ion transmission efficiency as the droplet streams are not focused (inset of Fig. 2.3). Furthermore, desolvation at this orifice is limited when the original ESI ion source is replaced with the AMUSE device, as in this particular instrument the heated desolvating element is located in the electrospray needle housing.

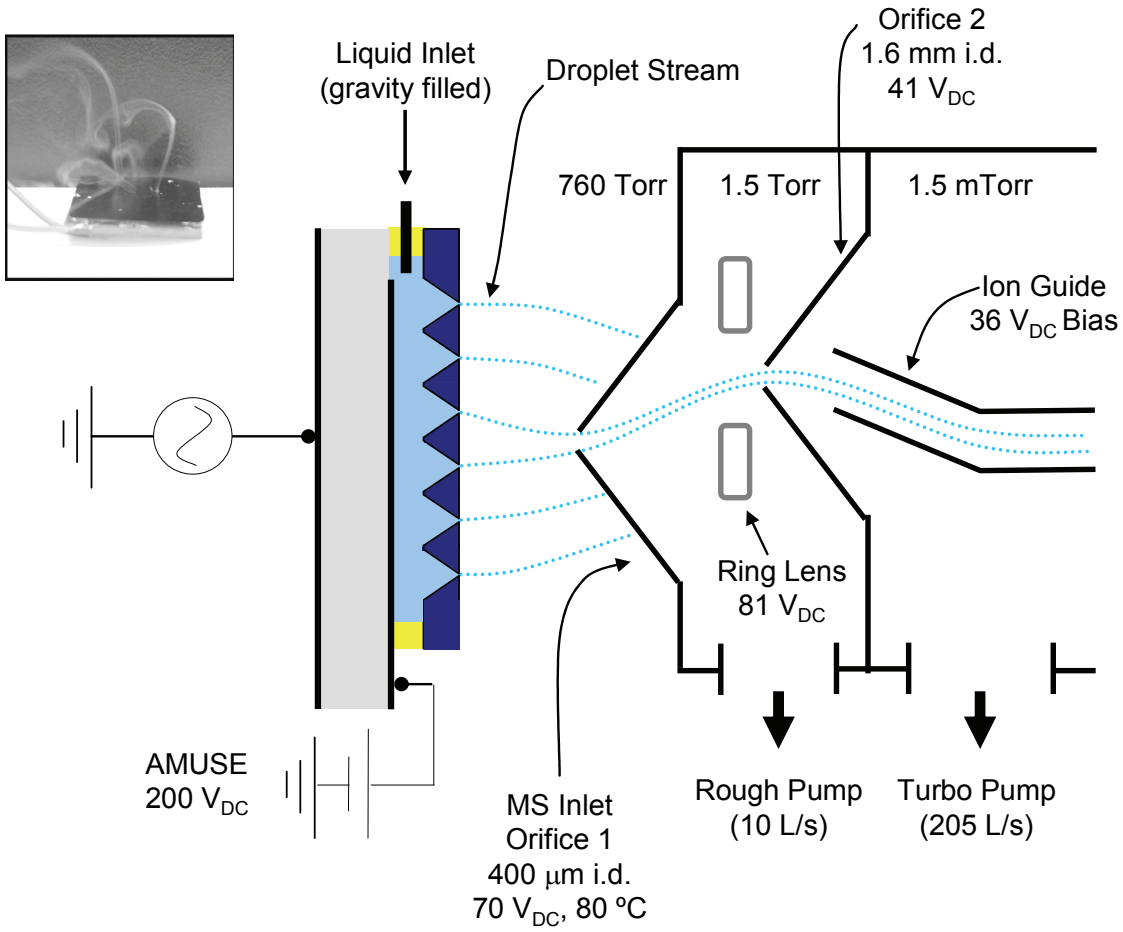

Figure 2.3. Schematic of the AMUSE-TOF instrumental configuration. Inset shows AMUSE droplet production (AMUSE was assembled using protocol 1, see section 2.3.2).

Follow-up experiments involved coupling of AMUSE to a triple quadrupole (QqQ) mass spectrometer (PE-Sciex API III$^+$, Perkin Elmer, Waltham, MA) which utilized a curtain gas interface. In this interface, a N_2 curtain gas flows around the orifice to prevent orifice clogging by non-volatile material, to assist in droplet evaporation and to aid in declustering of ion-solvent clusters by collisions with gas molecules. AMUSE experiments in this instrumental configuration (Fig. 2.4) were unsuccessful primarily due to the outflow of N_2 from the orifice which tended to blow away the low-linear velocity AMUSE droplet streams as discussed in section 2.4.

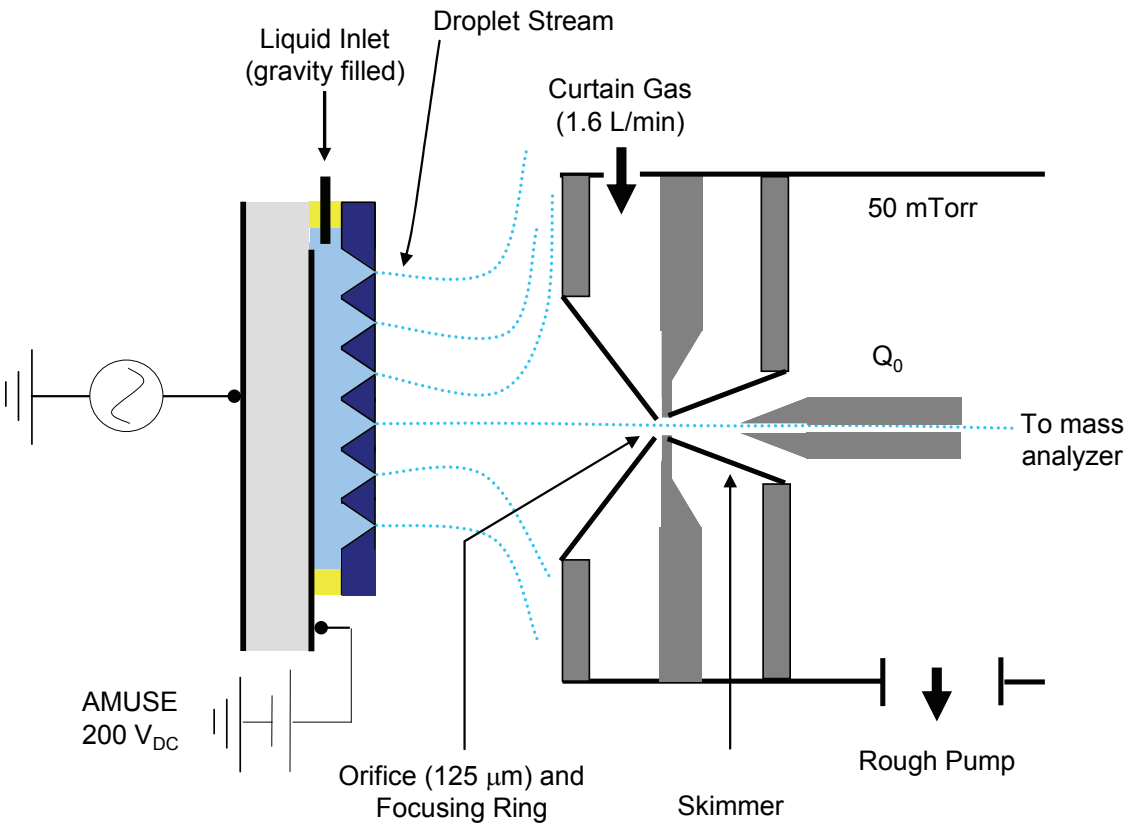

Figure 2.4. Schematic of the AMUSE QqQ instrumental configuration.

These difficulties were circumvented by coupling the AMUSE to an ion trap (IT) mass spectrometer which uses a long (17.8 cm) heated capillary as the first element of the API as shown in Figure 2.5. Despite the substantial improvement in the performance of the device, sensitivity was still lacking leading to speculation that incorporation of a Venturi device may provide improvement in performance.

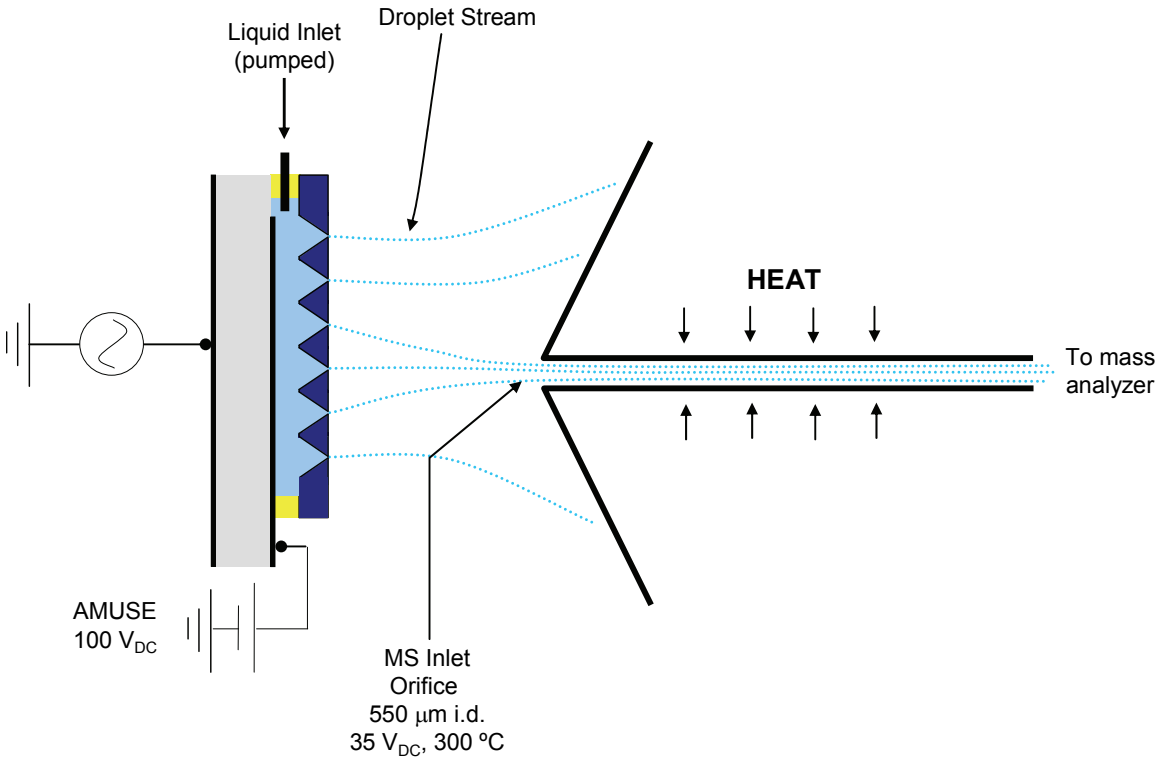

Figure 2.5. Schematic of the AMUSE-IT instrumental configuration.

Venturi devices are devices that rely on the Venturi and Coanda effects.[210] They have been applied to the task of focusing a charged droplet cloud towards the mass spectrometer inlet by Zhou, et al.,[210] Hawkridge, et al.,[216] Yang, et al.,[168] and Dixon, et al.[213, 217] The device consists of two threaded metal cylinders which, when attached, create an annular gap through which a high pressure gas flows. Compression of the gas at

this gap increases the velocity of the gas. This high velocity gas flowing along the walls creates a low pressure region in the center of the device, which provides suction as shown in Figure 2.6. Incorporation of a Venturi device in the AMUSE assembly and the characterization of this source for the analysis of model compounds are described in more detail below.

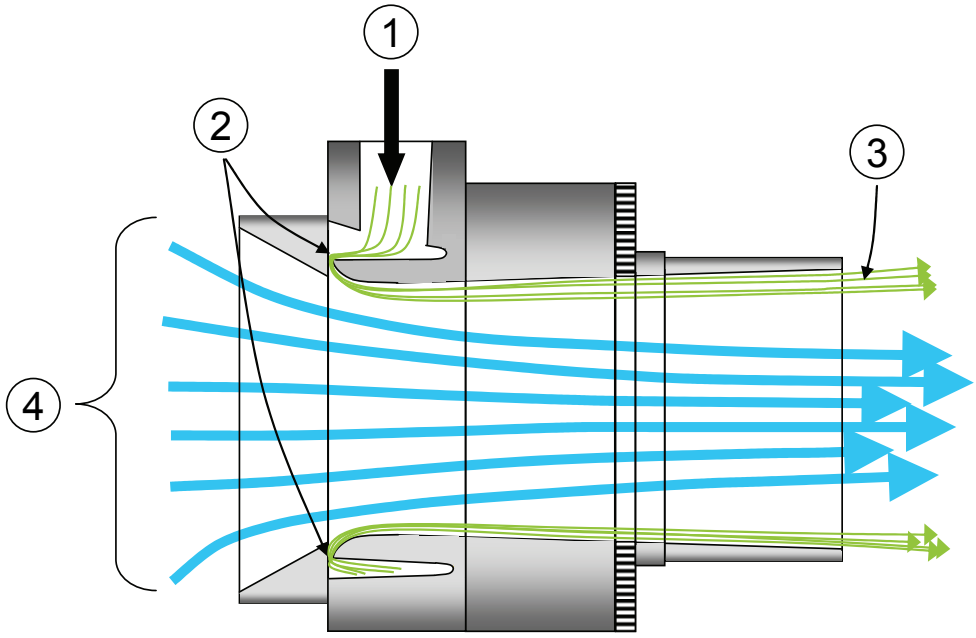

Figure 2.6. Overview of Venturi device operation. (1) Compressed N_2 enters the device and is (2) forced through a constriction. N_2 then (3) flows along the curved inner surface at a high velocity creating (4) suction of the droplet cloud.

2.3. Experimental Details

2.3.1. Materials

Reserpine (Sigma, St. Louis, MI), horse heart cytochrome C, (Acros Organics, Geel, Belgium), and leucine enkephalin (YGGFL, American Peptide, Sunnyvale, CA) were purchased and used without additional purification. Methanol (HPLC grade) was

purchased from Fisher (Hampton, NH). Working solutions of each compound (1–10 μM) were prepared in nanopure water (18 MΩ cm^{-1}, Barnstead International, Dubuque, IA) containing 0.1% (v/v) glacial acetic acid (Sigma-Aldrich, St. Louis, MO). Except for initial exploratory experiments with reserpine, no organic solvent was added to the working solutions. The sample solution was delivered to the analyte reservoir at flow rates ranging from 30 to 100 μL min^{-1}, equivalent to 75–250 nL min^{-1} per nozzle.

2.3.2. Acoustic Micromachined Array Assembly

The AMUSE assembly has undergone continuous modifications since its introduction in 2004.[130] In initial experiments, the device was sealed using a combination of cyanoacrylate (Loctite SuperGlue®, Rocky Hill, CT), epoxy (2-ton epoxy®, Devcon, Danvers, MA), and double-sided polyimide tape (Kapton®, Dupont, Wilmington, DE) (Protocol 1) as shown in Figure 2.7.

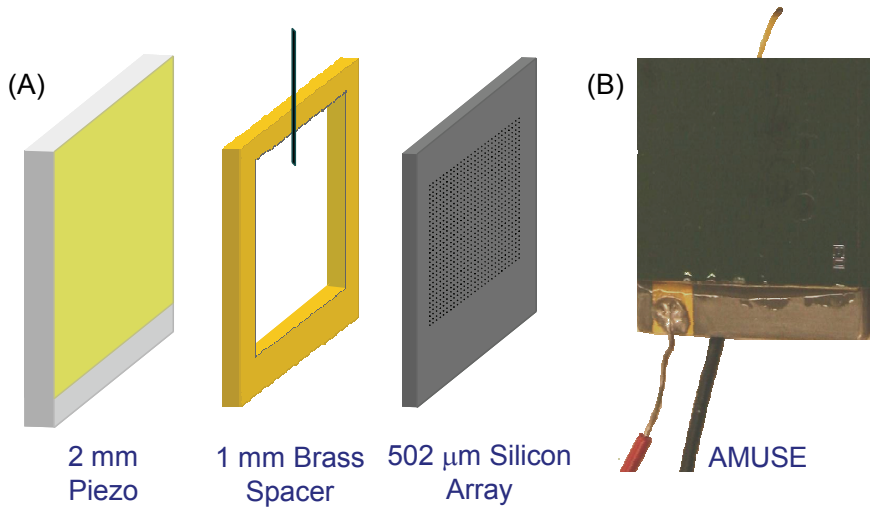

Figure 2.7. (A) AMUSE assembly components and (B) image of intact device assembled using protocol 1.

In this protocol, a 2-cm long liquid inlet tube (360 μm OD x 150 μm ID polytetrafluoroethylene (PTFE) tubing, Upchurch, Oak Harbor, WA) was glued into a 375 μm-deep channel etched in a 0.5 mm-thick brass spacer using cyanoacrylate. The spacer was then attached to a gold-coated lead zirconate titanate piezoelectric transducer (PZT-880, American Piezo Ceramics, Inc., Mackeyville, PA) using double-sided Kapton® tape. Double-sided tape was also used to adhere the opposite side of the spacer to the micromachined 25-mm x 25-mm x 500-μm silicon wafer containing the array of 400 pyramidally-shaped cavities each capped with a 5-μm orifice at the apex. A thin layer of epoxy was applied to the edges of the device and allowed to cure for 24 hours producing a water-tight seal around the entire device.

This assembly protocol allowed for the execution of preliminary proof-of-principle experiments but was not amenable to mass spectrometric analysis due to need to fully disassemble and decontaminate the prototype device when switching sample solutions. Use of this assembly protocol was further hindered by dissolution of the epoxy when using samples incorporating some organic solvent and difficulty in preventing leaks, which tended to trip the DC power supply due to shorts in the electrical circuit.

To circumvent these issues, the assembly protocol was modified by Thomas P. Forbes, a collaborator working in the research groups of Drs. F. Levent Degertekin and Andrei G. Fedorov in the George W. Woodruff School of Mechanical Engineering at the Georgia Institute of Technology (personal communication). The current AMUSE assembly incorporates the ability to rapidly assemble and disassemble the device and is shown in Figure 2.8.

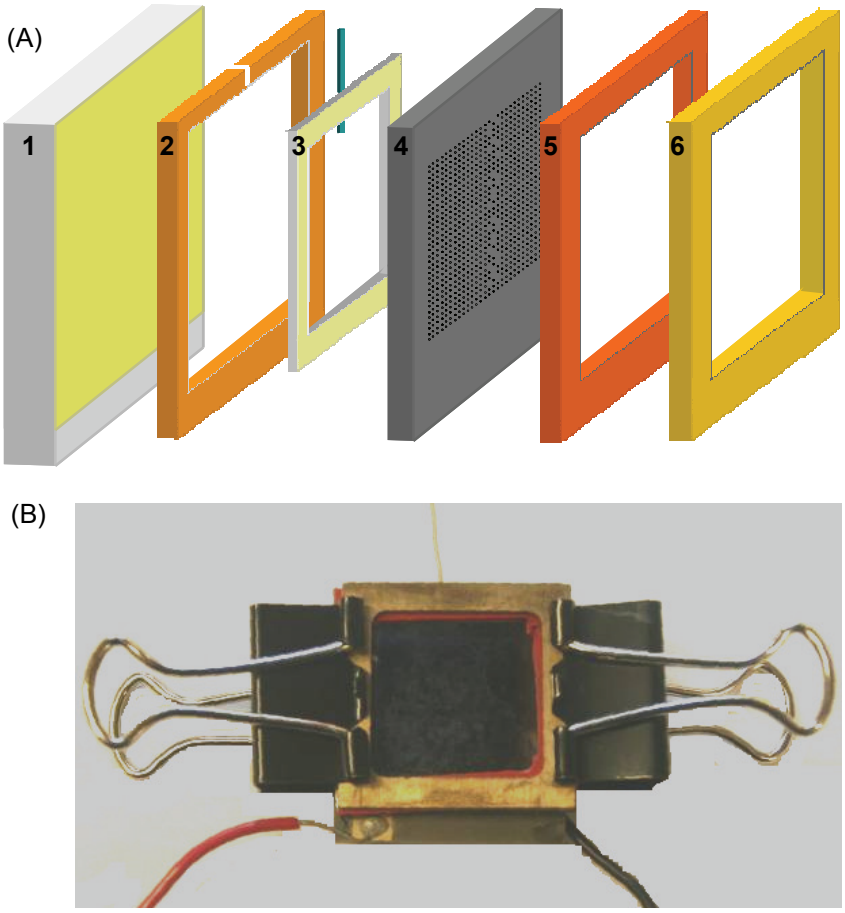

Figure 2.8. (A) AMUSE assembly components including (1) piezo, (2) Kapton® spacer, (3) silicone insert with PEEK sample inlet tube, (4) silicon array, (5) silicone spacer, and (6) brass spacer. (B) Image of intact device assembled using protocol 2.

This assembly consists of six components compressed together using spring-loaded clips. To assemble the device, a 2-mm thick gold-coated piezoelectric transducer (1) is topped by a 730-µm thick spacer made of double-sided Kapton® tape (2) and containing a 790-µm thick silicone insert (McMaster-Carr, Atlanta, GA) (3). This spacer is used to define the thickness of the 105-µL analyte reservoir. One edge of the silicone insert is pierced by a 3-cm long piece of 255-µm i.d. 510-µm o.d. poly-ether-ether-ketone (PEEK) tubing (Upchurch Scientific, Oak Harbor, WA) that is connected to the external sample flow circuit via a 1-mm slit cut into one side of the Kapton® spacer. The 24x24-

mm micromachined nozzle array (4) containing 400 pyramidally-shaped 125-nL cavities each capped with a 3- or 5-μm diameter nozzle, is then placed on top of the spacer/insert assembly sealing the reservoir. A second silicone spacer (5) is placed on top of the nozzle array to protect it from accidental damage during the sealing process and is topped with a 1-mm thick brass seal (McMaster-Carr, Atlanta, GA) (6) that provides a rigid surface for compression by a pair of spring-loaded clamps.

2.3.3. AMUSE Setup and Operation

Operation of the AMUSE required an electrical lead to be soldered to the electrode on each side of the piezoelectric transducer. In initial experiments (Fig. 2.9.A). The lead wire soldered to the interior electrode was directly connected to the active lead of a DC power supply (Stanford Research Systems Inc., Sunnyvale, CA) while the lead wire soldered to the exterior electrode was connected to an RF amplifier (ENI 350L, Electronic Navigations Industries, Rochester, NY) which amplified a 980 MHz sine wave generated by an external function generator (DS345, Stanford Research Systems, Inc., Sunnyvale, CA). The ground wires from each of these power sources were connected to a common ground. Sample was introduced into the reservoir by connecting the PEEK tube protruding from the assembled device to a 10-mL syringe via a Luer tip. In this configuration the AMUSE is self-pumping, therefore, no attempt was made to control the sample flow rate in these early experiments and gravity was used to ensure that the sample reservoir was replenished.

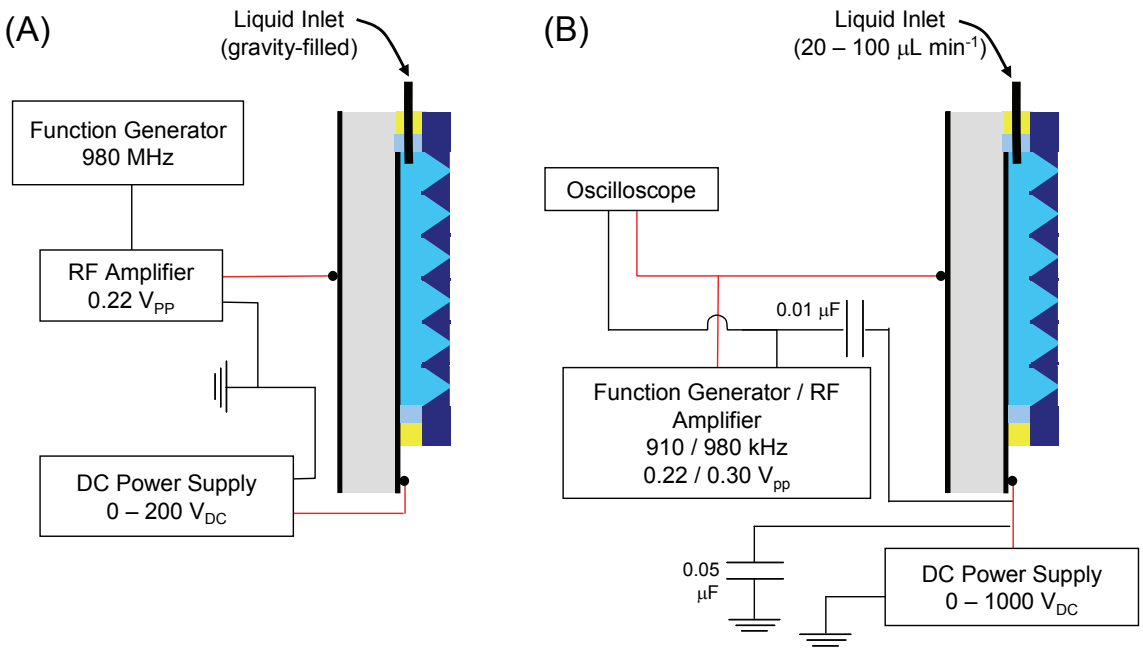

Figure 2.9. Electrical circuit used for (A) initial and (B) current AMUSE experiments (connections shown correlate to operation in DC-AMUSE mode).

To determine the detection limits of this system, it became necessary to mechanically pump solution into the device which was accomplished by connecting the protruding PEEK tube to a piece of 508-µm i.d. PEEK tubing (Upchurch Scientific, Oak Harbor, WA), which was attached to a liquid handling pump (Valco Instruments Co., VICI M6, Houston, TX.). The optimal flow rate for each array was determined by balancing the solution and ejection flow rates. This was accomplished by pumping solution into the AMUSE reservoir using a low flow rate (20 µL min^{-1}) until solution emerged from the nozzles, indicating that the AMUSE reservoir was full, and then turning on the RF amplifier to allow ejection. After 1 minute, the amplifier was turned off and the time required to refill the reservoir was recorded. The solution flow rate was increased by 10 µL min^{-1} and the process repeated until the refill time was less than 5 seconds, the approximate refill time when using the self-pumping setup.

During initial experiments, it was observed that droplet ejection using the AMUSE was enhanced by directly connecting the RF ground wire to the interior lead wire (Fig. 2.9.A). However, this caused cross-talk between the DC power supply and RF amplifier resulting in tripping of the DC power supply and damage to the RF amplifier. The RF amplifier was replaced by a unit that incorporated a function generator (T&C Power Conversion Inc., Rochester, NY) and cross-talk between this unit and the DC power supply was overcome by the inclusion of two capacitors into the electrical circuit as shown in Figure 2.9.B. An oscilloscope (Tektronix, Beaverton, OR) was also included to allow monitoring of the amplified RF signal.

Two AMUSE operating modes were explored. In DC-AMUSE operating mode, the electrical circuit shown in Figure 2.9.B is used and in addition to the RF signal, a DC potential $\leq$ 1000 V_{DC} is applied to the inner electrode. Under the operating conditions used in this study, droplets approximately have an average diameter that is 1–2 μm larger than the orifice diameter.[132] In RF-only AMUSE operating mode (Fig. 2.10), the connection between the exterior piezo electrode and the DC power supply was removed. Instead, the ground lead of the RF amplifier was directly connected to the interior piezo electrode and the only potential applied to the AMUSE is the RF potential which is in the frequency range of 900 kHz – 1 MHz with 0.220 – 0.300 V_{PP} amplitude.

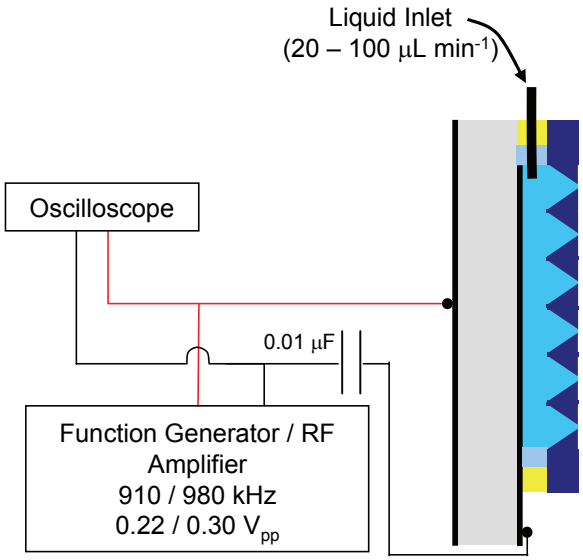

Figure 2.10. Electrical circuit used for RF-only AMUSE experiments.

Prior to mass spectrometric experiments, the AMUSE was placed approximately 2 mm from the inlet of a stainless steel Venturi device (HMC Brauer Co., Milton Keynes, England) operated with N_2 at rates of 0 – 17 L min^{-1}. The N_2 flow rate was controlled using a differential pressure flowmeter (Bel-Art, Pequannock, NJ). The N_2 gas was used at room temperature except for experiments with proteins, where the N_2 was heated using an inline air circulation heater (Omega, Stamford, CT) and a temperature controller (Eppendorf, Hamburg, Germany).

2.3.4. MS Experimental Setup

Initial experiments with 5-μm AMUSE devices were performed with a linear ion trap (LiT) mass spectrometer (LTQ, ThermoFinnigan, Waltham, MA). Access and training on the use of this instrument was provided by Dr. Charlene Bayer and Dr. Victor de Jesus in the Georgia Tech Research Institute. These experiments, which were carried

out in 2005, provided the framework for subsequent experiments using 3-μm devices performed with a quadrupole ion trap (QiT) mass spectrometer (LCQ Deca XP+, ThermoFinnigan, Waltham, MA) acquired by our group in early 2006. In both cases, the standard electrospray ion source was removed, and the Venturi device was positioned directly in front of the heated capillary inlet of the mass spectrometer as shown in Figure 2.11.

For LiT experiments, the following mass spectrometer settings were used: 13 – 34 V_{DC} inlet capillary voltage, 275 ºC capillary temperature, 100 – 200 ms trapping time. For QiT experiments, the following settings were used: 8 – 23 V_{DC} inlet capillary voltage, 300 ºC capillary temperature, 100 ms trapping time. Settings were optimized for the respective protonated molecules using the auto tune function of the mass spectrometer. Prior to mass spectrometric analysis, the liquid reservoir of the AMUSE device was primed with the sample to be analyzed, and after stable liquid ejection was visually verified, gas was supplied to the Venturi device and mass spectral data was acquired in positive ion mode. Conventional pESI and nESI experiments were performed on the QiT with the standard commercial ion sources provided by the mass spectrometer manufacturer (ThermoFinnigan, Waltham, MA), at a flow rate of 10 μL min^{-1} and 4.5 kV_{DC} for pESI, and 0.8 μL min^{-1}, and 2.5 kV_{DC} for nESI. Nanospray emitter tips (30-μm i.d.) were obtained from New Objective (Woburn, MA).

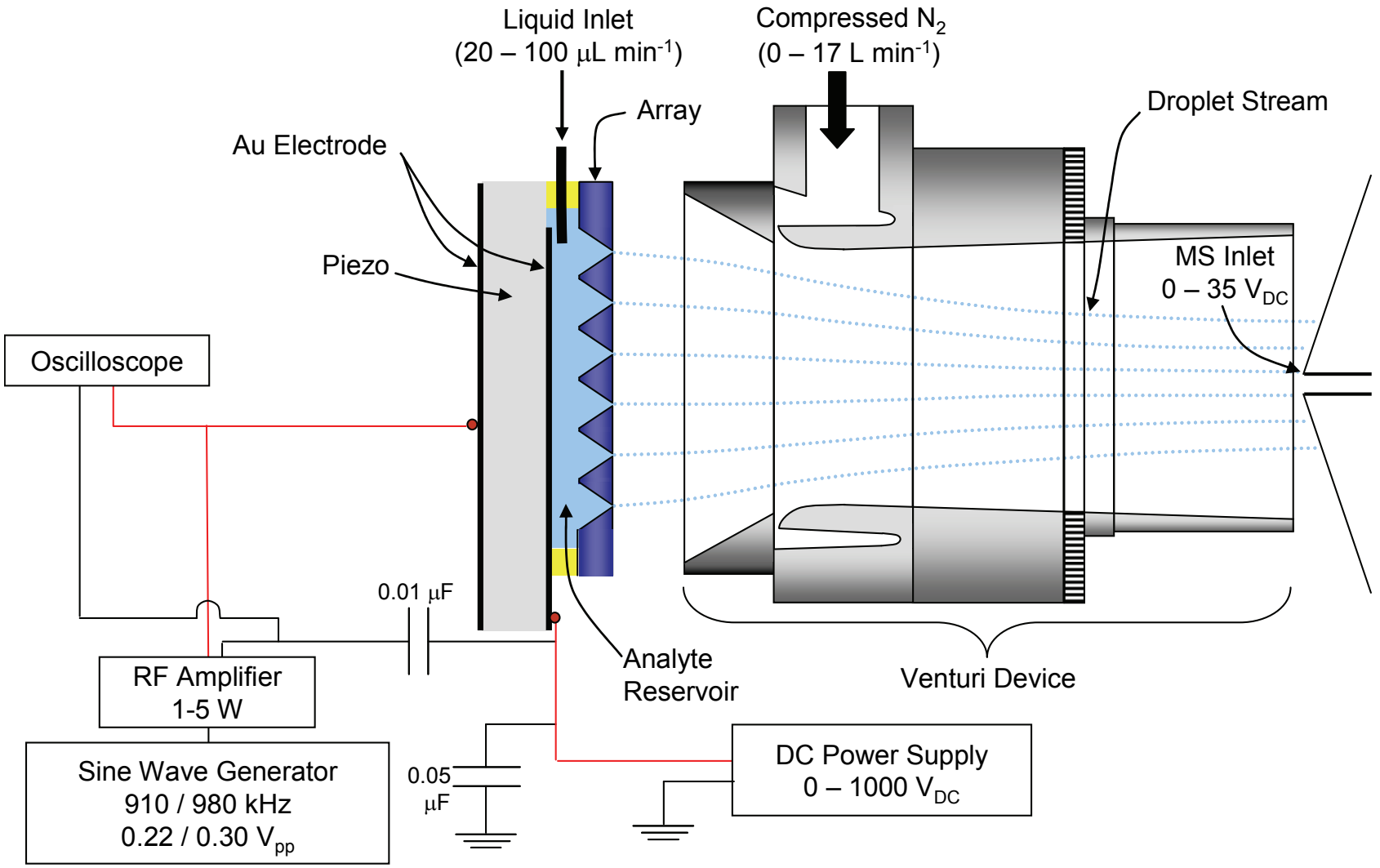

Figure 2.11. Schematic of Venturi-assisted AMUSE-MS setup.

2.4. Effect of Venturi Device on Signal Intensity and Stability

Visualization studies performed by Meacham, et al. showed that droplet ejection from the AMUSE produces droplets with velocities in the 10 – 20 m s^{-1} range which decelerate rapidly due to Stokes drag.[131, 132] In terms of coupling this device to a mass spectrometer, this behavior translated into unstable focusing of the AMUSE-generated droplets on the mass spectrometer inlet. Zhou, et al. reported that the incorporation of a non-biased Venturi device can lead to a 5-fold increase in the $[M+H]^+$ ion intensity of electrosprayed reserpine relative to signal obtained without the Venturi device, due to improved focusing of the highly-charged diverging nanodroplet cloud formed during ESI.[210] Therefore, we speculated that the coupling of such a device to the AMUSE would provide the necessary droplet stream stabilization, focusing and desolvation to achieve more stable ionization of polar biomolecules.

Figure 2.12 shows the mass spectra obtained for a reserpine solution ionized by the application of 100 V_{DC} charging potential to a 5-μm AMUSE device with and without Venturi-assisted droplet desolvation. Reserpine was chosen as it is easily ionized and because it serves as a sensitive standard compound used by most instrument manufacturers.

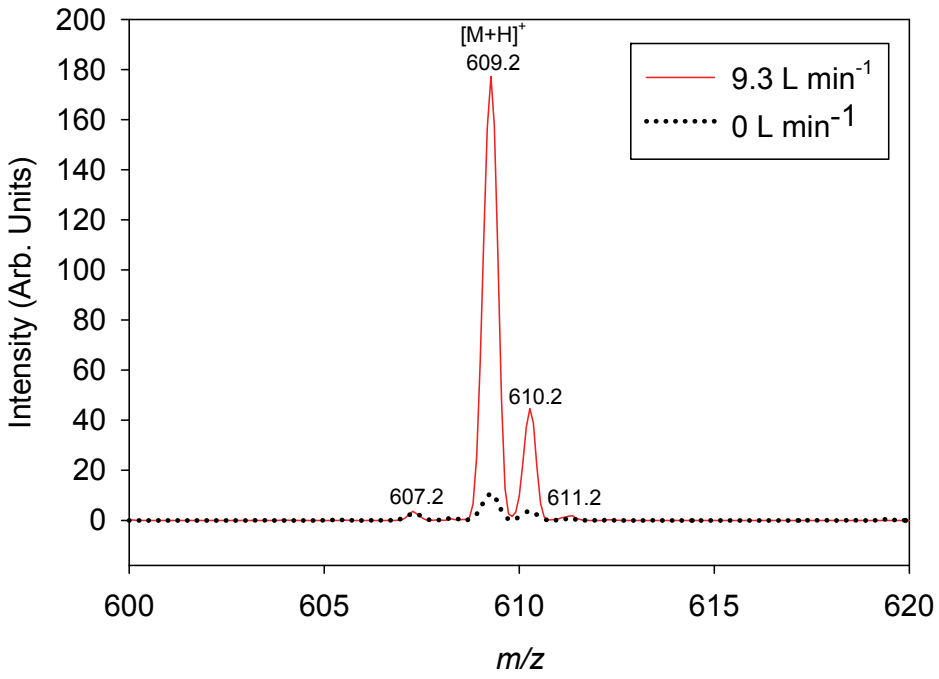

Figure 2.12. Mass spectra for 4 pmols reserpine nozzle^{-1} ionized by a 1st generation AMUSE array (5-μm apertures), with (9.3 L min^{-1}) or without (0 L min^{-1}) Venturi-assisted droplet desolvation and focusing. The solvent used in both cases was 10:89.9:0.1 (v:v:v) methanol:water:glacial acetic acid. AMUSE settings: 100 V_{DC}, 40 μL min^{-1} liquid flow rate, LiT detection.

As can be seen in the figure, the signal intensity of the protonated molecule (*m/z* = 609.2) obtained using the Venturi device was increased 10-fold with respect to that obtained without it. A similar gain in signal-to-noise (S/N) ratio was observed. This gain is a result of both the improved stabilization and transmission of the ejected droplet stream into the heated capillary inlet, and of the aforementioned desolvation effect afforded by the Venturi device.

The greater sensitivity gain obtained here (10x) compared to that reported by Zhou, et al. in the absence of a potential applied to the Venturi device (5x), can most likely be attributed to the improved sampling of the multiple droplet streams when the AMUSE is used in the Venturi mode. Figure 2.13 shows the total ion trace obtained for

the reserpine mass spectrum obtained when the gas flow to the Venturi device is shut off (Fig. 2.13.A) and when the device is operated at a flow rate of 9.3 L min^{-1} (Fig. 2.13.B). As can be seen in Figure 2.13.A, unstable droplet collection when there is no Venturi assistance causes the signal to oscillate precipitously throughout the analysis, leading to a large instability in the detected signal (% relative standard deviation (RSD) = 202%). Incorporation of a Venturi device increased the overall stability of the source to 47% RSD, but sensitivity was still lower than expected, most likely due to the relatively large initial droplet diameter produced by the 5-μm nozzle array.

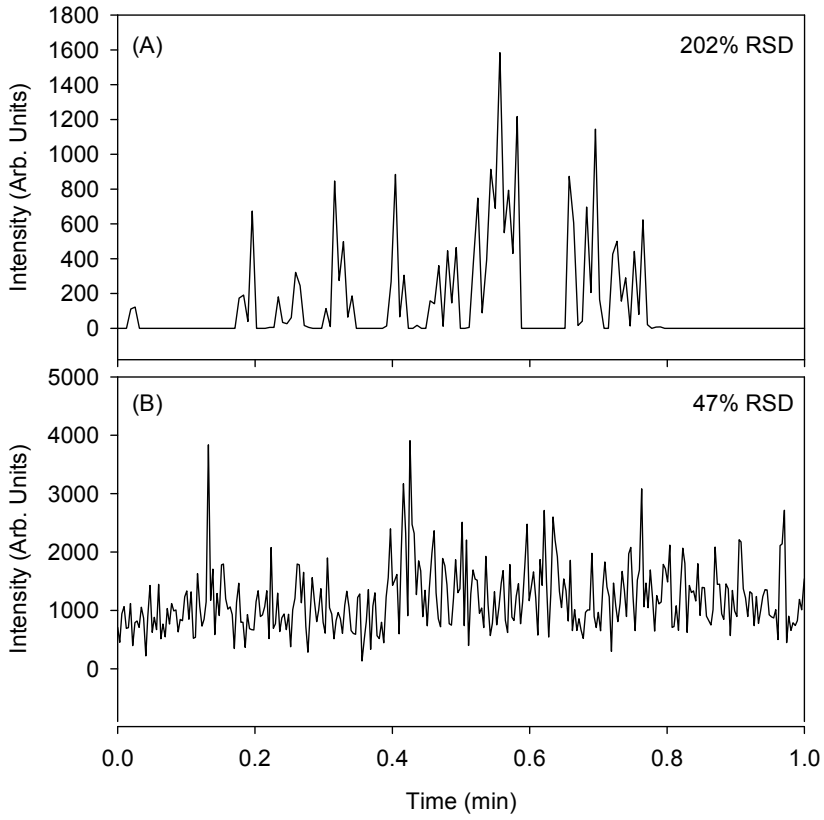

Figure 2.13. Total ion trace for 4 pmols reserpine $nozzle^{-1}$ ionized by a 1st generation AMUSE array (5-μm apertures) with no N_2 flowing through the Venturi device (A) and with 9.3 L min^{-1} N_2 flowing through the Venturi device (B). The solvent used was 10:89.9:0.1 (v:v:v) methanol:water:acetic acid. Operating conditions: 100 V_{DC}, 40 μL min^{-1} liquid flow rate, LiT detection.

2.5. Comparison of 1st and 2nd Generation Arrays

As demonstrated by the higher sensitivity afforded by nESI and μESI relative to that of ESI, droplet size has a significant impact on the quality of mass spectra obtained. To that end, experiments were performed to compare the absolute signal intensity and S/N ratio observed for the analysis of reserpine and YGGFL solutions prepared using nanopure water with 0.1% acetic acid using a 1st generation array having 5-μm apertures (6-7 μm diameter droplets) and a 2nd generation array having 3-μm apertures (4-5 μm diameter droplets).[132] The droplet ejection and Venturi focusing conditions were optimized for each device type. An applied DC potential of 100 V_{DC} was used in all cases, which represents a 20- to 45-fold decrease in charging voltage if compared to traditional electrospray operation. The results of these studies are shown in Figure 2.14.

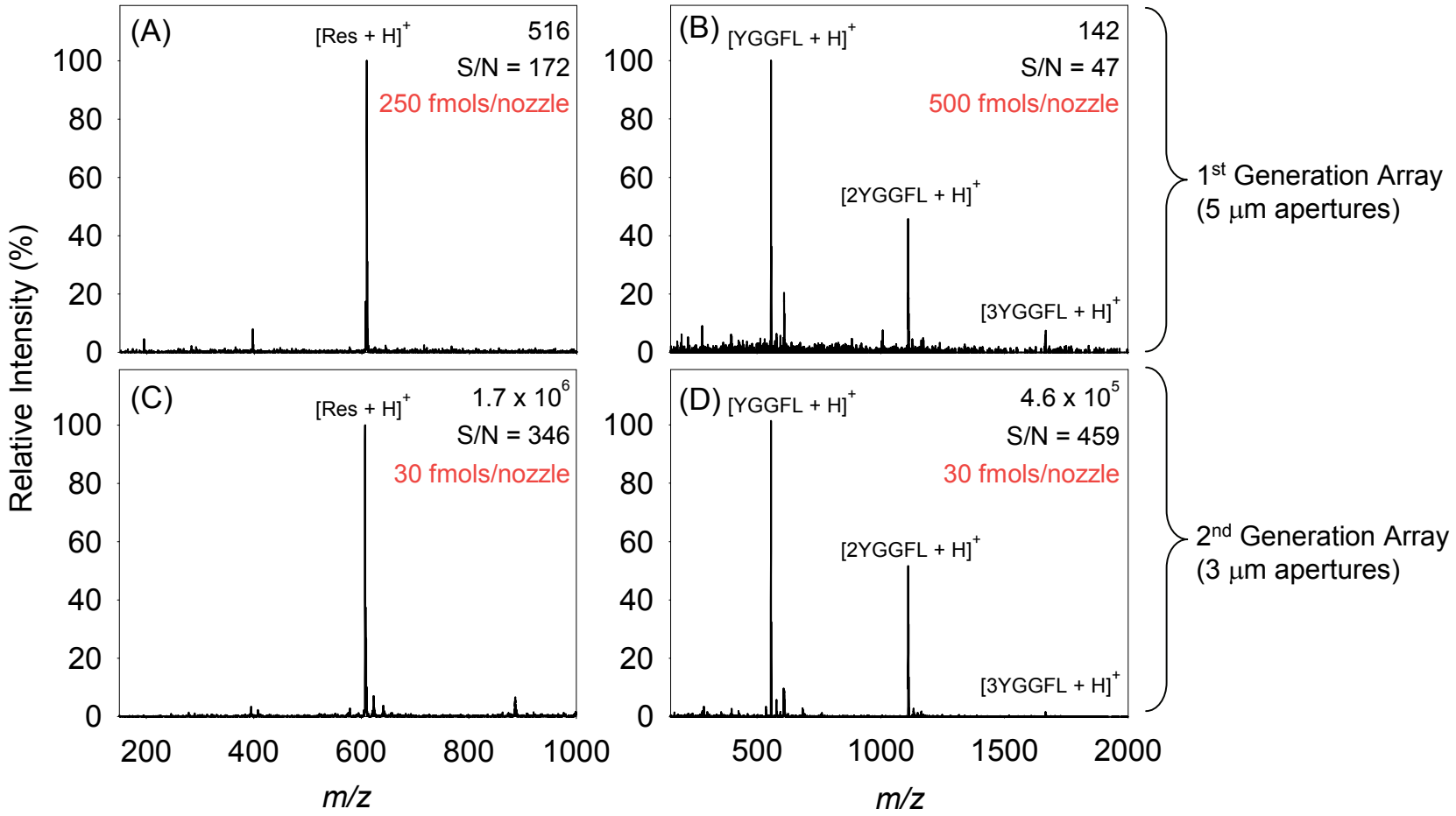

Figure 2.14. AMUSE mass spectra produced by averaging 1.2 sec of data obtained using a 1st generation array (5-μm apertures) for (A) 5 μM reserpine and (B) 10 μM YGGFL or a 2nd generation array (3-μm apertures) for (C) 5 μM reserpine and (D) 5 μM YGGFL. Operating conditions: (A-B): 100 V_{DC}, 100 μL min^{-1} liquid flow rate, 7.5 L min^{-1} N_2; (C-D): 100 $_{VDC}$, 30 μL min^{-1} liquid flow rate, 9.3 L min^{-1} N_2. The absolute intensity of the base peak is given in the upper right corner of each panel.

The ion intensity of the $[M+H]^+$ peak of reserpine (*m/z* = 609.2) using the 3-μm device was more than 30,000 times greater than that of the 5-μm device, while the overall S/N ratio was increased from 172 for the 5-μm device to 345 for the 3-μm device. Improvements were also observed for the ionization of YGGFL, where the absolute signal gain was greater than 3,000, while the S/N ratio showed a 10-fold increase. When examining these improvements, it must also be considered that LiT MS detection was used to measure ions produced by the 5-μm device while QiT MS detection was used to measure ions produced by the 3-μm devices. As LiT detection is more sensitive than QiT detection due to a larger ion trapping capacity, these results suggest that had the experiments using the 3-μm device been performed on the LiT, the improvement in response could have been even greater.

One interesting observation arising from inspection of the AMUSE mass spectra of YGGFL is the relatively abundant peaks of the dimer ($[2M+H]^+$; *m/z* = 1111.1) and trimer ($[3M+H]^+$; *m/z* = 1666.1) ion species (Fig. 2.14 B and D). These peaks are generally not observed in pESI mass spectra (Fig. 2.15), therefore, their presence in mass spectra obtained using AMUSE ionization suggests that the ionization processes in AMUSE may differ from those of ESI.

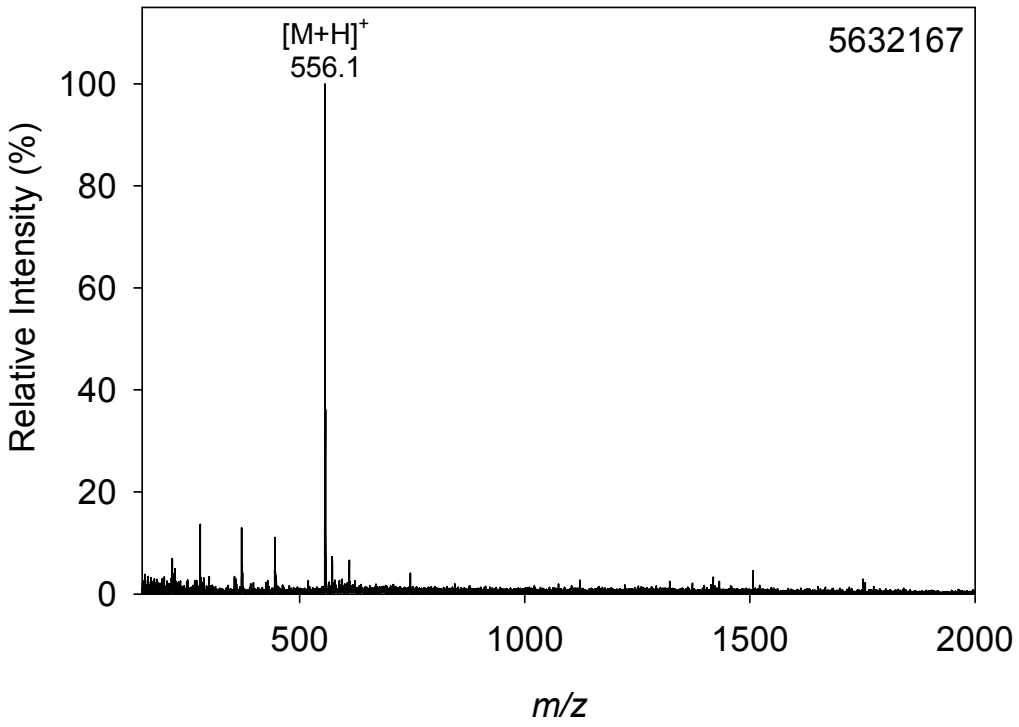

Figure 2.15. Mass spectra for a 1 μM YGGFL solution prepared in 99.9:0.1 (v:v) water:acetic acid obtained using pESI (10 pmol; 10 μL min^{-1}, 4500 V_{DC}, OiT detection.)

In the AMUSE, droplets production does not rely on Taylor cone electrohydrodynamic instability and vigorous Coulombic explosions as is typical in ESI. The lower DC potential applied to the droplets produced by the AMUSE is still capable of inducing droplet charging by electrophoretic charge separation or electrochemical reactions. This fundamentally different ionization mechanism possibly favors ion formation by evaporation of solvent from the charged droplets rather than ion evaporation, thus, favoring the stabilization of non-covalent interactions and possibly producing softer ionization than ESI. This suggests that AMUSE ionization may find applicability for the ionization of labile species such as non-covalent protein complexes.

Because individual liquid ejection from each cavity is not yet implemented in the prototype devices evaluated here, it is not possible to estimate the number of droplet streams being sampled by the inlet capillary. Thus, detection limits can only be estimated, but not accurately calculated, until development of a fully multiplexed AMUSE device, which enables ejection from a single nozzle, is accomplished. The amount of reserpine giving rise to the mass spectrum in Fig. 2.14.A (5-μm nozzle array) was 10 picomoles. Extrapolation of this signal, which gave S/N = 172, to signal having S/N = 3 corresponds to a theoretical detection limit of 174 femtomoles reserpine. For the reserpine signal detected from a 3-mm nozzle array, the theoretical detection limit was 26.1 attomoles reserpine. These theoretical limits of detection are on the same order as those for other common spray-based ionization techniques such as ESI,[31] pESI,[51] UA-ESI,[70] and nESI,[218] which are typically in the low femtomole – attomole range for common protein and drug standards. Calculation of the amount of analyte ejected per nozzle required that the number of ejecting nozzles be visually estimated. It was observed that the average number of nozzles ejecting at a given time was typically 10% for the 5-μm arrays and 25% for 3-μm arrays. This corresponds to a theoretical detection limit of 4.4 femtomoles reserpine/nozzle for the 5-μm devices and 0.26 attomoles reserpine/nozzle for 3-μm devices.

The Venturi device N_2 flow rate was found to have a marked effect on the intensity of the $[M+H]^+$ (*m/z* = 556.1) YGGFL ion. The results shown in Figure 2.16 suggest that the optimum flow rate of N_2 to the inlet of the Venturi device is between 7 – 10 L min^{-1} which is amplified 10-fold at the outlet, according to the manufacturer's specifications.[219]

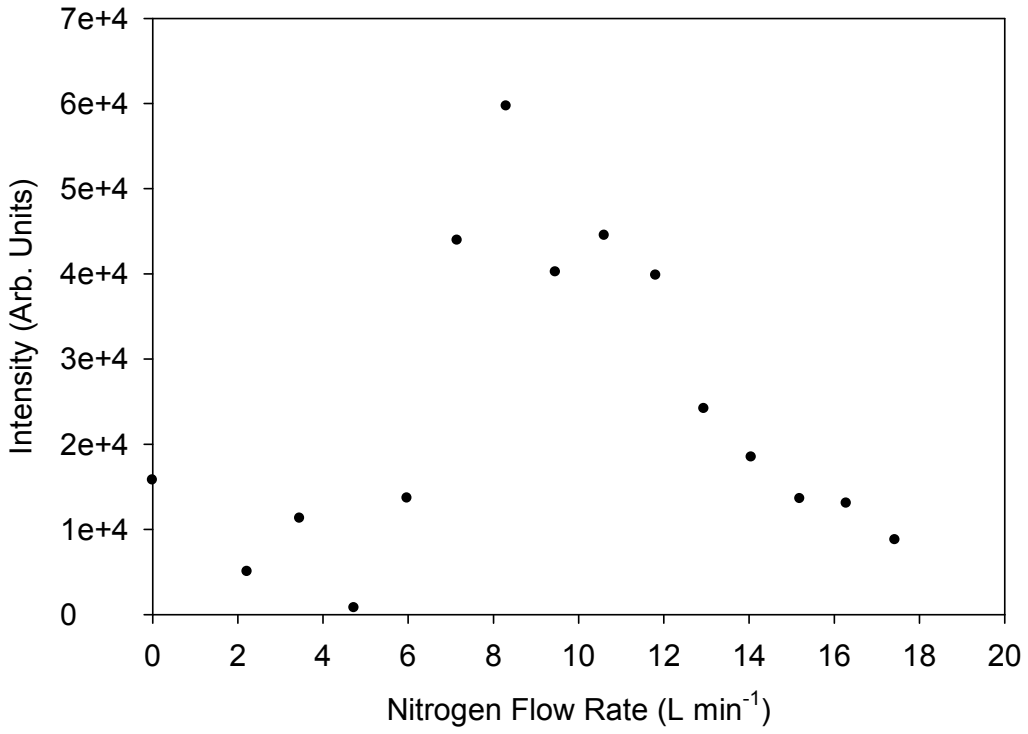

Figure 2.16. Intensity of $[M+H]^+$ ion of YGGFL vs. Venturi device N_2 flow rate for a 1 μM solution in 99.9:0.1 (v:v) water:acetic acid using an array with 3-μm nozzles. Operating conditions: 100 V_{DC}, 35 μL min^{-1} liquid flow rate, QiT detection.

The use of 3-μm arrays in combination with the Venturi device not only increased sensitivity, but also increased the stability of the ion signal, as seen in Figure 2.17, which shows the total and extracted ion traces for the ionization of a 5 μM solution of YGGFL. The 3-μm devices were shown to be stable (8.5% RSD) for up to 30 minutes at the liquid flow rates assayed here. Using these optimized conditions, the effect of changing the bias voltage used for droplet charging during ionization was explored.

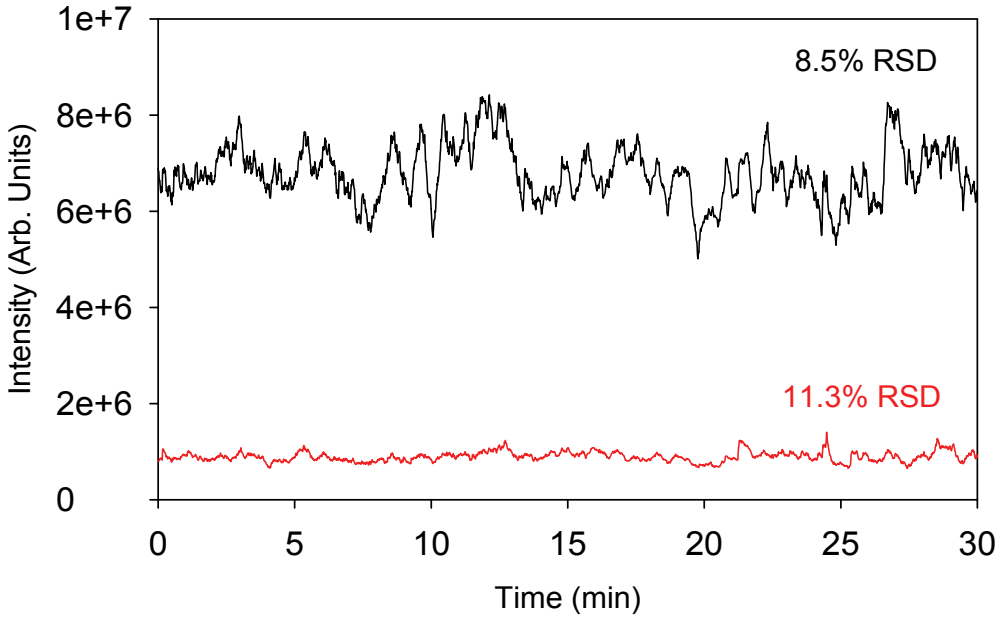

Figure 2.17. Total ion trace (black) and extracted ion trace for $[M+H]^+$ = 556.1 (red) for the continuous ejection of 5 μM YGGFL using a 3 μM AMUSE array. Operating conditions: 100 V_{DC}, 30 μL min^{-1} liquid flow rate, 4.0 L min^{-1} N_2, QiT detection.

2.6. Effect of Varying the Applied DC Potential

Despite the use of the word "electrospray" in the AMUSE acronym to provide familiarity, ionization by the AMUSE is accomplished in a different manner than in conventional electrospray due to decoupling of droplet formation and charging. The decoupling of these two processes enables the stable ionization of peptides and small molecules dissolved in acidified aqueous solutions at potentials of a few hundred volts. This results in safer operation of the ion source and enables placement of the AMUSE assembly in close proximity to the Venturi device inlet without generating electrical discharges, which provides improved droplet suction into the device and better focusing.

To further explore the dependence of AMUSE ion generation on the applied DC charging potential, a series of spectra were collected for the analysis of a 1 μM YGGFL

solution at different DC bias voltages. Figure 2.18 shows the intensity of the protonated molecule of YGGFL (A) as well as the corresponding S/N ratio (B) as a function of the applied DC potential.

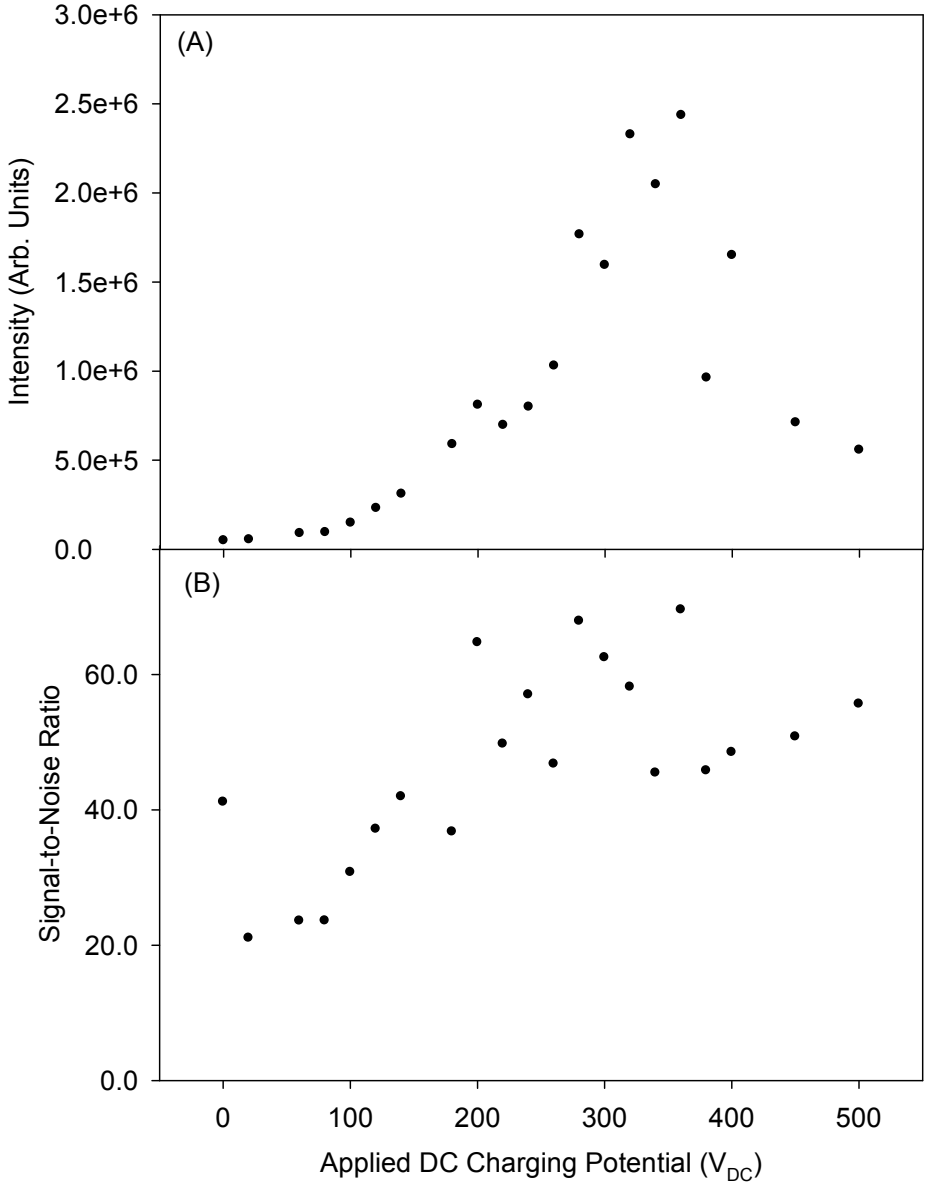

Figure 2.18. (A) Absolute intensity and (B) S/N for the YGGFL $[M+H]^+$ ion vs. DC charging potential for a 1 μM solution using an AMUSE array with 3-μm nozzles. Operating conditions: 40 μL min^{-1} liquid flow rate, 7.2 L min^{-1}, QiT detection.

As can be seen in this figure, it is possible to obtain ionization using a range of potentials, or even without any DC potential at all (RF-only AMUSE mode). The absolute intensity appears to be at a maximum at approximately 350 V_{DC} while the corresponding S/N ratio appears to increase throughout the entire range of applied DC potentials, with a local maximum at 280 V_{DC}. Although Fig. 2.18.A shows that signal intensity for RF-only AMUSE is low compared to that obtained using a DC charging potential, RF-only AMUSE provides higher S/N due to a simultaneous reduction in baseline noise as discussed in detail in section 3.9. For charging voltages of 350 V_{DC} and higher, significant liquid buildup on the device surface was observed, which hindered droplet ejection from some nozzles or nozzle clusters. This phenomenon was accompanied by a concomitant reduction in signal intensity. One possible explanation to this phenomenon is that the negatively-charged hydroxyl group on the tungsten oxide array surface may attract the positively-charged liquid meniscus produced at the onset of the droplet ejection event.[220] Higher potentials cause higher surface droplet charging, and thus could favor wetting of the tungsten surface. Covalent chemical modification of the array surface via silane chemistry to minimize this effect is currently being investigated and is described in Chapter 4.

Devices with smaller nozzle orifice diameter appeared to produce the most stable signal with no DC potential applied at all. Figure 2.19 shows the mass spectrum and total ion trace obtained for a 1 μM YGGFL solution when the AMUSE was operated in RF-only mode. The S/N ratio of the $[M+H]^+$ peak obtained using this mode was 41, while the total ion trace showed a 2.6% RSD over the course of one minute. In this ionization mode, the RF voltage signal induces periodic charging on the electrode facing the analyte

solution. With amplification, the amplitude of the RF signal needed for ejection approaches 50 – 150 V_{PP}, so the period-averaged positive potential seen by the sample is + (50 – 150) V_{PP} / (2π) = (8 – 24) V, sufficient for droplet charging, as observed from experiments with time-invariant DC potentials. In other words, we speculate that droplet charging still occurs even though the DC bias is not applied to the electrode. It must be noted, however, that this mode is less efficient, as the analyte "sees" the positive potential only half of the time, thus leading to the lower S/N ratio observed.

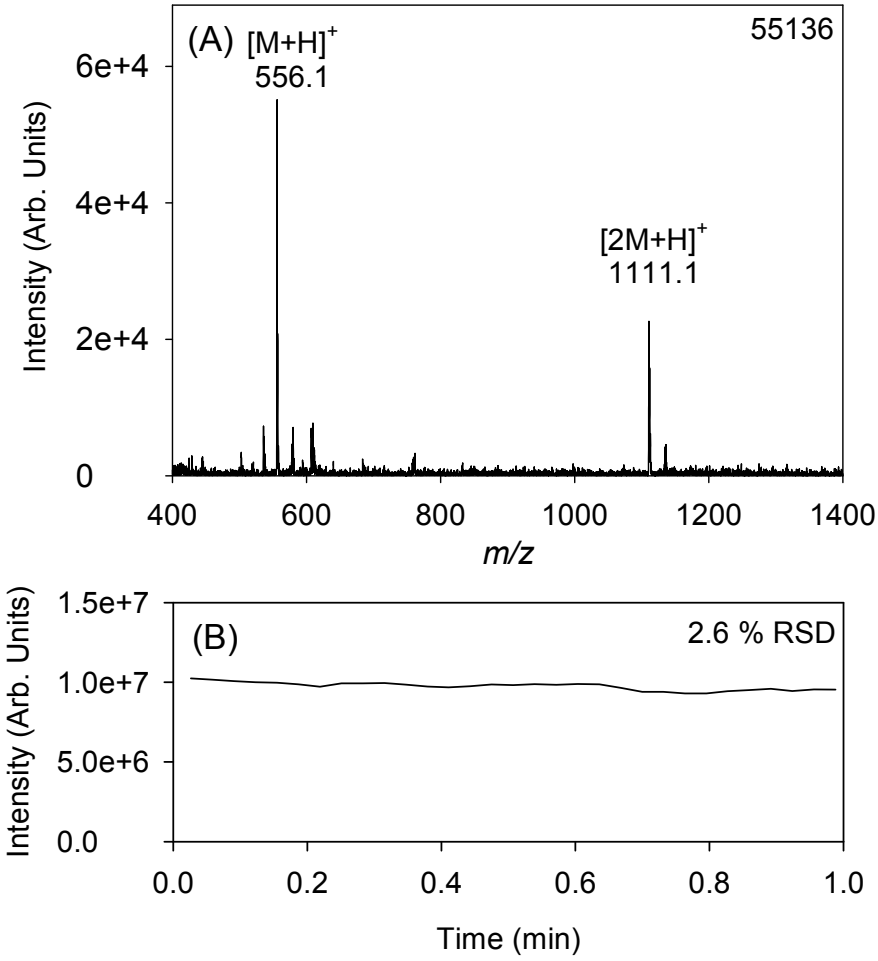

Figure 2.19. Mass spectrum (A) and total ion trace (B) obtained for 1 μM YGGFL in RF-only AMUSE mode using an array with 3-μm nozzles. Operating conditions: 0 V_{DC}, 40 μL min^{-1} liquid flow rate, 7.2 L min^{-1} N_2, QiT detection.

2.7. AMUSE Ionization of Proteins

To further explore the usefulness of AMUSE as a viable ionization technique for biological MS, the feasibility of ionizing a model protein from aqueous media was investigated. Initial experiments with 4 μM cytochrome C in 0.1% acetic acid (pH 3.2) yielded spectra with low S/N ratio, as shown in Figure 2.20.A. This can most likely be attributed to incomplete protein ion desolvation, as proteins are more difficult to desolvate due to their larger number of hydrogen-bonding sites.

To improve desolvation, a heater was used to increase the temperature of the N_2 flowing through the Venturi device. Figure 2.20.B shows the spectrum obtained for the same solution and identical conditions to the spectrum in Figure 2.20A but with the addition of N_2 heated to 40 ˚C, as measured at the outlet of the Venturi device. The use of heated N_2 caused a slight narrowing of the charge state distribution generating a spectrum with an average charge state of 8.8, and a S/N ratio of 55 for the +8 charge state as compared to an average charge state of 10 and S/N ratio of 7 for the +11 charge state in the spectrum obtained using ambient temperature N_2.

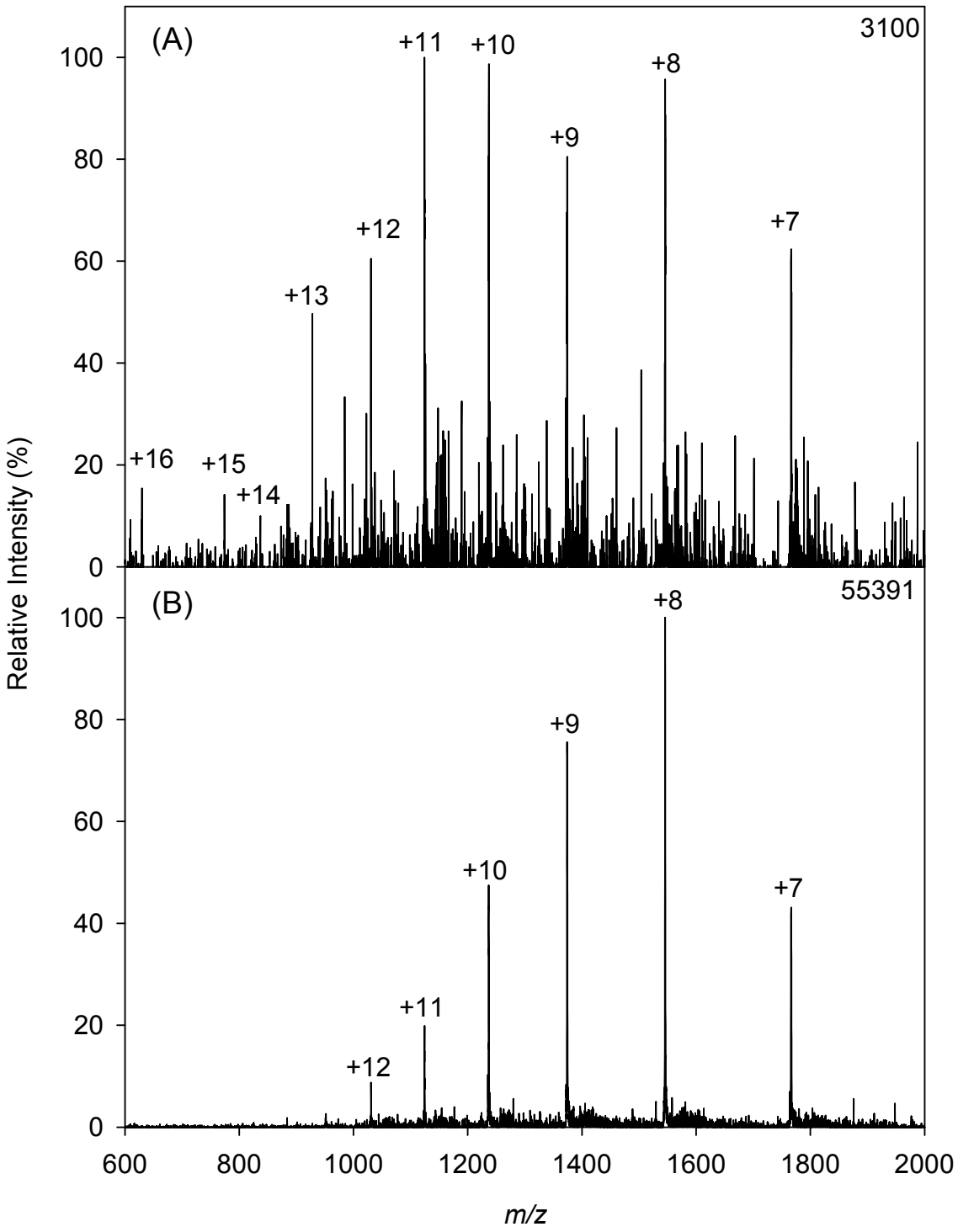

Figure 2.20. Mass spectra of cytochrome C (2.4 pmol nozzle^{-1}) obtained using an array with 3-μm apertures and flowing (A) room temperature N_2 or (B) 8 L min^{-1} N_2 heated to 40 ºC through the Venturi device. Operating conditions: 60 μL min^{-1} liquid flow rate, 100 V_{DC}, QiT detection

Additional experiments demonstrated that it was also possible to ionize cytochrome C in RF-only AMUSE mode, as shown in Figure 2.21. In this spectrum, the +8 charge state peak had an S/N ratio of 21 and the average charge state of the entire distribution was 8.9, which almost identical to the value obtained for the spectrum shown in Figure 2.20.B.

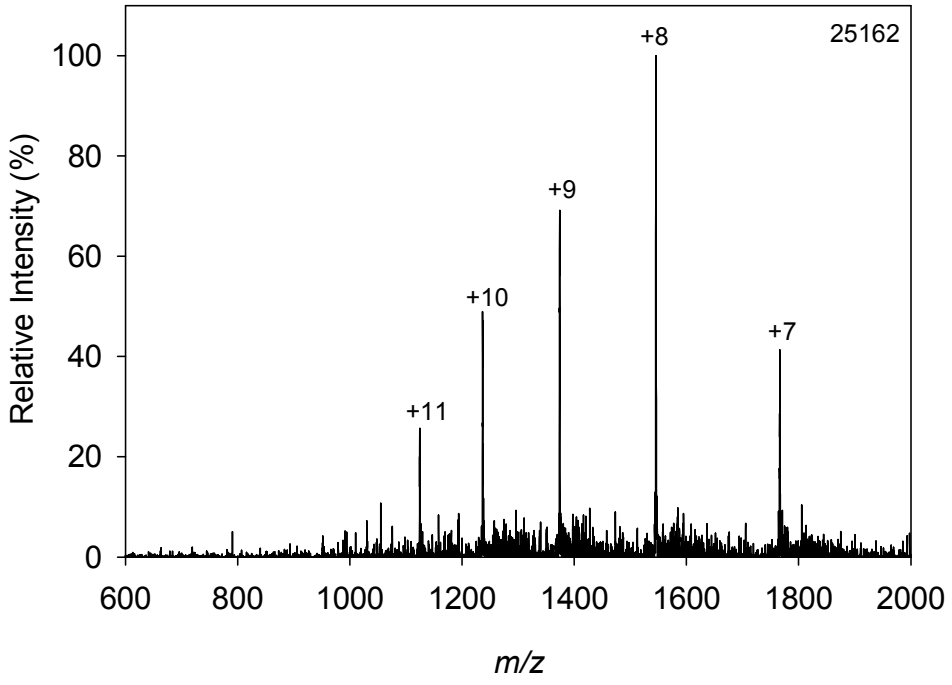

Figure 2.21. RF-only AMUSE mass spectrum of cytochrome C using an array with 3-μm apertures (240 pmol total). Operating conditions: 0 V_{DC}, 60 μL min^{-1} liquid flow rate, 8 L min^{-1} N_2 heated to 40 ºC, QiT detection.

Figure 2.22 shows the nESI mass spectrum obtained for the exact same solution previously ionized with the AMUSE. As can be seen in the figure, the charge state distribution in this case was quite narrow, yielding an average charge state of 9.24, which is higher than what was obtained using the AMUSE.

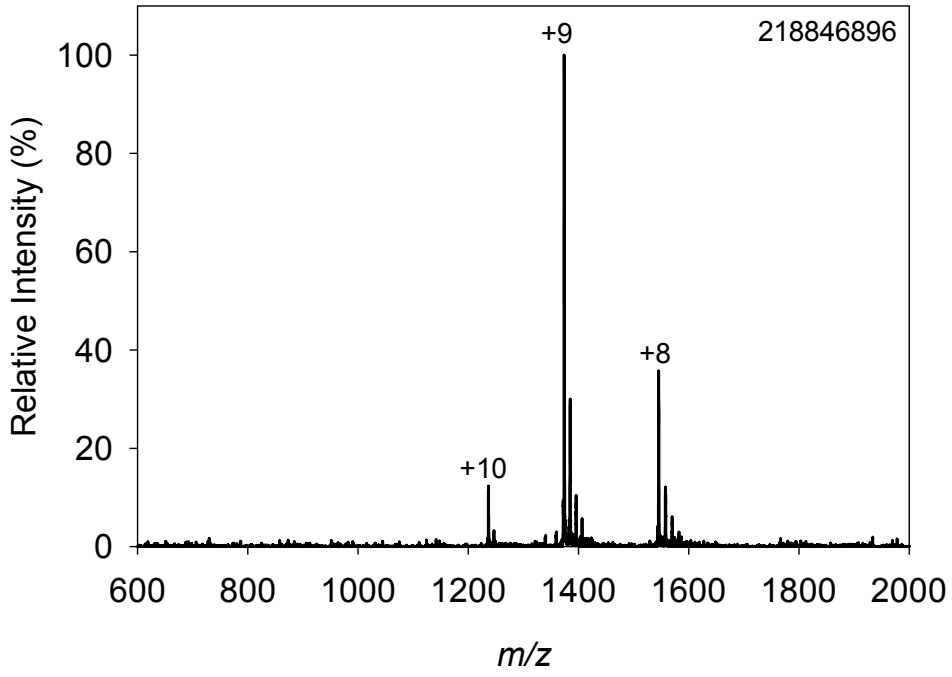

Figure 2.22. Mass spectrum of cytochrome C in 99.9:0.1 (v:v) water: acetic acid obtained with nESI (0.8 pmol, 0.8 μL min^{-1}, 2500 V_{DC}, QiT detection).

This charge state distribution is consistent with previous reports for cytochrome C solutions containing no organic solvent and at a pH higher than 3.[221] The slight decrease in the average charge state observed using the AMUSE relative to that using nESI could be attributed to the gentler ionization provided by the Venturi device as reported by Yang, et al.[168] This could also possibly be attributed to the AMUSE ionization process itself. By comparison, pESI (Fig. 2.23.A) and nESI (Fig. 2.23.B) using the more standard 1:1 methanol:water with 0.1% acetic acid solvent mixture (pH 4.0) and under the exact same instrumental conditions produced spectra having wide charge state distributions and an average charge state of 16.

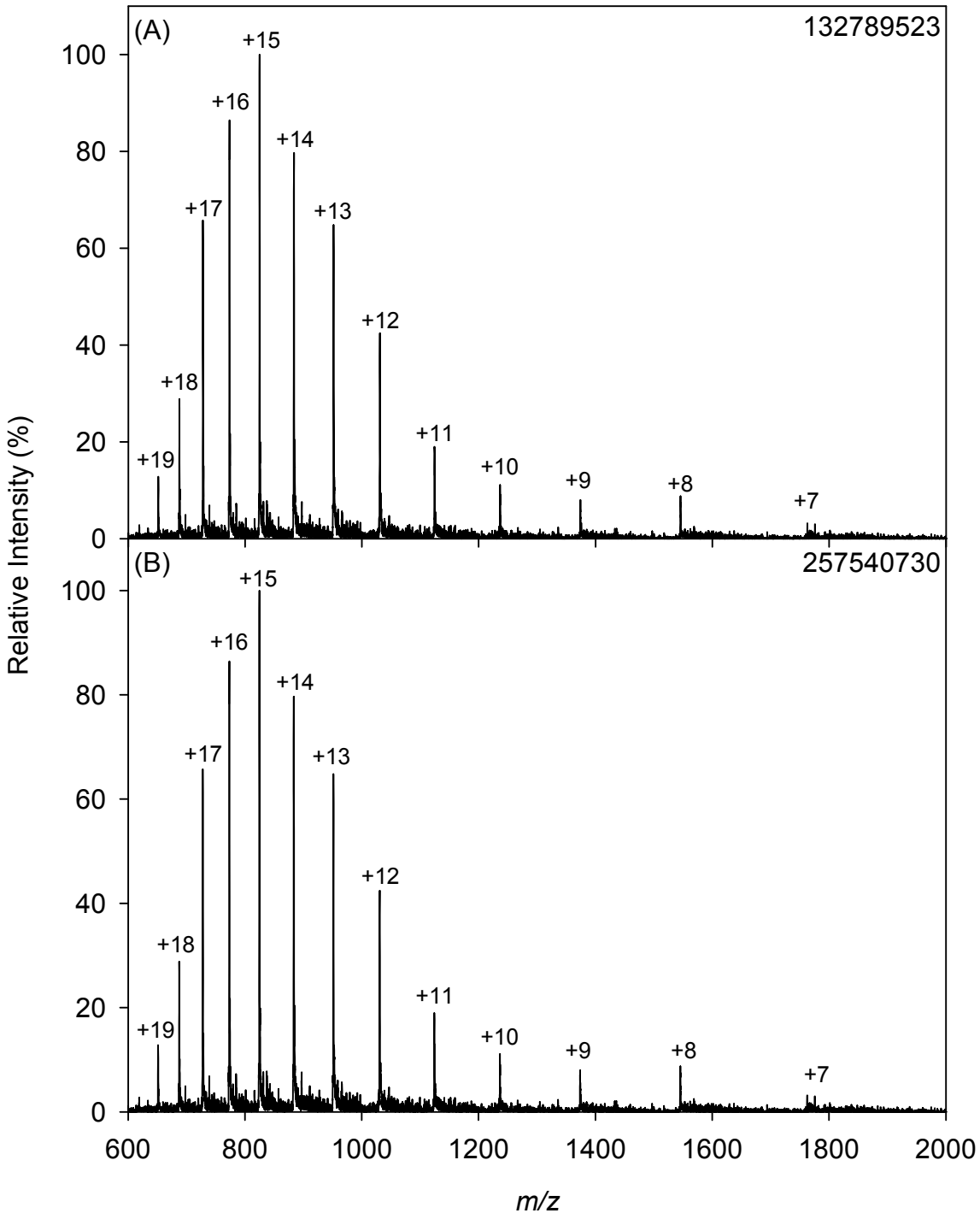

Figure 2.23. Mass spectra of cytochrome C in 50:49.9:0.1 (v:v:v) methanol:water:acetic acid obtained with (A) pESI (10 μL min^{-1}, 4500 V_{DC}, OiT detection) and (B) nESI (0.8 pmol, 0.8 μL min^{-1}, 2500 V_{DC}, QiT detection).

2.8. Conclusion

The results presented here are the first demonstration of the sensitive and stable ionization of proteins and peptides at femtomole levels per nozzle by using the Venturi-AMUSE ion source. This was possible without the addition of organic solvent into the analyte mixture and using very low, or no, applied charging potential, thus opening new avenues for the production of gas-phase ions for biological MS. The incorporation of the Venturi device provided a 10-fold gain in both the signal and S/N ratio for a reserpine spectrum obtained using a 5-μm array as well as a 4-fold reduction in the relative standard deviation of the corresponding total ion trace indicating an overall increase in sensitivity and stability as a result of the improved droplet desolvation and focusing efficiency of this setup.

Modifications to the fabrication protocol to generate 3-μm arrays led to an increase in sensitivity by at least 3 orders of magnitude and a 2- to 10-fold increase in the S/N ratio. The stability of the signal produced by the AMUSE was also much improved using the new arrays yielding a relative standard deviation of 11.3% in the intensity as measured over 30 minutes while that measured over 1 minute was generally 2-3%. The effectiveness of this device for the soft ionization of cytochrome C in aqueous media was also examined, yielding spectra with an average charge state of 8.8 when analyzed with a 100 VDC charging potential. Ionization of model proteins was also possible in RF-only AMUSE mode. The reduced average charge state for cytochrome C when interrogated by AMUSE provided further support for the need for experiments to investigate AMUSE ionization mechanisms which is described in the next chapter.

CHAPTER 3. INTERNAL ENERGY DEPOSITION OF VENTURI-ASSISTED ESI AND AMUSE

3.1. Abstract

A detailed comparison of the internal energy (IE) deposition of Venturi-assisted AMUSE, with and without the application of a DC charging potential, and Venturi-assisted ESI using the "survival yield" (SY) method on a series of para-substituted benzylpyridinium salts is presented in this chapter. An explanation of the importance of ion energetics in MS is provided followed by a tutorial explanation of the SY method for measuring the mean internal energy (<E>) of a given ion population. Under conditions previously shown to provide maximum ion yields for standard compounds when analyzed by either Venturi-assisted AMUSE or Venturi-assisted ESI, the observed <E> between these two techniques were nearly identical (1.93 – 2.01 eV). AMUSE operation without N_2 flow to sustain the Venturi focusing effect generated energetically-colder ions with <E> that were up to 39% lower than those for ESI. This suggested that a balance between improved ion transfer, adequate desolvation and favorable ion energetics could be achieved by selection of optimum operational ranges for the parameters that most strongly influence the ion population, namely the Venturi device gas flow rate and API capillary temperature. An investigation of the effect of these parameters on ion energetics is presented and the chapter concludes with a discussion of the effect of varying these parameters on the quality of MS signal obtained.

3.2. Importance of Ion Energetics in MS

Internal energy (IE) is defined as the "total energy of a species above its electronic, vibrational and rotational ground state."[222] In MS, IE has a profound effect on the reactivity of gas-phase ions and a significant influence on the ion species observed in the mass spectrum of a given compound as the amount of IE deposited on a molecule during ionization is one of the biggest predictors of whether the analyte will survive intact or fragment prior to reaching the mass analyzer.

3.2.1. IE Deposition by Various Ionization Techniques

As MS measurements are performed under vacuum, ions are effectively isolated from their environment once in the mass spectrometer. Thus unwanted IE deposition most generally occurs prior to the ions entering the mass analyzer, i.e. during ionization or, for instruments utilizing differential pumping, during transmission of ions from AP to the vacuum region of the mass spectrometer via an API. Although energy can also be intentionally deposited on the ions once they are in the mass analyzer to induce dissociation via either collisions with a gas, surface, or electrons, these processes are controlled and do not affect the *initial* IE of the ions and thus will not be included in this discussion.

Three factors determine the initial IE of an ion (1) the IE of the analyte prior to ionization, (2) the number of degrees of freedom (DOF) in the analyte, and (3) the amount of energy deposited during ionization and subsequent transmission through the API. Most ionization techniques can be loosely classified as being either *hard* or *soft* depending on the amount of IE they deposit on the ions, as briefly mentioned in section

1.2 during the discussion of the proto-typical examples of hard and soft ionization techniques, EI and CI. However, strictly speaking, EI and CI can be placed into either category depending on the energy of the primary electron beam used to ionize the analyte (EI) or the choice of reagent gas (CI), and on our particular definitions for "hard" and "soft", with regards to IE deposition. In general terms, a hard ionization technique is defined as a technique that produces spectra containing abundant fragment ions while a soft ionization technique is defined as a technique that produces spectra dominated by the presence of an intact analyte ion. Clearly, this is also a function of the chemical structure of the ions being considered, and the nature of the chemical bonds present (covalent and non-covalent). As an example of the extreme difference between spectra obtained using hard and soft ionization techniques, consider Figure 3.1.

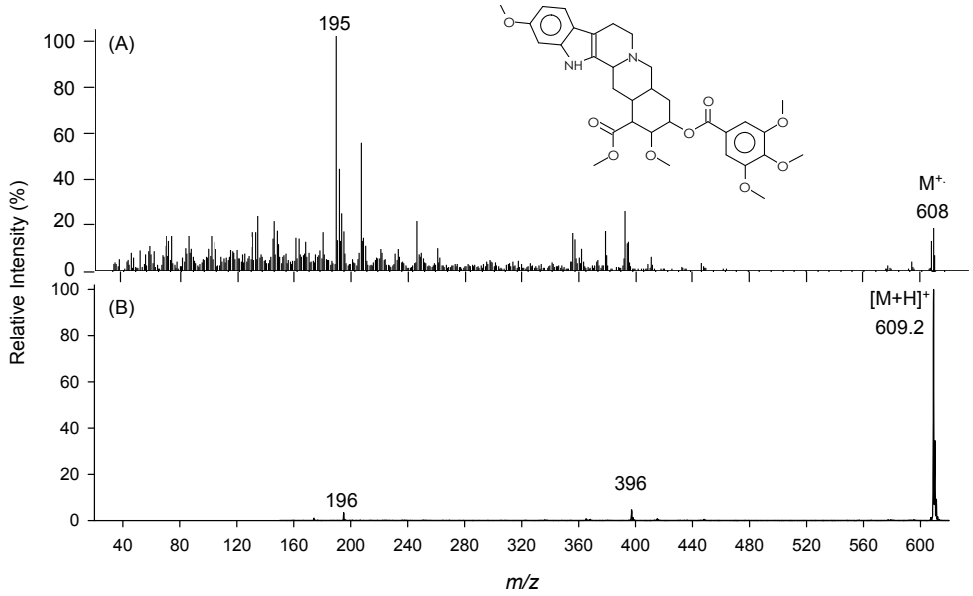

Figure 3.1. (A) EI mass spectrum of reserpine showing $M^{+\cdot}$ and significant fragmentation (reproduced from the NIST database[223]). (B) ESI-QiT mass spectrum of 1 μM reserpine in 50:49.9:0.1 (v:v:v) methanol:water:acetic acid showing $[M+H]^+$ and fragments at *m/z* 196 and 396 (10 μL min^{-1}, 5000 V_{DC}).

Figure 3.1 shows mass spectra of reserpine obtained using EI-MS (Fig. 3.1.A) and pESI-QiT (Fig. 3.1.B). The EI-MS spectrum clearly demonstrates the extensive fragmentation that is typical for hard ionization techniques while the relatively clean pESI-QiT mass spectrum shown in Fig. 3.1.B is dominated by the presence of $[M+H]^+$ and shows very few fragment peaks.

Hard ionization techniques, such as EI, typically produce, high-IE ions ("hot" ions, 10's of electronvolts[222]) which tend to fragment in the timeframe prior to reaching the detector of the mass spectrometer as a result of electronic and vibrational excitation of the ions induced by collision with energetic electrons (70 eV). As a result, mass spectra produced via EI may show some signal due to the intact radical ion ($M^{+\cdot}$, formed by the loss of an electron from the valence shell of the gas-phase molecule, M), but also show extensive fragment ion species. This type of spectral data is particularly useful for the identification of organic compounds as the fragments observed can be matched against databases and correlated to the cleavage of specific bonds in the molecule as it undergoes gas-phase unimolecular dissociation. Since the energy deposited by these sources is typically fixed and ionization occurs under vacuum, spectra are highly reproducible; thus, mass spectral databases can be transferred among different types of instruments. However, as explained in section 1.2, these methods are not amenable to the analysis of labile species, and may be impractical for the identification of molecules not in the database, as molecular weight information may be missing.

The generation of low-IE ions is particularly important for the study of fragile organic and biological compounds and non-covalent biological species, such as protein complexes. The development of soft ionization techniques now considered routine was

motivated by the need to ionize large species without fragmentation. Examples include MALDI (mean IE = 3-5 eV[224, 225]) and ESI (mean IE = 1-3 eV[226], pESI,[226] μESI,[227] and nESI[227] also show IE deposition in the same range). These techniques produce low-IE ions ("cold" ions, < 10eV[222]) which typically reach the mass spectrometer detector intact. These "survivors" generally appear as intact ions formed by adduction of an ion to the molecule, such as the protonated molecule ($[M+H]^+$), in the mass spectrum. However, fragment ions or cluster ions may also be observed if the appearance energy of the molecule (E_{app}, the minimum IE required to observe a given fragment ion) is low or if the ion source parameters are modified to allow for high IE deposition as described in section 3.2.2.

Despite the widespread appeal of MALDI and ESI, there has been considerable activity towards the development of even "softer" methods. For example, AP-MALDI,[34] sonic spray ionization (SSI),[228] electrosonic spray ionization (ESSI),[229] and cold spray ionization (CSI)[230] were developed with the intent of exploring improved ways for detecting biological species such as peptides,[231] proteins,[232, 233] non-covalent complexes,[234] and nucleic acids.[235]

AP-MALDI has been shown to produce ions with mean IE similar to ESI (1-3 eV[236]). This is colder than conventional vacuum MALDI as the IE of the AP-MALDI ion population is reduced through low-energy collisional cooling with ambient gas prior to entering the mass spectrometer and within the API. In SSI, droplets are produced by the flow of solution through a fused silica capillary with a high velocity gas flow coaxial to the capillary. The technique is similar to pESI but differs in that no potential is applied between the capillary and the counter-electrode and the gas flow rates are 100 times

higher than those of pESI. Although ion generation in SSI is not completely understood, one possible mechanism is that charging occurs via the statistical charging model proposed by Dodd[237] which states that, although the bulk liquid is electrically neutral, microscopic fluctuations in the ion concentration in the bulk liquid lead to the formation of some droplets having a positive or negative charge. Although SSI has been shown to form more clusters than ESI,[231] suggesting that it is softer than ESI, recent experiments by Zenobi and coworkers demonstrated that the actual IE deposited on the ion population in SSI is the same as that of ESI (1 – 3 eV).[227] Like SSI, ESSI, which is essentially SSI but with a potential applied to a union through which the analyte flows before it enters the SSI probe, has been shown to have an IE deposition similar to that of ESI.[227]

In CSI, the temperature of both the sample probe (similar to the design used in ESI, pESI, or SSI) and desolvation chamber is reduced to temperatures ranging from -80 to 10 ºC, causing a concomitant reduction in the IE of the system prior to ionization.[226, 230, 235] No measurements of the IE deposited on ions by CSI have been reported, thus it is unclear if the reduction in system IE translates into a reduction in the final energy of the fully desolvated ions. However, Albiz and coworkers recently compared the performance of CSI and ESI for the characterization of protein conformation and ionization of noncovalent complexes and found a shift to lower charge states in the CSI protein mass spectra suggesting that these ions may indeed be colder than those of ESI.[238] Like CSI, AMUSE ionization of proteins has also demonstrated a shift to lower charge states as shown in Section 2.7 suggesting that AMUSE ions could also be colder than those of ESI and providing motivation for an investigation of IE deposition by this technique.

3.2.2. Parameters Affecting IE Deposition in AP Spray-Based Ion Sources

In AP spray-based ion sources, the parameters which most strongly affect IE deposition can be loosely categorized as parameters which affect droplet desolvation[226] and parameters affecting ion transmission.[239] Efficient droplet desolvation in spray-based sources is critical to obtaining high ion yields from most analytes as evidenced by the increased sensitivity for peptides using nESI (subattomole[68]) in comparison to ESI (femtomole[240]). This is a direct result of the smaller nESI average droplet radius (<200 nm[50]) compared to that by ESI (1 μm[53]). Consequently nESI droplets experience enhanced desolvation,[68] tolerate higher salt concentrations (and consequently have lower background noise) due to the decreased amount of solvent in these smaller droplets,[68, 241] and show higher ion surface activity due to the higher surface-to-volume ratio, which enhances ion evaporation mechanisms.[68] However, in spray-based ion sources the excess energy not used to aid in droplet desolvation can be imparted into IE modes; thus, by modulating the parameters that affect droplet desolvation, it is possible to reduce IE deposition although reduced signal intensities may also result. The parameters which most strongly effect desolvation are the ion source pressure,[242] acceleration potential in the skimmer region of the API,[239, 243] and incorporation of heat in the ionization probe via use of a heating block encasing the probe,[46] prior to entry into the API via heated gas,[133, 244, 245] or in the API via a heated capillary.[246]

Karas and coworkers used nESI to monitor the signal intensity of maltopentaose, a carbohydrate that requires harsh desolvation conditions, and its corresponding fragment species. This data was used to determine the *relative* IE deposition upon changing the source pressure by calculating the fragmentation ratio (fragment ion intensities /

precursor ion intensity) and comparing this ratio for each set of conditions tested.[242] Increasing the source pressure from 0.84 to 2.0 mBar (0.6 to 1.5 mTorr) was found to improve desolvation and to cause a decrease in IE deposition as indicated by an 80% decrease in the fragmentation ratio. This effect can be explained by considering the interdependence of the droplet evaporation and ion activation processes. Gomez and Tang demonstrated that ESI droplet sizes are represented by a bimodal distribution in which the larger diameter distribution represents residual parent droplets while the smaller diameter distribution is due to progeny droplets, which usually become fully desolvated and are detected.[50] By raising the source pressure, this lower abundant desolvated fraction of the ion population may undergo ion activation after colliding with gas in the source. However, the more abundant large diameter droplets will be desolvated due to an increase in the number of low-energy inelastic collisions resulting in energy transfer to the gas molecule. These droplets will also experience a concomitant reduction in kinetic energy prior to entering the mass analyzer and being detected. This collisional cooling of the droplets translates into a mass spectrum having a lower fragmentation ratio indicating lower IE deposition. This effect was verified by Gabelica et al. who studied the shape of the IE distributions obtained using the SY method (section 3.3) and observed a reduction in IE deposition and narrower distributions when the source pressure was increased from 1.65 Torr to 2.93 Torr, also indicating more efficient desolvation.[247]

Increasing the potential gradient in the first skimmer region has been shown to cause an increase in IE deposition,[248, 249] and this is the basis of in-source collision induced dissociation (CID) experiments. This can be attributed to an increase in kinetic energy in a medium pressure region caused by the acceleration voltage. Hoxha et al.

performed ion trajectory calculations to gain an understanding of this phenomenon and observed that 90% of the IE uptake occurs at the first stage of the API suggesting that activation occurs primarily as a result of high energy collisions in this region.[250] Frictional heat as a result of these collisions also contributes to the increased IE.[251]

De Pauw and coworkers demonstrated that the addition of thermal energy generated mass spectra showing a higher fragmentation extent.[247] This thermal energy, which was supplied to the analyte by increasing the temperature of the mass spectrometer's capillary inlet, resulted in improved desolvation leading to an excess of IE that was no longer needed to aid in desolvation.

As mentioned in section 2.2.3, AP ionization techniques suffer from ion transfer losses of up to 99% of ions.[207-209] In our previous work, we observed that coupling a Venturi device to the AMUSE resulted in a 10-fold gain in S/N ratio of 10 μM reserpine accompanied by a 77% reduction in %RSD of the signal.[133] We attributed these improvements to the increased droplet velocity and droplet desolvation; thus, it is likely that use of Venturi devices will contribute to the overall IE deposition due to increased kinetic energy of the entrained droplets as they pass through the low pressure region of the device and due to improved desolvation. However, no measurements of the IE deposition by these devices had ever been reported. Therefore, we performed an investigation of the effect of these devices when coupled to AMUSE and ESI focusing on the effect of varying the flow rate of N_2 through the Venturi device and the API capillary inlet temperature as those parameters most strongly affect desolvation. The survival yield (SY) method developed by Kenttämaa and Cooks was used to measure the IE deposition.[252]

3.3. Measuring IE Deposition – The Survival Yield Method

The SY method correlates the fragmentation extent of a thermometer molecule with the IE deposited on it during the ionization process.[252] Thermometer molecules are generally small, well-characterized compounds that undergo a specific dissociation(s) at a known critical energy (E_0, the minimum energy of the precursor ion needed to overcome the dissociation energy barrier). Several compounds such as benzylpyridinium salts,[247, 249, 251, 253-255] peptides such as YGGFL,[236, 254] and protonated esters[254] have been used as probe ions. Collette and De Pauw introduced the use of substituted benzylpyridinium salts as probe ions because they undergo a simple cleavage reaction at known dissociation energies to form a benzyl cation and pyridine (Scheme 3.1).[249]

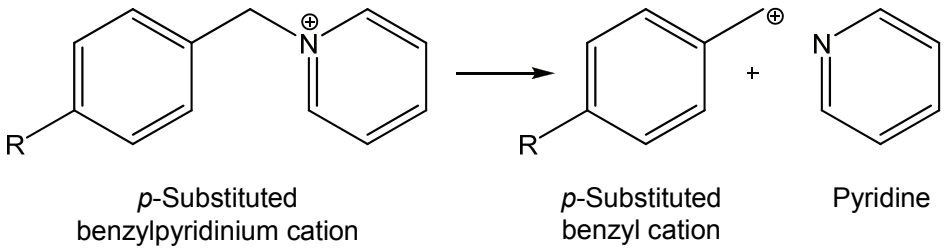

Scheme 3.1. Scheme showing the dissociation reaction of *p*-substituted benzylpyridinium ions to produce neutral pyridine and a *p*-substituted benzyl cation.

By using a series of *p*-substituted benzylpyridinium salts which have a similar number of DOF but differing dissociation energies,[247] the simultaneous measurement of SY for each molecule under controlled experimental conditions is obtained. The critical energy can be empirically calculated as the heat of the fragmentation reaction (ΔH_r), which is the difference in ground state energy between the precursor ion ($\Delta H_f(Py^+R)$, heat

of formation of benzylpyridinium cation) and its fragment ions (heat of formation of pyridine (ΔH_f(Py) and the benzyl cation ($\Delta H_f(R^+)$)) as shown in Equation 3.1.[253]

$$E_0 = \Delta\Delta H_f = [\Delta H_f(Py) + \Delta H_f(R^+)] - \Delta H_f(Py^+R) \qquad \text{(Eq. 3.1)}$$

The critical energies for the *p*-substituted benzylpyridinium salts used in these studies having tert-butyl- (tBu), methyl- (CH_3), fluoro- (F), chloro- (Cl), cyano- (CN) and nitro- (NO_2) substituents are given in Table 3.1.

Table 3.1. Nominal *m/z* for precursor and product ions, critical energies, and DOF for the *p*-substituted benzylpyridinium compounds used. *Critical energies taken from Gabelica et al.[247]

R	Precursor$^+$ (*m/z*)	Product$^+$ (*m/z*)	E_0 (eV) *	DOF
OCH_3	200	121	1.508	81
tBu	226	147	1.738	105
CH_3	184	105	1.767	78
F	188	109	1.867	69
Cl	205	125	1.899	69
CN	195	116	2.097	72
NO_2	215	136	2.352	75

The SY method is predicated by two assumptions: (1) all ions having the same DOF have identical P(E) and (2) ions do not dissociate until their IE surpasses their intrinsic dissociation threshold. SY for a thermometer ion (Equation 3.2) can be determined experimentally by measuring the fraction of ions below ($Int_{Product}$, the intensity of the product ion peak in the mass spectrum) and above ($Int_{Precursor}$, the intensity

of the precursor ion peak(s) in the mass spectrum) the dissociation threshold (critical energy) of a given molecule.

$$SY = \frac{Int_{Precursor}}{Int_{Precursor} + Int_{Product}} \qquad \text{(Eq. 3.2)}$$

This is theoretically equivalent to the value of the integral below the P(E) curve evaluated from E=0 to E_0, the dissociation energy of the molecule. The SYs of these compounds plotted against their respective dissociation energies can then be fitted to a sigmoidal function with the general form described in Equation 3.3 and differentiated to yield P(E), the probability of a species having a particular IE.

$$SY_{Fitted} = \frac{a}{1 + e^{-\left(\frac{Energy - x_o}{b}\right)}} = \int_0^\infty P(E)\,dE \qquad \text{(Eq. 3.3)}$$

The parameters a, b and x_0 in Equation 3.3 are variables fitted to the experimental data. Finally, the mean internal energy (<E>) of the ions (which give the average IE of the entire ion population) is calculated by finding the centroid of P(E) (Equation 3.4).

$$\langle E \rangle = \frac{\int_0^\infty E \cdot P(E)\,dE}{\int_0^\infty P(E)\,dE} \qquad \text{(Eq. 3.4)}$$

The observed <E> deposition not only depends on the intrinsic dissociation rate constant and activation energy, but is also strongly influenced by the time scale of the mass spectrometric experiment, manifested as the excess energy ("kinetic shift") required to observe dissociation products. For absolute measurements or for comparative measurements utilizing different types of mass analyzers, correction for this kinetic shift is necessary but can be a challenging task as it requires knowledge of the ions' residence times as they are transported and analyzed within the different stages of the mass spectrometer. However, a comparison of the *relative* changes in P(E) as a result of using different ionization techniques with the same mass analyzer can be accurately obtained if the residence time remains consistent throughout all experiments or/and if the SYs of the ions used in calculating P(E) do not vary significantly within the experimental time scale.

3.4. Experimental Details

3.4.1. Synthesis and Preparation of Thermometer Compounds

Pyridine, nitromethane, anhydrous diethyl ether, anhydrous ethanol and the para-substituted benzyl halide starting reagents were purchased from Sigma-Aldrich (St. Louis, MO) and used without further purification. All compounds except the methoxy-substituted salt (OCH_3; Arkat USA, Inc., Gainesville, FL) were synthesized by Catherine Silvestri, an undergraduate student who spent a semester working in our group. Para-substituted benzylpyridinium salts with tBu, CH_3, F, Cl, CN and NO_2 substituents were synthesized using a method based on that reported by Katritzky, et al.[256] The basic protocol involves condensation of the *p*-substituted benzyl halide with pyridine followed by recrystallization from diethyl ether. In general, synthesis was accomplished by

combining 0.01 mol of the starting reagent with 0.015 mol pyridine and stirring the mixture at room temperature for 7 – 24 hours. (Synthesis of the F, Cl, CN, and NO_2 salts also required the addition of 3 mL nitromethane to the reaction vessel prior to the addition of pyridine.) The mixture was then diluted with 30 mL diethyl ether and chilled before the product was filtered from the solution. Specific synthesis details are given in Table 3.2.

Table 3.2. Reaction details for synthesis of *p*-substituted benzlypyridinium compounds.

Alkyl Salt	Starting Reagent	Nitromethane Added?	Reaction Time (hrs)	Product Appearance
OCH_3	---	---	---	White salt
tBu	*p*-Tertbutylbenzyl chloride	No	16	White salt
CH_3	*p*-Methylbenzyl chloride	No	24	Clear oil
F	*p*-Fluorobenzyl chloride	Yes	24	Yellow oil
Cl	*p*-Chlorobenzyl chloride	Yes	12	Yellow, prism-like crystals
CN	*p*-Cyanobenzyl bromide	Yes	9.5	White, needle-like crystals
NO_2	*p*-Nitrobenzyl bromide	Yes	7	White, needle-like crystals

Mass spectral analysis was performed to assess the purity of the synthesized compounds that were stored in a -80 ºC freezer until needed. Unless otherwise specified, an equimolar mixture (5 μM each) was freshly prepared prior to analysis in either a 50% methanol solution (HPLC grade, Sigma-Aldrich, St. Louis, MO) or nanopure water

(Barnstead International, Dubuque, IA) and delivered to the ion source under investigation at a flow rate of 20 μL min^{-1}, the minimum flow rate possible for this particular AMUSE device. No organic acid was added as the analytes are pre-charged.

3.4.2. AMUSE Fabrication, Assembly, Setup and Operation

Fabrication of the 2nd generation 20x20 array of 5-μm nozzles in silicon was accomplished as described in section 2.2.2[132] and assembled using protocol 2 (see section 2.3.2). Experiments were performed using the RF-only AMUSE and DC-AMUSE operational modes as described in section 2.3.3 with the electrical circuit shown in Figure 2.9.B. The AMUSE was positioned as close as possible to the Venturi device inlet (4 mm) and the Venturi device outlet was flush with the QiT capillary inlet resulting in a total distance of 77 mm between the point of droplet emission and the inlet orifice (255 mm between the point of droplet emission and the skimmer) as shown in Figure 3.2.

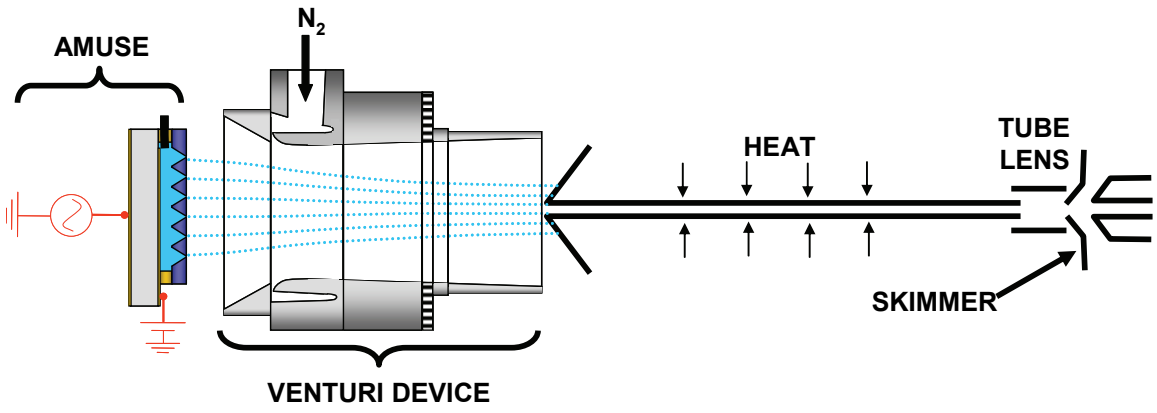

Figure 3.2. Setup of the Venturi-assisted experiment and relevant compounds of the mass spectrometer's API.

3.4.3. Venturi-Assisted ESI Setup

The needle assembly of a commercial pESI source (ThermoFinnigan, Waltham, MA) fitted with an 83 μm i.d. spray capillary (Small Parts, Miramar, FL) was removed from the source housing and mounted to a post using a clamp. The needle was centered with respect to a Venturi device and positioned so that the needle tip-Venturi device distance was equal to that used for the AMUSE. A 4 kV_{DC} electric potential was applied to the needle using the built-in power supply of the QiT mass spectrometer to produce stable electrospray. No N_2 was used to aid in nebulization. The source was positioned 4 mm in front of the inlet of the Venturi device, the minimum distance possible using the current AMUSE assembly, while the outlet of the Venturi device was positioned flush with the QiT capillary inlet as shown in Figure 3.3.

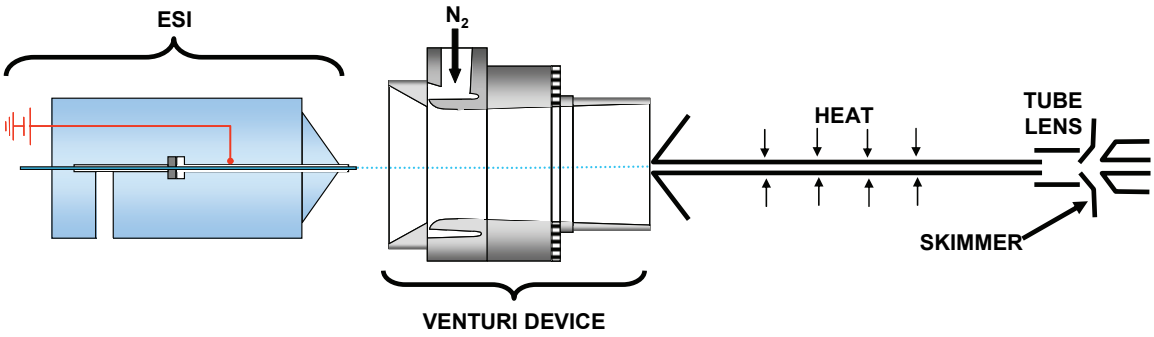

Figure 3.3. Setup of the Venturi-assisted ESI experiment and relevant components of the mass spectrometer's API.

3.4.4. Venturi Operation

A differential pressure flow controller (Bel-Art, Pequannock, NJ) controlled the flow rate (0 – 10.6 L min^{-1}) of industrial grade N_2 gas (130 psi, Airgas, Radnor, PA) used to provide suction of the droplet streams through the low pressure region in the center of

the Venturi device. Table 3.3 provides the gas pressures that correspond to the experimental flow rates that would be observed if gas flow was controlled solely by a pressure regulator. These values were obtained by fully opening the flow controller valve and adjusting the gas pressure at the regulator until the desired reading (flow rate) was achieved on the controller.

Table 3.3. List of experimental flow rates used with the Venturi device and corresponding gas pressures. Flow rates requiring gas pressures lower than the measurable range on the pressure regulator used are indicated by dashes.

Flow Rate (L min^{-1})	Pressure (psi)
0.00	--
0.96	--
2.23	--
3.45	--
4.37	--
5.98	10
7.16	20
8.31	30
8.76	35
9.46	40
10.61	50

3.4.5. Measurement of Droplet Size Distributions

Droplet size distributions (Sauter mean diameter (D[3,2]) vs. frequency) were measured in triplicate with a laser diffraction particle size analyzer equipped with a 63 mm focal length optical collection system (Model 2600C, Malvern, Worcestershire, UK). The correct performance of this instrument was verified by interrogating a calibrated graticule (46.5 μm nominal particle size), and particle size measurements were found to

be accurate within 4%. All particle size measurements were performed perpendicular to the ejection axis, with the laser measurement area placed immediately at the exit of the Venturi device. The area over which time-averaged particle-size measurements were obtained is approximately cylindrical in shape, and 22 mm long by 7 mm diameter.

3.4.6. Mass Spectrometry

A commercial pESI source was interfaced to the QiT and used to optimize the ion optics and mass analyzer settings to obtain maximum signal intensity for the base peak (*m/z* 226; precursor ion of the tBu compound) using the auto tune function. These settings were used for all subsequent experiments. For all experiments performed, the inlet capillary voltage was set to -30 V while the capillary temperature was varied between 230 – 300 ºC and the tube lens offset voltage (TL), which is equivalent to a capillary-skimmer voltage in this instrument, was varied from 0 – 100V to modify the desolvation/declustering conditions. The automatic gain control (AGC) was kept on and set to a maximum of 5x 10^7 ions, with a maximum trap time of 100 ms (3 microscans) for all experiments. Mass spectra were acquired in profile mode for 1 minute using the built-in mass spectrometer software (Xcalibur 2.0, ThermoFinnigan, Waltham, MA) and exported into Excel (Microsoft, Auburn, WA).

3.5. Data Analysis

Data analysis of preliminary mass spectral results required several steps to be performed after the acquired mass spectra were exported into Excel. The first step was to determine the precursor and product ion intensities for each of the thermometer

compounds present in the mass spectrum (seven compounds, fourteen peaks of interest). Figure 3.4 shows a typical AMUSE mass spectrum for a solution containing a mixture of *p*-substituted benzylpyridinium compounds with the peaks of interest labeled.

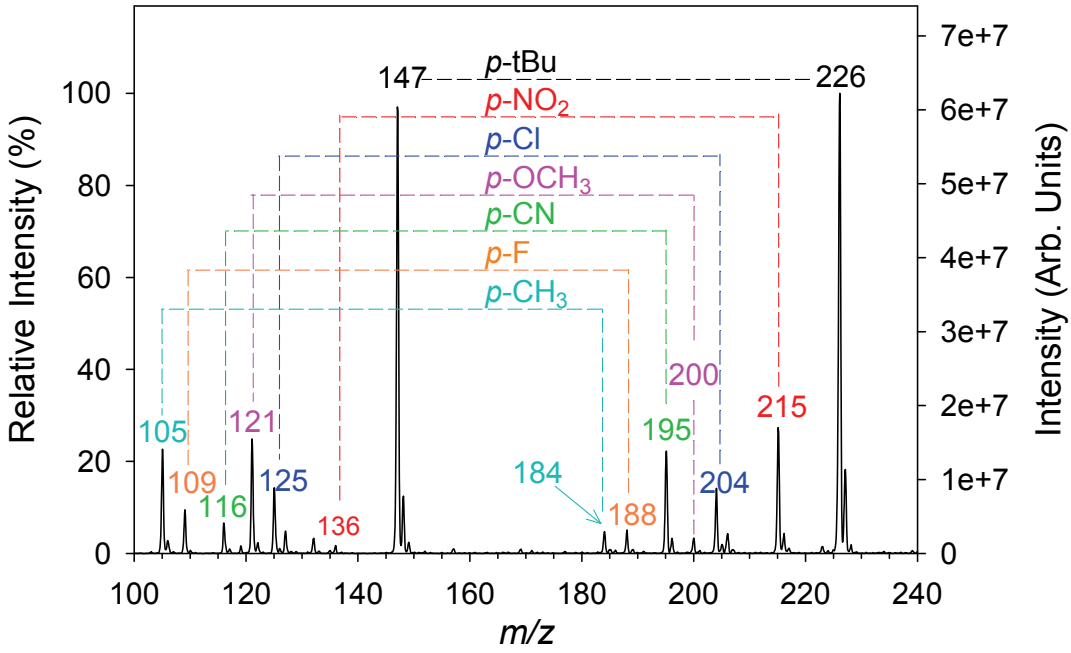

Figure 3.4. Mass spectrum for an aqueous 5 μM mixture ionized by RF-only AMUSE at TL = 40V. Operating conditions: 300 ºC capillary, 8.76 L min^{-1} N_2.)

Examination of the mass spectrum shows two clear peak distributions with a set of seven peaks on the left (*m/z* 105, 109, 116, 121, 125, 136, and 157) corresponding to fragment ions of the precursor ion peaks located in the set of seven peaks in the upper mass range of the spectrum (*m/z* 184, 188, 195, 200, 204, 215, 226). An assessment of the IE deposition can be determined visually by inspection of the relative heights of the sets of peaks. In this spectrum, matching precursor-fragment ion peaks across both sets of peaks have the same intensity which indicates SY = 0.5. If no precursor ions are detected,

then SY = 0, which corresponds to maximum IE deposition conditions. Conversely, for spectra showing no fragment ion peaks, SY = 1.0, which corresponds to minimum IE deposition conditions.

Although the analyte mixture is equimolar, the spectrum shows significant variations in intensity due to the wide variability in ionization efficiency as a result of the difference in hydrophobicity of the substituent which increases as follows: CN < OCH_3 < NO_2 ≈ F < CH_3 < Cl << tBu. This trend in hydrophobicity matches the relative intensities of the corresponding peaks in the mass spectrum and correlates well with the relative intensities observed by ESI. This can be explained by the higher abundance of the more hydrophobic components on the aqueous droplet surface; thus, these analytes are desorbed more readily from the droplet leading to high mass spectral intensities.[257] Gabelica et al. suggested the use of dilution factors to normalize the mass spectrometer response, however, preliminary experiments using equiresponse mixtures showed the same <E> as those for the equimolar mixture, therefore the equimolar mixture was used to preserve sample.[247]

Next, the SY for each compound in the mass spectrum was calculated using Equation 3.2. In step 3 of the data analysis protocol, the breakdown curve (SY vs. parameter of interest) was plotted to ensure that the experimental SYs were distributed over the entire SY range (0 – 1) increasing the probability that the subsequent data processing steps will yield good results. Figure 3.5 shows the breakdown curves as a function of TL obtained for a series of RF-only AMUSE mass spectra (the legend lists the compounds in order of highest to lowest E_0).

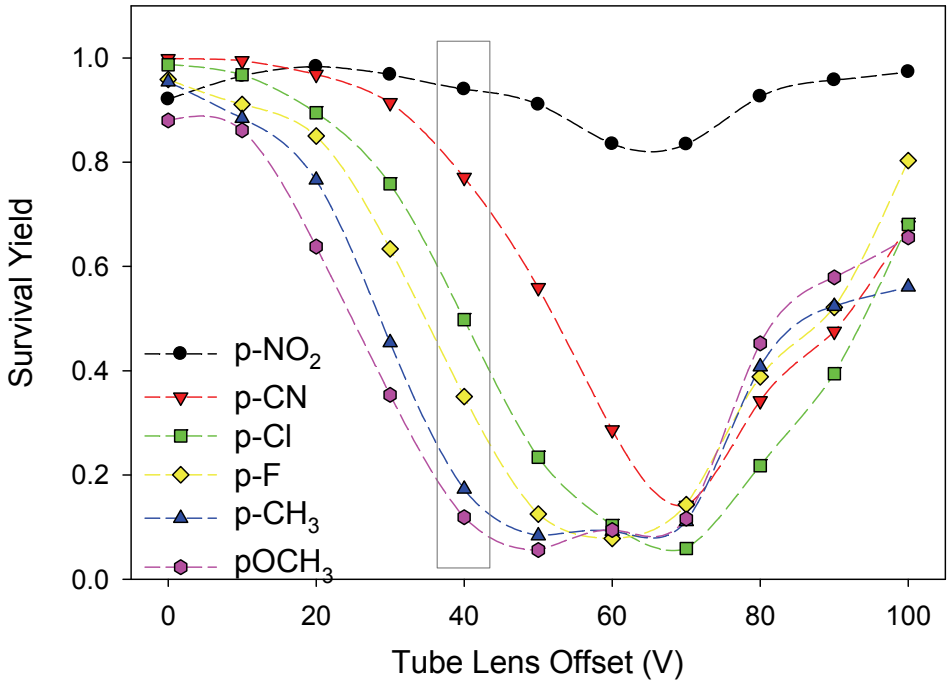

Figure 3.5. Breakdown curves as a function of TL for all compounds analyzed during collection of eleven mass spectra for an aqueous 5 µM mixture ionized by RF-only AMUSE. Operating conditions: 300 ºC capillary, 8.76 L min^{-1} N_2. The black box indicates the TL that provides the optimal spread of SYs.

As can be seen in Figure 3.5, the tBu compound (pink circle) does not fall between the OCH_3 (blue circle) and CH_3 (dark blue triangle) compounds as expected from their relative E_0's. This can be attributed to the higher DOF of the tBu compound (DOF = 105) relative to that of the other compounds. The actual energy required to observe dissociation of tBu is greater than expected due to the dispersion of IE to each oscillator, i.e. due to the presence of a kinetic shift; thus, tBu was not included in subsequent steps of the data analysis workflow. A detailed investigation of the effect of ion residence time on the SYs obtained is described in detail in section 3.5. Another interesting observation from Figure 3.5 is the increased SY with higher TL voltages. This can be attributed to further fragmentation of the product ion species, which was not

accounted for in our SY calculations but was verified experimentally. Figure 3.6 shows the intensity of the precursor and product ion peaks of the OCH_3 compound at various TL.

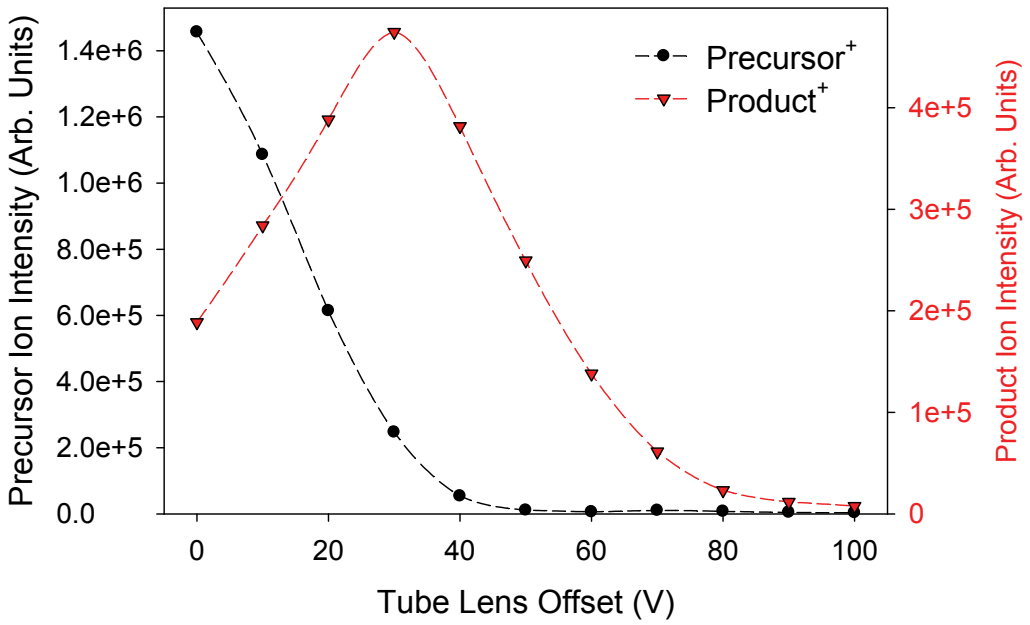

Figure 3.6. Ion intensities for the precursor and product ions of the CH_3 compound analyzed during collection of eleven mass spectra for an aqueous 5 μM mixture ionized by RF-only AMUSE for TL = 0 – 100 V. Operating conditions: 300 ºC, 8.76 L min^{-1} N_2.

As can be seen in Figure 3.6, the intensity of the precursor ion decreases rapidly with increasing TL up to 40 V and is negligible at higher potentials. The product ion intensity increases rapidly with increasing TL up to 30 V and then decreases until it reaches 80 V, at which point it too becomes indistinguishable from the baseline noise. In other words, the product ion begins to fragment at 30 V causing a corresponding inflation of the SY as these new fragments are not incorporated into the denominator of the SY equation. Other thermometer compounds showed similar trends; thus, any spectra that

fall into regions where the SY begins to increase (at high TL) must be carefully interpreted and possibly discarded.

In step 4, the experimental SYs were plotted as a function of E_0 and fitted using either 1 sigmoid as shown in Equation 3.3 or 2 sigmoids (in the 2-sigmoid fit, the first sigmoid is used to fit OCH_3 and CH_3 while the second is used for CH_3, F, Cl, CN, and NO_2) which are linked at their crossing point and smoothed to avoid steps in the derivative. These two alternate methods of fitting the experimental SY curves were implemented by Gabelica et al.[247] to account for deviation of the breakdown curve at low critical energies caused by a slight increase in SY for OCH_3 and CH_3 due to further fragmentation of the product ion species as demonstrated in Figure 3.6. Figure 3.7 shows a plot of SY vs. E_0 fitted using both methods.

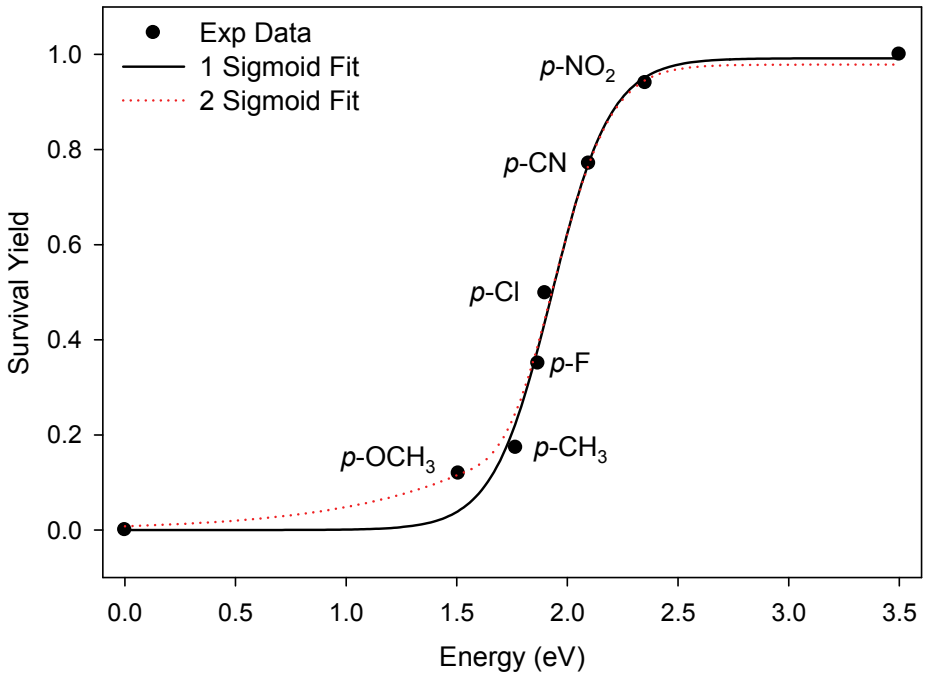

Figure 3.7. Breakdown curve showing 1 sigmoid and 2 sigmoid fits to data from an aqueous 5 μM mixture ionized by RF-only AMUSE at TL = 40 V. Operating conditions: 300 ºC, 8.76 L min^{-1} N_2.

Visual inspection of Figure 3.7 clearly indicates that the 2 sigmoid curve function provides a better fit of the data. However, determination of the method providing a better fit may be ambiguous in some datasets. Thus, the residual error associated with each fit type was also calculated, and the fit providing the highest correlation coefficient was chosen for subsequent analysis. In step 5 of the data analysis workflow, P(E) was determined by calculating the derivative of the sigmoidal curve chosen during step 4. The last step of the data analysis protocol was to calculate <E> using Equation 3.4. Figure 3.8 shows the P(E) curves of the sigmoidal curves in Figure 3.7 and lists <E> for each fit.

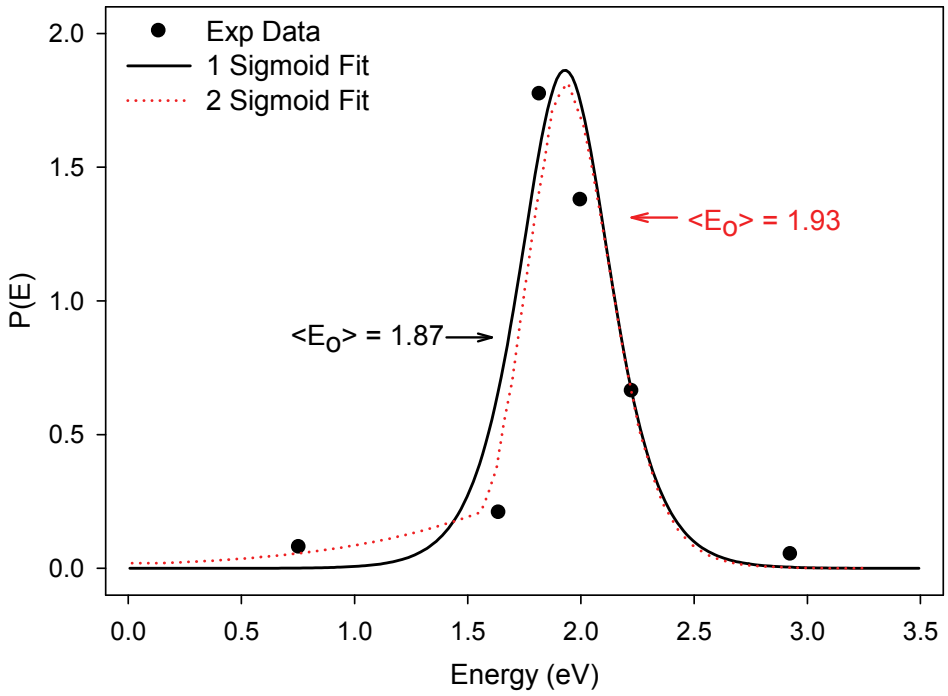

Figure 3.8. P(E) curves and <E> for sigmoidal fit data from an aqueous 5 μM mixture ionized by RF-only AMUSE at TL = 40V. Operating conditions: 300 ºC, 8.76 L min^{-1} N_2.

Initially, the data analysis workflow was performed manually and required several hours for a single spectrum. A set of macros generated in Excel and in SigmaPlot (Systat

Software Inc., San Jose, CA) was used to expedite the data analysis process. The Excel macro was used to identify the peak maxima for each of the ions of interest and to calculate SY for each species. The SY values were then exported into SigmaPlot and plotted against their respective critical energies. A series of SigmaPlot macros and transforms were used to fit the experimental SYs to a sigmoidal curve (using both fitting methods) and to calculate the residual error of each fit, P(E), <E>, and full width half maximum (FWHM) of the distribution. Use of these macros provided a significant reduction in analysis time (2 min / spectrum) and enabled us to perform studies that were previously considered unfeasible due to the lengthy data analysis times that would have been required.

3.6. Effect of Trapping Time on IE Deposition

In commercial QiT mass spectrometers, AGC is used to control MS signal sensitivity and peak resolution by automatically varying the trapping time. Generally, this is accomplished by either increasing the trapping time, which improves the signal intensity, or by decreasing the trapping time, which improves peak resolution by minimizing space-charge effects and detector saturation. With the AGC on, a pre-scan is first performed during which the QiT determines the flux of incoming ions so that it can adjust the trapping time of the following analytical scan to provide maximum sensitivity and resolution. However, it is sometimes beneficial to turn the AGC off, particularly for experiments that require a fixed time scale (as when monitoring kinetic reactions) or when performing comparative experiments with ionization sources exhibiting different ionization efficiencies.

Previous experiments to determine the sensitivity and stability of the Venturi-assisted AMUSE demonstrated that a trapping time of 100 ms, with 3 microscans and the AGC set to 5 x 10^7 provided the best sensitivity and resolution for the analysis of reserpine, YGGFL and cytochrome C. To verify that these conditions were optimal for the analysis of the thermometer compounds and to verify that the kinetic shift was constant within the range of assayed trapping times, experiments were performed with the AGC turned off while all other parameters were held constant (Fig. 3.9).

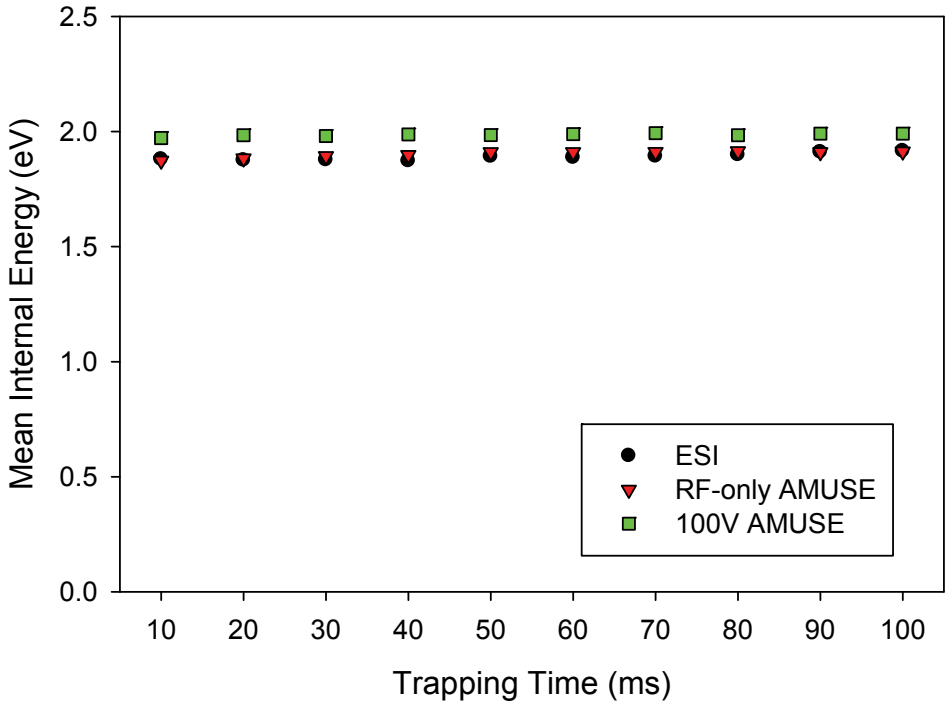

Figure 3.9. Plot of <E> measured for a 5 μM aqueous mixture at trapping times ranging from 2 – 100 ms. Operating conditions: TL = 40 V, 300 ºC, 8.76 L min^{-1} N_2.

<E> for these three ionization methods at all trapping times increased by 2% with increasing trapping time, which is within experimental error, suggesting that there is no appreciable difference in the kinetic shift at any of the trap times tested. It was observed

during subsequent experiments that when the AGC was on, the typical trapping time per scan automatically selected was 3-5 ms regardless of the ionization method used, and that the SYs of each compound varied by <1%. This indicated that the P(E) curves would not be significantly affected, even if fluctuations in ion source intensity caused the trapping time to be automatically adjusted by the instrument's software.

3.7. IE Deposition Under Optimized Desolvation Conditions

In our prior studies of Venturi-assisted AMUSE ionization, it was found that maximum ion yields for a variety of test compounds were obtained using an API capillary temperature of 300 ºC and 8.76 L min^{-1} flowing through the Venturi device. The mass spectra obtained for ESI, RF-only AMUSE, and DC-AMUSE ionization of a 5 μM mixture of thermometer molecules prepared in 50% *methanol*, with and without the use of ambient N_2 flowing through the Venturi device, are shown in Figure 3.10 while the corresponding IE distributions are shown in Figure 3.11.

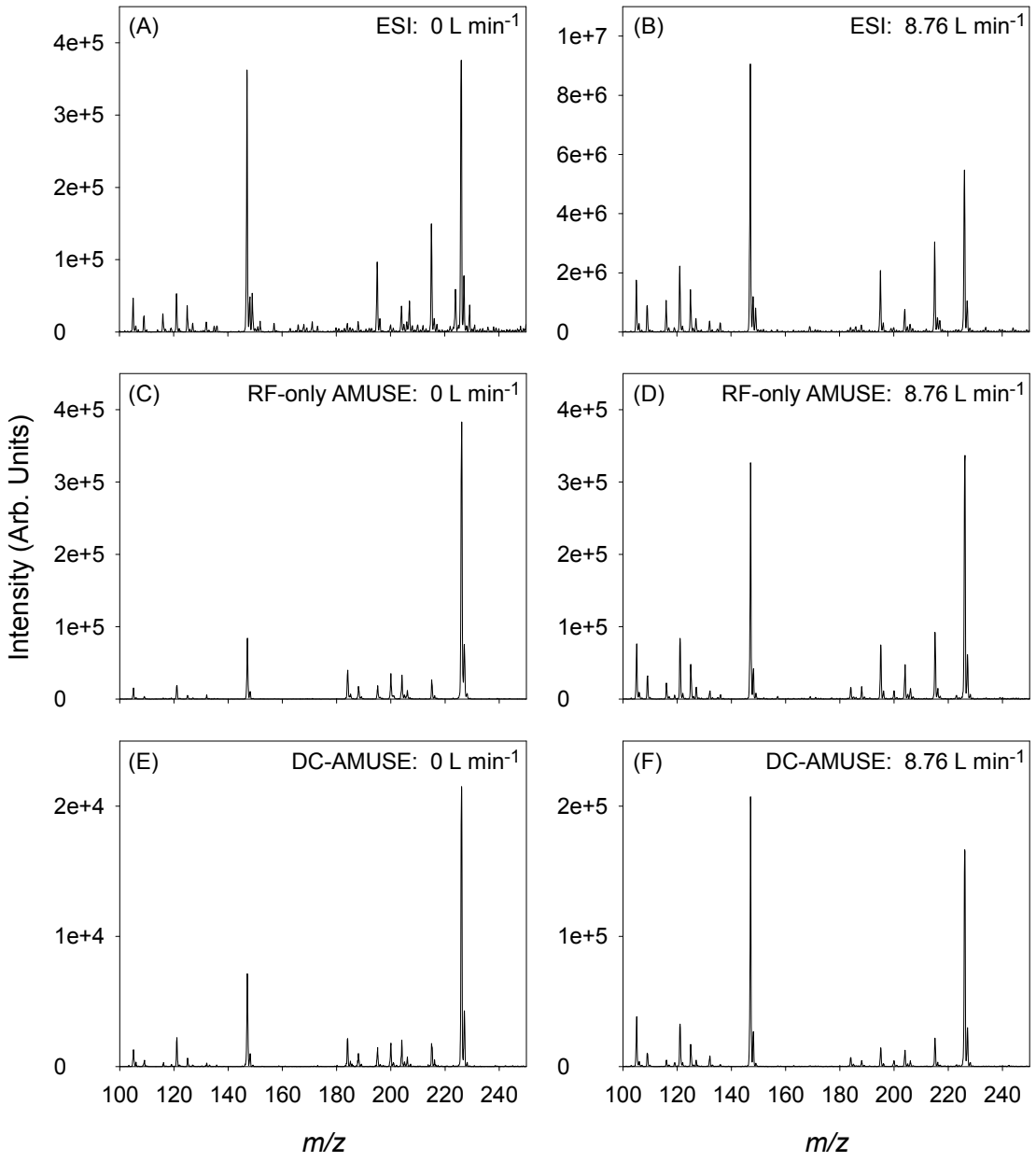

Figure 3.10. Mass spectra for ESI (A and B), RF-only AMUSE (C and D), and DC-AMUSE (E and F) ionization of a 5 μM mixture of thermometer compounds prepared in *50% methanol* without Venturi focusing (A, C, and E) or with 8.76 L min^{-1} N_2 (B, D, F). Operating conditions: TL = 40 V, 300 ºC.

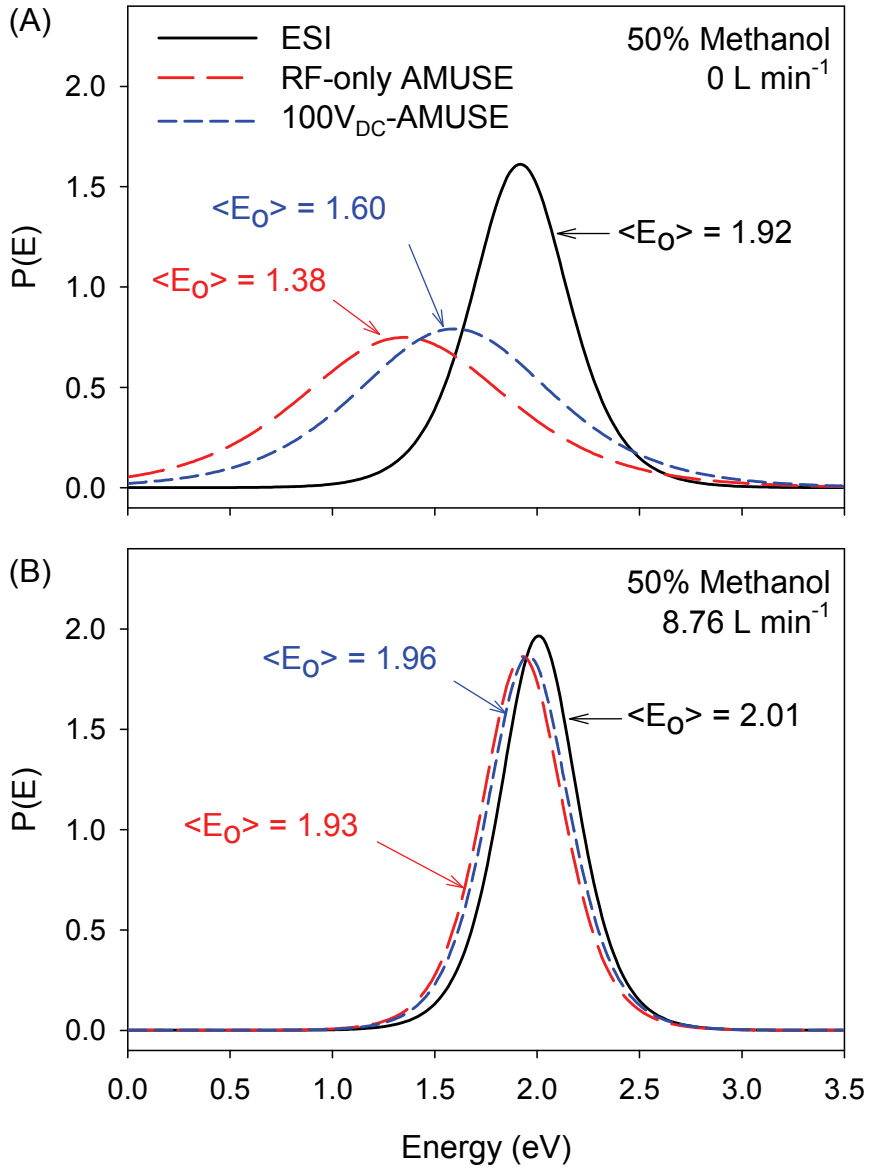

Figure 3.11. P(E) curves for ESI, RF-only AMUSE, and DC-AMUSE ionization of a 5 μM mixture prepared in *50% methanol* without Venturi focusing (A) or with 8.76 L min^{-1} N_2 (B). Operating conditions: TL = 40 V, 300 ºC.

Examination of the ESI spectra (Fig. 3.10 A and B) showed a clear improvement in signal intensity with a relatively small difference in the relative intensities of the precursor and product ion mass spectral distributions. This corresponded to a small difference in <E> for operation with and without N_2 flowing through the Venturi device

(Fig. 3.11 A vs. B). This effect was not as obvious for the AMUSE spectra (Fig. 3.10 C-F) as there was also a marked decrease in signal intensity of the precursor ions which translates into an increase in <E> (Fig. 3.11 A vs. B). However, an improvement in signal intensity upon using the Venturi device with AMUSE was previously observed for the analysis of less labile compounds.[133] In the absence of N_2 flowing through the Venturi device (Fig. 3.11.A), RF-only AMUSE ionization was the softest of all techniques, with <E> = 1.38 eV, which is 39% lower than the corresponding value observed for ESI (1.92 eV). For DC-AMUSE ionization, <E> was also lower than that for ESI but was slightly higher than for RF-only AMUSE (1.60 eV), possibly due to decreased mass transfer as a result of liquid buildup on the array surface as discussed in more detail below.

Flowing N_2 through the Venturi device at 8.76 L min^{-1} resulted in a marked increase in <E> for AMUSE ionization in both modes but only resulted in a 4% increase for ESI. With Venturi focusing, <E> for RF-only AMUSE was only marginally lower than that of DC-AMUSE and ESI resulting in <E> of, 1.93, 1.96 and 2.01 eV, respectively. The moderate increase in <E> observed for ESI when utilizing Venturi focusing indicates that, under optimum focusing conditions, the use of a Venturi device does not have a detrimental effect on the IE deposited on ions. The variation in observed <E> between the different ionization methods can be attributed to changes in the droplet size distribution upon use of the Venturi device which has been shown to be an important factor in P(E) when using spray-based ionization techniques.[255]

The decreased droplet size due to use of the Venturi device can be attributed to the increase in droplet velocity which causes a reduction of droplet/ion residence time before entering the heated inlet of the mass spectrometer and results in an effective

decrease in ion sub-cooling associated with solvent evaporation. Increased frictional droplet heating due to hydrodynamic friction within the flowing N_2 is not expected to be of any significance because N_2 viscosity is very small and there are no significant velocity gradients along the center axis (parallel to the walls) of the Venturi device. Even if there is any small gas heating, the heat capacity of the liquid is much larger than that of the gas, so no appreciable increase in droplet temperature due to this effect could be expected. Since droplets are carried by the flowing air because of their low inertia due to small size, the relative tangential droplet-to-N_2 velocity is zero. In other words, no slip is expected, as droplet and flowing N_2 gas are moving at the same velocity, resulting in minimal frictional heating. The ESI droplet size distributions produced in this configuration with and without Venturi focusing are shown in Figure 3.12.

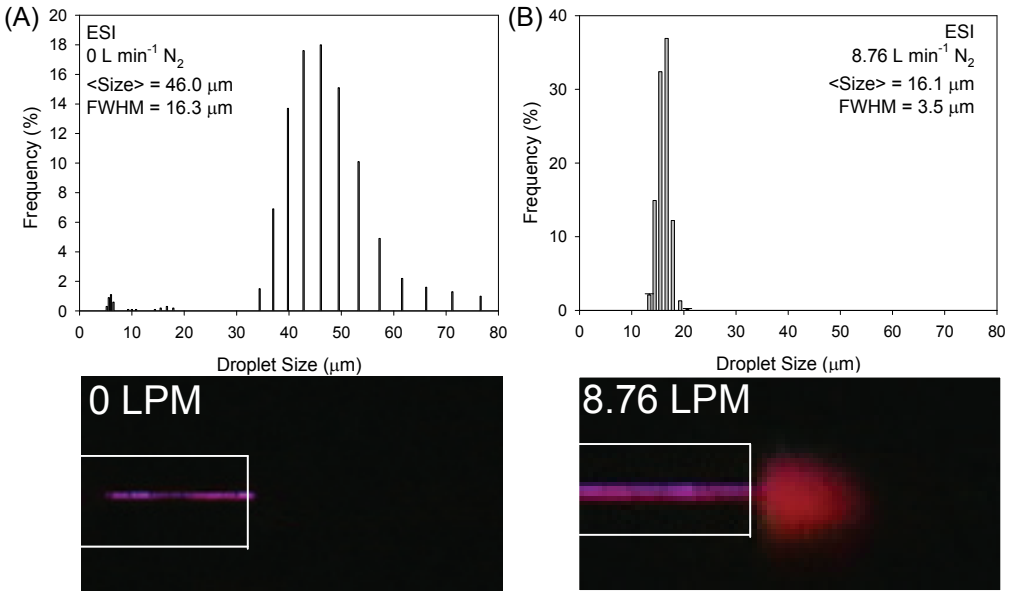

Figure 3.12. Droplet size distributions (top) and images of light scattered by spray (bottom) observed for a *50% methanol* solution sprayed using ESI without Venturi focusing (A) or with 8.76 L min^{-1} N_2 (B). (The white box in the image outlines the edge of the Venturi device.)

Without the use of Venturi focusing, the mean droplet diameter was 46.0 μm with a FWHM of 16.3 μm for ESI (Fig. 3.12.A), which is indicative of considerable droplet coalescence during the transit from the ESI capillary to the MS inlet. Close examination of the droplet size distribution obtained by ESI shows the additional presence of a low-abundance droplet population with a wide diameter distribution ranging from 5 to 20 μm. The presence of multiple droplet size populations when no N_2 flows through the Venturi device is not unexpected and can be attributed to the long residence time of droplets, which allows some droplets to emerge individually while others coalesce and exit as larger droplets. The distribution obtained with 8.76 L min^{-1} N_2 flowing through the Venturi device (Fig 3.12.B) shows a more uniform droplet population with a significantly lower mean diameter and FWHM, 16.1 μm and 3.5 μm, respectively, compared to that obtained without Venturi-assisted droplet entrainment. As the probability of generating ions via desolvation of the more abundant large-diameter population is low, it is likely that the mass spectrometric signal observed during the non-Venturi focusing experiment is due mostly to the low abundant small-diameter droplet population mentioned above. This would explain the similarities observed for ESI IE distributions between Figs. 3.11.A and 3.11.B as the spectrometer is sampling from droplet populations having similar diameters.

Comparative measurements of the droplet size distribution were also performed for RF-only AMUSE droplets. Figure 3.13 shows these distributions (top) and also shows images of light scattered by spray (bottom) observed for a *50% methanol* solution sprayed using RF-only AMUSE with and without Venturi focusing.

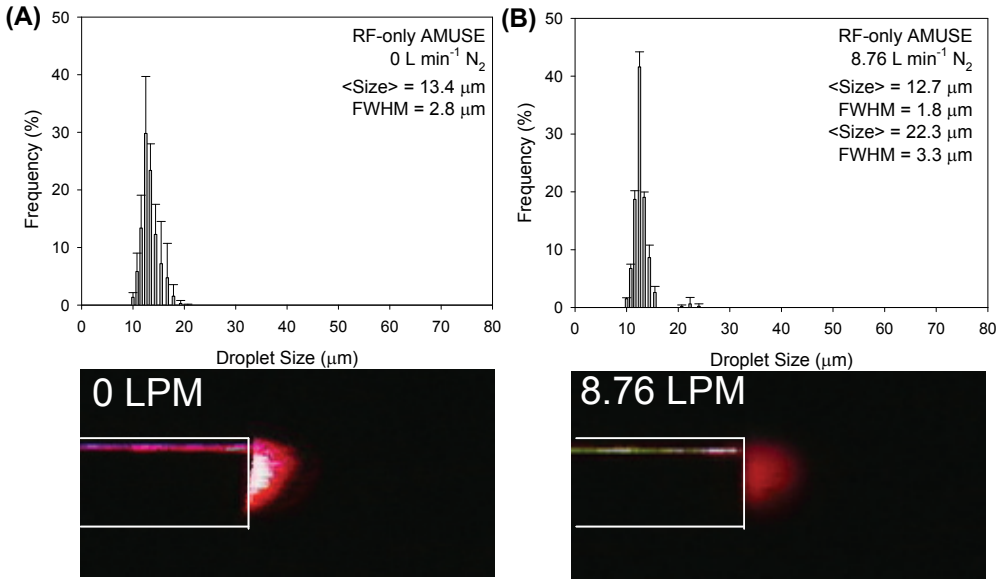

Figure 3.13. Droplet size distributions (top) and images of light scattered by spray (bottom) observed for a *50% methanol* solution sprayed using RF-only AMUSE without Venturi focusing (A) or with 8.76 L min^{-1} N_2 (B).

The mean diameter and FWHM of droplets produced by RF-only AMUSE (Fig. 3.13.A) without Venturi-assisted transmission were 13.4 μm and 2.8 μm, respectively, with a tail reaching values as high as 20 μm. Since upon ejection AMUSE-generated droplets have uniform size of 5-7 μm (defined by the nozzle aperture),[132] this increase in the mean diameter suggests droplet coalescence during transport to the MS inlet capillary. These larger droplets could be responsible for the lower <E> observed in Figure 3.11.A. The mean droplet diameter and FWHM decreased to 12.7 μm and 1.8 μm when 8.76 L min^{-1} N_2 was flowed through the Venturi device (Fig. 3.13.B) with a concomitant increase in <E> (Fig. 3.11.B). The intensity of scattered light increased for ESI upon use of the Venturi device (Fig. 3.12 A and B, lower panels), following the creation of a spatially-concentrated population of smaller droplets. The scattering intensity correlates with the total number of scatterers/droplets per unit volume and

relative size of the droplets as compared to the wavelength of light. For RF-only AMUSE, the intensity of light scattered by the spray (Fig. 3.13 C and D, lower panels) was reduced when N_2 was flowed through the Venturi device, suggesting that desolvation is enhanced by the Venturi device.

To investigate the behavior of Venturi-assisted AMUSE and ESI with solvent systems that are more compatible with biological species, the previous experiments were repeated using pure water solutions. The mass spectra obtained for ESI, RF-only AMUSE, and DC-AMUSE ionization of an *aqueous* 5 μM mixture of thermometer molecules, with and without the use of ambient N_2 flowing through the Venturi device, are shown in Figure 3.14 while the corresponding IE distributions are shown in Figure 3.15.

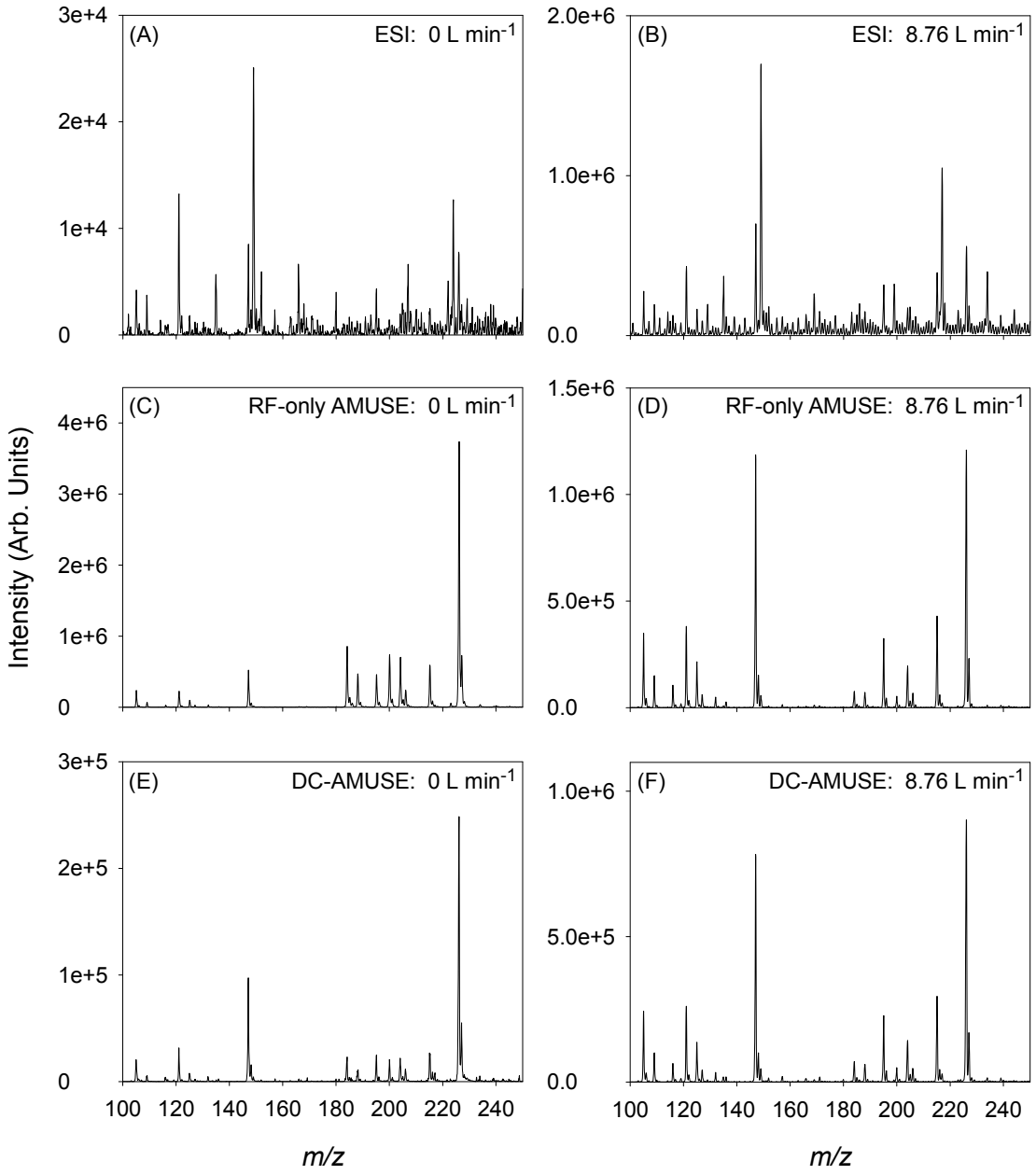

Figure 3.14. Mass spectra for ESI (A and B), RF-only AMUSE (C and D), and DC-AMUSE (E and F) ionization of an *aqueous* 5 μM mixture without Venturi focusing (A, C, and E) or with 8.76 L min^{-1} N_2 (B, D, and F). Operating conditions: TL = 40 V, 300 ºC capillary.

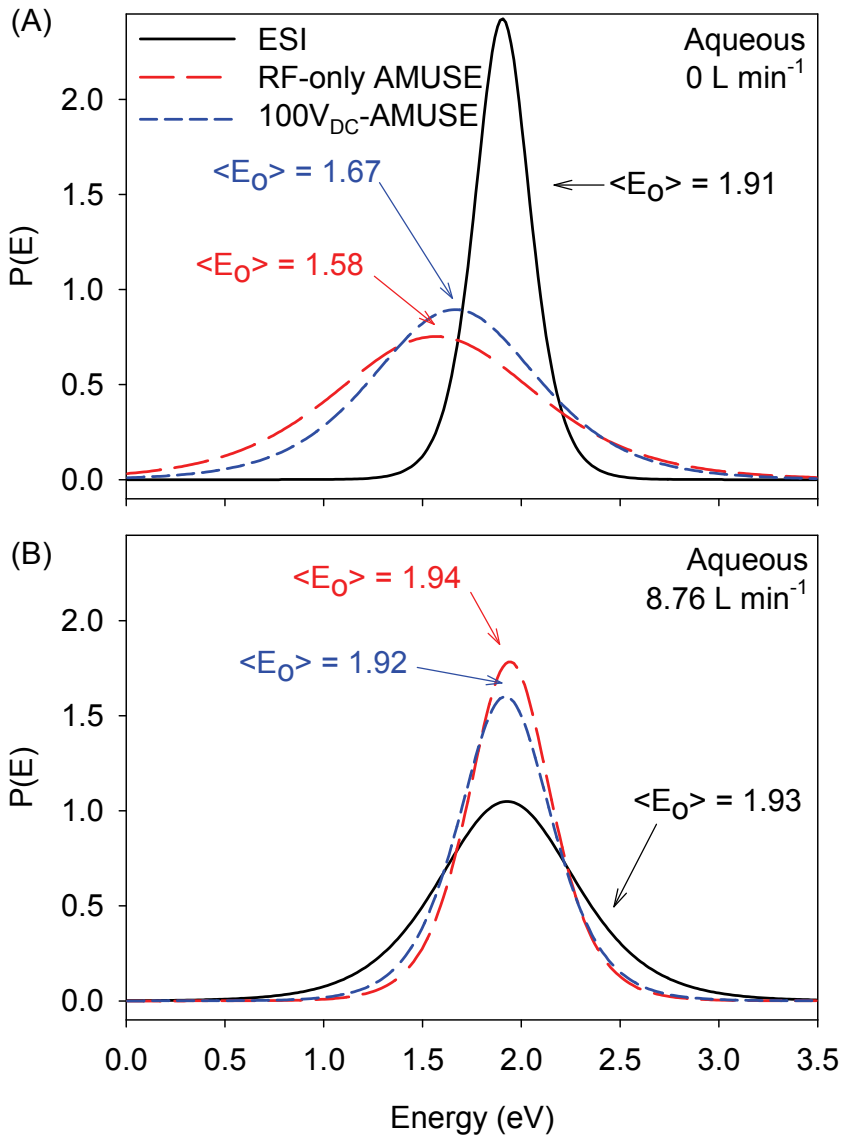

Figure 3.15. P(E) curves for ESI, RF-only AMUSE, and DC-AMUSE ionization of an *aqueous* 5 µM mixture without Venturi focusing (A) or with 8.76 L min^{-1} N_2 (B). Operating conditions: TL = 40 V, 300 ºC capillary.

Comparison of the P(E) curves shown in panels 3.11.A vs. 3.15.C and 3.11.B vs. 3.15.D shows that <E> for aqueous ESI, RF-only AMUSE and DC-AMUSE were within 5% of the values obtained using a 50% methanol solution. The slightly higher <E> observed for DC-AMUSE, relative to that for RF-only AMUSE, when operating in non-

Venturi mode (3.11.A and 3.15.C) can be attributed to decreased mass transfer caused by the buildup of liquid on the external surface of the ejector nozzle array, possibly due to electrowetting.[258] This led to significant variations in the ejection flow rate due to sporadic blockage of ejector orifices and thus experiments using this approach were not further pursued. An investigation of the effect of functionalizing the ejector nozzle array to increase the hydrophobicity of the surface is discussed in section 4.4.

The most salient difference upon changing the solvent system was the 0.5 eV increase in FWHM of the P(E) curve for Venturi-assisted ESI (3.11.B vs. 3.15.D). The explanation of this observation is not straightforward. This is possibly caused by a decreased evaporative droplet cooling rate,[259] or variations in the droplet size distribution upon changing the solvent composition. There has been only one report on the influence of solvent composition on P(E) curves for electrosprayed droplets. These studies showed a shift to higher <E> and wider P(E) curves when less volatile solvents with lower vapor pressures are used.[249] However, this is not an obvious result of general value, as although less volatile solvents do indeed evaporate at the lower rates, their latent heat of vaporization is generally much higher and thus they are capable of inducing more significant sub-cooling. Figure 3.16 shows droplet size distributions measured for droplets produced from an *aqueous* solution using ESI with and without Venturi focusing.

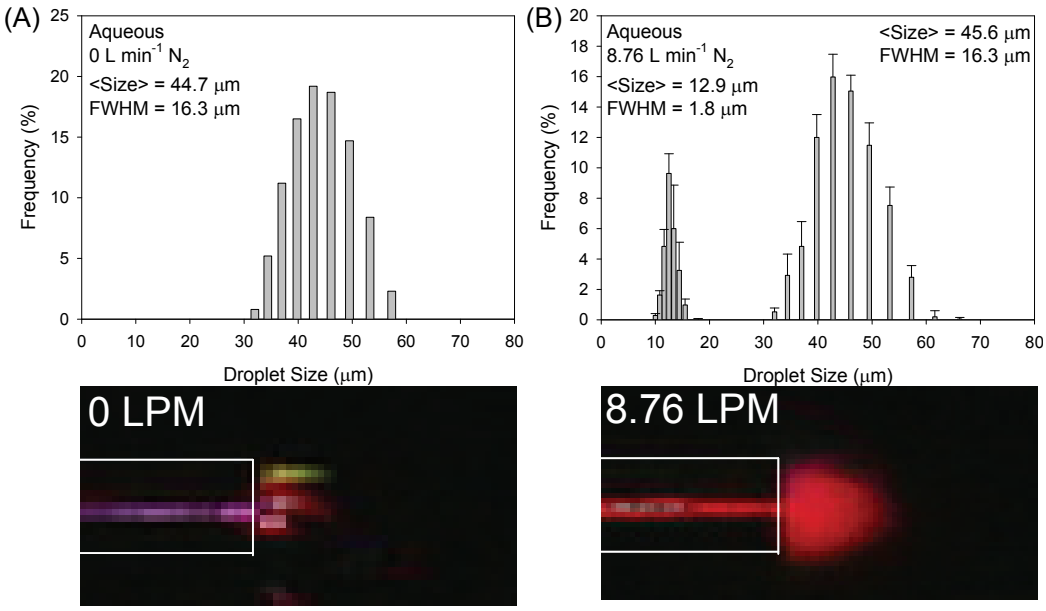

Figure 3.16. Droplet size distributions (top) and images of light scattered by spray (bottom) observed for an *aqueous* 5 μM mixture sprayed using ESI without Venturi focusing (A) or with 8.76 L min^{-1} N_2 (B). (The white box in the images outlines the edge of the Venturi device.)

Without Venturi focusing, a wide droplet size distribution having a mean droplet diameter of 44.7 μm and FWHM of 16.3 μm was observed (Fig. 3.16.A). However, when Venturi focusing was utilized, bi-modal behavior leading to two distinct droplet size distributions was observed (Fig. 3.16.B) The smaller-size population showed a mean droplet diameter and FWHM of 12.9 μm and 1.8 μm, respectively, while the more abundant population overlaps with the distribution measured without Venturi assistance. The presence of these multiple droplet size populations may also explain the broader P(E) observed for ESI (Fig. 3.15.D) as Gabelica et al. showed that there is a direct correlation between desolvation efficiency, as inefficient desolvation leads to multiple droplet populations in varying stages of desolvation, and the shape of P(E).[247] The lower desolvation efficiency observed for aqueous ESI is also reflected by the increase in

scattered light intensity (Fig. 3.12.B vs. 3.16.B, lower panels), indicative of the presence of a higher volume concentration of droplets. The droplet size distributions and scattered light intensities obtained for RF-only AMUSE ionization of an aqueous solution (Fig. 3.17) were found to be similar to those obtained for the methanolic solution. The focus of all further experiments was on measuring the effect of the API capillary temperature and N_2 flow rate on the IE landscapes of ESI and RF-only AMUSE.

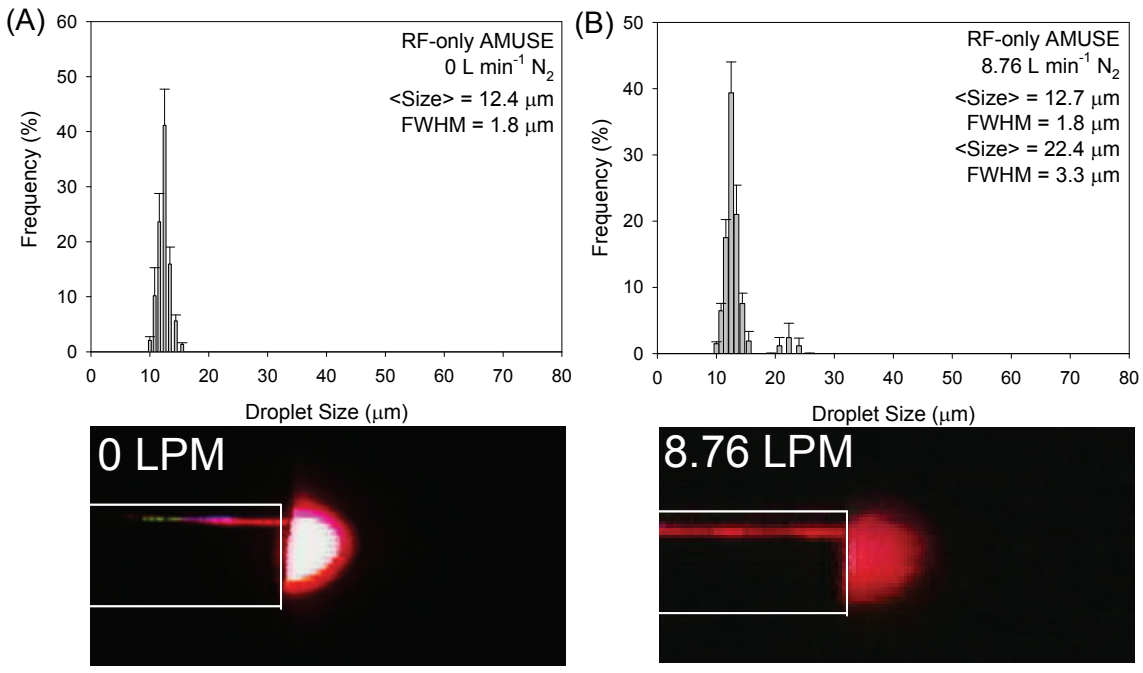

Figure 3.17. Droplet size distributions (top) and images of light scattered by spray (bottom) for an *aqueous* 5 μM mixture sprayed using RF-only AMUSE without Venturi focusing (A) or with 8.76 L min^{-1} N_2 (B). (The white box in the images outlines the edge of the Venturi device.)

3.8. Influence of Capillary Temperature and Venturi Device Flow Rate on IE Deposition

Recent experiments by Dixon et al.[217] indicated that the use of a Venturi device in combination with ESI provides both a focusing effect and improved droplet desolvation. Varying the Venturi gas flow rate provides control over both the desolvation efficiency and the aerodynamic focusing of the droplets, which results in improved ion transport. These two effects are strongly coupled and are expected to influence both P(E) and S/N as demonstrated by the work of Drahos and co-workers, who showed that for quadrupole and Fourier Transform mass spectrometers operated at various ion source temperatures (25-150 °C), P(E) of ESI ions can be approximated by a Boltzmann distribution with different characteristic temperatures.[251] For capillary temperatures of 50 – 75 °C, Gabelica et al. have shown that P(E) curves exhibit a low energy tail, indicating the presence of partially-solvated ions reaching the capillary-skimmer region of the mass spectrometer.[247]

These previous reports prompted us to perform additional experiments to determine the combined effect of the API capillary temperature and N_2 flow rates on the IE deposited by Venturi-assisted ESI and AMUSE and to explore the IE landscapes of these techniques. Figure 3.18 shows a 3D surface plot of <E> for ions produced by Venturi-assisted ESI (3.18.A) or RF-only AMUSE (3.18.B) vs. capillary temperature and N_2 flow rate.

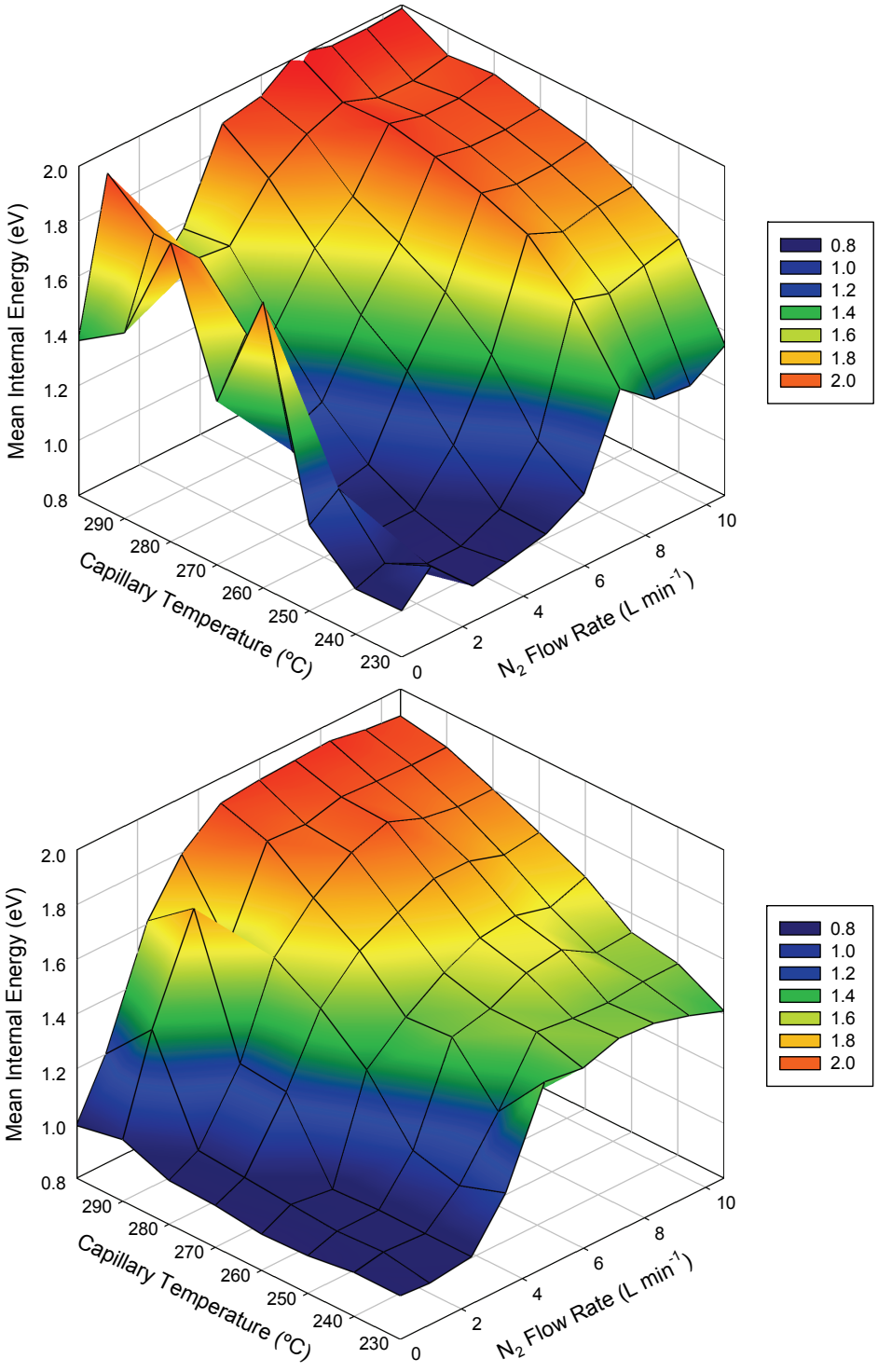

Figure 3.18. <E> deposited on ions produced from an aqueous 5 µM mixture using (A) ESI or (B) RF-only AMUSE at capillary temperatures ranging from 230 – 300 ºC and N_2 flow rates from 0 – 10.6 L min^{-1}. Operating conditions: TL = 30V.

The overall shape of these surfaces differs in several aspects. Venturi-assisted ESI is characterized by the presence of a low-IE (<E> < 1.5 eV) valley in the regime map, occurring at conditions with capillary temperatures of 230 – 275 °C and N_2 flow rates between 0 – 7 L min^{-1}. A region with <E> ≤ 1.0 eV was present at capillary temperatures up to 250 ºC and N_2 flow rates between 2 – 4 L min^{-1}. The RF-only AMUSE landscape was characterized by a low IE (<E> < 1.5eV) region present at all capillary temperatures tested with N_2 flow rates up to 5 L min^{-1}. A region with <E> ≤ 1.0 eV was present at capillary temperatures up to 280 ºC and N_2 flow rates up to 2.5 L min^{-1}. Ions with <E> < 1.5 eV were obtained in 42% of the conditions tested by ESI and in 46% of conditions tested by RF-only AMUSE. Ions with <E> ≤ 1.0 eV were obtained in 9 and 13% of conditions tested by ESI and RF-only AMUSE, respectively. The average <E> obtained by RF-only AMUSE was 7% lower than that obtained by ESI under all conditions examined.

The shape of the ESI landscape implies that ions of high IE can be produced at either high capillary temperatures *or* high N_2 flow rates. The fact that flow rates between 7 – 10 L min^{-1} also result in ions with higher mean IE, even for capillary temperatures as low as 250 °C, is inherently related to the decrease in residence time as the flow rate of N_2 is increased. Shortening the droplet/ion residence time causes a reduction in evaporative cooling, and thus leads to a higher IE. The characteristic droplet temperature[251] increases with increasing droplet velocity resulting in ions being ejected with higher internal energies. Interestingly, at low N_2 flow rates and high capillary temperatures, a region of high IE ESI ions is also observed. In this case, the sensible heat

convectively transferred to the droplets during their transit in the heated capillary seems to be sufficient to significantly elevate the ion's IE.

The generation of AMUSE ions with high <E> requires conditions combining both high temperatures *and* high flow rates. Because of the different principle used for liquid atomization in AMUSE, the droplets produced are uniform in size,[132] even at the extremes of Venturi device flow rates (Fig. 3.13 and 3.17). These droplets are also expected to have lower charge density due to the lower charging potential effectively applied to the liquid reservoir during each RF half-period, resulting in lower Coulombic explosion rates. This translates into larger AMUSE droplets surviving longer within the heated capillary. The increase in <E> measured for AMUSE ionization can be attributed to: (1) the increase in capillary temperature resulting in an equivalent increase in the rate of convective heat transfer to the droplet in combination with (2) the increase in flow rate resulting in an increase in the convective heat transfer coefficient, which in turns results in increased sensible heat transfer to the droplets. At high flow rates but lower capillary temperatures, the energy transferred at the API inlet results in ions with intermediate <E>.

3.9. Comparison of Spectral Quality Under High– and Low-IE Deposition Conditions

An investigation of the S/N of ions produced by Venturi-assisted ESI and RF-only AMUSE at the upper and lower limits of the sampled capillary temperatures was also performed. The *p*-CH_3-substituted thermometer compound was selected for this experiment as it has the second lowest critical energy of the compounds tested and can be

easily fragmented while still providing a measurable signal for the intact ion (*m/z* 184). The S/N for this ion at increasing N_2 flow rates and capillary temperatures of 230 °C (Fig. 3.19.A) and 300 °C (Fig. 3.19.B) is presented in Figure 3.19.

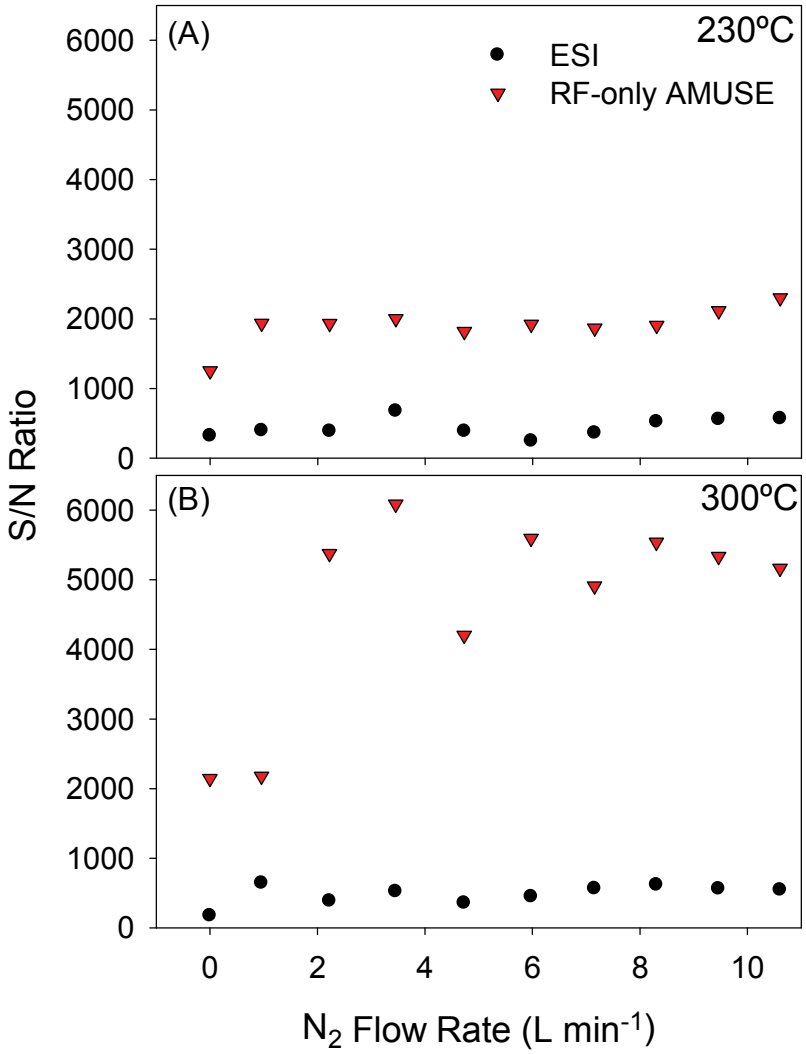

Figure 3.19. S/N of *m/z* 184 peak (precursor of *p*-CH_3 compound) for Venturi-assisted ESI and RF-only AMUSE ionization of a 5 µM aqueous mixture at flow rates ranging from 0 – 10.6 L min^{-1} N_2 and capillary temperatures of (A) 230 ºC or (B) 300 ºC. TL = 30 V for all experiments.

Examination of the ESI energy landscape (Fig. 3.18.A) at 230 °C suggests that the S/N of the intact ion should be relatively constant at most of the flow rates tested and should have a maximum value that corresponds to the flow rates which provide the minimum <E> (2 – 5 L min^{-1}). The observed S/N values appear to follow this trend reasonably well, with a maximum S/N observed between 4 – 6 L min^{-1}. The S/N obtained by AMUSE ionization at 230 °C increases with flow rates up to 2.5 L min^{-1} where it levels off. This correlates well with the AMUSE energy landscape (Fig. 3.18.B).

The differences in S/N observed for ESI and RF-only AMUSE cannot be solely explained by examination of their respective IE landscapes, but also requires consideration of the differences in spray divergence and electrochemical processes between these two methods. ESI droplets have a significantly higher charge density than AMUSE droplets and thus experience a greater degree of spray divergence. Therefore, Venturi focusing of this highly-divergent ESI plume produces a significant increase in the analyte signal intensity, as observed in the mass spectrum in Figure 3.14 A vs. B. This was not observed in the matching AMUSE mass spectra (Figure 3.14 C vs. D) due to the concomitant increase in IE deposition, which resulted in a reduction of the absolute intensity of the CH_3 precursor ion peak. Although the analyte signal intensity was higher in the ESI mass spectra, the background noise was also higher as a result of the high potential applied to the ESI sprayer which causes an increase in the rate of solvent oxidation processes[54] and also leads to ionization of volatile contaminants present in the laboratory air.[55] This is apparent upon inspection of the baseline noise in the mass spectra shown in Figures 3.10 and 3.14. In other words, although the analyte signal intensity in the AMUSE mass spectra was not as high as those for ESI, the reduction in background

signal in the AMUSE spectra resulted in a lower S/N for ESI at all assayed Venturi gas flow rates.

An examination of the S/N when the capillary is kept at 300 °C (Fig. 3.19.B) shows that the S/N for both ionization methods also correlates well with the trends suggested by their respective IE landscapes (Fig. 3.18). The ESI S/N has a local maximum between 1 and 3.5 L min^{-1} which levels off at higher flow rates while the AMUSE S/N decreases sharply as the flow rate is increased up to 3.5 L min^{-1} and exhibits a slower decrease at higher flow rates. The average S/N obtained using AMUSE ionization was five times higher using a capillary temperature of 230 ºC and eight times higher than that of ESI at 300 ºC.

3.10. Conclusion

We have shown that AMUSE ionization without Venturi assistance is inherently softer than ESI with a <E> that is 39% lower. AMUSE IE deposition was significantly modified by increasing the Venturi device gas flow rate, but a less marked effect was observed for ESI. Modulation of P(E) was accomplished by tuning the Venturi device N_2 gas flow rate and the API capillary temperature, as these parameters most strongly influence desolvation and droplet residence times. Examination of the energy landscapes obtained demonstrated that ions with <E> < 1.5 eV could be obtained using 46% of the conditions tested during RF-only AMUSE ionization compared to 42% of those tested during ESI. A low IE region (<E> ≤ 1 eV) was observed at capillary temperatures up to 250 ºC and N_2 flow rates between 2 – 4 L min^{-1} for ESI and at capillary temperatures up to 280 ºC and N_2 flow rates up to 2.5 L min^{-1} for AMUSE. Finally, it was shown that at

all N_2 gas flow rates tested, the average S/N of the intact *p*-CH_3-substituted thermometer ion by AMUSE was five times higher than ESI at 230 ºC and eight times higher at 300 ºC due to the difference in background noise observed between AMUSE and ESI spectra.

CHAPTER 4. TOWARDS AN EFFICIENT LC-MS COUPLING USING THE AMUSE ION SOURCE

4.1. Abstract

In this chapter, proof-of-principle results on the coupling of LC to MS via an AMUSE ion source are presented for the analysis of calpain inhibitors. A brief introduction to LC-MS, with an emphasis on the criteria required for optimum interfacing, is provided. Efforts to improve MS signal stability of the AMUSE by silanizing the ejector array are discussed in detail, concluding with results that demonstrate the first coupling of LC with AMUSE.

4.2. The Ideal LC-MS Interface

This chapter discusses the challenges for coupling LC to AMUSE with regards to long term stability of ejection and fidelity in reproducing the analytical pulse. As such, it would be beneficial to define a list of features that would be desired in the ideal LC-MS interface.[260, 261] (1) The interface must be tolerant to different solvent systems (including programmed solvent gradients and additives) and (2) varying flow conditions. (3) The ion yield must be high to provide good detection limits and (4) should be constant and independent of the nature and concentration of the solute while providing (5) high molecular weight detection capabilities. (6) There should be no loss of separation in the interface (i.e. there should be minimal dead volume). In essence, the ideal interface should allow decoupling of mobile phase selection from MS analysis while retaining chromatographic fidelity.

Despite the widespread appeal of pESI, nESI, and APCI for coupling LC with MS, none of these ionization techniques meet all of the criteria for an ideal LC-MS interface. AMUSE ionization has the potential to meet several of the aforementioned criteria. Since droplet ejection is primarily dependent on the resonant frequency of the reservoir,[130] AMUSE ionization is amenable to a wide variety of solvent systems including those with variable solvent composition (gradient elution) and containing additives such as acids, bases, or buffers. AMUSE ion yields using 2nd generation arrays are high with detection limits per nozzle that are on par with those of other spray-based techniques (section 3.2.2). Furthermore, the analysis of cytochrome C (section 2.7) demonstrated the wide mass range of compounds accessible to AMUSE ionization. Although it is likely that the AMUSE technique does show some dependence on the nature of the solute (as evident in the differing MS signal intensities observed for mass spectra of the thermometer compounds due to their varying hydrophobicities), ionization suppression effects as a result of charge or space competition have not yet been observed.

Long-term stability of AMUSE signal is highly affected by electrowetting of the surface. Karger and coworkers coated the outlet edge of their multichannel microchip for ESI-MS with a hydrophobic reagent to minimize electrowetting of their device.[93, 94] This strategy was implemented with AMUSE to improve signal stability, particularly when operating in DC-AMUSE mode. A detailed investigation of the effect of silanizing the array is presented here. To assess the analytical performance of LC-AMUSE-MS for potential "real-life" quantitation applications, experiments were performed using a candidate drug synthesized by Dr. Zhaozhao Li in the research group of Dr. James C. Powers at the Georgia Institute of Technology.[262] This drug, benzyloxycarbonyl-leucine-

4-aminobutyric acid-CONH-$(CH_2)_3$-4-morpholinyl (AK-295) has been shown to inhibit the activation of calpains, calcium dependent enzymes that play a role in initiating neuronal degeneration.[263] Quantitation of AK-295 was performed using an internal standard (ISTD), benzyloxycarbonyl-leucine-norvaline-CONH-$(CH_2)_3$-4-morpholinyl (ZLAK-74). ZLAK-74, an analog having a similar molecular weight and structure as AK-295 but which does not exhibit significant calpain inhibition, was added early in the sample preparation process to account for variation in LC-MS performance. Figure 4.1 shows the chemical structures of these drugs.

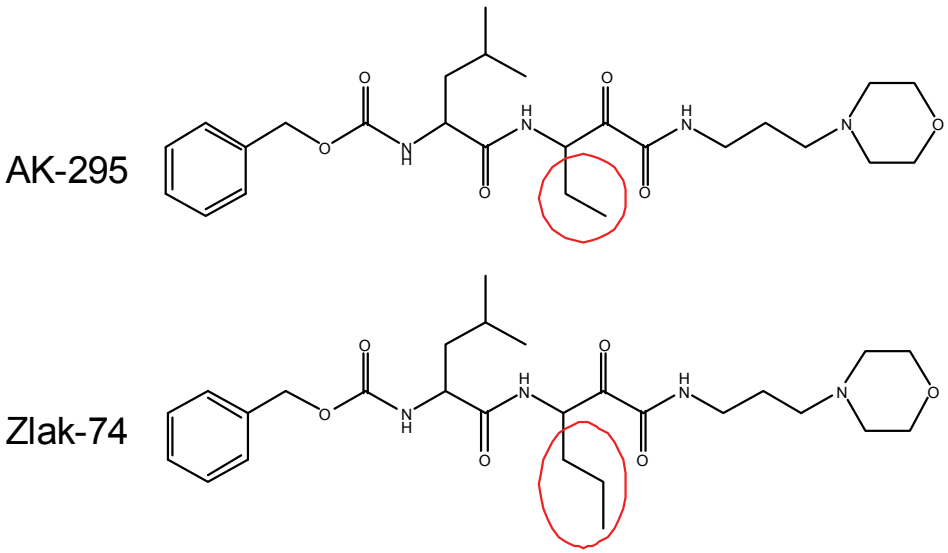

Figure 4.1. Structures of AK-295 and ZLAK-74. The main structural difference is indicated by a red circle.

4.3. Experimental Details

4.3.1. Materials

ACS-grade acetone and HPLC-grade acetonitrile, methanol, and ethanol were purchased from EMD Chemicals, Inc. (Gibbstown, NJ). ACS-grade sulfuric acid and

hydrogen peroxide (30% by weight) were purchased from Mallinckrodt (Phillipsburg, NJ). Anhydrous dichloromethane, HPLC-grade chloroform (Burdick and Jackson Morristown, NJ), *n*-hexadecane, *n*-octadecyltrichlorosilane (OTS) containing 5% branched isomers (Alfa Aesar, Ward Hill, MA), formic acid (88% by weight, Fisher Scientific, Hampton, NH), 99.9% glacial acetic acid (Sigma Aldrich, St. Louis, MO), and YGGFL (American Peptide, Sunnyvale, CA) were purchased and used without additional purification.

Stock solutions of AK-295 and ZLAK-74 prepared by dissolving 1 mg of each compound in methanol (1mg/mL) were pipetted into centrifuge vials in 50 μL aliquots and stored at -80ºC until needed.

4.3.2. AMUSE Array Silanization

Fabrication of the 2nd generation 20x20 array of 5-μm nozzles in silicon was accomplished as described in section 2.2.2. To improve AMUSE signal stability, the nozzle-side of the ejector array was functionalized with silane groups using a procedure based on that reported by Graham and coworkers.[220] Optimization of the silanization protocol for use with a newly-fabricated ejector array is depicted in Figure 4.2.

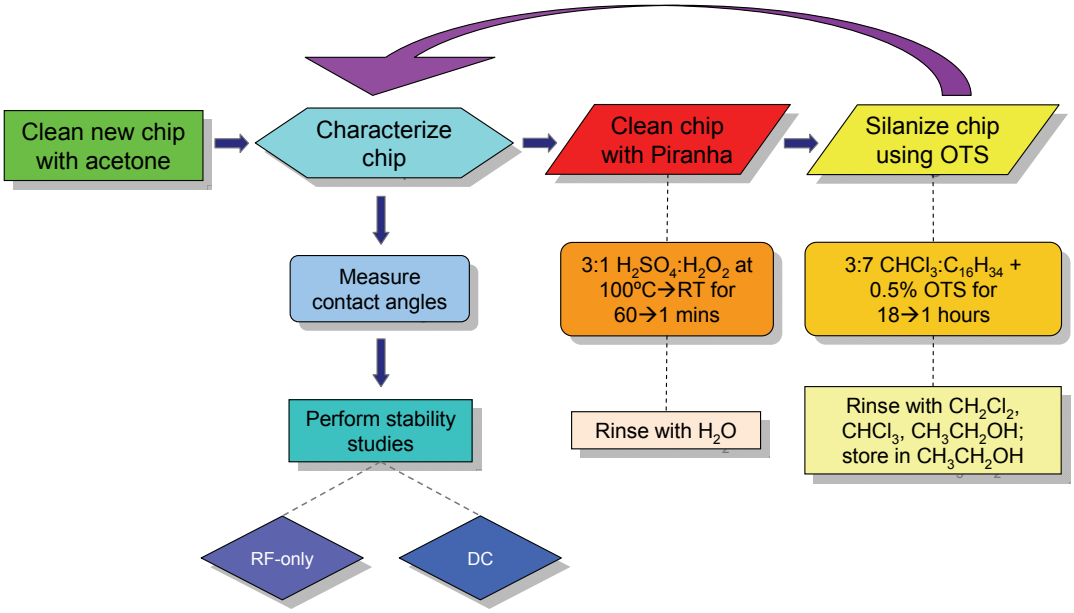

Figure 4.2. Workflow describing optimization of the silanization protocol via iterative characterization and reaction steps. Original protocol used was described by Graham and coworkers[220] and included a cleaning step in piranha solution at 100 ºC for 60 minutes and silanization for 18 hours. After optimization, room temperature piranha was used for 1 minute to clean the array and silanization was completed in 1 hour.

Upon arrival, the ejector array was rinsed with acetone to remove residual organic contaminants from the surface and dried using a low flow of industrial grade N_2. The array was then characterized to determine its average contact angle (see section 4.3.3) and to assess the stability of MS signal produced in each operational mode (RF-only AMUSE and DC-AMUSE as described in section 2.3.3). After characterization the array was cleaned and functionalized using the original protocol reported by Graham et al.[220] First, the array was immersed in 100 ºC piranha solution (3:1 sulfuric acid:hydrogen peroxide) for 60 minutes to remove organic contaminants and to promote hydroxylation of the surface. The array was removed from the piranha solution using Teflon tweezers rinsed twice with water, dried under N_2, and placed in a Teflon vessel with the nozzle-side facing upwards. To initiate silanization, 25 mL *n*-hexadecane and 10 mL chloroform

were added to the vessel followed by 175 μL OTS which was added under a stream of N_2. The vessel was immediately capped and placed into an enclosure with desiccant to reduce the probability of silane polymerization occurring as a result of the presence of excess moisture.[264] After 18 hours, the array was removed from the mixture and examined. Visual inspection of the array after completion of the protocol revealed that the tungsten oxide layer had been stripped from the surface. It was speculated that this was due to the relatively harsh cleaning conditions used during the piranha clean; thus, room temperature piranha was used instead but led to the same result. The optimal time for cleaning 2nd generation arrays (1 minute) was determined by immersing fragments of unusable 2nd generation arrays in piranha solution for successively shorter times. These fragments were also used to optimize the time required for the silanization reaction, which was ultimately reduced from 18 hours to 1 hour as shown in Figure 4.2.

4.3.3. Contact Angle Measurement

The change in hydrophobicity of the ejector array upon silanization was quantified by measuring the water contact angle (θ, Fig. 4.3.A) at nine different positions along the nozzle-side of the array (Fig. 4.3.B). Text indicating the orifice diameter etched onto a corner of each array during fabrication was used to ensure that the orientation of the array was consistent. All measurements were made using a goniometer assembled by Jenny Raynor from the research group of Dr. David Collard (Fig. 4.3.C).

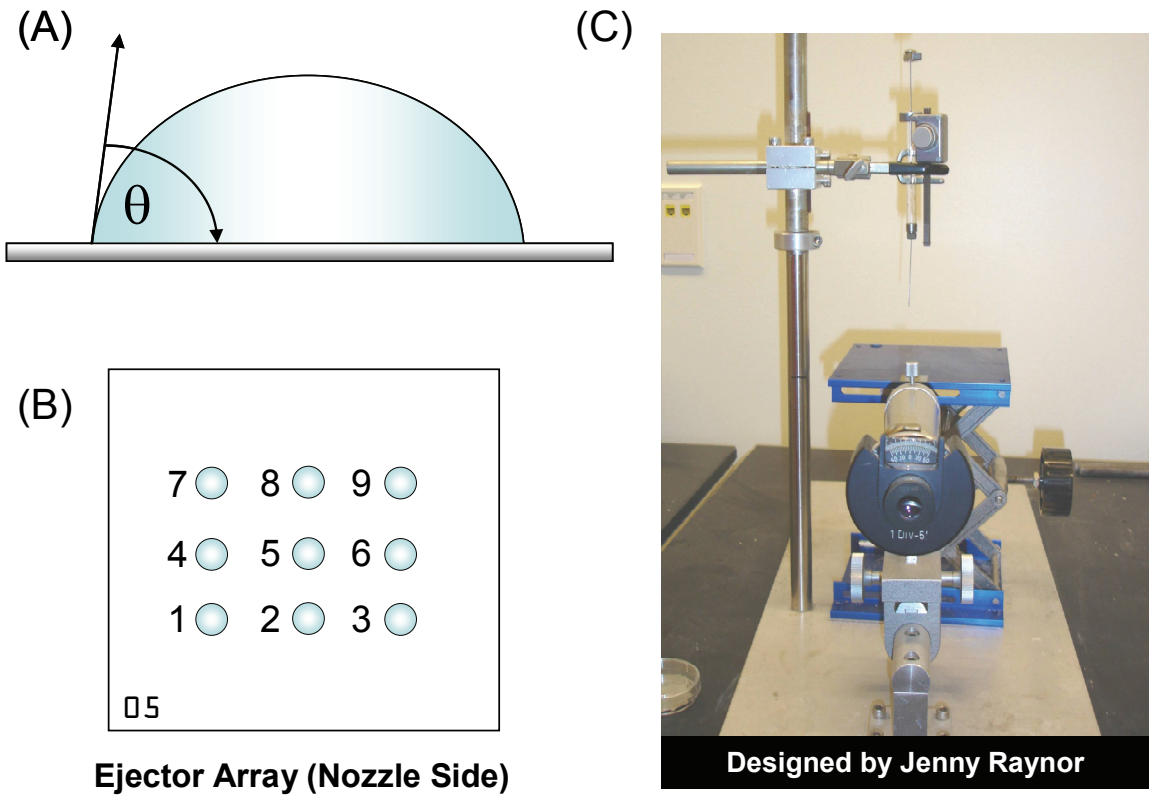

Figure 4.3. The water contact angle (A) was measured at nine positions on the nozzle side of the ejector array (B) using a goniometer assembled by Jenny Raynor (C).

For contact angle measurements, a 2-μL drop of nanopure water was suspended from a 10-μL syringe. The ejector array was placed on a jack that was raised until the suspended droplet was transferred to the chosen position on the array and the jack was lowered until the droplet was visible through the goniometer eyepiece. The cross-hairs in the eyepiece were aligned with the vertex of the contact angle and the eyepiece was rotated until the vertical cross-hair fell on the tangent with the droplet edge. The angular displacement of the vertical cross-hair, which was designated as 0º, was read from the scale on the eyepiece and the contact angle was calculated by adding this angular displacement to 90 (for $\theta > 90$ºC) or subtracting from 90 (for $\theta < 90$º). Triplicate

measurements were made at both sides of the droplet for all nine positions on the array. These measurements were performed in duplicate with a fresh drop deposited at each position and the average contact angle calculated.

4.3.4. AMUSE MS Signal Stability Studies

Stability studies were performed by continuously pumping a 5 μM solution of YGGFL prepared in nanopure water (18 MΩ cm^{-1}, Barnstead International, Dubuque, IA) containing 0.1% (v/v) glacial acetic acid into the AMUSE using a liquid handling pump. The optimal liquid flow rate for the array used in these studies, as determined using the method described in section 2.3.3, was 80 μL min^{-1}. Optimal settings for the ion optics and mass analyzer settings of the QiT were determined by tuning with the commercial pESI source installed on the front end. The capillary was set to 30 V and held at 300 ºC with TL = 10 V for all experiments. Experiments were performed in the RF-only AMUSE and DC-AMUSE operational modes using a 910 kHz sine wave amplified to 33 V_{RMS} for ejection in both modes and an applied potential of 100 V_{DC} in DC-AMUSE mode. The AMUSE was positioned 4 mm from the Venturi device inlet. The Venturi device outlet was flush with the QiT capillary inlet and 8.76 L min^{-1} N_2 was used to sustain the Venturi focusing effect.

4.3.5. LC-MS Operation

For LC-MS experiments, a series of calibration standards containing AK-295 (0 - 5 μM) and ZLAK-74 (1 μM, internal standard) were prepared in 30:69.9:0.1 (v/v) acetonitrile:nanopure water:formic acid. A commercial pESI source was interfaced to the

QiT mass spectrometer and used to optimize the ion optics and mass analyzer settings to obtain maximum signal intensity for both AK-295 (*m/z* 505.2) and the ISTD (ZLAK-74, *m/z* 519.2). The capillary inlet was set to 34 V and held at 275 ºC with TL = 25 V for all subsequent experiments.

An Agilent 1100 LC system (Agilent, Santa Clara, CA) equipped with a solvent degasser, a binary pump, an autosampler, and a thermostatic column compartment held at 25º was coupled to the QiT using either the commercial pESI ion source or the AMUSE ion source. A 15 μL aliquot of analyte was injected into a Symmetry Shield® reverse phase C18 column (3.5 μm, 1.0 x 150 mm, pore size 100Å; Waters, Milford, MA). The analytical column was preceded by a Zorbax® RX-C18 guard column (5.0 μm, 4.6 mm x 12.5 mm, pore size 2 μm; Agilent). The gradient LC method was optimized to provide high sensitivity for AK-295 and used A = nanopure water + 0.1% formic acid and B = acetonitrile + 0.1% formic acid as the mobile phases. The mobile phase flow rate was set to 80 mL min^{-1} and the following gradient program was used: 0.0 min – 30% B, 0.5 min – 30% B, 0.7 min – 100% B, 9 min – 100% B, 10 min – 30% B. Settings for the Venturi-assisted AMUSE setup were identical to those described in section 4.4.4.

4.4. Effect of Increasing Ejector Array Hydrophobicity on MS Signal Stability

Early experiments demonstrated that ejection stability, particularly when operating in DC-AMUSE mode, was affected by electrowetting of the array surface that sometimes tended to block nozzles and make ejection of droplet streams more difficult (section 3.7). It was speculated that electrowetting might be minimized by increasing the

hydrophobicity of the array surface. Measurement of the water contact angles suggested the existence of zones of varying hydrophobicities along the surface as indicated in Figure 4.4. This figure shows the profile image of the unsilanized array after deposition of water droplets and the contact angles measured at nine different positions on the array.

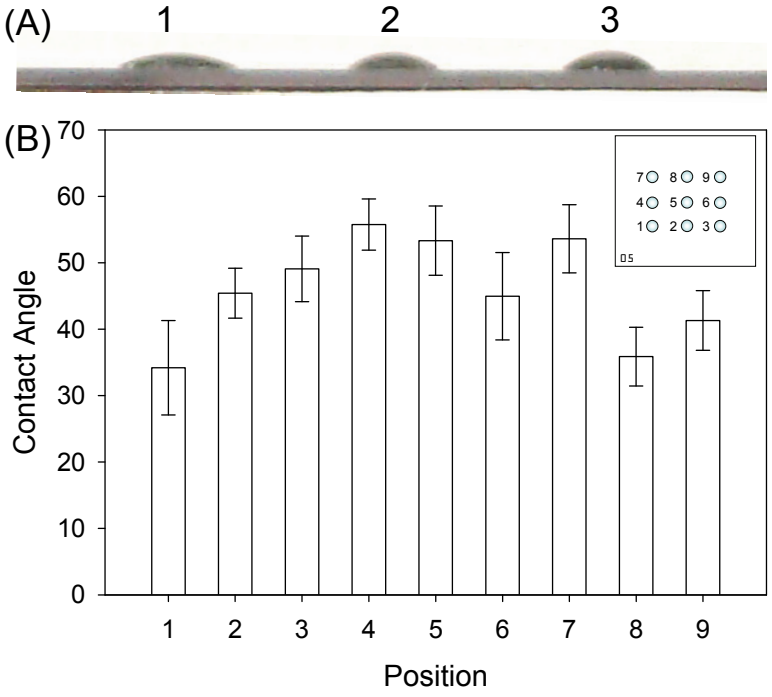

Figure 4.4. Profile image of the *unsilanized* array after deposition of water droplets (A) and contact angles measured prior to functionalization (B). Inset shows position of array corresponding to each measurement.

The average contact angle across the entire surface of the array prior to silanization was 47º ± 9º (mean ± standard deviation) with values ranging from 26º – 62º. Although arrays were cleaned by immersion in acetone and drying under N_2 and were only handled with gloves, it is likely that a large part of the variability in hydrophobicity along the array surface is due to residual contaminants transferred during fabrication and

handling. Microscopic surface defects may also contribute to this variability. Visual inspection of the array immediately after initiating ejection also showed variability in the location of the electrowetted area on the surface for DC-AMUSE which progressively grew over the entire array surface within the first minute. Wetting of the surface in RF-only AMUSE operating mode was also visually observed but to a much lesser extent. An examination of MS signal stability for YGGFL demonstrated that DC-AMUSE was less stable than RF-only AMUSE, probably because of the aforementioned difference in surface electrowetting tendency. Figure 4.5 shows the extracted ion traces for *m/z* = 556.1 ($[M+H]^+$ for YGGFL) corresponding to these two modes.

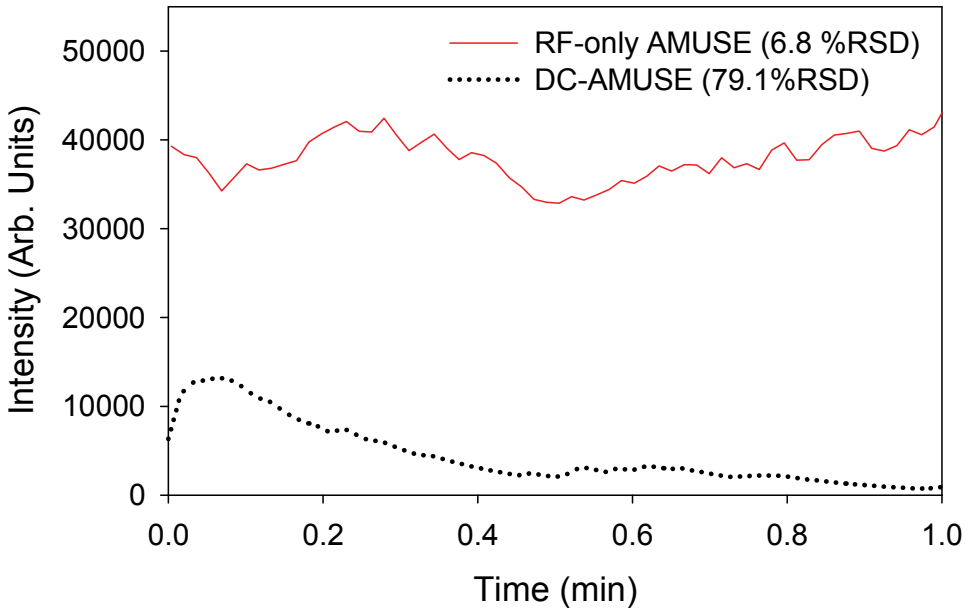

Figure 4.5. Extracted ion trace for $[YGGFL+H]^+$ (*m/z* = 556.1) from YGGFL using an *unsilanized* array with 5-µm nozzles operated in RF-only AMUSE (solid red line) or DC-AMUSE (dotted black line) modes.

Figure 4.6 shows mass spectra corresponding to the ion traces shown in Figure 4.5 also indicating a significant difference in the $[M+H]^+$ peak intensity of YGGFL.

Examination of these spectra provide further evidence of the deleterious effect of electrowetting on the AMUSE analytical performance, particularly when operating in DC-AMUSE operating mode.

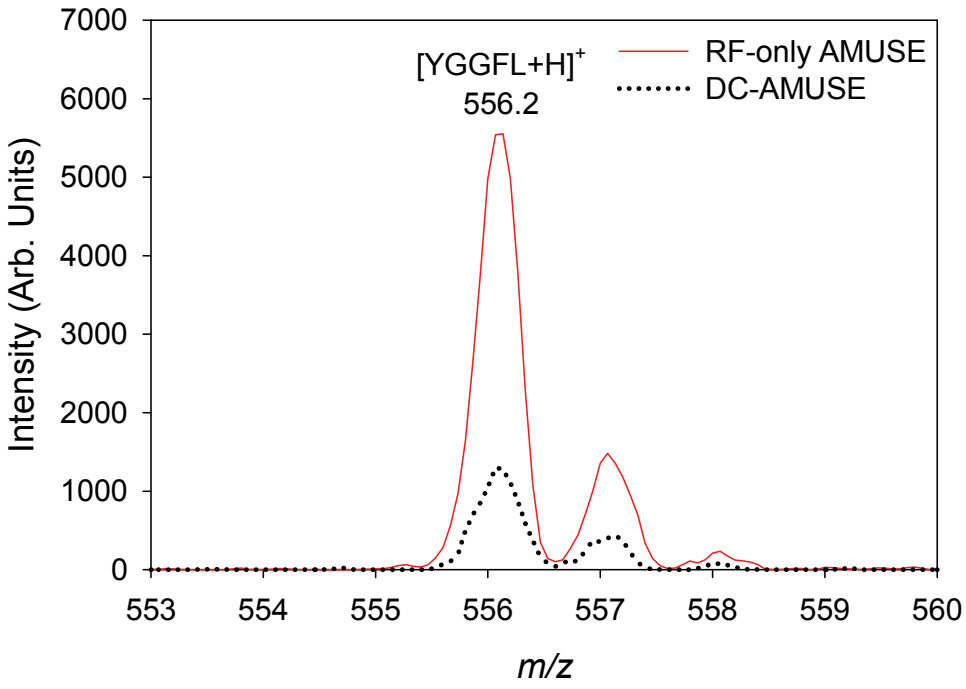

Figure 4.6. Mass spectra corresponding to averaged extracted ion traces shown in Figure 4.5 for an *unsilanized* array with 5-µm nozzles operated in RF-only AMUSE (solid red line) and DC-AMUSE (dotted black line) modes.

A dramatic improvement in long-term signal stability was observed following surface derivatization. After silanization, the average contact angle was observed to increase to 104.2º ± 0.6 º with values ranging from 103.0 – 106.5 º. A profile image of the functionalized array after droplet deposition and the contact angles measured at different positions on the array are shown in Figure 4.7.

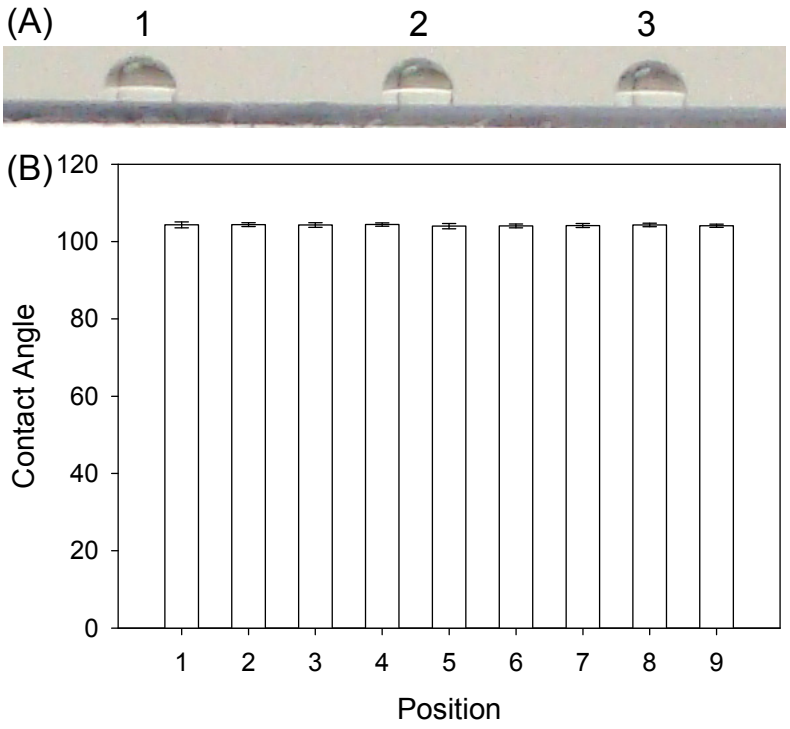

Figure 4.7. Profile image of the *functionalized* array after deposition of water droplets (A) and contact angles measured from a functionalize array (B). Positions match those shown in Figure 4.2.

The most striking difference in the relative hydrophobicity of this array before and after silanization is the improvement in hydrophobicity homogeneity across the surface. This can be attributed to the more rigorous cleaning provided by immersion in piranha solution immediately prior to silanization, which removes surface contaminants. Deposition of OTS on the array surface may have also mitigated the effect of microscopic surface defects, as these are probably covered by the silane layer(s). The MS signal stability observed for silanized arrays is presented in Figure 4.8.

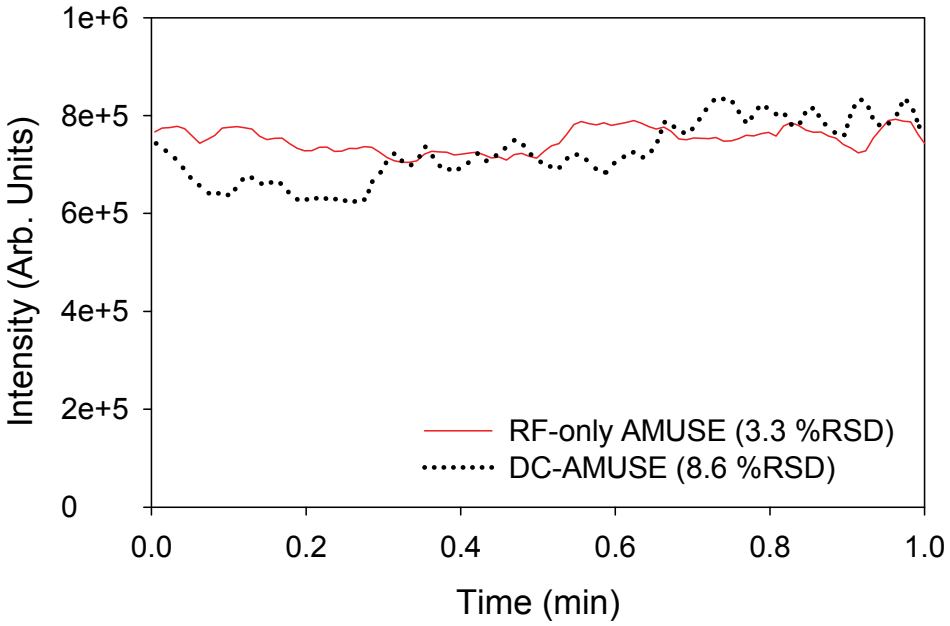

Figure 4.8. Extracted ion trace for $[YGGFL+H]^+$ using a *functionalized* array with 5-μm nozzles operated in RF-only AMUSE (solid red line) and DC-AMUSE (dotted black line) modes.

Functionalizing the array surface had a positive effect on the MS signal stability for both RF-only AMUSE and DC-AMUSE as indicated by the low %RSDs in the signals, 3.3% and 8.6%, respectively, obtained for ejection over the course of 1 minute. Clearly, reducing the wettability of the array surface by increasing the surface hydrophobicity minimized the effect of electrowetting and provided a significant improvement in DC-AMUSE signal stability with an 89% improvement in %RSD. The 51% improvement in %RSD for RF-only AMUSE signal can also be attributed to a reduction in electrowetting also occurring in RF-only AMUSE, but to a much lower extent due to the lower potential applied. Silanization resulted in a 2-fold increase in signal intensity for RF-only AMUSE and a 10-fold increase for DC-AMUSE, as shown

in Figure 4.9. Silanization of the array surface also enabled the collection of nearly identical RF-only AMUSE and DC-AMUSE mass spectra.

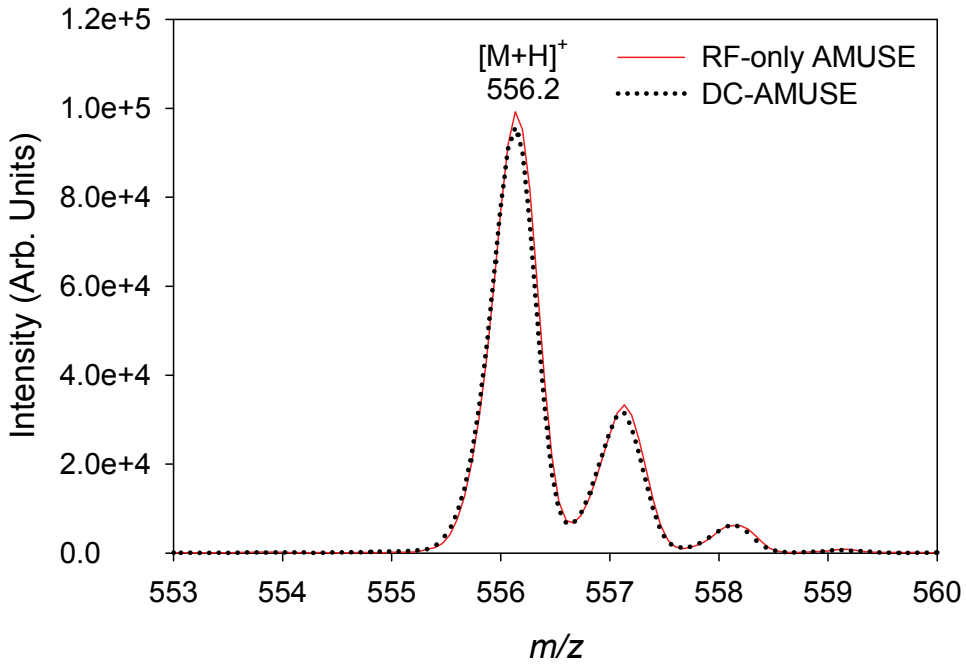

Figure 4.9. Mass spectra corresponding to extracted ion traces presented in Figure 4.8 for a *functionalized* array with 5-µm nozzles operated in RF-only AMUSE (red) and DC-AMUSE (black) modes.

4.5. LC-AMUSE-MS of AK-295

As a first step in using AMUSE in "real-life" applications, quantitation of candidate drugs for the treatment of peripheral neuropathy and chemotherapy-induced axonal damage by LC-MS was investigated using AMUSE as the chosen ion generation technique. These studies involved AK-295 (analyte) and ZLAK-74 (ISTD), as described in section 4.2. Figure 4.10 shows a mass spectrum for an equimolar solution of these two drug candidates obtained using RF-only AMUSE mode.

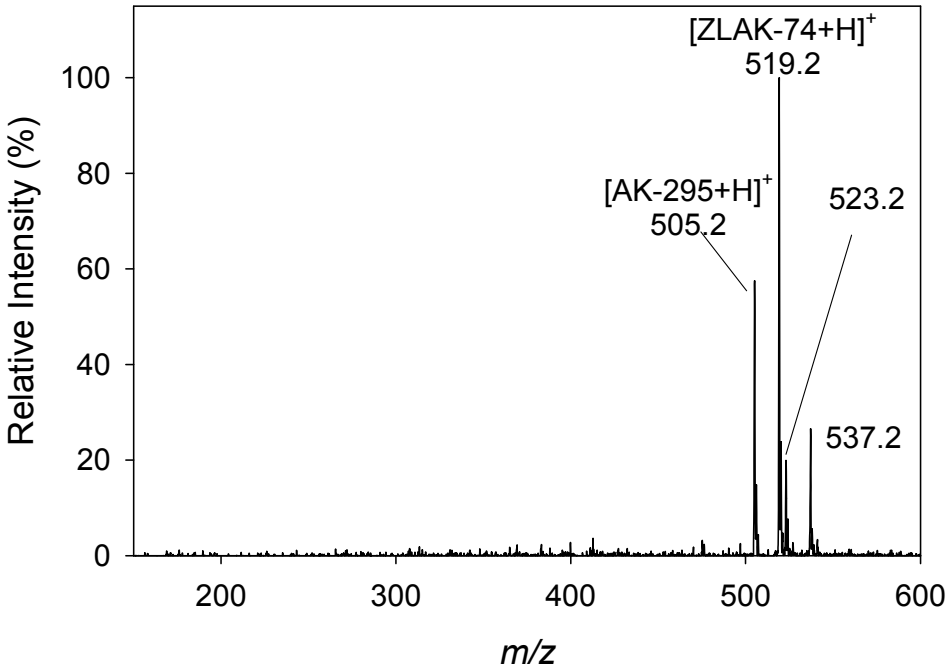

Figure 4.10. Mass spectrum of a solution containing 1 μM each AK-295 and ZLAK-74 analyzed by continuous-infusion RF-only AMUSE using a *functionalized* 2nd generation array with 5-μm nozzles.

The mass spectrum clearly shows $[M+H]^+$ peaks, as well as $[M+H_2O+H]^+$ peaks, for both AK-295 and ZLAK-74. The intensity of the $[ZLAK-74+H]^+$ peak at *m/z* 519.2 is roughly twice as high as that of AK-295 at equimolar concentrations. This difference in intensity is most likely due to differences in the purity of each compound in the samples provided, as there is not a significant difference in the polarity of these compounds, which would give rise to different ionization efficiencies.

One common method of enhancing the selectivity of LC-MS experiments is by performing selected reaction monitoring (SRM) experiments. In this type of MS scan, a precursor ion is selected and then fragmented in the collision cell giving rise to multiple product ions that are filtered so that the intensity of only the most specific and abundant product ion is monitored. In other words, in SRM mode the signal intensity corresponds

to one particular precursor-to-product ion transition. In our QiT mass spectrometer, up to 10 different scan functions can be run during a single acquisition; however, increasing the number of scan types also reduces the duty cycle for a given transition causing a concomitant reduction in sensitivity for each targeted compound. For LC-AMUSE-MS experiments, three scan types were alternated during each acquisition. The first scan was set to monitor the intensity of signal over *m/z* 150 – 2000, the second was an SRM scan for AK-295, while the third scan was an SRM scan for ZLAK-74. The transitions that would provide the highest sensitivity for these experiments were determined from product ion (MS/MS) spectra obtained for AK-295 and ZLAK-74 (Fig. 4.11).

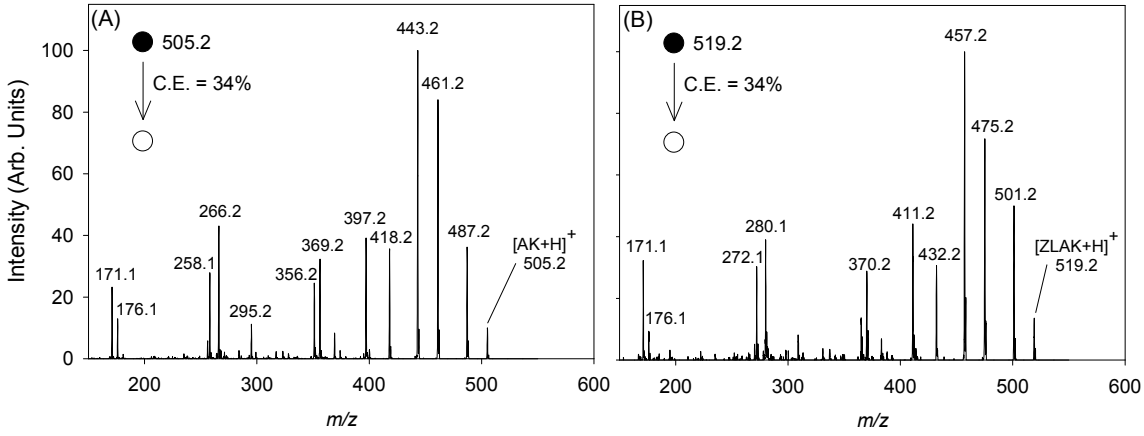

Figure 4.11. MS/MS mass spectra obtained by fragmenting the $[AK\text{-}295+H]^+$ ion (*m/z* = 505.2) (A) and $[ZLAK\text{-}74+H]^+$ (*m/z* = 519.2) (B) from a solution containing 1 μM each AK-295 and ZLAK-74 analyzed by continuous-infusion RF-only AMUSE using a *functionalized* array with 5-μm nozzles. Mass selection window width = 1.2 u, C.E. = normalized collision energy.

The fragment ion having the highest intensity in each spectrum was *m/z* 443.2 for AK-295 and *m/z* 457.2 for ZLAK-74. Thus, the SRM transitions chosen were *m/z* 505.2 → 443.2 for AK-295 and *m/z* 519.2 → 457.2 for ZLAK-74. Figure 4.12 shows

chromatograms for each scan type run during acquisition of a 1 μM AK-295 standard and ZLAK-74 by LC-RF-only AMUSE-MS while Figure 4.13 shows chromatograms for the SRM transition of AK-295 for two injections of a 2.5 μM AK-295 standard showing unwanted mixing effects.

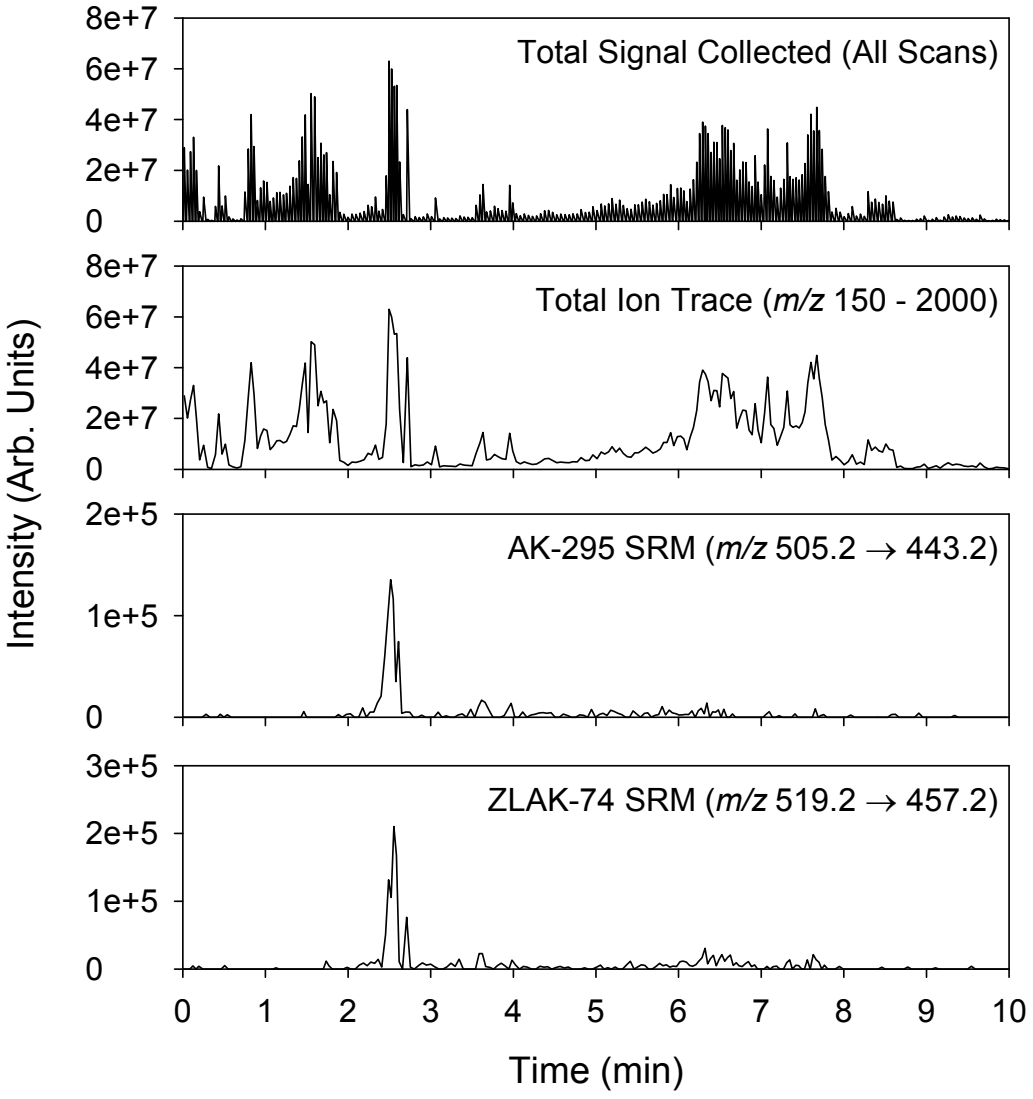

Figure 4.12. Chromatograms showing signal for all acquired scans (A), signal over entire mass range (B), signal for AK-295 SRM transition (C) and signal for ZLAK-74 SRM transition (D) for solution containing 1 μM each AK-295 and ZLAK-74 analyzed by LC-RF-only AMUSE using a *functionalized* array with 5-μm nozzles.

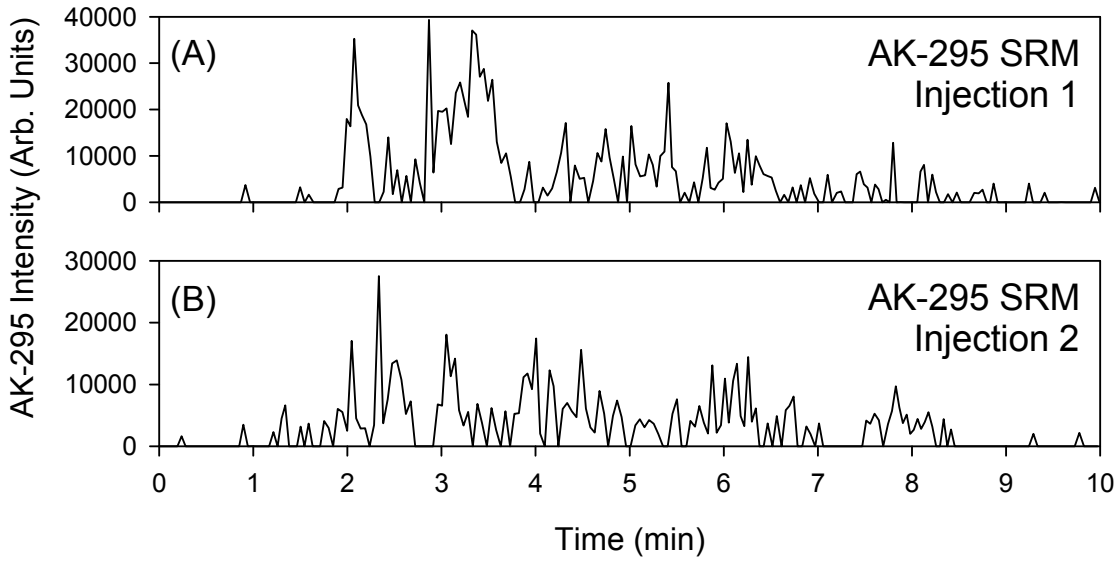

Figure 4.13. Chromatograms showing AK-295 SRM transition signal for two sequential injections of a 2.5 μM AK-295 standard analyzed by RF-only AMUSE using a *functionalized* 5-μm nozzle array.

As can be seen in these chromatograms, the peak shape of the AK-295 and ZLAK-74 signals can sometimes suffer severe distortions between runs. One limitation of the AMUSE assembly in its current configuration is the relatively large size of the analyte reservoir, 105 μL, which is seven times larger than the volume of sample injected into the column. Diffusional and convective broadening of the sample plug can occur within this compartment. It is well known by LC-MS practitioners that chromatographic band broadening, such as that occurring in the tubing connecting LC to the ion source mounted on a mass spectrometer, has to be carefully minimized to optimize peak shape and reduce memory effects. In LC-AMUSE-MS, the analyte reservoir is filled via a tube that is inserted approximately 3 mm into the reservoir from the center of the top-most edge of the AMUSE assembly. If ejection is actively occurring from the nozzles near the sample inlet tube, then it is likely that diffusion will be minimal and the chromatographic

peak will be relatively narrow as shown in 4.12.C. However, if no ejection hot spots are near the inlet, the sample will instead unevenly mix throughout the reservoir and will be sporadically ejected causing signal spikes and significant broadening of the chromatographic peak as shown in Figure 4.13. Attempts to minimize broadening due to the large reservoir volume by preparing silicone inserts (which define the reservoir volume as explained in section 2.3.2) having internal volumes as low as 20 μL were unsuccessful because of the poor ejection efficiency of this particular device (~10%) which made alignment of the reservoir with ejection hot spots extremely difficult.

Quantitation of drugs in biological samples with possible matrix effects is usually performed by calculating the area under the curve of the SRM chromatograms, and creating a calibration curve correlating the ratio of the area of the drug of interest (AK-295) / area of the ISTD (ZLAK-74) with the drug concentration ([AK-295]) in the sample. Calibration curves obtained following this approach by pESI, RF-only AMUSE and DC-AMUSE for the AK-295 standards are shown in Figure 4.14. Interestingly, despite the poor peak shape, the overall integrated peak intensity observed in SRM chromatograms still follows a linear relationship with analyte concentration, indicating quantitative elution and ionization of AK-295. These observations support our hypothesis of uneven mixing followed by ejection within the AMUSE ion source sample reservoir. The correlation coefficient for each calibration curve is > 0.98 indicating good fit between the experimental data and the regression line.

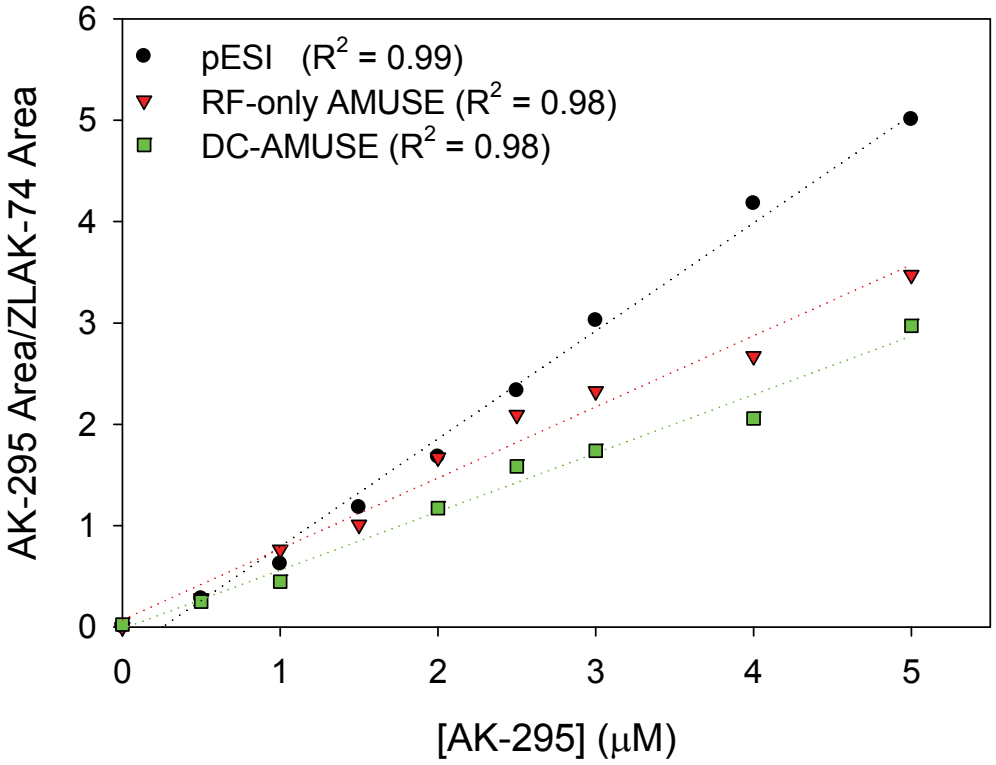

Figure 4.14. LC-MS calibration curves using pESI, RF-only AMUSE, and DC-AMUSE ion sources. The correlation coefficient for each curve is indicated in the legend. Peak areas for AK-295 and Zlak-74 were calculated using the QiT manufacturer's software (Xcalibur 2.0, ThermoFinnigan, Waltham, MA) by integrating over the entire SRM chromatograms.

One common pitfall with LC-ESI-MS quantitation using area ratios is deviation induced in the ratio due to ionization suppression when the analyte concentration becomes significantly larger than the concentration of the internal standard. In the pESI experiments, the ZLAK-74 peak area increased until [AK-295] > [ZLAK-74] at which point it steadily decreased with increasing AK-295 area as shown in Figure 4.15.

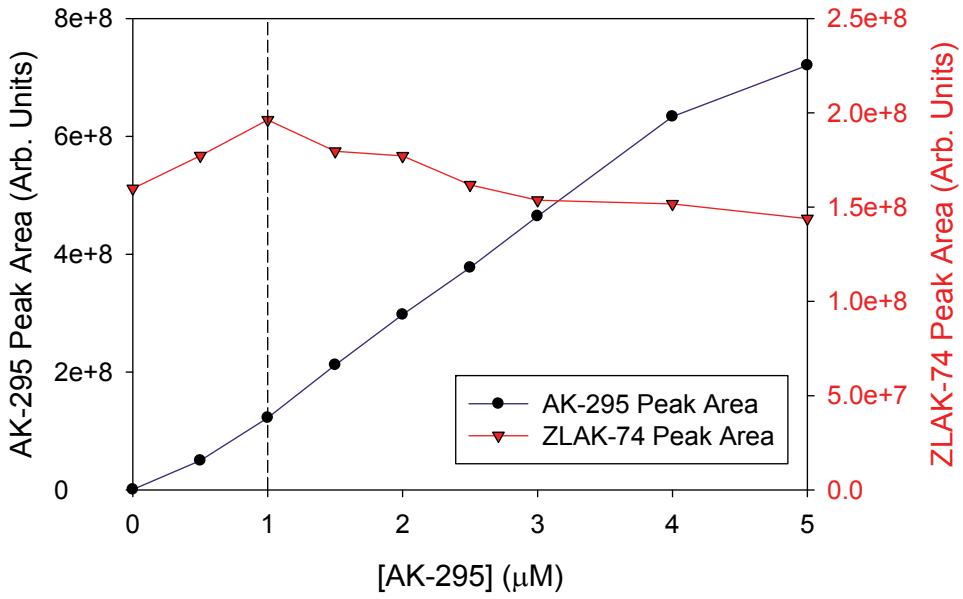

Figure 4.15. Peak areas for AK-295 (black circle) and Zlak-74 (red triangle) for LC-pESI-MS. The dashed line indicates the concentration of ZLAK-74 in the standards.

The decreased ZLAK-74 peak area with increasing [AK-295] causes the calibration curve to deviate to higher ratios for AK-295 concentrations that are higher than the concentration of ZLAK-74. Due to the inherently different ionization mechanisms, this distortion is not present in the calibration curves obtained with AMUSE suggesting that this technique is not significantly affected by ionization suppression. One minor experimental difficulty sometimes observed during these experiments was the presence of contaminant peaks in the LC-AMUSE mass spectra as shown in Figure 4.16.

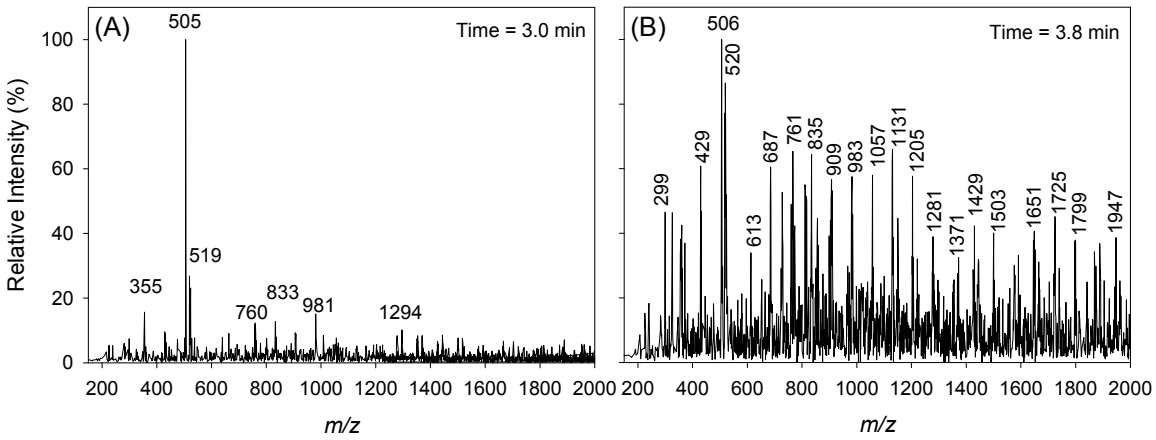

Figure 4.16. Mass spectra obtained for scans at (A) and after (B) the expected t_R of the chromatographic peak of AK-295 for a 5 μM standard analyzed using LC-RF-only AMUSE-MS. The corresponding SRM chromatogram is shown in Figure 4.13.C.

As can be seen in the spectrum at time = 3.0 min, the $[M+H]^+$ peaks for AK-295 and ZLAK-75 are apparent. However at 3.8 min, these peaks are completely obscured by the presence of a polymeric contaminant that has been identified as polydimethylcyclosiloxane (PDMS), an ubiquitous contaminant that has been shown to produce significant background signals in mass spectra.[265] The specific origin of this contaminant has not yet been identified; however, it was not observed in LC-pESI-MS studies performed prior to the LC-AMUSE experiments suggesting that it originates from the AMUSE assembly. PDMS is commonly found in silicone rubber so these signals may be due to leaching from the silicone insert used in the AMUSE assembly when the mobile phase was ramped to 100% acetonitrile. As these contaminants were not observed in the continuous-infusion experiments, which used 30% organic solvent, leaching because of the high organic content in LC-AMUSE is a strong possibility. Potential solutions to this problem include switching the insert material to polyethylene, latex, or

polyurethane, which are readily available in the same thickness as the silicone film used for the insert.

4.6. Conclusion

These critical proof-of-principle experiments demonstrated that increasing the hydrophobicity of the ejector array significantly improved MS signal stability for DC-AMUSE and RF-only AMUSE as indicated by decreases of up to 89% in %RSD of the MS signal. Furthermore, mass spectral peak intensities for DC-AMUSE and RF-only AMUSE were increased by 10-fold and 2-fold, respectively, upon silanizing the array. The first report of coupling of LC with AMUSE was also presented for the analysis of AK-295. However, several challenges need to be overcome before LC-AMUSE-MS can be used for routine separation and ionization of complex samples. Multiplexed AMUSE devices having smaller analyte reservoirs have recently been reported[134] and may aid in reducing diffusional/convective broadening of the chromatographic peak; however, the availability of these devices is still limited. Despite these remaining challenges, it is clear that the AMUSE ion source has clear potential for LC-MS experiments.

PART II: ADVANCES AND APPLICATIONS OF AMBIENT PLASMA-BASED IONIZATION TECHNIQUES

CHAPTER 5. DART-MS INVESTIGATION OF LOW-QUALITY MEDICINES

5.1. Abstract

In this chapter, results from screening experiments using DART-MS and LC-MS performed on a large collection of low quality drugs sold along the border between Thailand and Myanmar (Burma) are presented. The chapter begins with an explanation of the effect that distribution of low-quality drugs has on public health, with regards to the potential curative effect of these pharmaceuticals for patients and to the increasing prevalence of drug resistance, especially in areas most affected by *Plasmodium falciparum* (*P. falciparum*) malaria. This is followed by a description of the DART ionization technique. An examination of the effect of different DART experimental variables on the observed sensitivity for common drug molecules and a detailed study of the mass accuracy obtained during elemental composition determination of the ions generated is also presented. The chapter concludes with results of an investigation to identify the composition of these low-quality drugs via LC-MS and DART-MS.

5.2. Yaa Chud Medicine on the Thai-Myanmar Border

Multi-drug resistant *P. falciparum* malaria is a severe public health problem in Southeast (SE) Asia, particularly along the Thai-Myanmar border.[266-268] Traditional antimalarial medicines such as chloroquine, pyrimethamine+sulphadoxine, quinine, and mefloquine are no longer effective when used alone.[267] Instead, artemisinin derivative combination therapy (ACT), such as artesunate+mefloquine or artemether+mefloquine,

can be used to successfully treat *P. falciparum* malaria.[266, 267, 269, 270] Although these drugs are available from government clinics, many Thai villagers and Burmese migrant workers buy small packets of drugs over-the-counter from grocery shops and pharmacies as their first line of treatment for fever.

These small plastic bags, which contain 4-5 tablets or capsules are called "yaa chud" in Thai, or literally "combination medicine", and are sold to patients or their families without prescription or medical assessment.[271-273] Yaa chud are prepared by putting tablets and capsules, obtained from pharmaceutical wholesalers, in small plastic bags that are sold individually to patients according to the symptoms they present. They are often the first line of care for patients with malaria and "fever" and it has been estimated that 20 – 50% of total worldwide antimalarial distribution was through these informal outlets and sellers.[274]

There are many potential problems with the unregulated distribution of drugs in this way. Their use may reduce the effectiveness of antimalarial therapy.[275, 276] The medicines are unlabelled and in varied combinations, and are generally sold without instructions on how to take the drugs or what dosing regimens to follow. Furthermore, they are typically prepared by untrained staff who are probably unaware of drug interactions and contraindications and there is evidence that many yaa chud medicines are composed of inappropriate and/or unnecessary drugs.[271-273] Although the tablets and capsules within the bags may be genuine, yaa chud may also include counterfeit, substandard or degraded pharmaceuticals. However, without evidence of the chemical identity of these tablets and capsules, this is extremely difficult to determine. The use of yaa chud may also have important wider implications for public health as sub-therapeutic

doses may increase the prevalence of parasites, such as *P. falciparum,* that are resistant to the few remaining effective antimalarial drugs.[270, 277] Thus, the identification of AIs in these unlabelled drugs, which were purchased along the Thai/Myanmar border by a local volunteer, is of critical importance. These samples were provisionally identified by their appearance and the entire set was screened using DART-MS. A subset of these samples was further assayed using LC-MS and atomic absorption spectroscopy (AAS).

5.3. DART Ionization

DART has quickly gained popularity among MS practitioners due to the relative simplicity of obtaining useful data from chemical systems with sample throughputs of up to 3 samples per min.[189] At the core of the DART ion source (Fig. 5.1) is a point-to-plane glow discharge[38, 173] supported by a He stream.

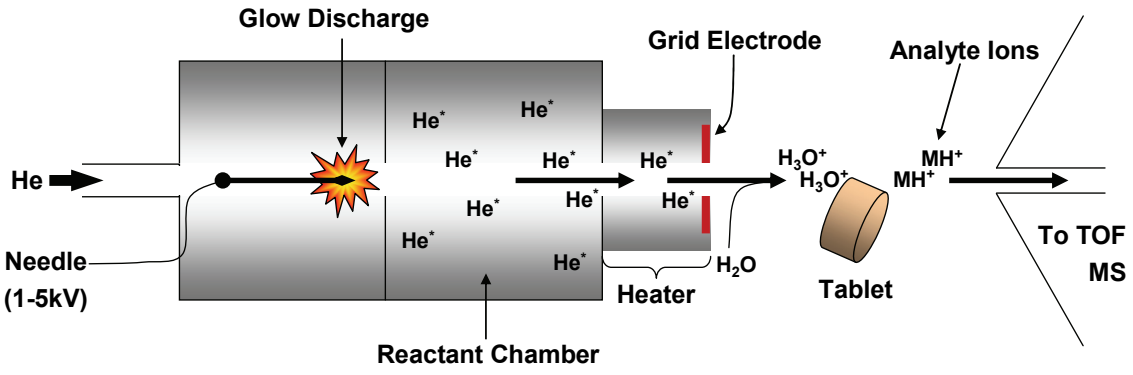

Figure 5.1. Schematic of the DART ion source depicting use for the analysis of a pharmaceutical tablet.

5.3.1. DART Desorption / Ionization Mechanism

A series of complex processes within this discharge region (electron-impact, ion-electron recombination) produces metastable He atoms (He^*, 2^3S_1, 19.8 eV) which are carried downstream by the He gas flow. N_2 can be used instead of He, in which case, the excited species correspond to energetic N_2 vibronic states. Ions and electrons also produced in the discharge region are filtered out by a perforated electrode positioned downstream. The He^*-containing gas stream can then be heated to temperatures varying from 200 to 450 °C prior to exiting the ion source. A second grid electrode at the exit of the ion source prevents ion-ion recombination.[38]

Cody et al have proposed several reasonable DART ionization mechanisms. Most of these mechanisms begin with reaction 5.1, where, upon exiting the ion source, the heated He^* stream induces Penning ionization[278] of atmospheric water, generating protonated water clusters.[38]

$$He^*_{(g)} + nH_2O_{(g)} \longrightarrow He_{(g)} + (H_2O)_{n-1}H^+_{(g)} + OH^-_{(g)} \qquad \text{(Rxn. 5.1)}$$

This mechanism for the formation of reactive protonated water clusters is supported by examination of the typical background mass spectrum obtained by DART-MS which shows clusters with n = 1 – 14.[38] Vaporized analyte(s) (AB) are generated via thermal desorption or chemical sputtering from the solid analyte surface by the heated He^* stream as shown in reaction 5.2.

$$AB_{(s)} \xrightarrow{\text{heat}} AB_{(g)} \qquad \text{(Rxn. 5.2)}$$

Proton transfer from the protonated water clusters to the analyte will occur for analytes having a higher proton affinity than water. Proton transfer from these water clusters to the gas-phase analyte can lead to the generation of protonated gas-phase molecules ($[AB+H]^+$) as shown in reaction 5.3.

$$(H_2O)_{n-1}H^+_{(g)} + AB_{(g)} \longrightarrow [AB+H]^{+\bullet}_{(g)} + (n-1)H_2O_{(g)} \qquad \text{(Rxn. 5.3)}$$

The predominance of this cluster-mediated mechanism seems to be consistent with most observations that $[AB+H]^+$ ions are the major species generated by DART-MS. However, fragmentation of the protonated molecule has also been observed for analytes having a much higher proton affinity than water and can be induced by increasing the DART gas temperature.[173]

Molecular ions have also been observed for analytes such as atmospheric gases and small organic molecules which have an ionization energy that is lower than the IE of the excited metastable (19.8 eV for He^*). The mechanism for the formation of $M^{+\cdot}$ ions from nonpolar species has been proposed to follow reaction 5.4.[173]

$$He^*_{(g)} + AB_{(g)} \longrightarrow [AB]^{+\bullet}_{(g)} + e^- \qquad \text{(Rxn. 5.4)}$$

Ionization in negative ion mode has also been reported.[38, 174, 184] In negative ion mode, ionization occurs via one of four mechanisms: electron capture, dissociative electron capture, proton transfer, and anion attachment as shown in reactions 5.5 – 5.8.[174]

$$AB_{(g)} + e^- \longrightarrow AB^{+\bullet}{}_{(g)} \quad \text{(Rxn. 5.5)}$$

$$AB_{(g)} + e^- \longrightarrow A^-{}_{(g)} + B^\bullet{}_{(g)} \quad \text{(Rxn. 5.6)}$$

$$AB_{(g)} + X_{(g)} \longrightarrow [AB-H]^-{}_{(g)} + [HX]^+{}_{(g)} \quad \text{(Rxn. 5.7)}$$

$$AB_{(g)} + Cl^-{}_{(g)} \longrightarrow [AB+Cl]^-{}_{(g)} \quad \text{(Rxn. 5.8)}$$

Following ionization, the combined forces exerted by the He flow towards the spectrometer inlet, the suction from the API orifice, and the weak electrical field applied to the ion source exit electrode contribute to transmit ions into the first differentially pumped region of a mass spectrometer utilizing orthogonal acceleration TOF[38, 173, 176, 183, 184, 186, 188, 190-192, 195] or triple quadrupole[194] mass analyzers.

5.3.2. Effect of DART Experimental Parameters on Ion Transport and Signal Intensity

Although qualitative analysis via DART-MS has been applied to a wide variety of problems, there have been few systematic studies on the factors influencing mass accuracy, ion yield, and thermal ion activation in DART-MS. Recent work by Harris and Fernández focused on investigating the parameters which most strongly affect ion transport.[279] Simulations of the effect of thermal gradients induced by the heated gas, convective gas currents, sample position, and electrical fields on the intensity of DART-MS signal showed that optimal signal could be obtained by aligning the DART ion source with the mass spectrometer inlet and placing the target analyte near the ion source at a position that is slightly below the center axis formed by the source and inlet. This phenomenon was verified experimentally and it was proposed that signal was enhanced

due to enhanced thermal desorption as a result of the higher temperature in this region and due to more efficient particle transport via gas currents.

Cody has recently investigated the effect of several parameters, including the distance between the ion source and mass spectrometer inlet, temperature, voltage on the discharge needle, and grid voltage on the relative abundances of molecular ions vs. protonated molecules of the same analyte.[173] It was found that by increasing the distance between the source and inlet, the abundance of the protonated molecule increased (due to the higher availability of water molecules) while the abundance of the molecular ion decreased. Increasing the voltage on the discharge needle caused a corresponding increase in the ion current but also increased analyte oxidation which tends to promote hydride extraction rather than protonation or electron transfer, resulting in a decrease in the abundance of both the molecular ion and the protonated molecule. Increasing the grid voltage was found to increase fragmentation in the mass spectra, an observation that was supported by the simulations performed by Harris.[279]

To extend these fundamental investigations of the effect of varying the DART source parameters on MS signal intensity, analyses using common drug molecules were performed. Specifically, the effect of changing the He^*-stream temperature, gas flow rate, and grid voltage on signal sensitivity was monitored. A study of the effect of the He stream temperature on the time-resolved appearance of fragment ions during the ionization of labile drugs was also performed. These results allowed us to optimize instrumental settings for the screening of a collection of yaa chud with the intent of identifying, by accurate mass measurements, the AIs present in these low quality pharmaceuticals.

5.4. Experimental Details

5.4.1. Sample Collection

Sample collection was organized by Dr. Paul N. Newton (Wellcome Trust-Mahosot Hospital-Oxford Tropical Medicine Research Collaboration and Centre for Clinical Vaccinology and Tropical Medicine, University of Oxford).

Between July 2000 and January 2001 a Thai, Burmese and Karen speaking researcher, dressed as a Burmese migrant worker from Myanmar, visited "kong cham" shops in 16 villages astride the Thai-Myanmar border in Mae Sot District, Tak Province, Thailand and adjacent Myawaddy District, Myanmar. The area is endemic for multidrug resistant *P. falciparum* malaria, and the first diagnosis to consider this area would be malaria. A total of 50 yaa-chud containing 254 tablets and capsules with a median (range) of 5 (1-8) tablets or capsules per plastic bag was purchased from 44 shops – 31 (70%) shops were in Thailand and 13 were in Myanmar. A further 20 shops visited did not have yaa chud. The median (range) retail price per bag and per tablet/capsule were 5 (4-12) and 1 (0.7-5.0) baht, respectively (5 baht was worth ~0.12 and 0.14 US$ in 2000 and 2009, respectively). Figure 5.2 shows an image of the entire yaa chud collection.

Figure 5.2. Yaa chud collection.

The mystery shopper said that his "wife was pregnant, has bad fever and is drowsy, could I have some medicine please". A fictional pregnant patient was chosen as they are especially vulnerable to malaria and treatment is not straightforward. If the

shopper was offered a packet of yaa chud, he asked where the drugs came from, how many should be taken and when, will it work for malaria, and might it harm her or the baby.

Fifteen (34%) of the sellers indicated that the yaa chud were prepared on-site while the remaining sellers indicated that the yaa chud were purchased from shops in Mae Sot town. Shopkeepers usually recommended taking a single yaa chud (96%) once every 24 hours (35%), 8 hours (33%), 12 hours (30%), or 4 hours(2%). None said that one yaa chud packet was insufficient to cure the illness or gave any advice regarding the length of time to continue taking yaa chud. Shopkeepers said that 45 (90%) of yaa chud samples would work for malaria, while 4 (8%) said that they would not work and 1 (2%) did not know.

All samples were inspected, described and reviewed by local pharmacists (Mae Sot Hospital and Faculty of Pharmacy, Mahidol University, Bangkok) prior to chemical analysis. All samples were refrigerated (4 ºC) prior to analysis.

5.4.2. LC-MS Sample Preparation and Analysis

All LC-MS sample preparation and analyses were performed by Krystyn Alter-Hall, a master's student in the Fernández group, and Colleen McShane and Horace Leung, two undergraduate students who conducted research in our group.

Drug standards (Sigma-Aldrich, St. Louis, MO) and yaa chud samples were first crushed with a mortar and pestle. Approximately 30 mg of sample was suspended in 1 mL of methanol (Sigma-Aldrich, St. Louis, MO) and extracted on a rotary shaker for 2 hours. Following extraction, suspensions were filtered through a 0.45 μm PTFE

membrane filter (Pall Corporation, Ann Arbor, MI) and were diluted with methanol or 50:50 acetonitrile:water (v/v) as needed. Tablets and tablet extracts were kept refrigerated (4°C) until analysis.

LC separations were performed on an Agilent 1100 system equipped with a solvent degasser, a binary pump, a thermostatted column compartment (held at 25°C), an autosampler, and a diode array detector. An analytical Zorbax® Extend-C18 column (2.1 x 150 mm, 5 μm particles, 80 Å pore size Agilent) equipped with a Zorbax® RX-C18 guard column (4.6 mm x 12.5 mm, 5 μm particles, 2 μm pore size; Agilent) was used. The gradient LC method was optimized to provide good separation of a wide range of drugs and used A = nanopure water + 0.01% acetonitrile and B = acetonitrile. The mobile phase flow rate was set to 200 μL min^{-1} with an injection volume of 20 μL. The following gradient program was used: 0 min – 5% B, 7 min – 45% B, 8 min – 100% B, 12 min – 100% B. The system was set with a four minute post run time to re-equilibrate the column to the original mobile phase composition.

The LC system was coupled to a TOF mass spectrometer (AccuTOF, JEOL, Peabody, MA) via an orthogonal pESI interface operating at 2 kV. The mass spectrometer ion optics settings were as follows: inlet orifice = 80 ºC, 30 V; ring electrode = 8 V; orifice 2 = 5 V; ion guide bias voltage = 26 V; ion guide RF amplitude = 2 kV; nebulizing gas flow rate = 1.0 L min^{-1}; desolvation gas flow rate = 2.5 L min^{-1}; desolvation chamber = 250 ºC; detector = 2500 V. Spectra were collected with a data sampling interval of 0.5 nanoseconds and a spectrum recording interval of 0.4 seconds.

5.4.3. DART-MS Analysis

Sensitivity and fragmentation studies were performed by Arti Navare, a graduate student in the Fernández research group, and used paracetamol (acetaminophen, 500 mg, Tylenol®; McNeil-PPC Inc., bought in the USA) and erythromycin. Yaa chud experiments were performed by Christina Y. Hampton, Dr. Facundo M. Fernández, and Dr. Robert B. Cody of JEOL USA, Inc.

This technique did not require sample preparation and thus samples were analyzed as provided. A commercial DART ion source (IonSense, Saugus, MA) was coupled to the AccuTOF and both were operated in positive-ion mode. He gas was introduced into the DART discharge chamber at flow rates ranging from 4 – 7 L min^{-1}. The glow discharge was initiated by application of 3.5 kV to the DART needle electrode and the first DART ion source electrode was held at 150 V. The grid voltage ranged from 25 – 375 V while the DART gas temperature ranged from 150 – 450 ºC. For yaa chud experiments, the He gas flow was set to 4 L min^{-1} and heated to 275 ºC while the grid voltage was set to 250 V. The mass spectrometer ion optics settings were as follows: inlet orifice = 150 ºC, 54 V; ring electrode = 59 V; orifice 2 = 34 V; ion guide bias voltage = 29 V; ion guide RF amplitude = 1000 V; detector = 2800 V. Spectra in the 50 to 1000 *m/z* range were collected with a data sampling interval of 0.5 nanoseconds and a spectrum recording interval of 0.4 seconds. The distance between the DART ion source exit and the spectrometer inlet was fixed at 2 cm.

Uncoated tablets were held with a pair of metal tweezers in front of the DART ion source for an average time of 20 s for yaa chud experiments. Exposure times were 20 s for sensitivity studies, and 80 s for fragmentation studies. The distance between the tablet

and the TOF inlet was 1 cm. In the case of coated tablets, these were first broken in half, and the interior was analyzed by DART. Capsules were opened, and the contents were sampled with the open end of a melting point capillary (for powders, 1.5 mm o.d. x 90 mm long glass capillary), or with tweezers (for granules). For sensitivity and ion fragmentation studies, which required a careful measurement of ion intensities and thus a higher degree of sample positioning reproducibility, a sliding arm terminated with an alligator clip was used to position the samples. No memory effects were observed as long as care was taken not to contact the inlet orifice of the mass spectrometer with the tablet. The total acquisition time to screen the complete sample set was 142 minutes, which corresponded to a sample throughput of 3 samples min^{-1}.

Due to the poor yaa chud packaging, cross contamination between tablets was common and problematic for DART-MS analysis as contaminant particles embedded on the sample surface produced signals corresponding to AIs from other tablets in the package. This is evident in Figure 5.3, which shows the DART-MS mass spectra obtained for samples in a single yaa chud packet that is shown in the top left panel. Contaminants embedded on the sample surface produced signals corresponding to AIs from other tablets in the package (Fig 5.3, panels A – E). If cross contamination between samples in a given package was suspected, tablets were broken in half, and the internal surface of the tablets was also subjected to DART-MS. The AIs were thus assigned based on the common peaks observed for both the external tablet surface, and the internal surface of the broken tablet.

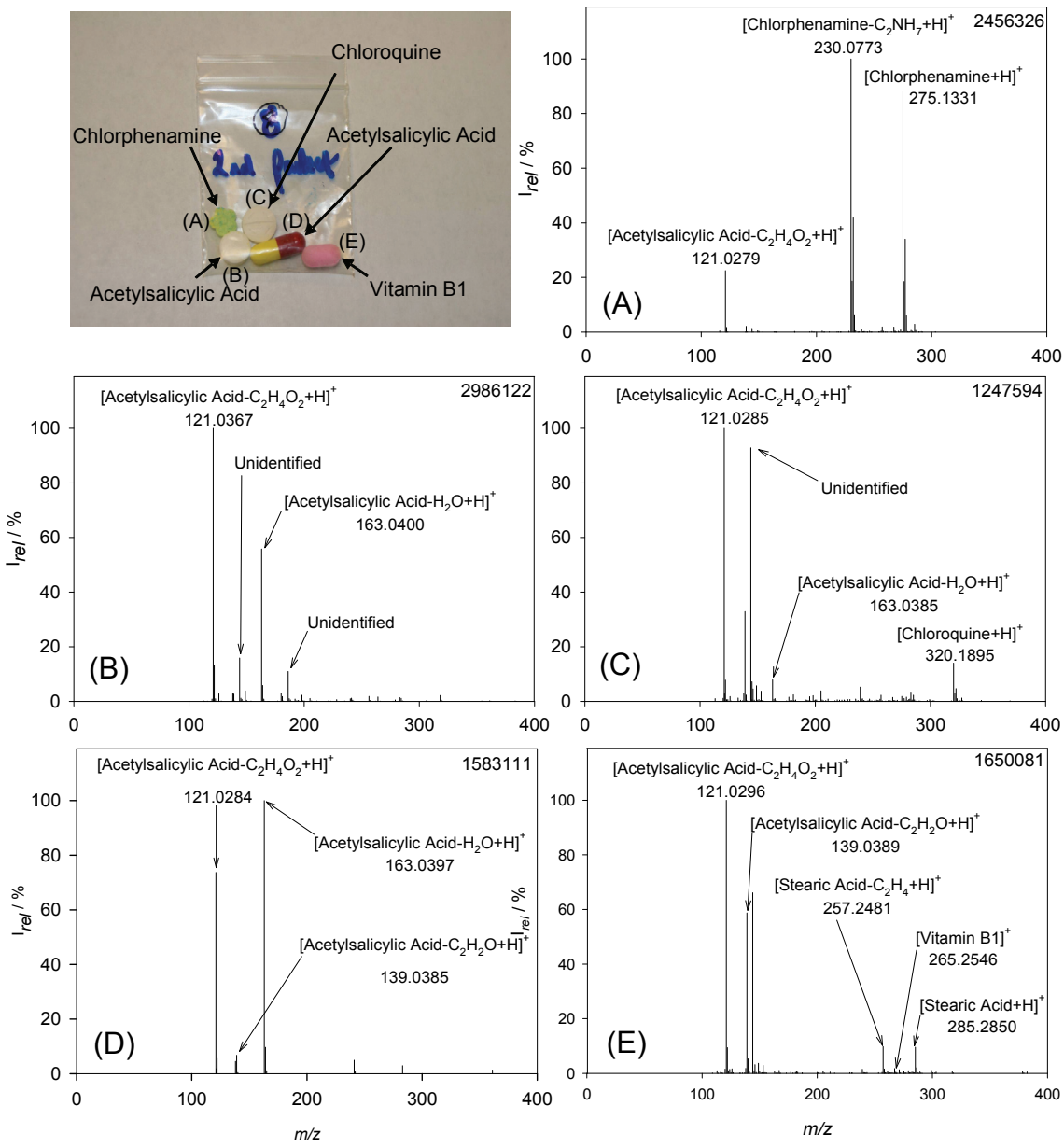

Figure 5.3. Accurate mass DART-MS mass spectra obtained from tablets and capsules found in a representative yaa-chud bag (shown in top left panel). Peaks were assigned if a match was found within a 5 mmu tolerance.

5.4.4. Mass Spectral Data Analysis

Spectra were continuously acquired over 10-20 minute runs, during which time drug samples and a melting point capillary dipped in neat poly(ethylene glycol) (PEG,

average molecular weight 600) were alternately placed within the DART ionization region. During data post-processing and analysis, a mass spectrum of each unknown was obtained by averaging the mass spectral data over the time interval corresponding to the exposure of the corresponding sample to the DART gas. Mass spectral background subtraction, data centroiding, and drift correction were performed using the built-in mass spectrometer software (MassCenter, version 1.3). Mass drift correction was performed by obtaining a reference mass spectrum using the PEG mass spectra acquired at the beginning of each sample run and immediately after each sample analysis during the run. AI identification was performed by importing the spectral peak list into Excel (Microsoft, Auburn, WA) and using a system of macros to search for matches against an in-house library of protonated molecules derived from the Model List of Essential Drugs published by the World Health Organization (WHO).[280] A match was considered positive if the difference between the experimental and theoretical *m/z* values was less than 5 mmu. Data on drug collection and identity was analyzed using Stata 10 (College Station, Texas, USA).

5.4.5. Elemental Analysis Using AAS

All AAS experiments were performed by Dr. Mabel B. Tudino and Natalia Mancuso of the Department of Inorganic, Analytical, and Physical Chemistry / INQUIMAE, at the University of Buenos Aires in Argentina.

Samples that were provisionally identified as containing either mineral supplements or antacids (3/132 or 2%) were analyzed using AAS using the method detailed by Newton, et al.[188] Briefly, 100 mg sample was digested in closed PTFE vessels

with 5 mL of 70 % w/w nitric acid using a microwave digestion system (MDS 2000, CEM Co, Matthews, NC, USA). After digestion, the PTFE vessels were cooled to room temperature and the final clear solution was diluted to a final volume of 10 mL with distilled water. Metal concentrations were determined by AAS (Shimadzu 6700 AAS, Kyoto, Japan) employing a flame air/acetylene atomic source (Hamamatzu single hollow cathode lamps, Cu, Fe, Mn, Zn, Ca and Mg, Shimadzu). The metal concentrations in the samples were obtained by the working curve methodology.

5.5. Factors Affecting DART-MS Sensitivity

As paracetamol was one of the most common AIs provisionally-identified in the yaa chud collection, it was selected as a probe molecule to better understand the effect of DART helium flow rate and exit (grid) electrode voltage on the observed DART-MS sensitivity. Figure 5.4 shows the results obtained by repetitively exposing identical paracetamol tablets to the DART stream under varying gas flow and voltage conditions.

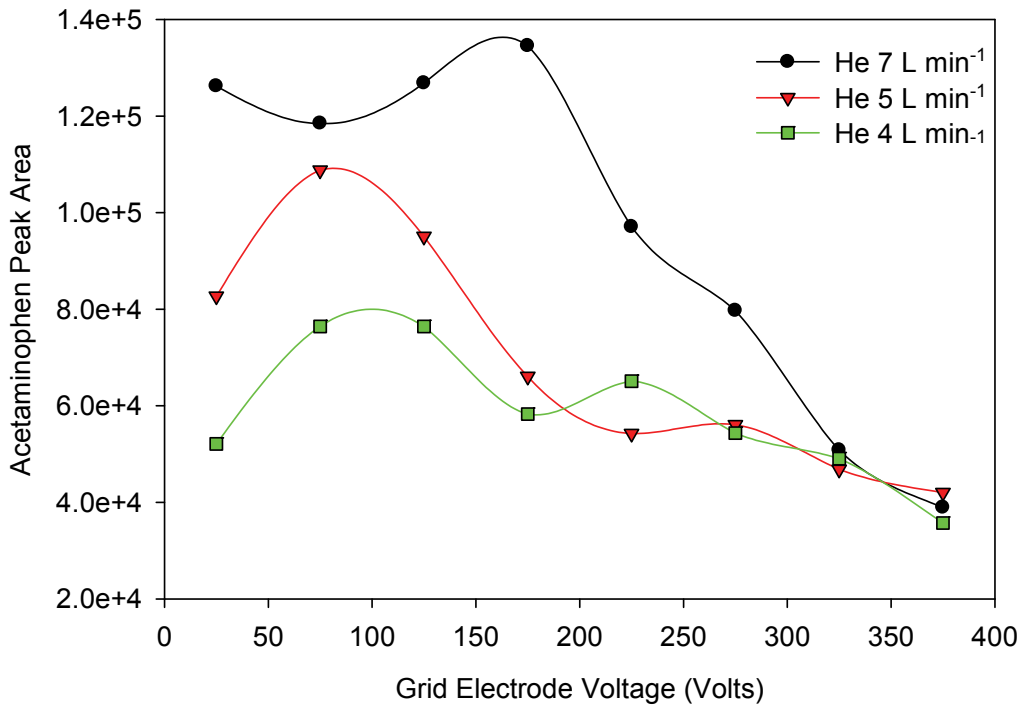

Figure 5.4. Effect of He gas flow and grid electrode voltage on the observed DART-MS ion yield for a paracetamol tablet. DART gas temperature: 200 °C, ion guide peaks voltage: 600V. Other conditions were as described under experimental.

It was observed that for the protonated paracetamol ion ($[M+H]^+$; m/z = 152), sensitivity increased with increasing He flow rate. One possible explanation for this effect is that, as He flow rate is increased, more heat is transferred to the sample per unit time, thus resulting in an increase in the paracetamol desorption rate (Rxn. 5.2), with a concomitant increase in ion yield (Rxn 5.3). This was also observed in simulations performed by Harris and Fernández.[279] Despite the increase in sensitivity at increased He flow rates, the S/N was still sufficient for detecting the major sample components even at the lowest flow rates assayed, and thus, from a practical standpoint, lower flow rates may be preferable if reducing He consumption is an important factor.

In DART, efficient transmission of ions into the vacuum of the mass spectrometer is crucial, because once formed, ions are rapidly dispersed. Ions formed externally by DART, must enter the TOF mass spectrometer through a small orifice (400 μm i.d.). Thus, a significant fraction of the ions formed are lost. In this sense, an additional factor to explain the increase in sensitivity observed with increased He flow, is improved ion transmission into the first differentially-pumped region of the mass spectrometer due to enhanced convective ion transport. Higher He flow rates effectively transport more ions to the inlet orifice before ion diffusion into the atmosphere takes place.

Prior to entering the mass spectrometer, ions are also subjected to a constant electrical field exerted by the grid electrode. Originally, this field was put in place to prevent ion/ion recombination.[38] In our experiments, it was observed that at the lowest He flow rate assayed (4 L min^{-1}), increasing the grid electrode voltage had only a small effect on the abundance of the $[M+H]^+$ paracetamol ion. However, as He flow rates were increased from 4 to 5 and 7 L min^{-1}, sensitivity became more dependent on the exit electrode voltage. Higher sensitivities were observed at lower exit electrode voltages, which was also observed in the simulations performed by Harris,[279] and in this case, an optimum value between 75 and 125 V was determined. Voltages higher than 175 V resulted in a systematic decrease of the ion abundance, as can be seen in Figure 5.3. At higher values, the grid voltage also affects ion transmission. Following ionization, ions are transported towards the mass spectrometer inlet under the influence of various forces, including the force created by the He flow, the spectrometer's intake airflow, and the static electrical field from the exit electrode. At low electrical fields, the air inflow is sufficient to attract ions near the inlet orifice, but at higher voltages, the ion's kinetic

energy is such that the intake airflow is not sufficient for effectively sampling ions that are not closely on-axis with the inlet. Thus, more ions are forced to collide with the mass spectrometer's front plate resulting in a decrease in the overall ion transmission.

5.6. Effect of Temperature on the Fragmentation of Labile Molecules

During DART-MS analyses, fragment ions are sometimes observed.[38, 173, 184] One potential origin of these fragment ions is thermal activation, either in the gas phase within the open air ionization region in front of the DART, or in the solid phase, prior to desorption. It was observed that, in most cases, fragment appearance was significantly reduced at lower temperatures (e.g. 200 °C), but a short lag time of 5-20 seconds (depending on the size of the tablet) between the introduction of the sample into the DART stream and the appearance of ions was noticed. This effect could be attributed to the finite time required to heat a solid sample in order to produce a detectable amount of volatile AB species following reactions 3.2 and 3.3. It was also noticed that at temperatures lower than 275 °C, the *m/z* range of the signals observed was significantly reduced to ~600 and accompanied by a decrease in the overall signal intensity. It was concluded that for the majority of samples being screened, a He gas temperature of 275 °C was a good compromise to minimize thermal ion activation and maintain the ability of desorbing unknowns with higher *m/z*.

To further study the effect of He gas temperature on the appearance of fragment ions, temperature-resolved DART-MS experiments were performed on a large (250 mg) erythromycin tablet. The reasons for choosing this sample were three-fold. First, for larger tablets such as these, the heating and desorption rates are probably significant with

respect to the time scale of the DART measurement. Thus, higher temperatures may be required for effective desorption, which may bring a concomitant increase in thermal ion activation. Secondly, erythromycin (Fig. 5.5) is known to readily dehydrate at 55 °C and lose neutral desosamine ($C_8H_{16}O_2N$) to form a fragment ion at *m/z* = 558 at 165 °C.[281, 282]

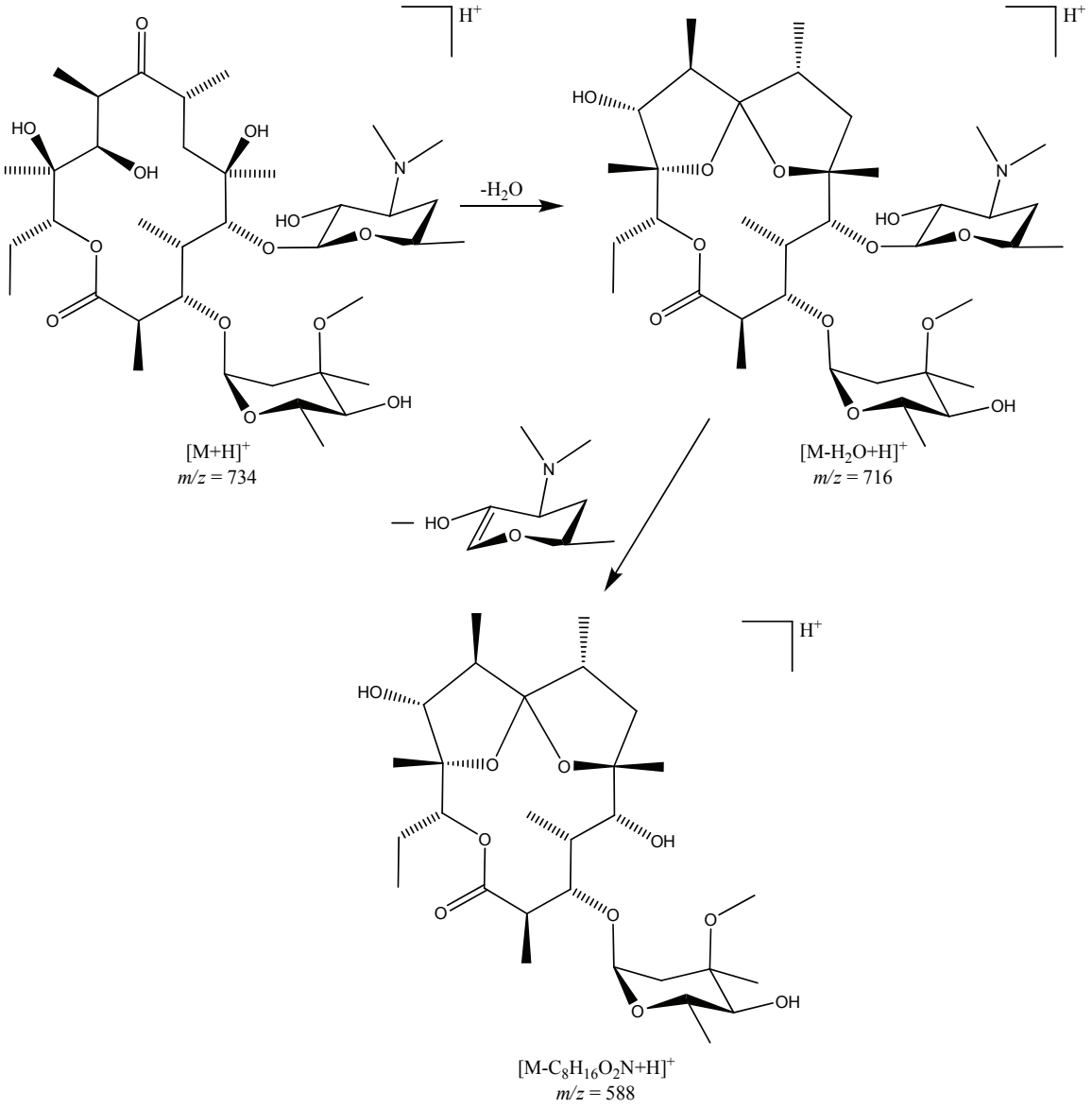

Figure 5.5. Fragmentation scheme for erythromycin.

The appearance of these ions can thus be monitored as an indicator of increased IE deposition during the ionization process. Thirdly, the erythromycin protonated molecule (*m/z* 734) is at the upper range, in terms of molecular weight, of the drugs contained in our database, and thus, its efficient desorption at a given temperature indicates that efficient desorption of other molecules in a mass range equal to this would also be feasible. Figure 5.6 shows DART-MS spectra of four identical erythromycin tablets obtained using variable He gas temperatures.

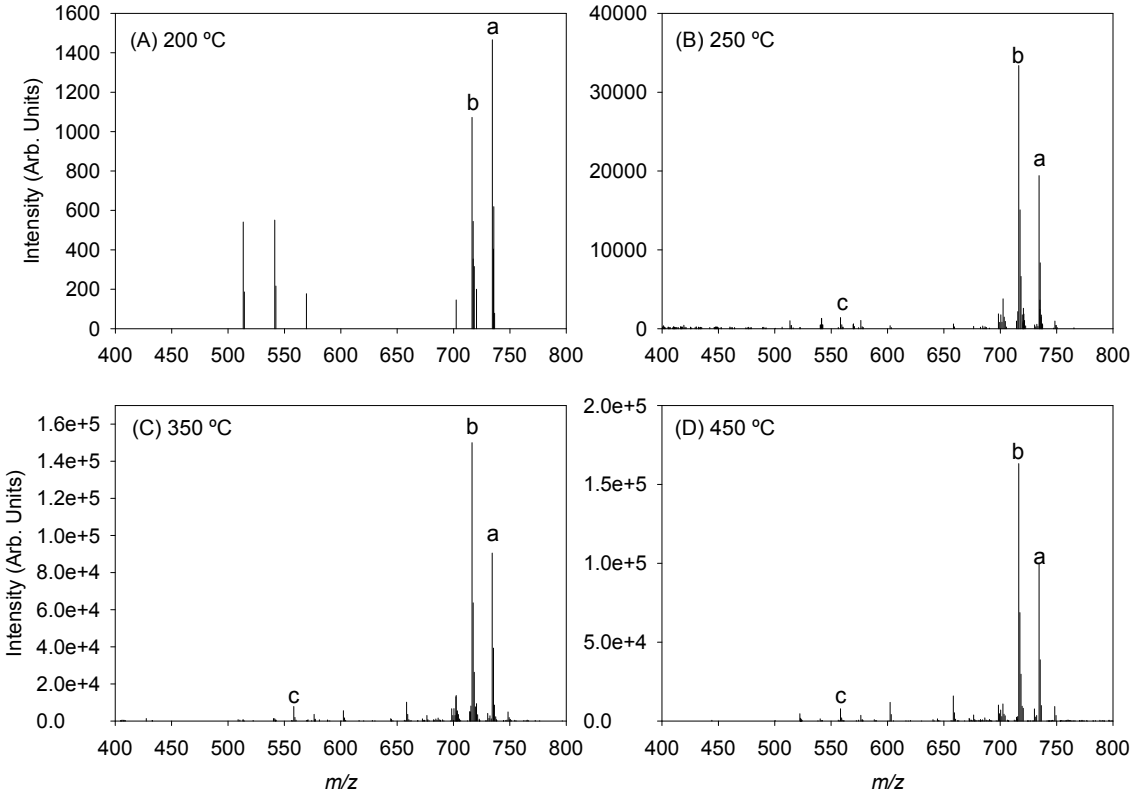

Figure 5.6. DART-MS mass spectra obtained for an erythromycin tablet exposed for 30s to a He stream at varying temperatures. Ion guide peaks voltage:1400 V. Other conditions as described under experimental. a = $[M+H]^+$ (*m/z* = 734), b = $[M-H_2O+H]^+$ (*m/z* = 716), c = $[M-C_8H_{16}O_2N+H]^+$ (*m/z* = 558).

It was observed that the S/N for the erythromycin $[M+H]^+$ ion was maximized at temperatures between 300 ºC and 350 ºC. At 200 ºC, the observed S/N was less than desirable, whereas at temperatures of 150 ºC, no ions were observed. From Figure 5.6, it can also be observed that the $[M-H_2O+H]^+$ (*m/z* = 716) ion was detected at temperatures of 200 ºC and above. As the ratio between the *m/z* 716 and 734 ions increased as a function of temperature, it was concluded that the *m/z* 716 ion, corresponding to dehydroerythromycin, was produced, at least partially, by thermal activation of the $[M+H]^+$ ion or thermal degradation of erythromycin in the solid sample.

The $[M-C_8H_{16}O_2N+H]^+$ fragment ion (*m/*z 558) was also observed with significant intensity. The abundances of this ion, the dehydroerythromycin ion and the erythromycin $[M+H]^+$ ion were not only a function of He gas temperature, but also a function of the exposure time to the DART ionizing gas. Figure 5.7 shows the temporal evolution observed for the $[M+H]^+$, $[M-H_2O+H]^+$, and $[M-C_8H_{16}O_2N+H]^+$ ions as a function of time.

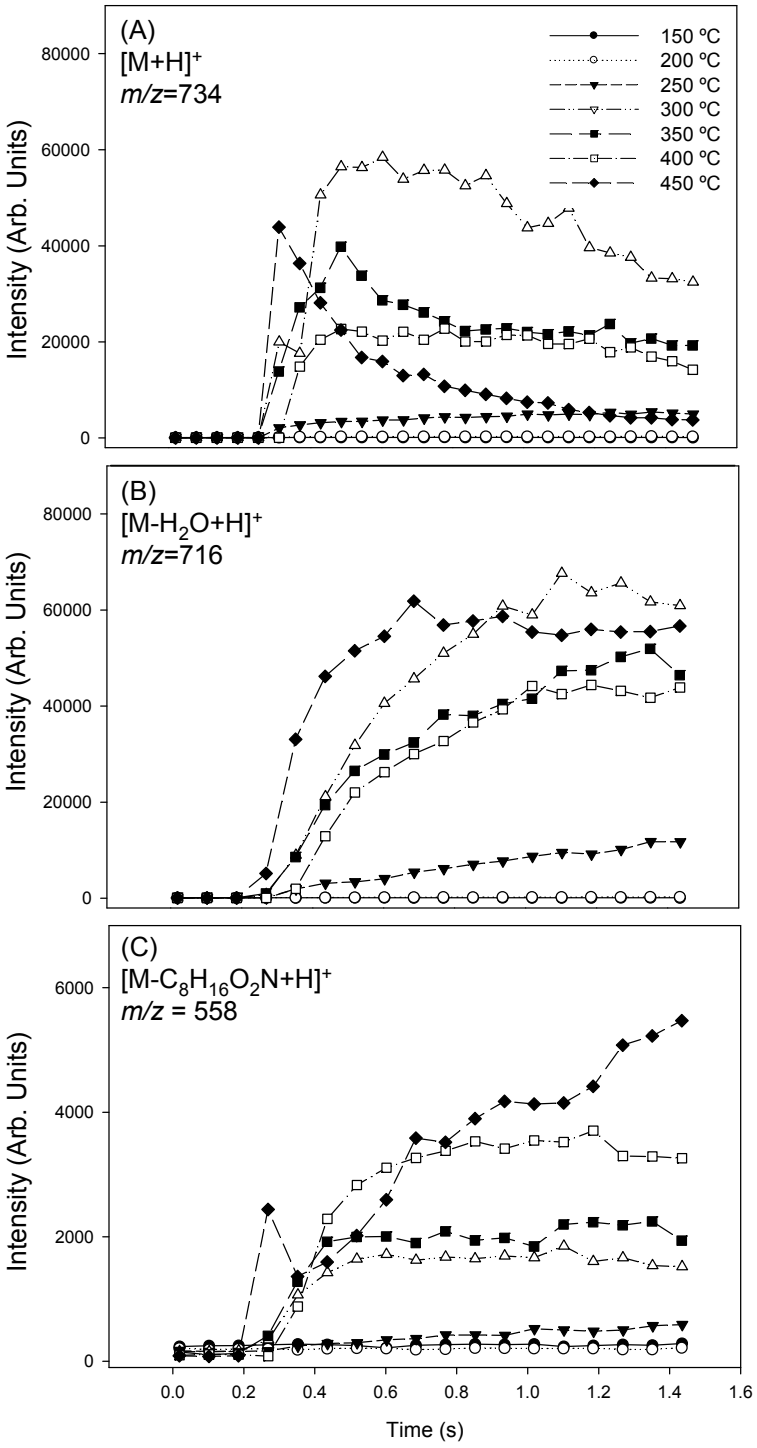

Figure 5.7. Time-resolved DART-MS selected ion traces for (A) the erythromycin protonated molecule ($[M+H]^+$, (B) $[M-H_2O+H]^+$, and (C) $[M-C_8H_{16}O_2N+H]^+$. Spectra were acquired every 0.5 s. A fresh sample was introduced into the DART stream at t = 0.2 min for each measurement.

At temperatures of 350 ºC and higher, the mass spectra obtained by averaging the first few seconds of data were significantly different than the ones obtained by averaging the data collected after having exposed the sample to the heated DART gas stream for more than a minute. For temperatures higher than 350 ºC, an initial spike signaling the abrupt desorption of erythromycin from the tablet was observed and quickly followed by an increase in the relative abundance of the $[M\text{-}H_2O+H]^+$ ion, and at longer times, of the *m/z* = 558 fragment ion. These experiments highlight the importance of selecting the appropriate DART gas temperature to avoid artifacts in the spectra arising from thermal sample degradation, or thermal ion activation.

5.7. Accurate Mass DART-MS Analysis

The identification, by accurate mass measurements, of the AIs and impurities present in yaa-chud pharmaceuticals is of critical importance, as these may contain drugs contraindicated in pregnancy or childhood, give rise to clinically confusing adverse events, and, if used in subtherapeutic courses, engender antimicrobial drug resistance. The identification process involves obtaining accurate *m/z* values for the constituents ionized by DART in each sample. Although a single mass calibration check per day or per week is generally sufficient to ensure the accuracy of *m/z* measurements for most mass analyzers, it is a good practice to incorporate a mass drift correction when performing long analyses, such as for long LC runs, or if temporal shifts in the local environment are expected, as in the case of DART-MS analyses.

As mentioned in section 5.4.4, each sample was preceded and followed by a PEG standard to facilitate correction of the polynomial coefficients used in the mass

calibration file and to compensate for drifts in the *m/z* scale. When screening sample collections containing in excess of 254 samples, such as in this survey, this approach can be time consuming, as it involves repeating the mass drift correction procedure 254 times. Any drift in mass calibration during a DART run is usually due to a temperature change, since both the power supply output and the length of the flight tube are a function of temperature.[283] Evaluating the extent to which these changes affect the observed mass accuracy is thus important in deciding the limits for matching candidates in our database, and for the calculation of elemental compositions using software tools. If the mass accuracy threshold is set too low, then it is possible to miss the actual compound. If the mass accuracy threshold is set too high, then too many matches can be obtained. To estimate the mass accuracies obtainable by alternative DART-MS data processing strategies, two approaches were evaluated – a single mass drift correction and a time-dependent mass drift correction.

In the single mass drift correction approach, multiple peaks (> 5) within the PEG spectrum collected at the beginning of the DART run are compared to a reference file and are used to create a single calibration file. This calibration file is then applied to all sample spectra collected within the run. The primary benefit of this approach is the reduction in time required to collect and analyze the data. However, the advantage of increased throughput using this method may be offset by lowered mass accuracies. To explore this further, a second mass drift correction approach was performed. For the time-dependent mass drift correction, an individual calibration file is created for each PEG spectrum collected during the run, which contains alternating PEG and analyte mass spectra. The calibration file for the PEG spectrum collected immediately after a given

sample spectrum is then applied as a correction for that sample, thus, each sample spectrum is corrected using the PEG reference spectrum most closely associated to the sample spectrum in time. Figure 5.8 shows mass accuracies observed for drugs identified in the analysis of yaa-chud samples during 3 different DART-MS runs.

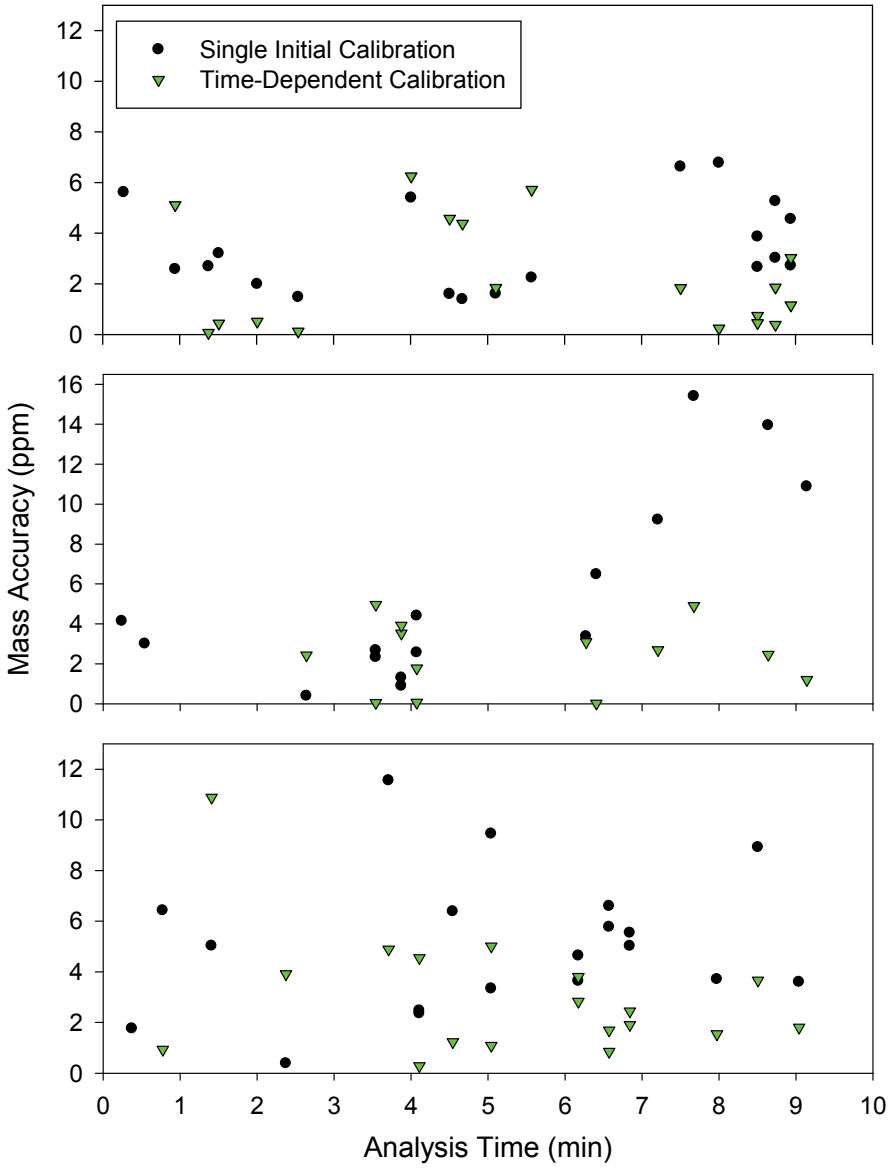

Figure 5.8. Observed mass accuracies for drugs analyzed during three independent DART-MS runs. Full circles show mass accuracies observed when a single initial mass drift correction was employed for the whole run. Green triangles show mass accuracies obtained for each individually-corrected sample (time-dependent calibration).

The average mass accuracy for each DART run was 3.3 ± 1.7 ppm, 5.7 ± 5.1 ppm and 5.3 ± 2.7 ppm (average ± standard deviation) using the single initial calibration method, and 2.2 ± 2.1 ppm, 2.4 ± 1.7 ppm and 3.0 ± 2.5 ppm using the time-dependent calibration. Significant statistical differences in the observed mass accuracies were observed for individual runs between the two mass calibration approaches tested. The differences in observed mass accuracy were greatest for samples analyzed at the end of the runs emphasizing the importance of using the more rigorous time-dependent calibration approach for analyses with long run times. The average mass accuracy of each run was better using the time-dependent calibration for each sample; however, the throughput of this approach is lower. For example, using the average time it took us to collect a spectrum (22.1 seconds), 4.1 minutes would be required to collect data for 10 samples (and 1 PEG spectrum) analyzed in a single run using the single mass drift correction approach. Using the time-dependent approach requires the analysis of an additional nine reference spectra, which adds 3.4 minutes to the collection time. The data analysis time would also be increased using this method.

The decision as to whether throughput or accuracy is the determining factor for which of these approaches to apply is dictated by the requirements of the experiment and the use of shorter run times would appear to negate this conflict entirely. The mean mass accuracy observed for all PEG standards was 3.8 ± 3.2 ppm, which is comparable with the manufacturer's specification of 5 ppm for ESI-TOF accurate mass measurements, indicating that the DART ion source did not introduce additional variables that negatively influenced mass accuracy. As the time-dependent calibration produced better mass accuracies, it was used for subsequent correction of yaa chud spectra.

5.8. Identification of Yaa Chud Contents

An attempt was made to visually identify the tablets and capsules in yaa chud using knowledge as to what was locally available along the Thai-Myanmar border, but this proved to be extremely difficult; thus, chemical identification was necessary. Of the 254 samples analyzed via DART-MS and/or AAS, 96% could be correlated to a particular AI and the percentage (number) of samples identified as having a particular AI is given in column 2 in Table 5.1. A subset of 100 physically-distinct pills (39%), representing all the "taxa" of medicine with different shape, printed codes and color that were present in the collection was also analyzed using LC-MS and/or AAS. An AI was identified in 89% of this subset and the percentage (number) of samples corresponding to a given AI within this subset is given in column 3. The frequency with which a given AI was identified in a single yaa chud packet is given in column 4 of Table 5.1 while adverse effects for these pharmaceuticals, as specified by the U. S. Food and Drug Administration (FDA), are given in column 5.[284]

Table 5.1. Composition of 50 yaa chud (N = 254 pills). G1 = gastrointestinal; Antacid 1 contains Cu, Zn, Mg, Fe, Ca, and Mn; G6PD = glucose-6-phosphate dehydrogenase; Antacid 2 contains Mg, Fe, and Ca. †FDA pregnancy categories are shown in brackets ([C] = animal studies show toxicity but there is insufficient human data, [D] = evidence of human risk, but clinical benefits outweigh risks).[284]

Drug	No. (%) of pills (N=254)	No. (%) of physically-distinct pills (N=100)	No. (%) of yaa chud containing AI (N=50)	FDA pregnancy category† & potential negative consequences (adverse effect)
Paracetamol	56 (22.0)	18 (18)	39 (78)	
Chlorpheniramine	34 (13.4)	12 (12)	30 (60)	Drowsiness, anti-muscarinic
Chloroquine	32 (12.6)	7 (7)	29 (58)	Not efficacious against P. falciparum malaria
Tetracycline / Doxycycline	29 (11.4)	12 (12)	26 (52)	[D] Efficacious against *P. falciparum* malaria in combination with quinine or artemisinin derivative. Upper GI irritation
Quinine	13 (5.1)	2 (2)	11 (22)	Remains effective if given for 7 days in combination with tetracycline. Tinnitus, hypoglycaemia
Vitamin B6	12 (4.7)	3 (3)	12 (24)	------
Chlorpheniramine + Paracetamol	12 (4.7)	2 (2)	8 (16)	Drowsiness, anti-muscarinic
No AI detected	11 (4.3)	11 (11)	0	-----
Acetylsalicylic acid	11 (4.3)	5 (5)	8 (16)	[D] Acidosis
Metamizole	10 (3.9)	5 (5)	10 (20)	[D] Agranulocystosis
Vitamins B_3 & C	5 (2.0)	2 (2)	4 (8)	
Ampicillin	5 (2.0)	2 (2)	4 (8)	Rash
Antacid 1	3 (1.2)	1 (1)	3 (6)	Negative interaction with doxycycline absorption
Paracetamol + Sulphamethoxazole	3 (1.2)	1 (1)	3 (6)	[C] Neonatal haemolysis, methaemoglobinaemia
Dexamethasone	2 (0.8)	2 (2)	2 (4)	Immunosuppression
Indomethacin	2 (0.8)	2 (2)	2 (4)	[D] Gastric irritation
Primaquine	2 (0.8)	1 (1)	2 (4)	[C] Haemolysis in G6PD deficiency
Thiamin	2 (0.8)	2 (2)	2 (4)	
Pyrimethamine	1 (0.4)	1 (1)	1 (2)	
Chloroquine + Paracetamol	1 (0.4)	1 (1)	1 (2)	Not efficacious against P. falciparum malaria
Alprenolol	1 (0.4)	1 (1)	1 (2)	[C] Bradycardia
Tolperisone	1 (0.4)	1 (1)	1 (2)	Contraindicated in pregnancy
Amitriptyline	1 (0.4)	1 (1)	1 (2)	Anti-muscarinic
Prednisolone	1 (0.4)	1 (1)	1 (2)	Immunosuppression
Prazepam	1 (0.4)	1 (1)	1 (2)	Habit forming
Vitamin B_3, B_6 B_7	1 (0.4)	1 (1)	1 (2)	
Diclofenac	1 (0.4)	1 (1)	1 (2)	[D] Gastric irritation
Antacid 2	1 (0.4)	1 (1)	1 (2)	Negative interaction with doxycycline absorption

Throughout the survey, there was good agreement between the DART-MS and LC-MS results providing an additional level of confidence about the identity of the AI(s) in any given sample. As an example, consider Figure 5.9 that shows mass spectra for sample 22-2, which was provisionally identified according to its shape and color as paracetamol.

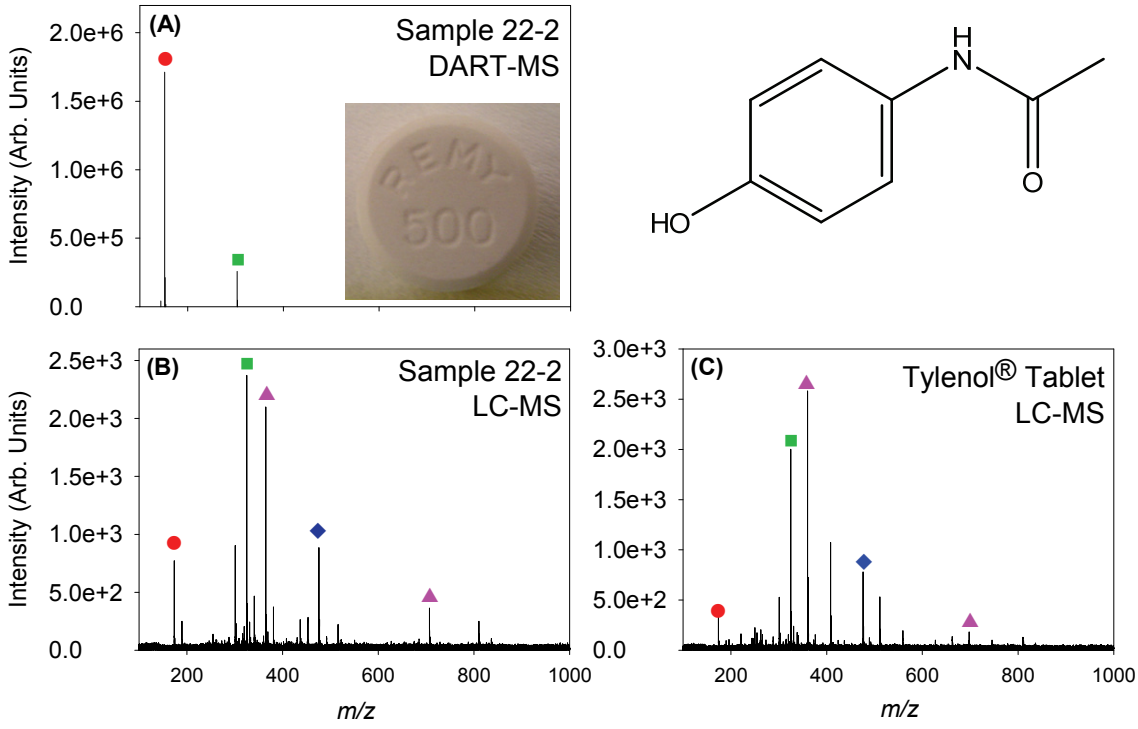

Figure 5.9. (A) DART-MS spectrum of a sample visually identified as paracetamol (code 22-2; inset shows an image of this tablet), (B) LC-MS spectrum of sample 22-2, and (C) LC-MS spectrum of a paracetamol tablet (Tylenol®). The peaks observed correspond to the monomer ion (●; $[M+Na]^+$ for LC, $[M+H]^+$ for DART), dimer ion (■; $[2M+Na]^+$ for LC, $[2M+H]^+$ for DART), $[3M+Na]^+$ (◆), and excipient (▲).The structure of paracetamol is shown in the upper, right corner.

The DART-MS mass spectrum for this sample (Fig. 5.9.A), which only shows peaks corresponding to the protonated paracetamol monomer and dimer species, is

relatively clean when compared to the LC-MS mass spectra of sample 22-2 (Fig. 5.9.B). The identification of this tablet as paracetamol was verified experimentally by comparison to the LC-MS mass spectrum of a paracetamol reference standard (Tylenol®, Fig. 5.9.C), which shows sodiated paracetamol monomer, dimer, and trimer peaks, formed by the adduction of sodium to the neutral paracetamol molecules, as well as the presence of lactose/sucrose as an excipient.

Sporadic, low intensity signals due to impurities and partially extracted excipients were frequently observed during collection of mass spectral data, but their assignment to known chemical substances was outside the scope of this study. In eleven (4.3%) of the samples, no AI could be identified in either the mass or atomic spectra collected suggesting that these drugs may be composed of degraded or counterfeit drugs, or may not contain any AI. A database of color photographs of the tablets, mass spectral peak lists, and compounds identified is available for viewing on the Fernández group website.[285]

Of 132 yaa chud capsules and/or tablets that had both a provisional identity, based on physical appearance, and also a confirmed identity from chemical analysis, 85 (64%) were identified correctly by visual inspection. Of the samples that could not be provisionally identified, 82% were subsequently identified via MS, further emphasizing the need for rapid chemical analysis as visual inspection of tablets and capsules cannot be used to definitively assign AIs to pharmaceuticals of unknown composition. Moreover, visual inspection by pharmacists also yielded a number of incorrect AI's including diazepam, phenylbutazone, chloramphenicol, co-trimoxazole, ergotamine tartrate, ambroxol, vitamin A & E compound and phenylpropapanolamine & belladonna

alkaloids. Figure 5.10 shows mass spectra obtained from a sample that had been visually identified as diazepam. The MS analysis of this sample revealed that this sample contained chlorpheniramine and not diazepam, as can be concluded by comparison of the sample mass spectra obtained by both DART-MS (Fig. 5.10.A) and LC-MS (Fig. 5.10.B) with the mass spectrum of a chlorpheniramine standard (Fig. 5.10.C).

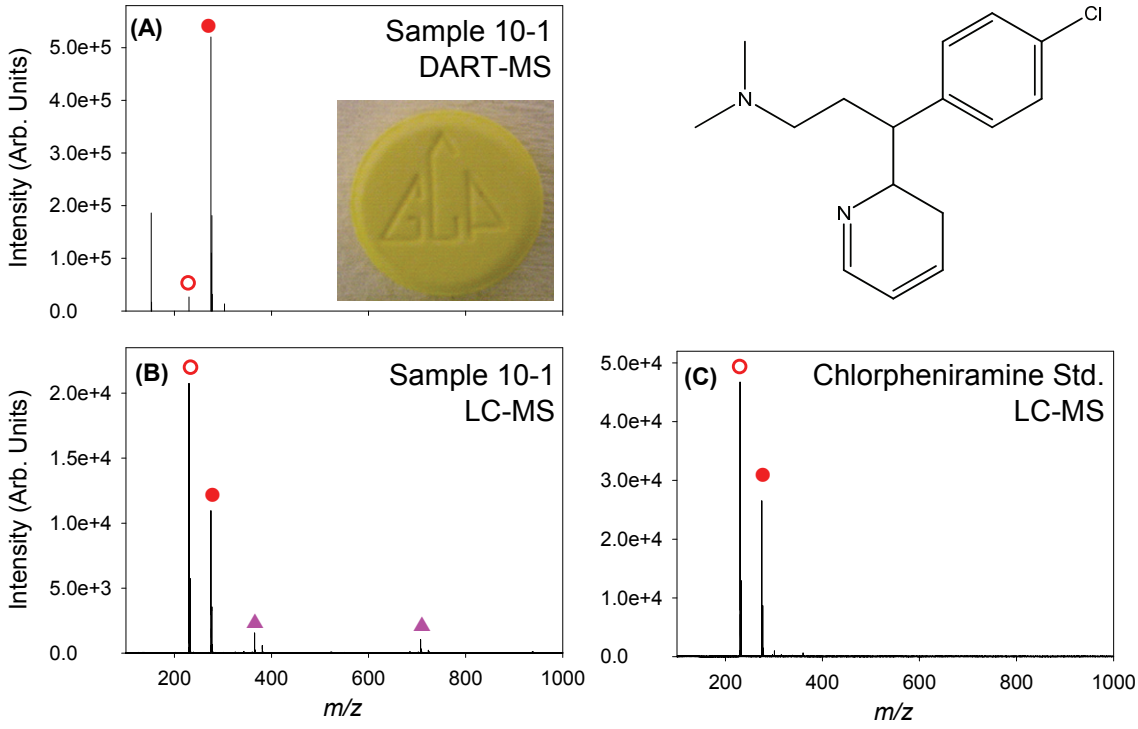

Figure 5.10. (A) DART-MS spectrum of a sample that had been visually identified as diazepam (code 10-1; inset shows an image of this tablet), (B) LC-MS spectrum of sample 10-1, and (C) LC-MS spectrum of a chlorpheniramine standard. The peaks observed correspond to $[M+H]^+$ (●), a major fragmentation product $[M\text{-}NHC_2H_6+H]^+$ (○) and excipient (▲).The structure of chlorpheniramine is shown in the upper, right corner.

5.9. Implications of These Results for Public Health

Only 7 yaa chud (14%) contained medicine that could have potentially cured *P. falciparum* malaria if taken as part of an appropriate dosing regimen. The remainder of

yaa chud had no potential curative effect for malaria. All but one of the yaa chud contained medicines that may have alleviated some symptoms (fever, headache) but would have caused harm by delaying access to curative antimalarials, which are freely available through local Thai hospitals and governmental agencies. Using the FDA pregnancy categories[284] and the British National Formulary[286] guidelines, 41 (82%) of the yaa chud were contraindicated for pregnancy. This indicated that in addition to not being efficacious, the use of these medicines may be harmful to pregnant patients and their fetuses. Even if the yaa chud contained effective antimalarials, they were unlikely to be efficacious if taken as recommended by the sellers.

These yaa chud were collected in 2000 and 2001 and malaria treatment has changed locally since then as considerable effort has been expended to improve the use of ACT therapy.[266] Mainland SE Asia has had great importance in the spread of drug-resistant malaria and preliminary reports that artemisinin resistance has arisen on the Thai/Cambodia border are of considerable concern.[287, 288] If the consumption of yaa chud containing inadequate antimalarial therapy or with inadequate dosing leads to treatment failure, the spread of drug-resistant parasites to other communities may occur.[268, 289] Therefore, further work to determine if artemisinin derivatives and mefloquine are now used in yaa chud and also to determine how often yaa chud is taken by malaria patients is needed to assess the current threat of yaa chud consumption on public health.

5.10. Conclusion

The benefits of rapid screening via accurate DART-MS were presented for studies to identify AIs of drugs present in mixed therapeutics. A detailed study of combination drug packets screened by DART-MS demonstrated the ability of this latest generation of ionization methods to achieve high throughput accurate mass identifications of 96% of samples analyzed during this survey. An investigation of the effect of temperature and flow rate of the helium gas stream, as well as the potential applied to the grid electrode, demonstrated that improved sensitivity for the protonated paracetamol peak was generally accessible by increasing the temperature and flow rate and decreasing the grid electrode. However, some experimental conditions can also induce fragmentation and/or oxidation of the protonated molecule resulting in decreased sensitivity. Two approaches to performing mass calibrations were explored to identify the factors that most influence the quality of mass spectral data obtained during accurate mass experiments. The results emphasize the importance of using a mass correction methodology that addresses the needs of the experiment being executed. The following were the most common compounds identified in the yaa-chud collection: paracetamol (33.5%), chlorpheniramine (18.1%), and chloroquine (16.5%).

CHAPTER 6. DART-MS INVESTIGATION OF COUNTERFEIT DRUGS

6.1. Abstract

Since 1998, the serious public health problem in SE Asia of counterfeit artesunate, containing no or subtherapeutic amounts of the active antimalarial ingredient has led to deaths from untreated malaria, reduced confidence in this vital drug, caused large economic losses for legitimate manufacturers, and led to concerns that artemisinin resistance might be engendered.[186] This chapter presents work aimed at developing rapid screening methods to identify counterfeit drugs, and discusses an international collaborative effort (named operation Jupiter) led by Dr. Paul N. Newton that is geared towards determining the source of these counterfeits.

6.2. Background on Operation Jupiter

Counterfeit drugs are defined as those which are "deliberately and fraudulently mislabeled with respect to identity and/or source" and may include products with the "wrong" ingredient(s), without AI(s), or with an insufficient amount of AI(s).[290] In recent years, a particularly alarming case of drug counterfeiting has been reported by field researchers[202, 203, 291] who have detected counterfeit products that mimic vital antimalarial medicines containing artesunate (Figure 6.1), an antimalarial artemisinin derivative that was first developed in the People's Republic of China[292] and is widely used throughout SE Asia and Africa for the treatment of *P. falciparum* malaria.[201, 292, 293]

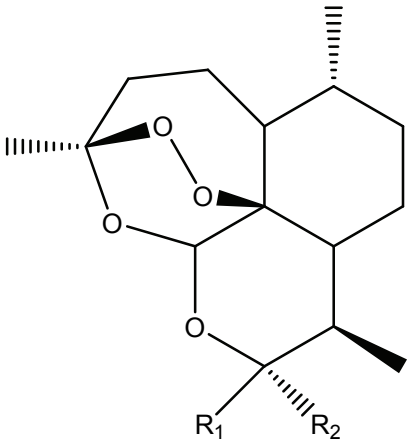

Artemisinin	$R_1, R_2 = O$
Dihydroartemisinin	$R_1 = H, R_2 = OH$
Artemether	$R_1 = H, R_2 = OCH_3$
Ateether	$R_1 = H, R_2 = OCH_2CH_3$
Artelinic acid	$R_1 = H, R_2 = OCH_2CH_6H_5CO_2H$
Artesunic acid	$R_1 = O_2CCH_2CH_2CO_2H, R_2 = H$

Figure 6.1. Structure of artemisinin derivatives including artesunic acid (artesunate).

It is believed that the consumption of fake antimalarials has resulted in many deaths, some of them fully documented,[204-206] and evidence suggests that production of counterfeit artesunate tablets is on an industrial scale. For example, one health care organization in SE Asia purchased 100,000 artesunate tablets, all of which were later shown to be counterfeit.[291] Classic hyphenated analytical techniques, such as LC-MS, are capable of discriminating between genuine and counterfeit pharmaceuticals but lack the required sample throughput to survey such large numbers of samples in a reasonable amount of time.[294]

Although most patients with malaria would survive if provided with timely access to affordable, effective medicines, over one million people die each year as a result of the disease.[290, 295] Unfortunately, due to the global spread of drug resistance and the practical difficulty of delivering health care to rural communities, most people who are at risk of contracting malaria have not had such access until very recently. The current resurgence in activity to eradicate malaria can be attributed to the development of ACT treatment and to the accumulation of international financial support allowing for inexpensive, or

free, distribution of antimalarials to at-risk populations.[293] However, the poor quality of antimalarial medicines available in the tropics has been a major obstacle in the struggle to reduce the prevalence of malaria. Furthermore, recent data has indicated that antimalarials have been particularly targeted by counterfeiters, which has had a detrimental effect on the situation.[186]

Since 1998 an epidemic of multiple types of counterfeit artesunate tablets have been identified in mainland SE Asia. Ad hoc surveys conducted from the year 2000 until present times in Myanmar, Lao People's Democratic Republic (Lao PDR, Laos), Cambodia, Vietnam, and along the Thai-Myanmar border suggested that 33-53% of bought artesunate was counterfeit, containing either no or subtherapeutic quantities of artesunate.[185, 202, 203, 291, 296-298] In SE and East Asia there are at least 16 manufacturers of artemisinin and its derivatives[299] and millions of tablets are produced each year both for consumption in Asia and export to Africa. Of these manufacturers, one major producer of artesunate, Guilin Pharmaceutical Co. Ltd. (Guilin, Guangxi autonomous region, China), has been exclusively targeted by counterfeiters. Counterfeit artesunate pharmaceuticals containing no or subtherapeutic quantities of artesunate have recently been described in Asia.[185] Such counterfeits, which may foil simple screening tests, will engender the selection and spread of artemisinin-resistant *P. falciparum* parasites, which would be disastrous for malaria control in Asia and thereafter in Africa.

Since the first description of fake artesunate in 2000, there has been little action in comparison to its public health consequences. With little progress and worsening contamination of the supply of antimalarials in the Greater Mekong sub-Region, a confidential meeting was held in Manila in May 2005 at the Western Pacific Regional

Office (WPRO) of the WHO. The meeting brought together WHO officials, physicians, pharmacists and scientists working in the region with the International Criminal Police Organization (INTERPOL) to discuss what could be done. It was decided that a joint effort be made to investigate where the counterfeits were being manufactured and to develop an intelligence document that could be presented to concerned governments with a request that measures be taken to stop the lethal manufacture and trade in counterfeit artesunate. This chapter presents the analytical screening methodology developed during this investigation and summarizes the findings relevant to public health.

6.3. Experimental Details

6.3.1. Sample Collection and Details

Sample collection was organized by Dr. Paul N. Newton. From 1999 – 2006, 391 counterfeit and genuine artesunate tablets were collected in a wide area of SE Asia encompassing Laos (115), Myanmar (137), Vietnam (75), Cambodia (48), and along the Thai-Myanmar border (16) and were kept refrigerated (4° C) until analysis. These samples underwent Fast Red Trypaflavine (TR) Dye testing[300, 301] and/or HPLC and ambient MS. A subset of 27 fakes and 5 genuines sent, along with four fake (collected in Cambodia) and two genuine samples from the United States Pharmacopeia (USP) Drug Quality and Information program, also underwent detailed forensic chemical and botanical examination as part of the Jupiter operation. In addition, five samples seized by the subsequent Ministry of Public Security (MPS) investigation in China were analyzed. All laboratories performed the analyses blinded to the results from other laboratories.

6.3.2. Analysis of Physical Appearance

The physical appearance and text on packets, leaflet inserts and blisterpacks were examined by Paul Laurin of the Royal Canadian Mounted Police Forensic Laboratory Services National Anti-Counterfeiting Bureau in Ottawa, Ontario, Canada.

The tablets were compared with known genuine Guilin Pharmaceutical Co. Ltd artesunate obtained directly from the company. Packets, leaflets and blisterpacks were examined with a 6x hand lens, 100x stereo microscope and a handheld UV (375nm) light source and then electronically scanned. Batch numbers, expiration and manufacture dates, the color, clarity and text of printing on the blisterpack, packet and leaflet (when present) were documented. Guilin provided information about the validity of batch numbers.

6.3.3. Botanical Analysis

Botanical analyses were performed by Dallas C. Mildenhall from GNS Science, Lower Hutt, New Zealand as described in Newton, et al.[188] Briefly, tablets were dissolved in hot distilled water or 10% hydrochloric acid yielding two fractions of material in which the top fraction, which contains spores and pollen, was dissolved in 9:1 (v:v) acetic anyhydride:sulfuric acid. Mineral material remaining was removed by 50% hydrofluoric acid and was filtered through a 6 μm mesh. All residues were mounted on glass microscope slides and examined at a magnification of 125-250x. Suspected pollen grains were identified by comparison with reference spore and pollen material

6.3.4. X-Ray Diffraction and Stable Isotope MS Analyses

X-ray diffraction (XRD) analyses were performed by S. W. Ray Soong from GNS Science, Lower Hutt, New Zealand while stable isotope ratio MS was performed by Kevin Faure, also from GNS Science. The basic protocol was as follows: each sample was crushed and mounted as a slurry on a silicon plate and was analyzed by XRD (X'Pert Pro X-ray Diffractometer, Philips, Almelo) and isotope ratio analysis to determine the mineral composition. Values, in per mil (‰), are reported in $\delta^{18}O$ $\left(1000 \times \left(\left(\frac{^{18}O}{^{16}O}\right)_{Samp.} - \left(\frac{^{18}O}{^{16}O}\right)_{Std.}\right) \div \left(\frac{^{18}O}{^{16}O}\right)_{Std.}\right)$ and $\delta^{13}C$ $\left(1000 \times \left(\left(\frac{^{13}C}{^{12}C}\right)_{Samp.} - \left(\frac{^{13}C}{^{12}C}\right)_{Std.}\right) \div \left(\frac{^{13}C}{^{12}C}\right)_{Std.}\right)$ notation.[302] Samples were analyzed in duplicate and the values were averaged.

6.3.5. LC Diode Array Analysis

Tablets were processed and analyzed for artesunate using HPLC by Dr. Michael D. Green from the Division of Parasitic Diseases at the National Center for Infectious Diseases of the Centers for Disease Control and Prevention in Atlanta, GA.[300, 301]

A 150 x 4.6 mm octadecylsilica column with a mobile phase consisting of 45% acetonitrile and 55% 0.05 M perchlorate buffer (pH 2.5) effectively separated artemisinin, paracetamol, and artesunate. For quantitative paracetamol analysis, the mobile phase was changed to 10% acetonitrile and 90% perchlorate buffer. Components were detected using a diode array detector with wavelengths set at 220 and 254 nm. UV spectra of samples were compared with artesunate, artemisinin and paracetamol reference standards for validation.

6.3.6. DART-MS Analysis

DART-MS analyses were performed using a home-built DART ion source coupled to the AccuTOF mass analyzer and using a slightly modified version of the method described in section 5.4.3. The DART ion source and the AccuTOF were operated in positive-ion mode. He gas (350 ºC) was introduced into the DART discharge chamber at 2.8 L min^{-1}. The glow discharge was initiated by application of 3 kV to the DART needle electrode while the grid voltage was held at 300 V. The mass spectrometer ion optics settings were the same as those described previously with the following exceptions: inlet orifice = 80 ºC, 30 V; ring electrode = 5 V; orifice 2 = 34 V; ion guide bias voltage = 29 V; ion guide RF amplitude = 300 V; detector = 2950 V. Tablets were sampled as previously described. Data processing was also performed using the method described in section 5.4.3 and results were searched against an expanded library which included the drugs listed in WHO's List of Essential Medicines[280] and a list of 238 common drugs identified in human blood via LC-MS that was compiled by Gergov et al.[303] Reactive DART-MS was also performed to improve the specificity of artesunate analysis. For these experiments, the sampling region was exposed to ammonia vapors emitted from a beaker containing ammonium hydroxide (28% in water, Sigma Aldrich, St. Louis MO).

6.3.7. DESI-MS Analysis

DESI-MS experiments were performed by Leonard Nyadong, a graduate student in the Fernández Research Group.

As described briefly in section 1.4.1, in DESI-MS analysis, a high-speed electrically-charged liquid spray is directed at the surface of a solid for direct analysis of the surface composition. For pharmaceuticals, the charged spray is directed at the tablet under inspection as shown in Figure 6.2.

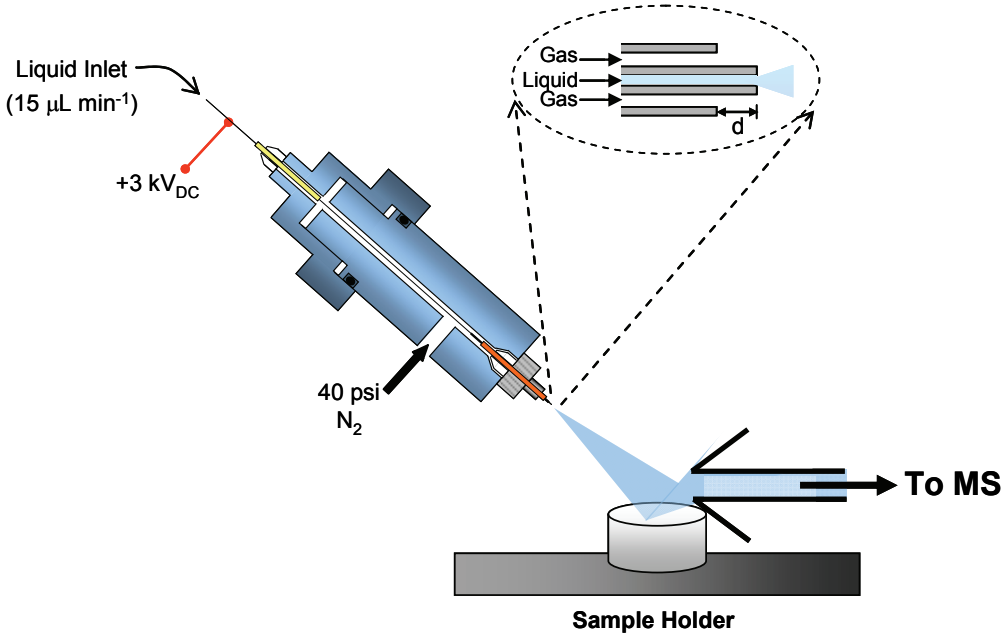

Figure 6.2. Schematic of the DESI-QiT setup.

The DESI spray progressively dissolves material from the tablet, giving a qualitative depth profile. The charged droplets containing tablet material are sampled downstream by a mass spectrometer, providing a spectrum of the sample components. As no tablet dissolution is required, this technique is well-suited for screening large number of samples. Several points on the tablet surface and interior were sampled during DESI analysis to obtain an accurate representation of the components present. A homebuilt DESI ion source was used in all experiments with QiT detection.[171] Two operational modes were explored – reagentless DESI and reactive DESI. In reagentless DESI, a

charged (3 kV_{DC}) solution of 75:25 (v:v) acetonitrile:nanopure water was sprayed onto the tablet at a flow rate of 5 μL min^{-1}. This mode allowed for non-specific detection of analytes having a larger molecular weight than those typically accessible via DART-MS. DESI MS was also performed in "reactive" mode, which allowed for the specific and sensitive detection of artemisinin derivatives. Reactive DESI experiments were performed by adding 100 μM dodecylamine (DDA) (Sigma-Aldrich) to the spray solution, and repeating the procedure described above.

6.4. Analysis of Tablet Packaging

A total of sixteen different hologram types that mimic the genuine packaging used by Guilin (Fig. 6.3.A) have been identified since 1999 and range in sophistication from crude stickers (Fig. 6.3.B) to highly sophisticated fake holograms such as the ones shown in Figure 6.3 C and D. Like the genuine Guilin packaging, the hologram in Figure 6.3.C includes the legend 'Guilin Pharma' in microscopic font below the illustrated river and the Chinese registration code 'X-52' visible under UV light. Upon close visual inspection, it is apparent that this packaging has some defects such as misalignment in the color, size, and arrangement of the blocks in the circular border at the edge of the hologram and also variation in the wavy lines at the bottom of the label. The wavy lines at the bottom of the fake hologram shown in Figure 6.3.D are more similar to those of the genuine packaging but this fake also shows distortion of the circular border and does not contain the UV stamp.

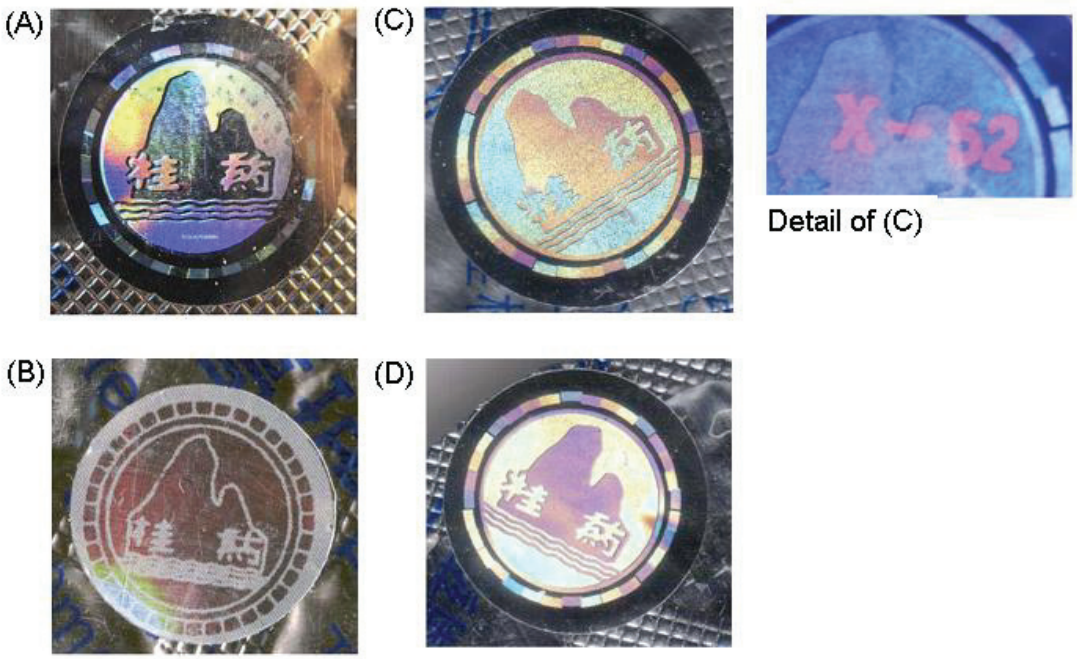

Figure 6.3. Examples of genuine and counterfeit holograms. (A) Genuine Guilin pharmaceutical artesunate blister pack hologram. (B) A type 2 sticker copy. (C) A type 10 hologram copy with the fake "X-52" stamp as seen under UV light. (D) Type 15 hologram copy from a counterfeit artesunate tablet seized from the China/Myanmar border.

As of May 2009, sixteen different types of fake packaging have been identified and are described in detail in Figure S-1 from Newton, et al.[188] One feature common to all of these counterfeit holograms is misalignment of the blocks forming the circular border of the Guilin logo. Other discrepancies noted between genuine packaging and these fakes include printing errors in boxes (including misalignment of letters or words), differences in font, spelling mistakes, and variable print quality. Figure 6.4 shows a map of the distribution of fake artesunate in relation to the fake packaging type.

Figure 6.4. Map of the distribution of fake artesunate, collected by Wellcome Trust-University of Oxford SE Asian Tropical Medicine Research Program and Collaborators. Map drawn by Mr. Chongkham Phonekeo and reproduced with permission from Newton, et al.[188]

6.5. Results of Palynological and Mineralogical Analyses

Most of the spores and pollen identified during this survey have a distinct northern Asian temperate signature with evidence of plants such as firs, pines, cypresses,

sycamores, alders, wormwood, willows, elms, wattles, and fern spores. Figure 6.5 shows photos of some of the debris found in these counterfeit tablets.

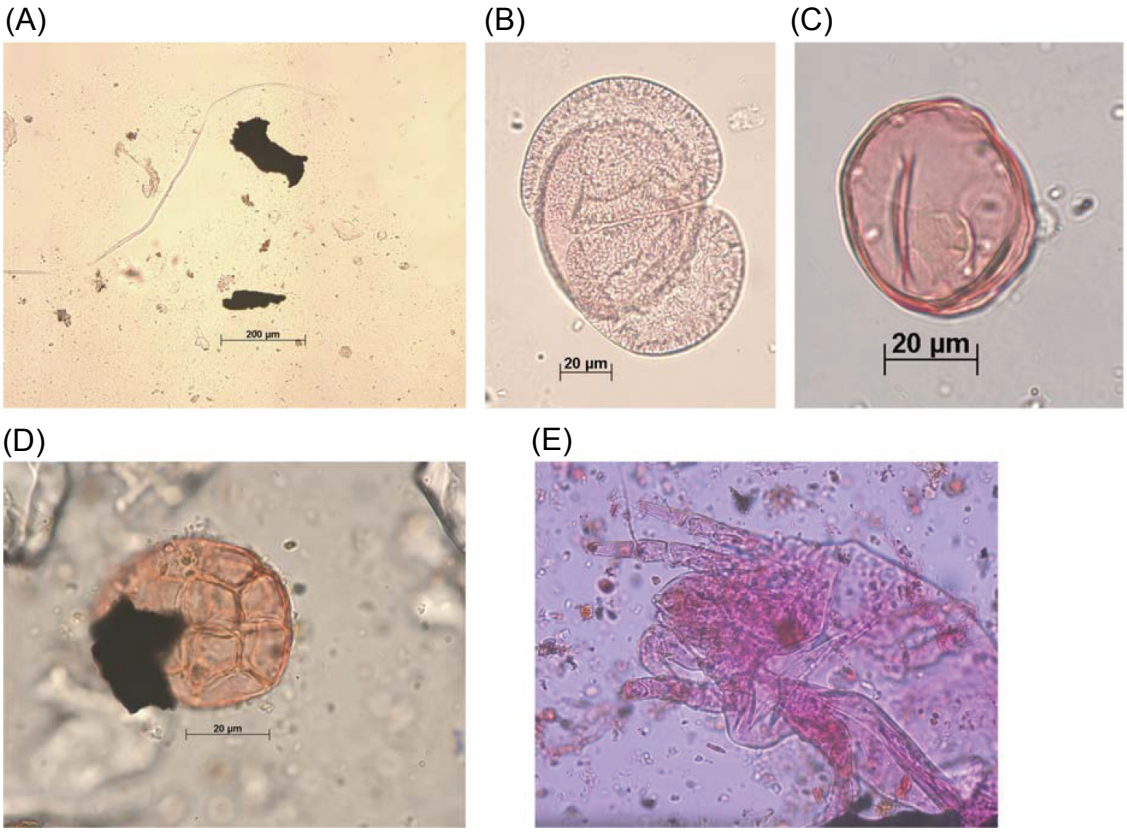

Figure 6.5. Photomicrographs of material found in fake artesunate tablets. (A) Debris, including charcoal fragments. (B) *Pinus* pollen grain. (C) *Juglans* pollen grain. (D) *Acacia* pollen grain with charcoal deposit. (E) *Dermatophagoides* mite nymph.

The estimated origin of the samples includes northernmost Vietnam, southern China, and near the mountains bordering Myanmar and Vietnam. Some of the plant remains, such as *Juglandaceae* pollen (walnut), *Carya* (wing nut), and *Pterocarya* (hickory), suggest manufacture in southern China.[304] In terms of botanical analysis for samples having different types of fake hologram/sticker, Type 2 differs from the others as it lacks fern spores, Type 1 contained little material but appeared similar to Type 3, and

Types 10, 11 and 12 had similar pollen signatures. Types 5 and 8 did not contain anything to enable comparisons to be made and Types 4, 6, 7, 9, 13 & 14 were not examined.

In addition to plant remains, five samples contained invertebrates, including a *Dermatophagoides* mite nymph (from Type 11, Vietnam, Fig 6.5.E) which is commonly found in house dust and has a global distribution. All fake artesunate tablets contained charcoal fragments and black chips, broken up by the processing for pollen. In some samples, charcoal was so abundant that it suggested the source was an area suffering severe air pollution.

XRD demonstrated great variability in tablet mineralogy. Although, maize starch is the main excipient in the genuine Guilin product, talc (hydrated magnesium silicate), calcite (calcium carbonate) and starch were the main excipients detected in the counterfeit tablets. Trace amounts of aragonite were present in two calcite-dominated fake tablets and traces of chlorite (iron-magnesium hydrosilicate) and quartz (silicon dioxide) were found in another two. Stable isotope analysis of the calcite fraction gave $\delta^{18}O$ and $\delta^{13}C$ values between -11 to +2% and +2 to + 25 %, respectively, as shown in Figure 6.6.

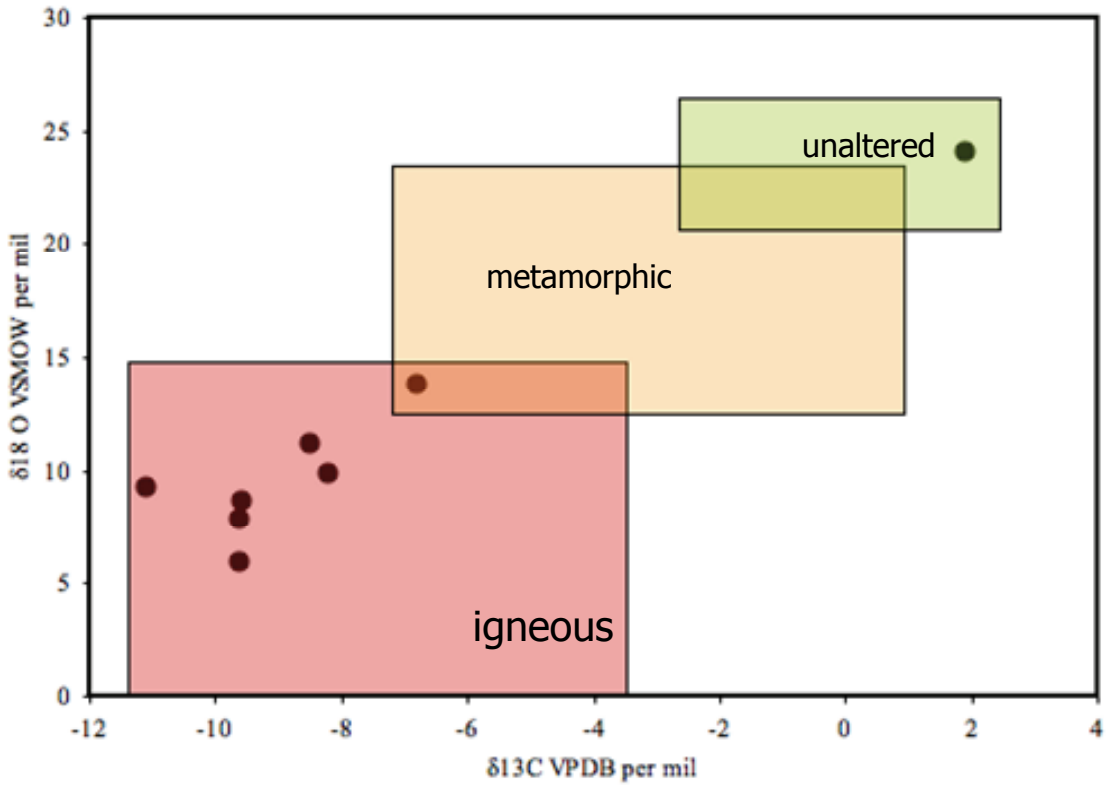

Figure 6.6. Plot of $\delta^{13}C$ and $\delta^{18}O$ values, in % of carbonate in tablets. Approximate values expected from calcite in different geological environments (pink = igneous; yellow = metamorphosed; green = unaltered) is also plotted. Sample 05/17 is represented by the top right data point.

Given the similar isotope signatures, the calcite in all (Types 2, 4, 5, 8, and 11) but one sample appears to come from the same source and is either hydrothermal or medical in origin. The one exception is sample 05/17 (Type 12) from southern Laos which, if the calcite is assumed to have been formed by natural geological processes, is typical of marine limestone.

6.6. DART and DESI Method Development for Screening Counterfeit Artesunate Antimalarials

One common pitfall in the analysis of artesunate by MS is its labile nature, which makes detection of ions corresponding to the intact molecule difficult. As artesunate is acidic, it was anticipated that negative mode ionization would yield an intense $[M-H]^-$ peak, however, this was not the case as can be seen in Figure 6.7, which shows the negative DART mass spectrum of a genuine (Fig. 6.7.A) and a counterfeit (Fig. 6.7.B) artesunate tablet.

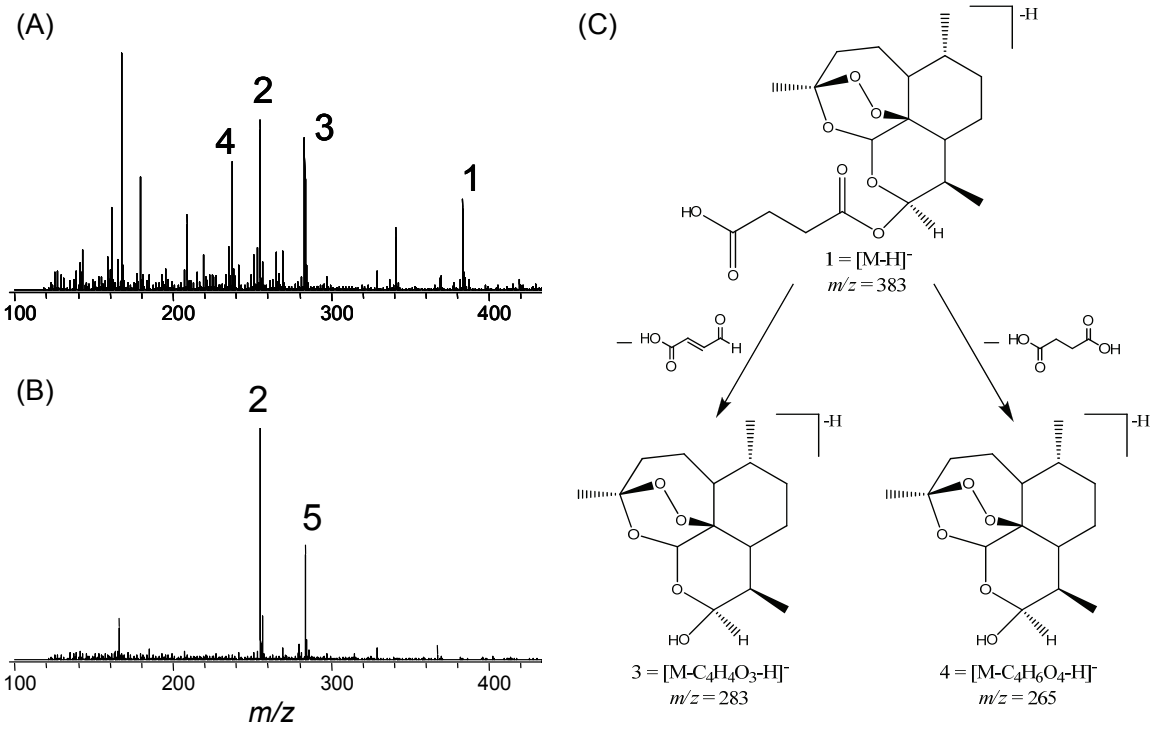

Figure 6.7. Negative mode DART-MS mass spectra for a genuine (A) and counterfeit (B) artesunate tablet. The structure of artesunate and its dominant fragment ions are shown in (C). (1) = $[M - H]^-$, (2) = [palmitic acid - $H]^-$, (3) = $[M - C_4H_4O_3 - H]^-$, (4) = $[M - C_4H_6O_4 - CO - H]^-$, (5) = [stearic acid - $H]^-$.

The mass spectrum shown in Fig. 6.7.A presents signals corresponding to the diagnostic $[M-H]^-$ artesunate anion (experimental *m/z* = 383.1702, theoretical *m/z* = 383.1711) and to palmitic acid, an ubiquitous contaminant. Artesunate fragment ions due to dissociation of the highly labile artesunate carboxylic side chain were also detected in this spectrum. The spectrum in Fig. 6.7.B, corresponding to a sample which had been classified as counterfeit by the Fast Red TR dye test,[300, 301] does not contain signal corresponding to any artesunate species. Only palmitate and stearate anions were detected (calcium stearate is a common pharmaceutical excipient).

As shown in Figure 6.7, negative ion mode DART-MS allows the rapid differentiation of counterfeit from genuine artesunate tablets. However, the high specificity of this DART ion mode prevents the detection of analytes that are not easily deprotonated. Not only is the absence of artesunate of concern in these tablets, but also the potential presence of other physiologically-AIs. These "wrong active ingredients" are sometimes added to counterfeit pharmaceuticals to either simulate alleviation of symptoms, or perhaps are waste powders left over from the manufacture of other pharmaceuticals.[305] For this reason, an ionization mode that allows screening for artesunate and for other common drugs is highly desirable.

To that end, positive ion mode DART-MS was performed, however, only a few artesunate fragment ions were detected. When the sample was exposed to ammonia vapors during DART ionization, the artesunate $[M+NH_4]^+$ ion was readily observed. Although the formation mechanism of this ion has yet to be studied, this doped-DART approach has proven to be extremely useful for analytical purposes. This approach is conceptually similar to the reactive DESI experiment performed by Takats, et al.[37] and to

the method developed by Nyadong, et al. for the analysis of artesunate.[171] Figure 6.8 shows the mass spectra of a genuine artesunate tablet obtained using doped-DART ionization (Fig. 6.8.A) and DESI ionization (Fig. 6.8.B).

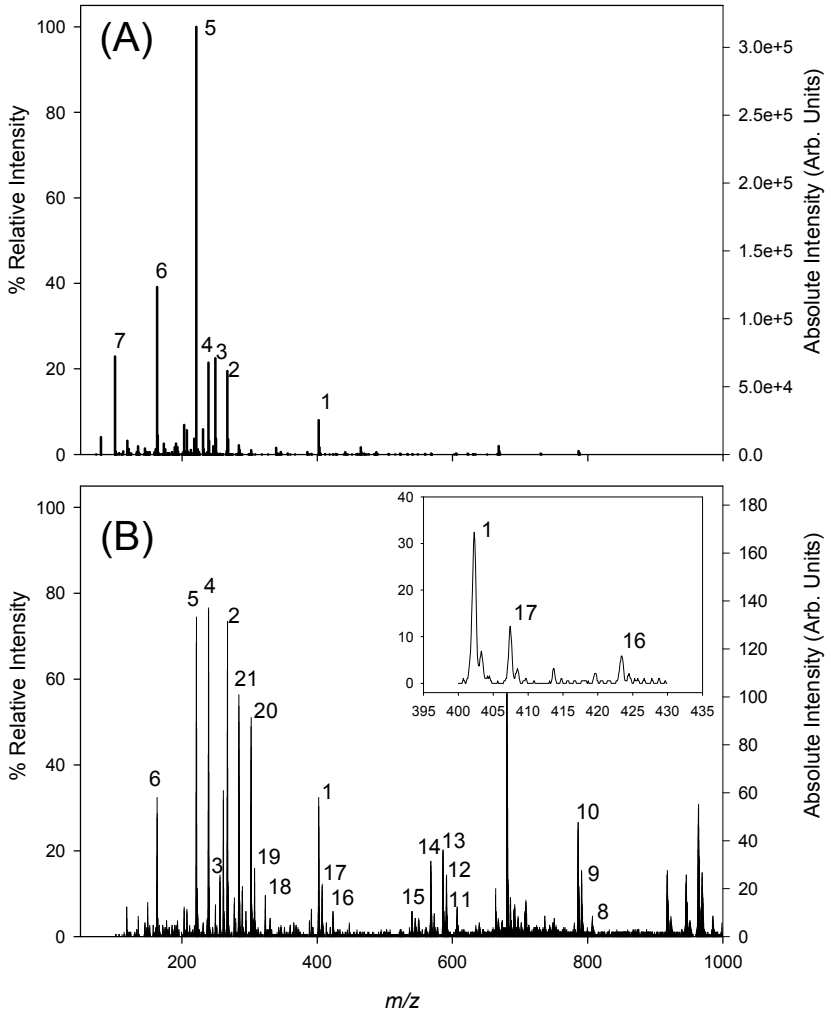

Figure 6.8. Screening of a genuine artesunate (M) tablet by (A) ammonia-doped DART-MS and (B) reagentless DESI-MS. (A = $C_4H_6O_4$ and B = $C_4H_4O_3$: 1 = $[M + NH_4]^+$, 2 = $[M – A + H]^+$, 3 = $[M – A - H_2O + H]^+$, 4 = $[M – A – CO + H]^+$, 5 = $[M - A – CO - H_2O + H]^+$, 6 = $[M – A - C_4H_7O_3 + H]^+$, 7 = $[A - H_2O + H]^+$, 8 = $[2M + K]^+$, 9 = $[2M + Na]^+$, 10 = $[2M + NH_4]^+$, 11 = $[2M – A – B + K]^+$, 12 = $[2M - A – B + Na]^+$, 13 = $[2M – A – B + NH_4]^+$, 14 = $[2M – A – B - H_2O + NH_4]^+$, 15 = $[2M – A – B - H_2O – CO + NH_4]^+$, 16 = $[M + K]^+$, 17 = $[M + Na]^+$, 18 = $[M - B + K]^+$, 19 = $[M – B + Na]^+$, 20 = $[M – B + NH_4]^+$, and 21 = $[M - A + NH_4]^+$.)

Reactive DART, as shown in Fig. 6.8.A, not only produced a diagnostic $[M+NH_4]^+$ ion, but also fingerprint fragment ions that could be assigned with an average error of 2.2 mmu. Together, the $[M+NH_4]^+$ and fragment ions accumulated 13.5 identification points enabling the positive identification of the target analyte in excess of what is recommended by new EU guidelines.[306, 307]

Both DESI and DART produced spectra with good S/N in five seconds, demonstrating an improvement of over two orders of magnitude in terms of sample throughput when compared to LC-MS. The DESI-MS mass spectrum also included several ions corresponding to adducts of the intact molecule (Fig. 6.8.B, insert), including $[M+H]^+$, $[M+Na]^+$ and $[M+K]^+$, as well as ammoniated, sodiated and potassiated fragment and cluster ions. However, lower DESI jet flow rates caused the relative abundances of these species to change. Despite the low amount of IE believed to be deposited into the analyte ions during DESI, fragmentation was also observed – an indication of the lability of the $[M+H]^+$ ion itself. A fragmentation pattern similar to 6.8.B is also observed in pESI mass spectra of artesunate.

6.7. Results of DART- and DESI-MS Screening

The success of the DART- and DESI-MS methods for differentiation of genuine and counterfeit antimalarials enabled further investigation of the entire set of counterfeit artesunate antimalarials. Figure 6.9 shows the DART-MS mass spectra of counterfeit artesunate samples of increasing sophistication.

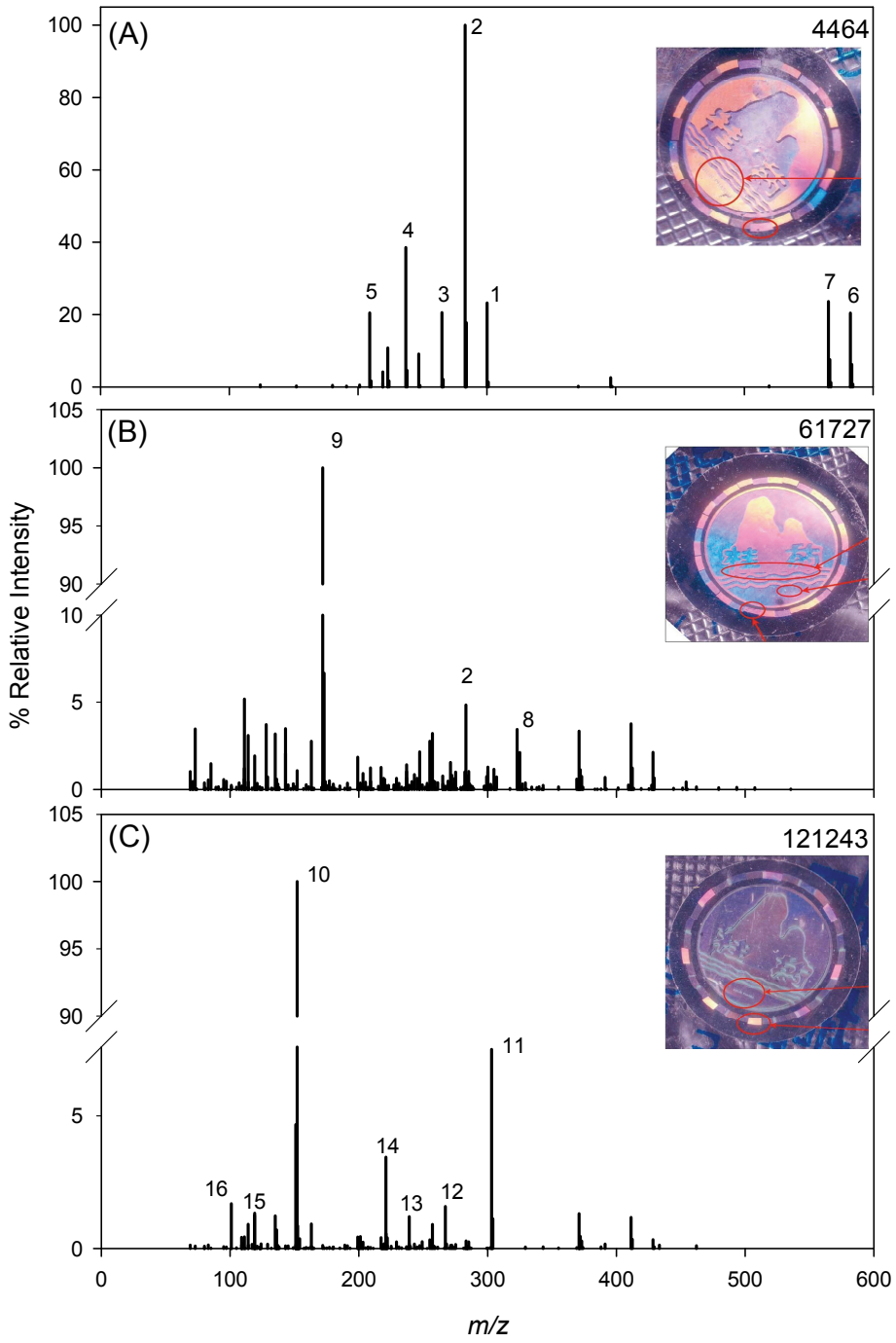

Figure 6.9. DART-MS spectra of sophisticated counterfeit artesunate samples collected from (A) Savannakhet, Laos, (B) Luang Nam tha, Laos, and (C) along the Thai-Myanmar border. (M = artesunate, N = arteminsinin, and A = $C_4H_6O_4$: 1 = $[N + NH_4]^+$, 2 = $[N + H]^+$, 3 = $[N - H_2O + H]^+$, 4 = $[N - H_2O - CO + H]^+$, 5 = $[N - H_2O - 2CO + H]^+$, 6 = $[2N + NH_4]^+$, 7 = $[2N + H]^+$, 8 = [chloramphenicol + $H]^+$, 9 = [metronidazole + $H]^+$, 10 = [paracetamol + $H]^+$, 11 = [2 paracetamol + $H]^+$, 12 = $[M - A + H]^+$, 13 = $[M - A - CO + H]^+$, 14 = $[M - A - CO - H_2O + H]^+$, 15 = $[A + H]^+$, and 16 = $[A - H_2O + H]^+$.

The sample shown in 6.9.A was collected in Savannakhet, Laos in June 2003 and had a type 7 fake hologram affixed to the blisterpack. Interestingly, this sample presented $[M+H]^+$ and $[M+NH_4]^+$ ions consistent with artemisinin, the naturally-occurring precursor for artesunate synthesis that is found in *Artemisia annua*. Artemisinin may have been unintentionally added during the poor quality production process or may have been added in an attempt to confer some antimalarial properties to the fake sample. Figure 6.9.B shows the DART-MS spectrum of a counterfeit sample collected in Luang Nam Tha, Laos in September 2004 with a well-crafted Type 6 fake hologram affixed to the blisterpack. The mass spectrum for this sample included peaks corresponding to chloramphenicol ($C_{11}H_{12}C_{l2}N_2O_5$, Δmass = 1.4 mmu) and metronidazole ($C_6H_9N_3O_3$, Δmass = 1.4 mmu), two commonly-used antibiotics.

Figure 6.9.C corresponds to a counterfeit artesunate sample collected along the Thai-Myanmar border in March 2005. Although this sample had a sophisticated (but fake) type 9 hologram affixed to the blisterpack, it produced a positive result in the colorimetric Fast Red TR test. DART-MS analysis of this sample revealed not only the presence of paracetamol, but also low-intensity (5%) signals corresponding to artesunate fragment ions. This alarming finding was further confirmed by LC, which showed that this tablet contained 10 mg of artesunate per tablet (20% of the expected amount). It has been hypothesized that this latest "innovation" was introduced by counterfeiters in an attempt to deceive the colorimetric authentication tests currently used in the field. The implications of this finding are far-reaching, as the continued administration of low doses of artesunate could genetically select for artesunate-resistant parasite strains and render this last-resource antimalarial medicine ineffective.

HPLC and/or DART- and DESI-MS confirmed that all specimens (195/391, 49.9%) thought to be counterfeit based on packaging analysis contained no, or very small, quantities of artesunate (up to 12 mg/tablet as opposed to 50mg per genuine tablet). One sample from Cambodia had apparently genuine packaging but contained only 21 mg artesunate and was therefore either substandard or had deteriorated in transit and/or storage.[297] Of 321 samples labeled as being manufactured by Guilin, 195 (61%) were counterfeit. A wide variety of unexpected "wrong" pharmaceuticals were also identified, including paracetamol (n = 24), sulphadoxine (n = 18), pyrimethamine (n = 11), dimethylfumarate (n = 17), erythromycin (n = 88), erucamide (n = 5), safrole (n = 6), artemisinin (n = 10), metamizole (n = 10), an analgesic suspected of causing serious bone marrow disorders,[308] 2-mercaptobenzothiazole (n = 5), chloramphenicol (n = 4), metronidazole (n = 2) and chloroquine (n = 2), an early generation antimalarial that is now ineffective against multidrug-resistant *P. falciparum* parasites.[296]

6.8. Interpretation of the Evidence

Although at first glance, the pooling of chemical, botanical and packaging evidence suggests a wide diversity of fake artesunate in SE Asia with strikingly different fake holograms and chemical signatures, some generalization can be made. For example, palynological evidence suggests that all counterfeits were produced in temperate areas along the borders between China and neighboring countries in SE Asia. Inspection of maps of the geographical distribution of fake artesunate suggests that there may be two different origins of counterfeit artesunate, with similarities between the samples in Myanmar, northern Laos, and along the Thai-Myanmar border in a westerly group, and

similarities between those recovered in southern Laos, Vietnam and Cambodia in an easterly group (Fig. 6.4). A significantly higher proportion of counterfeit drugs were found in the east than in the west (41% (62/151) vs. 79% (133/168), $p < 0001$). Of samples collected in the westerly group, 73% (37/51) contained invalid batch numbers used were invalid whereas only 1.5% (2/128) of samples in the easterly group were invalid ($\chi^2 = 107.8$, $p<0.0001$).

Fakes with stickers were only found in Vietnam and Cambodia while those with holograms were only found in Myanmar and along the Thai-Myanmar border. Both stickers and holograms were found in northern and southern Laos. All of the different fake holograms have mis-registration of the outer ring of the Guilin logo and although the errors differ between all Types, they have been made in the same way, suggesting the use of similar technology and machines. Types 2, 3, 5, 7, 11, and 12 were only found in the east while 6, 9, and 10 were only found in the west. Types 1, 4, and 8 were found in the east and the west but in varying proportions as 82% of Type 1, 17% of Type 4 and 25% of Type 8 were found in the west. With the exception of Type 4, all counterfeits containing calcite bore stickers and not fake holograms. However, the pollen signatures of Types 3, 11 & 12 (easterly) and 9 & 10 (westerly) were similar, suggesting that the manufacturing sites of these two groups may be in the same area of southern China, but that they are parts of separate operations having different distribution networks. Types 8, 11, and 12 all contain an error in the upper case font for ‘Mfg’ and ‘Exp’ suggesting a link between the producers of these three types of counterfeits. Cross-mixing of different types of fake blisterpack packaging and boxes was also evident. Specifically, the occurrence of a Type 10 blisterpack in a Type 4 box and a Type 13 blisterpack in a Type

9 box suggested the presence of a link between the producers and/or distributors of these particular fakes. All of this evidence supports the 'easterly' and 'westerly' distribution hypothesis.

The existence of two main sources is also suggested by DART- and DESI-MS analysis. Metronidazole and artesunate were only found in westerly group samples while sulphadoxine, pyrimethamine, erythromycin and erucamide were found only in the easterly group samples. Dimethylfumarate, 2-mercaptobenzothiazole, metamizole, safrole, paracetamol, and artemisinin were found predominantly in the east. Samples containing chloramphenicol, and chloroquine were in equal numbers in each geographical group.

Counterfeit artesunate with type 14 packaging was shown to contain some artesunate of the exterior surface suggesting that the counterfeit tablets may have been contaminated with genuine artesunate in the tablet press left over from the manufacture of genuine product at an unknown location.[171] The presence of sulphadoxine and pyrimethamine further suggests that the factory had been making, or had access to, sulphadoxine+pyrimethamine, an antimalarial combination therapy that is no longer effective in SE Asia. The discovery of safrole is of considerable concern and interest as it is a precursor in the synthesis of methylenedioxymethamphetamine (MDMA or Ecstasy) and is a banned chemical in the United Nations Convention Against Illicit Traffic in Narcotic Drugs and Psychotropic Substances.[309] However, MDMA was not detected in or on the counterfeits.

All of the counterfeits purchased from Vietnam, except for Type 12, contained calcite having stable isotope ratios that are consistent with what would be found in an

area being volcanic in origin rather than that originating from marine or terrestrial limestone or tap water precipitation. One such area having high temperature hydrothermal calcite is mined in an area west of Nanning, close to the Vietnam border (Fig. 6.4) and the calcite used in Types 2, 4, 5, 8 and 11 may have originated from these mines.

This combination of excipient composition and palynology results therefore suggested that at least some of the counterfeit artesunate were coming from southern China or close to its border with Vietnam, Thailand and Myanmar. Furthermore, the evidence suggests that there are at least two distribution routes followed for these counterfeit products with westerly origins via Myanmar and easterly origins via Vietnam with Laos in the middle, an area of overlap afflicted by Types of both groups.

The evidence described here was presented by the Secretary General of INTERPOL (Mr. Ronald K Noble) to the Assistant MPS (Mr. Zheng Shaodong) in March 2006 in Beijing, China. In response, a criminal investigation was carried out leading to the arrest of a native of Yunnan Province who, it was alleged, had bought 240,000 blisterpacks of counterfeit artesunate (Fig. 6.10) from a native of Guangdong Province, China, which is thought to be the origin of these counterfeits. As Guilin Pharmaceutical Co. Ltd. exported 272,000 blisterpacks to Myanmar and Thailand during this time, an estimated 47% of artesunate available in the market was fake which is consistent with previous estimates of the proportion of fake artesunate in mainland SE Asian shops.

Figure 6.10. Counterfeit artesunate samples seized during arrests made after reporting of findings of Operation Jupiter to Chinese government officials.

The seized samples appeared to be related to the more sophisticated westerly counterfeits found in Myanmar, Thai-Myanmar border and Laos bearing sophisticated holograms and without the plethora of wrong AIs (other than artemisinin). This assertion was also supported by the absence of calcite in these counterfeits. However, based upon the findings presented here, there is a strong possibility that there is a second trade route involving a different group of criminals distributing and/or manufacturing fake artesunate, with poor quality stickers and a variety of wrong ingredients with calcite, into Vietnam, Cambodia and southern Laos. If this hypothesis is correct, future examination of the prevalence of different types would be expected to demonstrate a reduction in the westerly distribution, but not that being fed by the easterly trade route.

6.9. Conclusion

It has been estimated that almost half of the current supply of artesunate sold in SE Asia is counterfeit.[188] Due to the widespread nature of this problem, an inter-disciplinary approach must be taken to determine the source of these counterfeits and stop the inflow of counterfeits on the market. In particular, the use of novel analytical tools such as DART- and DESI-MS has been shown to facilitate the detection of counterfeit artesunate antimalarials. Reactive DART- and DESI-MS methods were developed and have been shown to provide sensitive, specific detection of artesunate while non-reactive mode analyses are useful for the identification of wrong AIs. Of 391 tablets assayed using these methods, 196 (50.1%) were shown to be genuine artesunate samples while the remaining 195 samples contained AIs such as erythromycin, paracetamol, artemisinin, and safrole, as well as several other compounds. A collaborative effort by health workers, scientists, and law enforcement has prompted the Chinese Government to act quickly against the criminal traders identified in this work and has led to arrests and seizure of 240,000 blisterpacks containing counterfeit artesunate.

CHAPTER 7. CONCLUSIONS AND FUTURE OUTLOOK

7.1. Abstract

This chapter begins with a summary of the results of my work with AMUSE and DART. Specific challenges of these techniques, including limitations and possible solutions, are addressed. The chapter concludes with a discussion of the possible direction for continuation of this work and of applications that might benefit from the proposed improvements.

7.2. AMUSE Ionization

7.2.1. Summary of Accomplished Tasks in Development of the AMUSE Ionization Technique

Since inception of the idea for the AMUSE ionization technique, the AMUSE ion source has undergone several design modifications. The current prototype incorporates an ejector array having 3-5 μm orifices, which has been shown to provide improved signal intensities for model compounds. This has been attributed to the concomitant reduction in droplet diameter[132] which allows for more efficient desolvation. Incorporation of a Venturi device into the current setup provided a significant improvement in signal stability and intensity as shown in the low %RSDs of the MS signal for YGGFL during a 30 minute ejection interval.

Although comparison of the absolute signal intensities for ESI and AMUSE indicated that AMUSE absolute signal intensities are lower, an investigation of the baseline noise between these two ionization techniques showed that AMUSE spectra

have less noise. This was attributed to the use of much lower voltages than those typically used in pESI-based ionization techniques resulting in a corresponding reduction in solvent oxidation processes[54] and ionization of volatile contaminants present in laboratory air.[55] As a result of this cleaner baseline, S/N for peaks in AMUSE mass spectra are better than those for pESI mass spectra.

Soft ionization of cytochrome C, a model protein commonly used in MS, was also demonstrated. However, the use of heated N_2 flowing through the Venturi device was necessary to promote efficient desolvation. The average charge state in the cytochrome C charge state distributions observed for AMUSE, pESI and nESI was lowest for AMUSE suggesting that AMUSE ionization, which likely follows the charged residue ionization mechanism, is softer than either pESI or nESI and prompted an investigation of the mean IE deposited on AMUSE ions during the ionization process.

Experiments using the SY method showed that AMUSE ionization is inherently softer than ESI. Increasing the Venturi device gas flow rate caused a miniscule increase in <E> for ESI but yielded a significant increase in <E> for AMUSE ionization. When ionizing solutions containing organic solvent and using optimized desolvating conditions, it was found that <E> for ESI and AMUSE were similar within experimental error. Ionization of aqueous solutions under optimum desolvating conditions produced AMUSE ions with a slightly lower <E> than ESI ions.

Tuning of <E> of AMUSE and ESI ions was accomplished by modulating the Venturi gas flow rate and mass spectrometer capillary inlet temperature. An interesting observation arising from these experiments was that ESI ions with high <E> could be produced by either using high gas flow rates *or* high capillary temperatures. However,

AMUSE ions with high <E> could only be produced by conditions combining high gas flow rates *and* high capillary temperatures, demonstrating that AMUSE ionization is inherently softer than ESI.

One potential application of the AMUSE ionization technique is as an ion source for LC-MS. It was speculated that AMUSE would be amenable to LC-MS applications for several reasons. First, due to decoupling of the droplet formation and charging processes, AMUSE ionization is not dependent upon solvent composition. Therefore, AMUSE should be compatible with a greater variety of solvent systems than current spray-based ionization methods, making it attractive for use with LC-MS. AMUSE-MS analyses have been shown to have good detection limits (femtomole to attomole), indicating that low abundant analytes in complex sample matrices may be detected by LC-AMUSE-MS. Furthermore, multiply charged cytochrome C charge states have been detected using AMUSE ionization suggesting that like ESI-MS, AMUSE-MS can ionize compounds spanning a large mass range – from small drugs and peptides to proteins.

One phenomenon observed during AMUSE operation is the occurrence of electrowetting on the array surface, particularly in DC mode, which caused a concomitant reduction in signal stability. Silanization of the AMUSE ejector array increased the hydrophobicity of its surface causing a decrease in electrowetting and an increase in signal stability and signal intensities for both operational modes. LC-AMUSE-MS experiments using calpain inhibitors revealed that incompatibility between the sample injection volume and the reservoir volume resulted in a loss of fidelity of the chromatographic pulse. However, generation of a calibration curve using chromatographic areas calculated using SRM signal obtained over the entire LC-MS run,

rather than for individual chromatographic peaks, showed good correlation between the curve and experimental data suggesting that a reduction in reservoir volume should improve chromatographic fidelity.

7.2.2. The Long and Difficult Road to Commercialization

Critical proof-of-principle and characterization of the AMUSE setup has been accomplished. However, additional work must be performed to facilitate widespread acceptance and commercialization of this ionization technique. A retrospective examination of MS literature reveals the introduction of a plethora of ionization techniques over the last century – most of which have not been commercialized due to their difficulty of use or due to poor timing in their introduction in the market.

The development of ESI provides a clear example of how each of these factors contribute to the successful commercialization of a given ionization technique.[310] Investigation into the electrospray phenomenon has occurred over long intervals starting with experiments by Lenard in 1892 who studied electrification in raindrops[311] and followed by Chapman in 1930 who studied the electrification of liquids produced by spraying.[312, 313] In 1966, Hines investigated the physics of the electrospray method during use in electrostatic painting and described the interdependence of the applied voltage, fluid flow rate and physical properties of the solvent.[314] This was followed by the seminal work by Dole et al. in 1968 who was the first to recognize that large molecules could be analyzed by ESI.[29]

Dole's apparatus utilized a 70 cm AP desolvation chamber with an ESI needle at one end of a flange to a nozzle-skimmer system that was originally developed by

Kantrowitz and Grey[315] and allowed pressure reduction so as not to overload the vacuum system. Detection was accomplished using a Faraday cup detector rather than with a mass spectrometer. Up to 30 kV was applied to the needle forcing the production of charged droplets that were propelled through the AP desolvation chamber due to the effects of the electric field and a concurrent flow of N_2. Although Dole's apparatus incorporated several parameters that could be varied to allow optimization, such as the distance between the needle and nozzle-skimmer inlet, gas flow rate, and applied potential, this system also exhibited signal instability due to charge accumulation on the walls of their glass chamber and clogging of their needle because of the high liquid flow rate used (80 mL min^{-1}). Due to the lack of mass spectrometers allowing efficient ion transfer from AP to the vacuum region of the mass analyzer, Dole's findings remained largely unexploited for the next decade until 1972 when Evans and Hendrick introduced EHD,[15] which also suffered from signal instability and required the use of volatile solvents as described in section 1.2. A decade after Dole's work and nearly a century after the first reported studies of the electrospray phenomenon, Fenn and coworkers reignited interest in the ESI technique by demonstrating successful coupling of ESI to MS for the analysis of small organic molecules,[30] salts[30] and biomolecules.[31]

Fenn's apparatus used a liquid sample flowed at a rate of 10 μL min^{-1} through a needle held at 3 – 10 kV. A potential applied to a coaxial cylindrical electrode enclosing the needle was used to reduce spray divergence while a countercurrent gas flow of N_2 aided in desolvation and allowed the use of a shorter distance between the needle and the nozzle of the nozzle-skimmer interface used. One commercial version of Fenn's source, the Ion Max® source from Thermo Electron, utilized an off-axis ESI spray with a heated

metal capillary inlet.[316] Spraying off-axis prevented further transmission of large solvent clusters while lighter analyte ions entered the next vacuum stage because of the combined effect of suction and the potential gradient. The initial configuration of the IonSpray® ion source from PE/Sciex utilized a pESI source capable of handling high solution flow rates that was sprayed off-axis relative to the curtain gas API used in PE mass spectrometers.[317] More recently, pESI sprayers that are oriented orthogonal to the mass spectrometer inlet have been introduced by most manufacturers.[318] Many manufacturers have also employed either fused silica capillary or a metal hypodermic needle to enable low flow rate analyses, such as those required for protein MS analyses.[319] Modified techniques related to ESI, such as nESI and microchip ESI have also been commercialized.[310]

In order for AMUSE ionization to experience similar commercial success to ESI, several follow-up experiments should be performed to validate and test the robustness of this ionization technique. To that end, the following studies are recommended for future research:

1. Due to the limited availability of ejector arrays resulting from difficulties during the challenging fabrication process, the effect of batch-to-batch variability on MS signal intensities has not been investigated. From preliminary work to compare the performance of 1st and 2nd generation arrays, it is clear that changes in the fabrication process have a large effect on the quality of MS signal obtained. However, it was also observed that there was a significant difference in performance between arrays of the same type. As an

example consider the work performed to determine IE deposition by AMUSE. Those experiments utilized a 2nd generation array having 5-μm nozzles having an optimal liquid flow rate of 20 μL min^{-1}. LC-AMUSE-MS experiments were also performed using a 2nd generation array with 5-μm nozzles; however, it this case the optimal flow rate was 80 μL min^{-1}. Therefore, it is suggested that further optimization of the batch fabrication process be conducted followed by rigorous testing of the reproducibility of AMUSE MS signal for the model compounds reserpine, YGGFL, and cytochrome C ionized using different batches and types of arrays.

2. All AMUSE experiments were performed using a single array which was replaced if it became damaged during analysis. Damage to arrays assembled using protocol 1 generally occurred during device disassembly as the epoxy holding the device together needed to be completely removed. This particular issue was resolved by varying the assembly protocol. However, the large size of the current setup sets the minimum distance between the AMUSE and the Venturi/MS inlet. Therefore, it is recommended that a compression holder for the assembly be designed so that the array can be moved closer to the inlet.

3. No attempt was made to improve the design of the Venturi device used in the current AMUSE setup. The commercial Venturi device allows adjustment of the size of the annular gap that constricts gas flow causing an increase in the linear velocity of the gas. However, it is unlikely that the dimensions of the

Venturi device are optimized for this particular application. For example, comparison of the droplet diameter at the inlet (1-2 μm larger than the orifice diameter[132]) and outlet (~2-3 x the orifice diameter[135]) of the Venturi device demonstrates the occurrence of droplet coalescence during transit through the relatively long Venturi device used in these studies. It is recommended that computer simulations modeling the Venturi gas flow, liquid flow, and AMUSE droplet stream focusing be performed to aid in determination of optimal dimensions for the Venturi device, keeping in mind the ultimate goal of utilizing the multiplexing capability of the AMUSE. Other methods of improving ion transmission, such as incorporation of flared inlet capillaries,[212, 213] should also be explored.

4. Previous experiments demonstrated the importance of consistent alignment of the Venturi-assisted AMUSE setup. Mounting the various components onto a breadboard allowed for consistent coarse adjustment of the AMUSE but manual fine adjustment was necessary to optimize alignment. Therefore, it is also suggested that the AMUSE holder be designed to attach to a computer-controlled x,y-translational motion stage and that the entire assemblage, including the Venturi device, necessary electrical connections, and a digital camera, be packaged into a housing unit that also allows manual adjustment of the AMUSE in the z-direction. Utilizing computer control of the AMUSE position will likely allow for improved reproducibility of the AMUSE MS signal and will also provide the capability of optimizing the relative positions

of the MS inlet, Venturi device, and AMUSE. The AP-MALDI ion source offered by Masstech, Inc. (Columbia, MD) can serve as a model for the proposed AMUSE housing.

5. Silanization of the surface provided a reduction in electrowetting of the array surface and improved signal stability for an aqueous solution ejected in DC- and RF-only AMUSE modes. However, tests to monitor the long-term stability of the silane layer have not been performed, nor have experiments using different solvent systems. Therefore, it is suggested that follow-up experiments designed to assess these parameters be performed.

6. Several fundamental MS experiments also need to be performed to improve our understanding of how AMUSE ionization compares to more established techniques.
   a. Extrapolated detection limits for reserpine using arrays having 3- and 5-μm nozzles have been calculated but should be verified experimentally.
   b. One of the major challenges in the analysis of mixtures by ESI is the presence of ionization suppression due to a combination of charge competition and analyte partitioning within the droplet. Examination of AMUSE mass spectra obtained via analysis of an equimolar mixture of thermometer compounds showed evidence of some ionization suppression, most likely due to variation in the hydrophobicity of each compound. However, LC-MS analysis of a mixture of AK-295 and ZLAK-74 did not

show evidence of ionization suppression such as that observed for matching experiments using pESI. Therefore, it is recommended that experiments be performed with the intention of determining if ionization suppression effects are prevalent in AMUSE ionization. This could be accomplished using the methods described by Tang et al. who investigate charge competition in ESI-MS.[62]

c. The linear dynamic range of ESI is estimated to include analyte concentrations spanning three or four orders of magnitude. The minimum of the linear dynamic range for ESI is set by the detection limit for a given analyte while the maximum depends on the occurrence of ionization suppression and charge competition, which will have an adverse effect on signal for species that prefer to remain solvated in the droplet.[320] AMUSE mass spectra have exhibited low baseline noise relative to that of ESI mass spectra, indicating that the detection limit by AMUSE may be lower. As mentioned in point 6b above, it is also possible that ionization suppression may not occur in AMUSE ionization to the same extent that it is observed during ESI. These observations suggest that the linear dynamic range in AMUSE may be wider than that of ESI. Therefore, it is recommended that the linear dynamic range of AMUSE (in both operating modes) be determined using model compounds.

d. Mass spectra for the model compound reserpine revealed the presence of redox active species. It is well-known that ESI operates as a current-controlled electrochemical cell. Thus, ESI analyses of reserpine show

peaks corresponding to the protonated molecule, water adducts, and also to a reduced form of reserpine at *m/z* 607.2. Reduction of reserpine in the AMUSE ion source is most likely due to electrochemical reactions occurring on the inner electrode of the piezo. It is recommended that experiments be performed to characterize the properties of this ionization technique using either cyclic voltammetry or chronoamperometry. The findings of these experiments may also enhance our understanding of the mechanism by which droplet charging occurs.

7. Visual inspection of the AMUSE during ejection suggested that the ejection efficiency (number of nozzle ejecting a particular time) can range from 10 – 25 % (40 – 100 nozzles). This relatively low value may be due to fabrication issues or may be due to the use of a RF resonant frequency that promotes the formation of a droplet stream rather than a continuous jet of solution. Meacham performed visualization studies which demonstrated that at distances close to the array surface (<100 μm), three ejection modes exist including times when no ejection occurred, ejection of a droplet stream (discrete-droplet mode), and ejection of a continuous jet (jet mode).[131, 132] For a 2nd generation device with 5-mm nozzles, Meacham found that switching between these operating modes occurs over a 100 kHz range,[132] thus, it is possible that the MS signal stability using AMUSE might be improved by switching to a different ejection mode.

8. Recently, Forbes et al. demonstrated successful operation of an AMUSE ion source having two droplet reservoirs having less than half of the volume of the current device.[134] An investigation of the MS signal from this multiplexed using model compounds and for LC-MS studies of calpain inhibitors should be performed to assess the performance of this device – particularly with regards to retention of the chromatographic fidelity of LC-MS peaks.

9. Finally, it has been demonstrated that AMUSE ionization is inherently softer than ESI. AMUSE analysis using cytochrome C showed that the average charge state by AMUSE was lower than that of ESI suggesting that the conformation of cytochrome C during analysis using AMUSE was tighter. One application which should be further explored is the use of AMUSE for the analysis of non-covalent complexes, such as myoglobin, and specific non-covalent interactions such as antibody-antigen or enzyme-substrate interactions.

7.3. DART Ionization of Pharmaceuticals

7.3.1. Summary of Accomplished Tasks in Development and Applications of the DART Ionization Technique

DART ionization has proven to be a useful screening technique and a powerful addition to the arsenal of analytical tools for forensic analyses of counterfeit pharmaceuticals. Experiments were performed to characterize the effect that varying the DART parameters has on the intensity for tablets of known composition. An

investigation of the effect of increasing the He gas flow rate or the grid voltage, which has been speculated to remove ions from the metastable stream, demonstrated that higher signal intensities for a paracetamol tablet was obtained using higher He gas flow rates and lower grid voltages. This was later verified by experiments and simulations performed by Harris.[279]

The effect of increasing the He gas temperature was also investigated and it was found that the signal intensity of erythromycin generally increased with increasing temperature until thermal degradation induced fragmentation of the intact erythromycin signal, suggesting that the IE deposited on DART ions should be further investigated. Experiments to measure DART IE deposition are currently being pursued by two other graduate students in the Fernández research group using the methods and macros I generated during my investigation of the IE deposited on AMUSE ions.

Although obtaining useful DART data was rapid, analysis of the data – particularly with regards to calibrating the spectra – was a lengthy process. To that end, an investigation of two methods to perform mass drift correction via either a single initial calibration or a time-dependent calibration was conducted and demonstrated that calibration of the mass spectral data should be performed using the time-dependent calibration method.

Upon completion of these method development experiments, a collection of 50 yaa chud containing a total of 254 tablets and capsules was subsequently analyzed by DART-TOF-MS. It was found that the majority of these pharmaceuticals contained paracetamol as the AI. Only 32 of the 50 yaa chud sampled contained an antimalarial

compound, however, none of the yaa chud contained an antimalarial that would be useful against *P. falciparum* malaria.

DART-TOF-MS was also used to screen artesunate-containing pharmaceuticals as artesunate is a widely counterfeited drug that has been implicated in the deaths of patients with malaria patients.[185] Preliminary screening of a set of 52 tablets using negative mode DART-TOF-MS demonstrated the capability of detecting genuine artesunate tablets from counterfeits. Expanding this screen to include an additional 339 tablets further demonstrated the validity of this method for detecting counterfeit artesunate and ultimately led to the dismantling of a ring of counterfeiters by Chinese law enforcement officials.

7.3.2. Future Proposed Direction of DART Research

Although DART was introduced in 2005,[38] research into the fundamental physicochemical properties of this ionization technique, as described in section 5.3, have only recently been explored.[173, 174, 279, 321, 322] However, there are some questions that have yet to be investigated. To that end, the following studies are proposed for future research:

1. DART experiments were performed using either the commercial DART source or a home-built source. Both of these sources utilized an on-axis orientation of the gas exit of the DART with the mass spectrometer's inlet orifice. However, it might be beneficial to explore other possible orientations, as that would increase the types of analyses and samples that are accessible via this technique.

2. One of the biggest challenges in DART-MS is the low upper mass limit accessible via this technique. This is likely due to inefficient desorption of the analyte from the surface being analyzed. Glenn Harris, a 2nd year graduate student in our group has begun preliminary experiments to try to decouple these effects to determine which possibility is contributing to the low upper mass limit of DART. In addition to the experiments he devised, it is recommended that a quartz crystal microbalance be used to measure the mass of the sample before and after analysis to determine the extent of desorption occurring. Other members of the Fernández research group are exploring the possibility of combining laser desorption or spray-based desorption with DART, however, acoustic desorption[128] might be a better option as there are minimal surface interactions due to the mechanical desorption method used.

APPENDIX A. AK-295 DRUG ADME STUDIES

A.1. Abstract

This appendix presents results of LC-pESI-QiT studies for the quantitation of several calpain inhibitors including AK-295, benzyloxycarbonyl-leucine-4-aminobutyric acid-CONH-$(CH_2)_3$-adenine (ZLAK-3001), benzyloxycarbonyl-leucine-4-aminobutyric acid-CONH-$(CH_2)_3$-N-(1-methyl)piperazine (ZLAK-3002), and benzyloxycarbonyl-leucine-phenylalanine-CONH-$(CH_2)_3$-N-$(CH_3)_2$ (ZLAK-3005). These compounds were synthesized by the Powers group as part of a series of syntheses designed to make analogs of AK-295 that inhibit calpain activity but also increase the probability that the compound will permeate the blood brain barrier. This chapter presents preliminary Adsorption, Distribution, Metabolism, Excretion (ADME) studies of these drugs.

A.2. ADME Studies of Calpain Inhibitors

As mentioned in Chapter 4, AK-295 is a calpain inhibitor compound synthesized by the Powers research group in the School of Chemistry & Biochemistry at the Georgia Institute of Technology[262] that has been shown to prevent neuronal degeneration in rat models for stroke[323] and brain injury.[324] A quantitative LC-MS/MS method for detection of AK-295 in mouse plasma and tissue was developed with the aim of determining the permeability of this compound for crossing the blood brain barrier (BBB). This method was further extended to the analysis of several other analogs synthesized by the Powers group that have also shown to inhibit calpain activity.[325] The names and formulas of these compounds are given in Table A.1 while the structures are provided in Figure A.1.

Table A.1. Acronyms, chemical names, and formulae for compounds tested by LC-MS/MS. (Z = Benzyloxycarbonyl, Leu = leucine, Abu = 4-aminobutyric acid, Nva = norvaline.)

Acronym	Compound	Formula
AK-295	Z-Leu-Abu-CONH$(CH_2)_3$-morpholine	$C_{26}H_{40}O_6N_4$
ZLAK-74	Z-Leu-Nva-CONH$(CH_2)_3$-morpholine	$C_{27}H_{42}O_6N_4$
ZLAK-3001	Z-Leu-Abu-CONH$(CH_2)_3$-adenine	$C_{27}H_{36}O_5N_5$
ZLAK-3002	Z-Leu-Abu-CONH$(CH_2)_3$-N-(1-methyl)piperazine	$C_{27}H_{43}N_5O_5$
ZLAK-3005	Z-Leu-Abu-CONH$(CH_2)_3$-N$(CH_3)_2$	$C_{27}H_{38}N_4O_5$

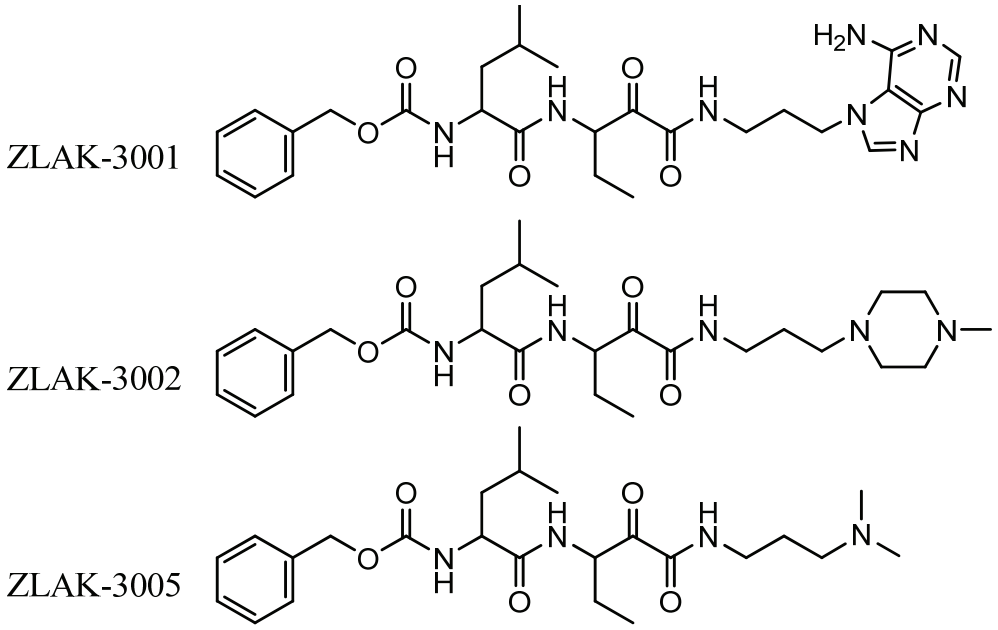

Figure A.1. Structures of calpain inhibitors analyzed by LC-MS/MS. Structures of AK-295 and ZLAK-74 are given in Section 4.2.

A.3. Experimental Details

A.3.1 Materials

HPLC-grade acetonitrile, methanol (EMD Chemicals, Inc., Gibbstown, NJ), and formic acid (88% by weight, Fisher Scientific, Hampton, NH) were purchased and used without additional purification. Stock solutions of all calpain inhibitors were provided by Dr. Asli Ovat of the Powers Research Group. These stocks were prepared by dissolving 1 mg of each compound in methanol (1mg mL^{-1}). Aliquots containing 50 μL of stock were pipetted into centrifuge vials and stored at -80 ºC until needed. Serum and tissue samples were prepared by Dr. Seneshaw A. Asress in the research group of Dr. Jonathan D. Glass at the Emory School of Medicine. Female C57BL/65 mice, aged 7 weeks, were dosed with the drug of interest (24 mg drug / kg body weight of mouse). Three methods of dosing were used: subcutaneous via a mini diffusion pump, oral gavage, and intravenous. After mice were sacrificed, their serum and tissues were collected and stored at -80 ºC until needed for analysis.

A.3.2 Standard and Sample Preparation

To eliminate possible matrix effects, control tissues from undosed mice were used to prepare calibration standards with concentrations of 0.10, 0.30, 0.50, and 1.00 μM for each compound investigated. Sample preparation for the spiked control tissues and the sample tissues was identical and was based on a protocol reported by Guo and coworkers.[238] First, the tissues were homogenized with water in a 5% (weight/volume) ratio (i.e. 5 g tissue / mL water) and 100 μL aliquots of each homogenate were pipetted into centrifuge tubes and spiked with 1.00 μM ZLAK-74. The mixture was sonicated for

10 minutes to ensure homogeneity in the sample and 300 μL of 99.9:0.1 v/v acetonitrile:formic acid was added to precipitate proteins. The sample was briefly vortexed and sonicated for 15 minutes followed by centrifugation at 13,000 g for 30 minutes. The supernatant was removed and evaporated at 45 ºC for 3 hours and the residue was reconstituted with 100 μL 30:69.9:0.1 v/v acetonitrile:water:formic acid. The final solution was filtered using a 0.45 μm syringe filter (Acrodisc, Pall) and analyzed by LC-MS/MS.

A.3.3 LC-MS/MS Operation

All measurements were carried out in an Agilent HPLC 1100 system coupled to a ThermoFinnigan LCQ Deca XP+ ion trap mass spectrometer using a pESI ion source operated in positive ion mode. For experiments with compound AK-295, an analytical Zorbax Extend® C18 column (1.0 x 150 mm, 5 μm particles, 80 Å pore size, Agilent) was used with the following gradient program: 0.0 min – 30% B, 0.5 min – 30% B, 0.7 min – 85% B, 2.5 min – 85% B, 2.70 min – 30% B, 5.5 min – 30% B.

For experiments using Zlak-3001, Zlak-3002, and Zlak-3005, an analytical Symmetry Shield® reverse-phase C18 column (1.0 x 150 mm, 3.5 μm particles, 100Å pore size; Waters) preceded by a Zorbax® RX-C18 guard column (4.6 mm x 12.5 mm, 5.0 μm particles, 2 μm pore size; Agilent) was used for all remaining experiments. The solvent gradient program used was: 0.0 min – 30% B, 0.5 min – 30% B, 0.7 min – 100% B, 4.5 min – 100% B, 5.0 min – 30% B, 6.0 min – 30% B.

The mobile phases used for all separations were: A = 0.1 % formic acid in water and B = 0.1 % formic acid in acetonitrile. The flow rate was 80 μL min^{-1}, with an injection volume of 15 μL.

The QiT was operated in multiple reaction monitoring mode using the following precursor → fragment transitions: AK-295: *m/z* 505.2 → 443.2, ZLAK-74: *m/z* 519.2 → 457.2, ZLAK-3001 : *m/z* 553.2 → 509.2, ZLAK-3002: *m/z* 518.3 → 410.3, and ZLAK-3005: *m/z* 462.2 → 418.2. The QiT was set as follows: needle voltage +4.0 kV; sheath gas 15 arbitrary units (~0.6 L min^{-1}); capillary temperature 275 ºC; capillary voltage 34 V (AK-295), 28 V (ZLAK-3001), 18 V (ZLAK-3002), 15 V (ZLAK-3005); capillary-skimmer voltage 25 V (AK-295), 55 V (ZLAK-3001), 45 V (ZLAK-3002), 55 V (ZLAK-3005). For all experiments, the mass analyzer was set with the automatic gain control on ($1x10^7$) with 2 microscans, 400 μs, 1.2 Da mass selection window and 34% normalized collision energy.

A.3.4 Data Processing

After acquisition, peak areas for the chromatographic peaks present in the extracted ion chromatograms for ZLAK-74 and the compound of interest were determined using the mass spectrometer software (Xcalibur 2.0, Thermofinnigan) with the Genesis peak detection algorithm (15 smoothing points, signal-to-noise ratio threshold = 3.0). The areas for the compound of interest and ZLAK-74 were exported to Excel and the ratio of the peak area of the compound of interest/peak area of ZLAK-74 was calculated. The amount of compound present in each sample was determined by

correlating the area ratio to a concentration using the calibration curves obtained during each experiment.

A.4. Results of Quantitation Studies

In our initial studies demonstrating axonal protection in the animal model of peripheral neuropathy, AK-295 was delivered continuously from a subcutaneous mini diffusion pump at a dose of 24 mg/kg/day.[263] These studies showed that AK-295 is an effective calpain inhibitor but subsequent LC-MS/MS experiments demonstrated that this compound does not penetrate into the brain

Although AK-295 could not be detected in the brain tissues provided, it has since been discovered that oral and intravenous delivery of AK-295 at doses of 50 or 100 mg/kg twice per day provides a similar degree of protection against axonal degeneration and clinical disease and at these levels, it is possible that AK-295 might be present in the brain. During initial studies using a dose of 24 mg/kg body weight, AK-295 was present in the liver, heart, kidney, and spleen at levels > 0.5μg/gram of tissue after a single subcutaneous dose as shown in Table A.2.

Table A.2. Amounts of AK-295 detected in the brain, heart, kidney, liver, spinal cord, serum, peripheral nerve, or spleen from mice dosed subcutaneously, orally, or intravenously with 24 mg AK-295/kg body weight. ND = not detected, NQ = not quantifiable. Each dosing study set included 2 mice.

Tissue	Subcutaneous (μg AK-295/g tissue)	Oral (μg AK-295/g tissue)	Intravenous (μg AK-295/g tissue)
Brain	ND	ND	ND
Heart	0.541 ± 0.008	NQ	0.561 ± 0.036
Kidney	0.936 ± 0.068	NQ	1.816 ± 0.161
Liver	1.550 ± 0.068	NQ	0.943 ± 0.052
Spinal Cord	ND	ND	ND
Serum	0.895 ± 0.196	NQ	NQ
Peripheral Nerve	NQ	NQ	0.333 ± 0.009
Spleen	1.380 ± 0.174	NQ	1.316 ± 0.067

As can be seen in Table A.2, AK-295 could not be detected in the brain for any of the dosing methods tested. Oral dosing provided the lowest levels of AK-295 detected but most of the LC-MS/MS signal intensity was too low to be quantified using the calibration curve created during the run. However, intravenous dosing provided quantifiable signal intensities for most of the tissue samples tested. Interestingly, after intravenous dosing, levels of 0.333 ± 0.009 μg AK-295/g tissue were detected in the peripheral nerve (Fig. A.2). This confirms that AK-295 is present in the target organ of interest, and is able to prevent axonal degeneration in the peripheral nerve, supporting its potential as a treatment to reduce axonal degeneration.

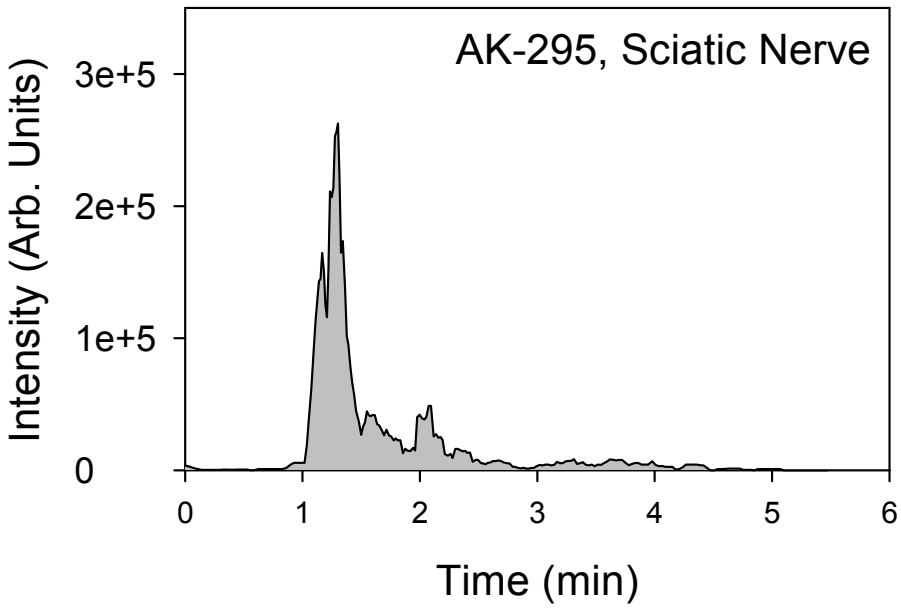

Figure A.2. Extracted ion chromatogram obtained using LC-MS/MS showing chromatographic peak from sciatic nerve of mouse dosed intravenously with 24 mg AK-295/kg body weight.

Early data from inhibitors ZLAK-3001, ZLAK-3002, and ZLAK-3005 demonstrated that ZLAK-3001 and ZLAK-3002 do penetrate into the brain but that ZLAK-3005 does not (Fig. A.3). The amounts of ZLAK-3001 and ZLAK-3002 quantified in the brain tissue sampled were 1.17 ± 0.01 μg/g tissue and 1.14 ± 0.02 μg/g tissue, respectively.

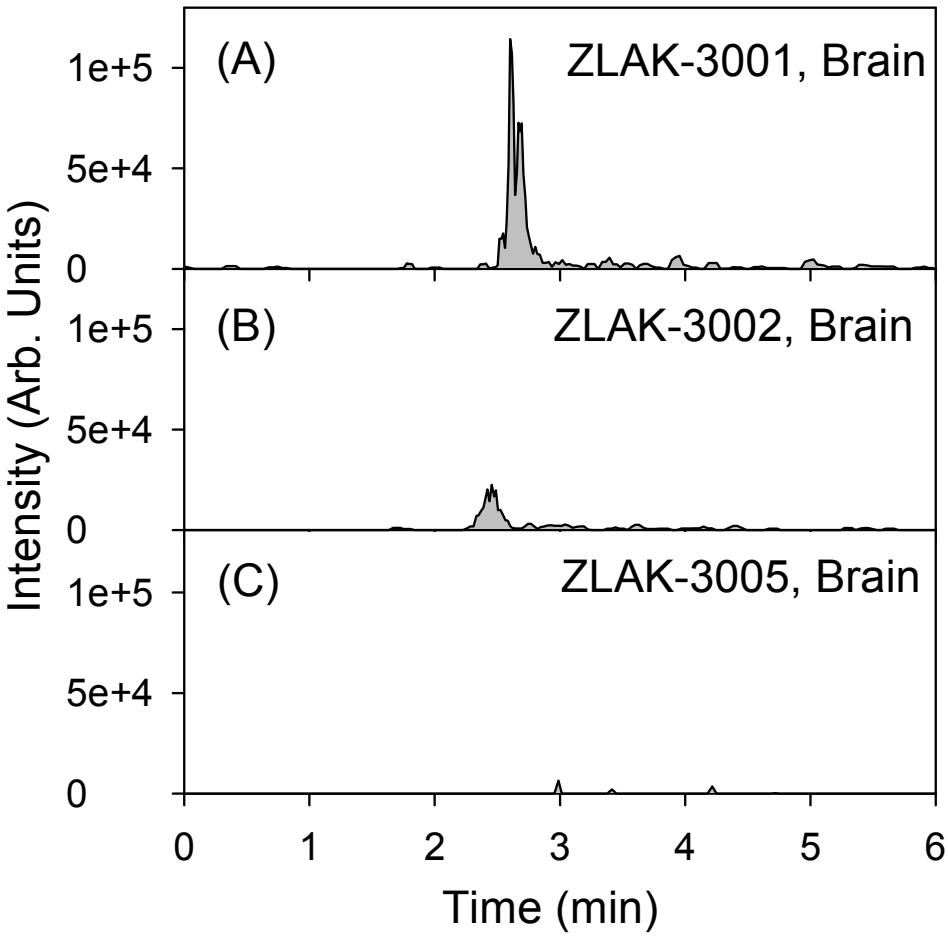

Figure A.3. Extracted ion chromatograms obtained using LC-MS/MS showing chromatographic peaks from brain tissue of mice dosed subcutaneously with 24 mg/kg body weight for compounds (A) ZLAK-3001, (B) ZLAK-3002, or (C) ZLAK-3005.

A.5. Conclusion

Work performed so far has demonstrated that AK-295 can cross the BBB, but only with limited efficiency, and appears to be primarily passed through the excretory system. Since then, several new drugs in the same family as AK-295 have been synthesized to find a compound that can penetrate the brain. Three of these compounds, ZLAK-3001, ZLAK-3002, and ZLAK-3005 have been analyzed using our quantitative method. ZLAK-3001 and ZLAK-3002 have been shown to have therapeutically useful

concentrations in the brain of mice that received a single subcutaneous dose, demonstrating the ability of these compounds to cross the blood brain barrier and suggesting that these compounds should be further investigated to determine their concentrations in other tissue types and with different dosing strategies.

APPENDIX B: DIFFERENTIAL OVARIAN CANCER SERUM METABOLOMICS

B.1. Abstract

Efforts to discover potential biomarkers for ovarian cancer have been primarily focused on identifying diagnostic proteins to improve the predictive power of current diagnostics tests. Metabolomics, the study of metabolic changes in biological systems, can be used to provide characteristic small molecule fingerprints (profiles) related to disease states. In this chapter, results are presented for the mining of potential metabolic biomarkers from LC-MS analyses of a small group of patients with ovarian cancer and controls, who may have benign tumors on their ovaries or may have another form of cancer.

B.2. Biomarker Discovery Efforts for Ovarian Cancer

In the U.S. ovarian cancer is the fifth most common cancer in women and is the leading cause of deaths from gynecological malignancies with estimates of more than 21,500 new cases diagnosed in 2009 and more than 14,600 deaths.[326] The high mortality rate is a direct consequence of the lack of effective early detection diagnostic tests. Due to the asymptomatic nature of the disease, most new cases involve women in the advanced stages of the disease (Stage III/IV) when the 5-year survival rate is less than 20%.[327] Current assays for ovarian cancer detection are based on examination using ultrasound or Doppler imaging of the ovaries or on measuring the physiological level of cancer antigen 125 (CA125), the only FDA-approved diagnostic test for ovarian cancer

detection. However, abnormally high CA125 levels are only present in 82% of advance stage patients while fewer than 50% of early stage patients show elevated levels.[328] As a result of this variability, the overall predictive value of CA125 has been reported to be less than 10%.[329] Despite the high degree of active research being conducted to screen for diagnostic ovarian cancer biomarkers, which has been on-going since the early 1970's,[330] no new biomarkers have been implemented in screening tests.

Most biomarker discovery studies reported in literature are based on the univariate or multivariate comparison of the high-throughput analyses that are focused on investigating qualitative or quantitative changes of large biomolecules such as DNA, RNA, glycans, or proteins.[331] In particular, researchers have focused on identifying changes in the concentrations or biotransformations such as methylation or glycosylation on these biomolecules. In contrast, metabolic biomarker discovery efforts (molecules < 1 kDa) have received considerably less attention and comprise ~6% of all reported potential ovarian cancer biomarkers.[327]

As metabolites are the end products of cellular regulator processes, their physiological concentrations can be correlated to genetic, pathophysiological or environmental stressors.[332] Therefore, human serum metabolic profiling, as defined by Fiehn and Kind,[333] can reflect the pathological state of various organs and may be useful in the search for early detection assays for ovarian cancer. For example, lysophosphatidic acid[334-336] and lipid associated sialic acid,[337-341] are two metabolic biomarkers identified using ^{1}H nuclear magnetic resonance (NMR) spectroscopy as being possible biomarker candidates for ovarian cancer detection.

On challenge in performing broadband metabolomic studies, which is aimed at simultaneously screening relative changes in the concentrations of thousands of metabolites, is the wide variation in concentrations and chemical properties of metabolites. Due to the wide dynamic range, reproducible quantitative properties,[342] and large peak capacity,[343] MS is an ideal tool for detecting these metabolic changes. MS has been successfully applied to the discovery of proteomic biomarker panels using either MALDI[344, 345] or a related technique, surface-enhanced laser desorption/ionization (SELDI),[329, 344, 346-349] which is similar to MALDI but uses functionalized target plates that promote sample clean-up and preferential protein binding, rather than the stainless steel target plates that are commonly used for MALDI. However, LC-MS technologies for probing the metabolome have not been as widely used as they are still evolving,[350] as are the bioinformatics techniques for the analysis of the resulting data.[351]

Denkert, et al. recently used GC-MS to investigate metabolic changes in ovarian tumor tissues and identified 51 metabolites that were significantly different between their control and patient groups.[352] Despite the promise of this approach, the limited accessible mass range in GC-MS, which more suitable for the detection of metabolites with m/z < ~350 Da, reduces the applicability of GC-MS for use in metabolite profiling experiments. However, LC-MS is widely used for the separation of complex biological samples and allows for the sensitive detection of compounds over a wide mass range.[353, 354] Recent technological advances in separation techniques for metabolomics such as ultraperformance liquid chromatography (UPLC),[355] capillary LC,[356] 2D-LC,[357] and drift tube ion mobility gas-phase separations,[358] which are all characterized by having high speed separations with improved peak capacity, have further expanded the capability of

MS combined with separation techniques for metabolomics. However, the difficulty in extracting useful diagnostic data from these massive datasets remains challenging and has only recently begun to be overcome by applying chemometric techniques to this data.[351]

Historically, principal component analysis (PCA),[359, 360] which identifies useful spectral features from the dataset by using principal components that capture the most relevant variance between disease and control populations, and partial least squares discriminant analysis (PLSDA),[335] which extracts the variation in the data as latent variables and uses discriminant analysis to generate a model that classifies the data as being part of the disease or control groups, have been applied to the analysis of metabolomic datasets. However, it has long been recognized that feature reduction improves the model quality as it eliminates non-informative data, makes the diagnostic process cheaper and targeted, and reduces the number of potential biomarkers, which aids in interpreting their biological significance. To that end, feature selection tools such as genetic algorithms (GA)[361-364] and recursive feature elimination (RFE)[365] have been combined to generate high classification models with good predictive ability.

Recently, support vector machines (SVMs)[366] have also been successfully applied to the classification of cancer vs. control sample sets obtained using SELDI-MS[367-369] and MALDI-MS.[344, 345] SVMs treat the input data (retention time (t_R) and *m/z* vs. intensity) as two vectors in space and optimize the classification performance of the system by maximizing the distance between any two neighboring points on these vectors using a hyperplane.

In this work, results from RFE feature selection combined with a nonlinear SVM for classifying LC-MS data of serum samples from ovarian cancer patients and controls

are presented. Panels of metabolic spectral features that are potentially useful in diagnosis are identified and chemical assignment of these biomarkers to endogenous human metabolites is attempted based on accurate mass measurements.

B.3. Experimental Details

B.3.1. Materials

Serum samples were collected by Benedict B. Benigno, of the Ovarian Cancer Institute, Atlanta, GA, and L. DeEtte Walker and John F. MacDonald, who are both affiliated with the Ovarian Cancer Institutes and the School of Biology at the Georgia Institute of Technology.

Serum samples for LC-MS metabolomics analysis were obtained from 37 patients with papillary serous ovarian cancer (mean age 60 years, range 43-79, stages I – II (9), stages III – IV (28)) and 35 controls (mean age 54 years, range 32-84). The control population consisted of patients with histology considered normal within limits (NWL) and women with non-cancerous ovarian conditions. All serum samples were obtained from the Ovarian Cancer Institute (OCI, Atlanta, GA) after approval by the Institutional Review Board (IRB). All donors were required to fast and to avoid medicine and alcohol for 12 hours prior to sampling, except for certain allowable medications, for instance, diabetics were allowed insulin. Following informed consent by donors, 5 mL of whole blood were collected at Northside Hospital (Atlanta, GA) by venipuncture from each donor into evacuated blood collection tubes that contained no anticoagulant. Serum was obtained by centrifugation at 5000 rpm for 5 min at 4 ºC. Two hundred and fifty μL aliquots of serum samples were frozen with dry ice immediately after centrifugation, and

stored at -80 ºC for further use. The sample collection and storage procedures for both ovarian cancer patients and healthy individuals were identical. All chemicals were obtained from Sigma-Aldrich (St. Louis, MO) and used without further purification. All aqueous solutions were prepared with nanopure water from a Nanopure Diamond laboratory water system (Barnstead International, Dubuque, Iowa).

B.3.2. Serum Sample Pretreatment and LC-MS Analysis

Serum samples were prepared and analyzed by Dr. Manshui Zhou, a post-doc in the Fernández research group. LC-MS data processing was done by Dr. Manshui Zhou, Dr. Facundo M. Fernández, and Christina Y. Hampton.

A stock sample of human serum purchased from Sigma (S7023, St. Louis, MO) was used during the development of the serum sample pretreatment and LC-MS analysis protocols. Upon arrival, the frozen stock sample was thawed and separated into 250 μL aliquots that were stored at -80 ºC for further use.

Serum samples were thawed, and proteins precipitated by addition of acetonitrile to the serum sample in a 5:1 ratio (1000 μL acetonitrile + 200 μL serum). The mixture was vortexed for 1 minute and incubated at room temperature for 40 minutes, then the sample was centrifuged at 13,000 x g for 15 minutes and the supernatant retained. The supernatant was vacuum-evaporated and the residue reconstituted in 80% acetonitrile/0.1% TFA.

LC-MS analyses were performed on a JEOL AccuTOF mass spectrometer coupled to an Agilent 1100 Series LC system (Santa Clara, CA) via a pESI source. The TOF resolving power measured at FWHM was 6000 and the observed mass accuracies

ranged from 5-15 ppm, depending on the S/N of the particular ion investigated. The injection volume was 15 μL in all cases. Reverse phase separation of serum samples was performed using a Symmetry® C18 column (3.5 μm, 2.1 mm x 150 mm, pore size 100 Å; Waters, Milford, MA) at a flow rate of 150 μL min^{-1}. The analytical column was preceded by a Zorbax® RX-C18 guard column (5.0 μm, 4.6 mm x 12.5 mm, pore size 2 μm; Agilent). The LC solvent mixtures used were: A = 0.1% formic acid in water and B = 0.1% formic acid in acetonitrile. After a pre-run equilibration with 5% B for 5 minutes, data acquisition was started and the solvent composition was varied according to the solvent program described in the Table B.1. After analysis of a given serum specimen, a 0.20mM sodium trifluoroacetate standard (NaTFA) was run for mass drift compensation purposes. For NaTFA analysis, 100% B at a flow rate of 300 μL min^{-1} was used and data was acquired for 10 minutes. After injection of the drift correction standard, the column was washed with 100% B for 30 minutes.

Table B.1. LC solvent gradient used in metabolomic experiments.

Time (min)	%B (acetonitrile/0.1% formic acid)	Flow Rate ($\mu Lmin^{-1}$)
Pre-Run Column Equilibration		
0.0	100	300
10.0	5	150
15.0	5	150
Sample Run		
0.0	5	150
5.0	5	150
10.0	20	150
20.0	25	150
28.0	30	150
38.0	35	150
50.0	40	150
90.0	45	150
100.0	50	150
110.0	60	150
120.0	75	150
130.0	85	150
160.0	95	150
180.0	100	150
Post-Run Column Wash		
0.0	100	300
30.0	100	300
NaTFA Standard Run		
0.0	100	300
10.0	100	300
Post-Run Column Wash		
0.0	100	300
30.0	100	300

Spectral data was collected in the 100-1750 *m/z* range with a spectral recording interval of 1.5 s and a data sampling interval of 0.5 ns for both positive ion mode pESI (+pESI) and negative ion mode pESI (-pESI). The settings for the TOF mass spectrometer for +pESI or -pESI were as follows: needle voltage: +/- 2000 V, ring lens: +8 V or -9 V, orifice 1: +30 V or -69 V, orifice 2: +6 V or -8 V, desolvation chamber

temperature: 250 ºC, orifice 1 temperature: 80 ºC, nebulizing gas flow rate: 1.0 L min^{-1}, desolvation gas flow rate 2.5 L min^{-1}, and detector voltage +/- 2800 V. The TOF analyzer pressure was $4.8x10^{-6}$ Pa during analysis. The RF ion guide voltage amplitude was swept to ensure adequate transmission of analytes in a wide range of *m/z* values. The sweep parameters were as follows: initial peaks voltage: 700 V, initial time: 20%, sweep time: 50%, final peaks voltage: 2500 V. After LC-MS data was collected, it was centroided, mass drift corrected using the NaTFA reference spectrum, and exported into NetCDF format for further mining.

To ensure maximum reproducibility in metabolomic experiments, all serum specimens were run consecutively within a 2.5 month period. Every cancer sample was randomly paired with a normal sample and run on the same day to ensure that no temporal bias was introduced in the way samples were analyzed. Sample pairs were run in random order and in duplicate.

B.3.3. LC-MS Data Mining

Data mining was performed by Dr. Manshui Zhou, Dr. Facundo M. Fernández, and Christina Y. Hampton.

All data were mined identically and simultaneously. Data mining was performed by loading NetCDF files into mzMine.[370] The data mining parameters were selected by visual inspection of their effect on the spectral features extracted. Data were smoothed by chromatographic median filtering with a tolerance in *m/z* of 0.1, and one-sided scan window length of 3 s. Peaks were picked with a *m/z* bin size of 0.15, chromatographic threshold level of 0%, absolute noise level of 200, absolute minimum peak height of 250,

minimum peak duration of 5 s, tolerance for *m/z* variation of 0.06, and tolerance for intensity variation of 50%. The method for de-isotoping was to assume +1 charge states, and monotonic isotopic patterns. The t_R tolerance for de-isotoping was 65 s and the *m/z* tolerance was 0.07. The chromatographic peak alignment *m/z* tolerance was 0.2, and the t_R tolerance was 12%, with a balance between *m/z* and t_R of 30. The minimum number of detections for rare peak filtering in the alignment results was set to 41. Spectral features not initially detected by the peak detection algorithm were subsequently added by a gap filling method using an intensity tolerance of 30%, *m/z* tolerance size of 0.2, and t_R tolerance size of 12%. Systematic drift in intensity levels between different data files was corrected for by linear intensity normalization using the total raw signal.

After the normalized alignment file containing all peak intensities was created, peak areas were exported to Excel and peaks of contaminants, dimers, redundant adducts, and isotopes not adequately detected were removed. Approximately 37% of the peaks from +pESI and 18% of the peaks from -pESI were eliminated after this filtering. Peak areas from duplicate runs were then averaged, and the mass spectral data were exported as ASCII files into Matlab (R2007a, The Mathworks, Natick, MA).

B.3.4. Feature Selection, Model Building, and Model Validation

Data processing, including feature selection, model building and model validation were performed by Wei Guan and Dr. Alexander Gray in the College of Computer Science, Georgia Institute of Technology.

Feature selection was performed using iterative RFE whereby an SVM is first trained with the currently selected feature set. The features are individually evaluated to

determine their importance and less important features are dropped from the feature set. The process is iteratively repeated until the smallest feature set that achieved the highest training accuracy is selected. The prediction performance was evaluated using leave-one-out-cross-validation (LOOCV, one sample is removed from the set of 72 samples, the model is built with the training set (N=71) and tested with the test set (M=1)), 12-fold-cross-validation (12-fold CV, 12 samples are excluded, the model is built with the training set (N=12) and tested with the test set (M=60)), and 52-20 split-validation (52-20 Split, 20 samples are excluded (N=52), the model is built using the training set (N=52) and tested with the test set (M=20)).

B.3.5. Metabolite Identification Protocol

Metabolite identification was performed by Dr. Manshui Zhou and Christina Y. Hampton. Compound identification was attempted only for those spectral features remaining after the feature selection process. Due to the biological complexity of serum samples, adduct ion analysis was first performed to ensure the unambiguous assignment of the signal of interest in each mass spectrum. Adducts formed in +pESI usually include $[M+H]^+$, $[M+NH_4]^+$, $[M+Na]^+$, $[M+K]^+$, $[M-H_2O+H]^+$, and $[2M+H]^+$ species; while adduct and dimer formation in -pESI include $[M-H]^-$, $[M+CH_3COO]^-$, $[M+Cl]^-$, $[M+HCOO]^-$, and $[2M-H]^-$. Adducts in centroided mass spectra corresponding to SVM-RFE-selected variables were identified by manually calculating the differences between the exact *m/z* values of peaks within the spectrum and comparing these differences to those between the common adduct species mentioned above. For spectra in which multiple adducts were not present, the accurate mass of the candidate neutral

molecule was calculated based on the assumption that the peak of interest corresponded to either $[M+H]^+$, $[M+Na]^+$, or $[M+NH_4]^+$ in +pESI or $[M-H]^-$, $[M+CH_3COO]^-$, $[M+HCOO]^-$, or $[M-CH_3]^-$ (for glycerophosphocholines) in -pESI yielding multiple possible neutral molecular masses for each *m/z* value.

Elemental formulae were estimated from the accurate mass spectra using a freely-distributed system of macros[333] that relies on a series of heuristic rules to identify possible formulae based on the mass accuracy of the peak of interest and the corresponding isotopic ratios. The mass of the neutral molecule and relative isotopic abundances were imported directly into the "seven golden rules" Excel spreadsheet.[371] The mass accuracy was set to 15 ppm, and the threshold for error in the relative isotopic abundance was set to 10%. The list of elements to include in the search was constrained to include C, H, N, O, P, S, Cl, and Br. The probability of a given formulae being the "correct" one is provided as a score calculated from the error rates in satisfying the aforementioned rules. The top hits in the list of filtered elemental formulae and accurate mass values obtained were searched in the following databases: Metlin,[372] KEGG,[373] HMDB,[374] MMCD,[375] and Lipid Maps (LM),[376] to determine the greatest possible number of candidate molecules. The criteria used for the assignment of a tentative chemical structure were: 1) a mass difference with the simulated formula lower than 15 ppm, 2) isotope abundance errors less than 10%, and 3) that the candidate found in the database corresponded to an endogenous metabolite (i.e. a small molecule that participates in cellular metabolism as an intermediate or product).

B.4. Results of LC-MS-Based Metabolomic Analysis of Human Serum Samples

Metabolomic investigation of LC-MS data from sera of patients with ovarian cancer and controls revealed 576 features (each feature represents a particular *m/z* value observed at a specific t_R) extracted by mzMine in +pESI and 280 in -pESI (giving a total of 856 features in the multimode feature set, which combines all +pESI and -pESI features). Detailed manual analysis of the entire dataset revealed the presence of additional redundant species (dimer, adducts, and isotopes) that were removed, thus reducing the final number of features (n) used to n = 360 +pESI, n = 232 -pESI, and n = 592 multimode features.

A 3-D serum metabolic profile for a typical stage III ovarian cancer serum sample is displayed in Figure B.1.A showing the capability of LC-MS to resolve hundreds of compounds in a wide mass range within 180 minutes. Despite the shallow solvent gradient chosen for the LC run, there is still evidence of co-elution as evidenced by the projection of Figure B.1.A onto the chromatographic axis (Fig. B.1.B). However, the high resolving power of the TOF mass analyzer allowed in most cases to resolve these signals by their selected monoisotopic ion chromatograms as shown in Figure B.1.C for an ion with *m/z* = 443.26 at a window width of 0.05 Da. The corresponding centroided negative ion mode spectrum obtained at t_R = 91 minutes is shown in Figure B.1.D.

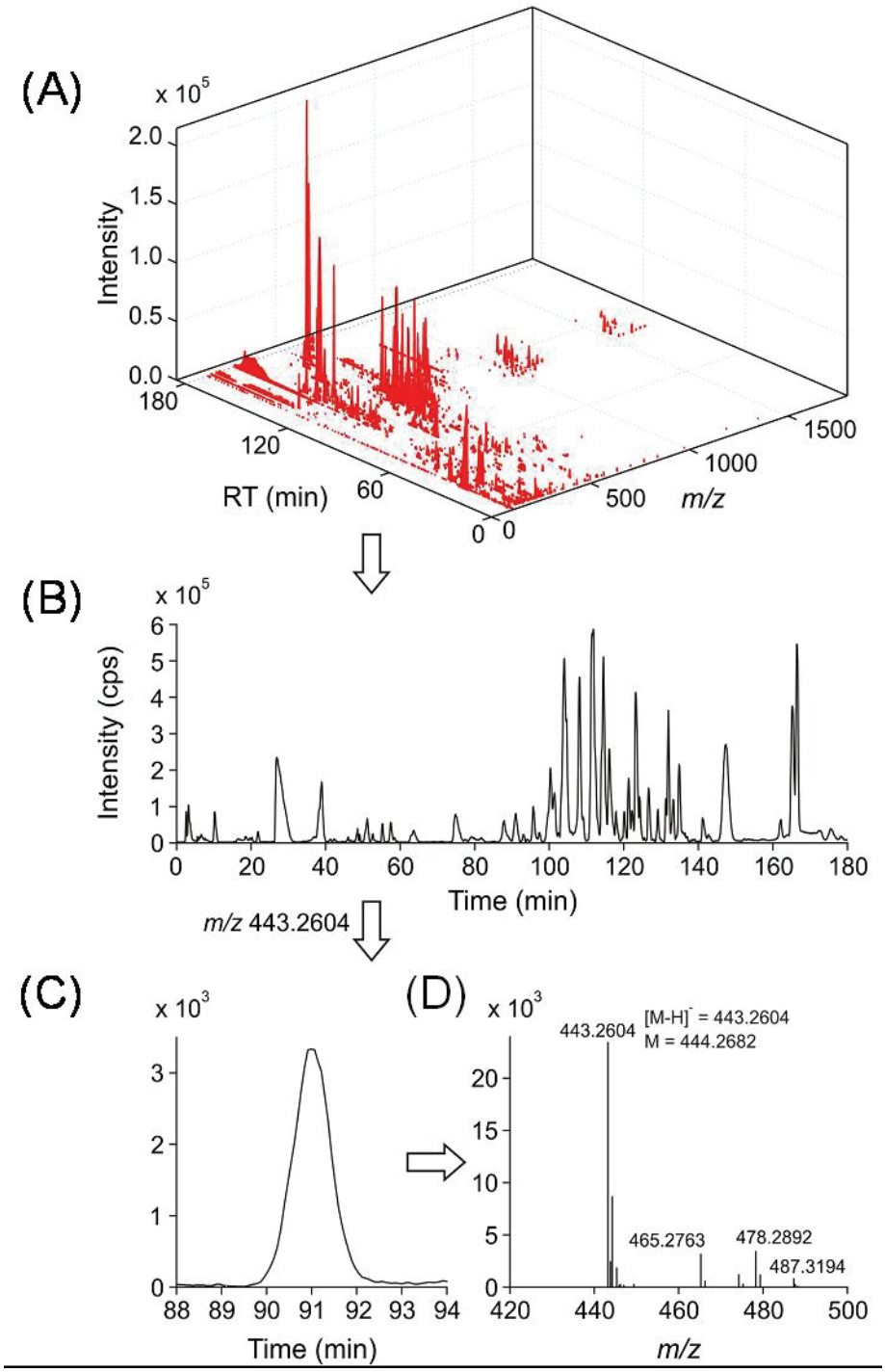

Figure B.1. Sample data obtained by –pESI-LC-MS analysis of a stage III ovarian cancer serum sample including (A) 3D intensity matrix, (B) total ion chromatogram (TIC), (C) selected ion chromatogram for the feature at *m/z* 443.26, and (D) mass spectrum at t_R = 91 minutes.

Due to the obvious complexity of these samples, the reproducibility of the LC-MS approach was tested in early experiments to rule out column memory effects. Lipids, fatty acids and other hydrophobic components in sera that are easily adsorbed onto the reverse phase column can act as a new stationary phase, causing a change of selectivity, memory effects and shifting retention times. If sufficient contamination occurs, backpressure increase or even complete blockage of the column may occur. Figure B.2 shows total ion chromatograms corresponding to 4 identical samples prepared in an identical fashion and analyzed by +ESI (Fig. B.2.A) and -ESI (Fig. B.2.B).

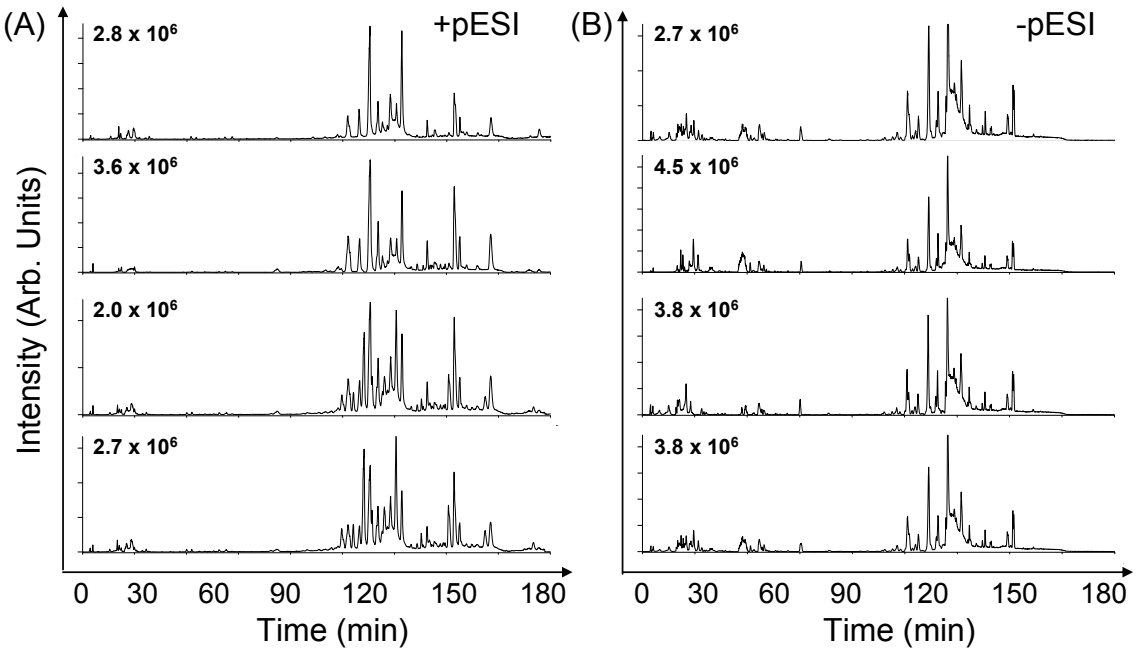

Figure B.2. Total ion chromatograms (TIC) of 4 aliquots of stock serum prepared in an identical fashion and analyzed by (A) +pESI and (B) -pESI.

The results indicate that good reproducibility was possible following the 30-minute washing step. Compound identification was not pursued at this stage, as in LC-MS experiments this is a more time-intensive task than in GC-MS experiments, where

automatic identification is accomplished in an unsupervised way by direct comparison of each EI spectra with existing databases, such as the one available from NIST. This difference in identification procedures arises from two fundamental properties of ESI that are different than for EI: (a) the formation of various adducts and dimers with varying abundances, which is a function of the LC solvents and the desolvation conditions used, and (b) the different extent to which different ESI sources impart varying degrees of IE to desolvated ions. This last property of ESI lends to producing varying degrees of fragmentation of labile species, most commonly dehydration, by in-source CID. Instead, compound identification was attempted *a posteriori*, for spectral features observed to be significant in SVM-RFE models.

B.5. Evaluation of Model Performance

The prediction performance for each dataset (+pESI, -pESI, and multimode) was evaluated for the SVM-RFE model. The results are summarized in Table B.2.

Table B.2. Prediction performance (%) evaluated for each dataset using LOOCV, 12-fold CV, and 52-20 Split.

Dataset	LOOCV	12-fold CV	52-20 Split
Multimode (n=592)	80.6	74.0	71.6
+pESI (n=360)	66.7	71.4	66.5
-pESI (n=232)	73.6	74.3	69.1

As can be seen in Table B.2, the prediction performance of the multimode dataset model was better than that of the +pESI and -pESI datasets for LOOCV and 52-20 Split validation. However, for 12-fold CV, the prediction performance of the -pESI dataset model is slightly better than that for the multimode dataset. The average number of features selected for the multimode, +pESI, and -pESI datasets was 32, 26, and 35 features, respectively. The sensitivity (how well cancer patients can be detected) and specificity (how well controls can be detected) of these models are summarized in Table B.3.

Table B.3. Sensitivity and specificity (%) for LOOCV validation.

Dataset	Sensitivity	Specificity
Multimode (n=592)	83.8	77.1
+pESI (n=360)	73.0	60.0
-pESI (n=232)	78.4	68.6

Although it is difficult to pinpoint which of the three models, multimode, +pESI, or -pESI, has the best prediction performance using the results in Table B.2, it is clear from Table B.3 that the multimode dataset provides a model having the best sensitivity and specificity. Therefore, we attempted to identify metabolites corresponding to the features selected in the SVM-RFE model of the multimode dataset.

B.6. Metabolite Identification

The calculated neutral masses, species investigated, and t_R's of the +pESI and -pESI features used by the multimode SVM-RFE model, as well as their corresponding chemical formulae, mass differences (Δm), and matching scores, are reported in Tables B.4 and B.5, while the corresponding mass spectra are shown in Figures B.3 and B.4.

This model consists of the relatively stable features (threshold 54%) obtained over the LOOCV validation as described above. Adduct analysis of the 18 and 27 features selected from +pESI and -pESI, respectively, provided 29 neutral masses to search against the databases as 16 features were found to be redundant.

Five of the SVM-RFE-selected +pESI features from the multimode dataset were tentatively identified as glycophospholipids. Due to the inability of single stage MS analysis to distinguish between isomeric compounds (compounds having identical chemical formulae but different structures), the features could not be definitively assigned to a particular glycophospholipid isomer. As such, all of the possible isomers corresponding to each feature are listed in Table B.4. The chemical formulae corresponding to these five features yielded 106 possible compounds with the total number of isomers attributed to each feature ranging from 3-32, mass accuracies between 0.4-11.6 ppm and matching scores between 42.6-99.0%. Examples of compounds that could be tentatively matched to the elemental formulae obtained in this investigation include LysoPC (18:2 (9Z, 12Z), PE-NMe (18:1 (19E) /18:1 (9E)), PC (14:0/20:1 (11Z)), PC (14:0/22:4 (7Z, 10Z, 13Z, 16Z)), and PC (14:0/22:1 (13Z)).

Nine of the SVM-RFE-selected -pESI features were tentatively identified as endogenous carboxylic acids, peptides, glycerophospholipids, and hormones. The total

number of isomers for these nine features ranged from 1 – 16 yielding 65 possible compounds with mass accuracies between 1.4 – 14.9 ppm and matching scores between 82.7 – 99.3%. One of the identified features could not be assigned to a single chemical formulae due to the absence of additional supporting adduct ions in the mass spectrum. This feature was attributed to either lithocholic acid glycine conjugate or any of 8 glycerophosphocholine isomers, such as PC (P-16:0/0:0). Potential matches for the possible identities of the selected features include palmitic acid, 12-hydroxy-8E,10E-heptadecadienoic acid, stearic acid, GlnHisAla, DHEA sulfate, PC (10:4/4:0), PE (9:0/10:0) and glycoursodeoxycholic acid 3-sulfate.

Although metabolites such as lysophosphatidic acid and lipid associated sialic acid have been investigated as metabolic biomarkers for ovarian cancer in literature, these were not identified during this study. However, the presence of several endogenous lipids as well as other endogenous metabolites in the set of selected features suggests that this approach has merit and should be further explored.

The wide variation in mass accuracies and scores observed can be attributed to two major factors: 1) ambient temperature variations during the lengthy LC analysis time affecting both the output of the TOF mass spectrometer power supplies and the length of the flight tube, and 2) low signal intensity of some of the features selected. The software provided by the mass spectrometer manufacturer provides two methods to perform post-analysis correction of the *m/z* values obtained – mass drift compensation and mass calibration. Mass drift compensation, which is typically used to correct for temporal drift during long analysis times, was found to be insufficient to accurately calibrate the entire run. Instead, a full recalibration of the sample run using a calibration curve generated

from the NaTFA standard run immediately after the sample was performed and provided a marked improvement in mass accuracy. It was further observed that inclusion of the isotope matching rule had a positive impact on decreasing the number of false-positive or negative entries on the hit lists. Confirmation of the annotation of these eighteen metabolites and identification of remaining features selected by SVM-RFE will require additional accurate mass MS/MS and ^{1}H-NMR experiments, and exceeds the scope of this study.

Table B.4. Tentative identifications of SVM-RFE-selected features from multimode dataset detected in +pESI. Matches to identified compounds were made using accurate mass measurements and isotope cluster matching. For species which could not be matched against metabolite databases, the top-five matching formulae (according to score) are listed (for features matching fewer than five formulae, all formulae are shown).[A]

Neutral Mass (Da)	Species Investigated	RT (min)	Estimated Formulae (in order of decreasing score)	Accuracy (ppm)	Score (%)	Tentative Identification	Source	Spectra
148.0129	$[M+H]^+$	116.8812	C_4N_6O, C_5H_9OPS, $C_4H_8N_2S_2$	0.1-11.7	99.5-90.1			B.3 (a)
204.0695	$[M+H]^+$	116.8743	$C_{12}H_{13}OP$, $C_6H_{12}N_4O_2S$, $C_{14}H_8N_2$, $C_{11}H_{12}N_2S$	3.7-12.8	96.5-91.5			B.3 (b)
278.1434	$[M+CH_3CN+Na]^+$	144.2175	$C_8H_{14}N_{12}$, $C_{10}H_{24}N_4OP_2$, $C_{11}H_{23}N_2O_4P$, $C_{12}H_{19}N_6P$, $C_7H_{18}N_8O_4$	3.1-13.9	96.3-99.0			B.3 (c)
495.3210	$[M+H]^+$	109.6750	$C_{21}H_{46}N_5O_6P$, $C_{21}H_{45}N_5O_8$, $C_{18}H_{37}N_{15}O_2$, $C_{19}H_{37}N_{13}O_3$, $C_{20}H_{47}N_7O_3P_2$	1.1-13.7	99.7-98.8			B.3 (d)
519.3330	$[M+H]^+$	100.1739	$C_{26}H_{50}NO_7P$	1.0	99.0	3 PC(18:2/0:0) isomers (e.g. LysoPC(18:2(9Z,12Z))	see footnote (B)	B.3 (e)
757.5678	$[M+H]^+$	127.8454	$C_{42}H_{80}NO_8P$	7.5	83.3	31 glycerophospholipid isomers (e.g. PE-NMe(18:1(19E)/18:1(9E)))	see footnote (C)	B.3 (f)
759.5775 [D]	$[M+Na]^+$	138.3808	$C_{42}H_{82}NO_8P$	0.4	42.6	18 glycerophosphocholine isomers (e.g. PC(14:0/20:1(11Z)))	see footnote (E)	B.3 (g)
781.5595 [D]	$[M+H]^+$	138.3808	$C_{44}H_{80}NO_8P$	3.4	46	32 glycerophosphocholine isomers (e.g. PC(14:0/22:4(7Z,10Z,13Z,16Z)))	see footnote (F)	B.3 (g)
787.6000 [G]	$[M+Na]^+$	136.6754	$C_{44}H_{86}NO_8P$	11.6	74.6	22 glycerophosphocholine isomers (e.g. PC(14:0/22:1(13Z)))	see footnote (H)	B.3 (h)
932.6173	$[M+NH_4]^+$	143.6995	$C_{54}H_{94}O_6P_2S$, $C_{53}H_{88}O_{11}S$, $C_{52}H_{88}N_2O_{10}S$, $C_{54}H_{95}O_4P_3S$, $C_{52}H_{84}N_8O_5S$	1.0-13.5	97.3-96.6			B.3 (i)

Table B.4, cont'd. Tentative identifications for SVM-RFE-selected features from multimode dataset detected in +pESI.

(A) For species having multiple isomers the following nomenclature is given: # isomers found including **name of isomer** *[source (cross-listed source, if any)]*.

(B) 3 isomers found including **PC(18:2/0:0)** *[LMGP 01050036 (HMDB 10386), 01050034, and 01050035]*.

(C) 31 isomers found including **PE-NMe(18:1/18:1)** *[LMGP 02010331 (MMCD cq_17959), 02010333, 02010338, 02010350]*, **PC(16:0/18:2)** *[LMGP 01010585, 01010586, 01010587, 01010588, 01010589, 01010590, 01010591, 01010592, 01010593, 01010594, 01010595, 01010596]*, **PC(16:1/18:1)** *[LMGP 01010678, 01010680, 01010687, 01010688, 01010689]*, **PC(17:1/17:1)** *[LMGP 01010726, 01010727, 01010728]*, **PC(18:0/16:2(2E,4E))** *[LMGP 01010745]*, **PC(18:1/16:1)** *[LMGP 01010886, 01010887]*, **PC(18:2/16:0)** *[LMGP 01010920, 01010926, 01010932, 01010933]*.

(D) Adduct analysis yielded several possible ion species for the selected feature. Only species having tentative matches are listed.

(E) 18 isomers found including **PC(14:0/20:1(11Z))** *[HMDB 07879]*, **PC(16:0/18:1)** *[LMGP 01010005, 01010575, 01010576, 01010577, 01010578, 01010579, 01010580, 01010581, 01010582, 01010583, 01010584]*, **PC(16:1/18:0)** *[LMGP 01010679, 01010686]*, **PC(18:0/16:1(9Z))** *[LMGP 01010744]*, **PC(18:1/16:0)** *[LMGP 01010874, 01010884, 01010885]*.

(F) 32 isomers found including **PC(14:0/22:4(7Z,10Z,13Z,16Z))** *[HMDB 07889]*, **PC(16:0/20:4)** *[LMGP 01010007, 01010629, 01010630, 01010631]*, **PC(18:0/18:4)** *[LMGP 01010772, 01010773, 01010774, 01010775, 01010776]*, **PC(18:1/18:3)** *[LMGP 01010897, 01010898, 01010899]*, **PC(18:2/18:2)** *[LMGP 01010918, 01010919, 01010921, 01010922, 01010923, 01010924, 01010925, 01010927, 01010928, 01010929, 01010930, 01010937, 01010938, 01010939]*, **PC(18:3/18:1)** *[LMGP 01010949, 01010955]*, **PC(20:4/16:0)** *[LMGP 01011049, 01011050, 01011056]*.

(G) Adduct analysis yielded several possible ion species for the selected feature. Only 1 species could be tentatively identified.

(H) 22 isomers found including **PC(14:0/22:1(13Z))** *[HMDB 07887]*, **PC(16:0/20:1(11Z))** *[LMGP 01010618]*, **PC(18:0/18:1)** *[LMGP 01010749, 01010750, 01010751, 01010752, 01010753,01010754, 01010755, 01010756, 01010757, 01010758, 01010759, 01010760, 01010761, 01010762, 01010763]*, **PC(18:1/18:0)** *[LMGP 01010840, 01010875, 01010888, 01010889]*, **PC(20:1(11Z)/16:0)[U]** *[LMGP 01011037]*.

Figure B.3. Mass spectra for SVM-RFE-selected features from multimode dataset detected in +pESI (structure and name of 1st isomer listed in Table B.4 is included as inset in spectra for those features that were matched to compounds).

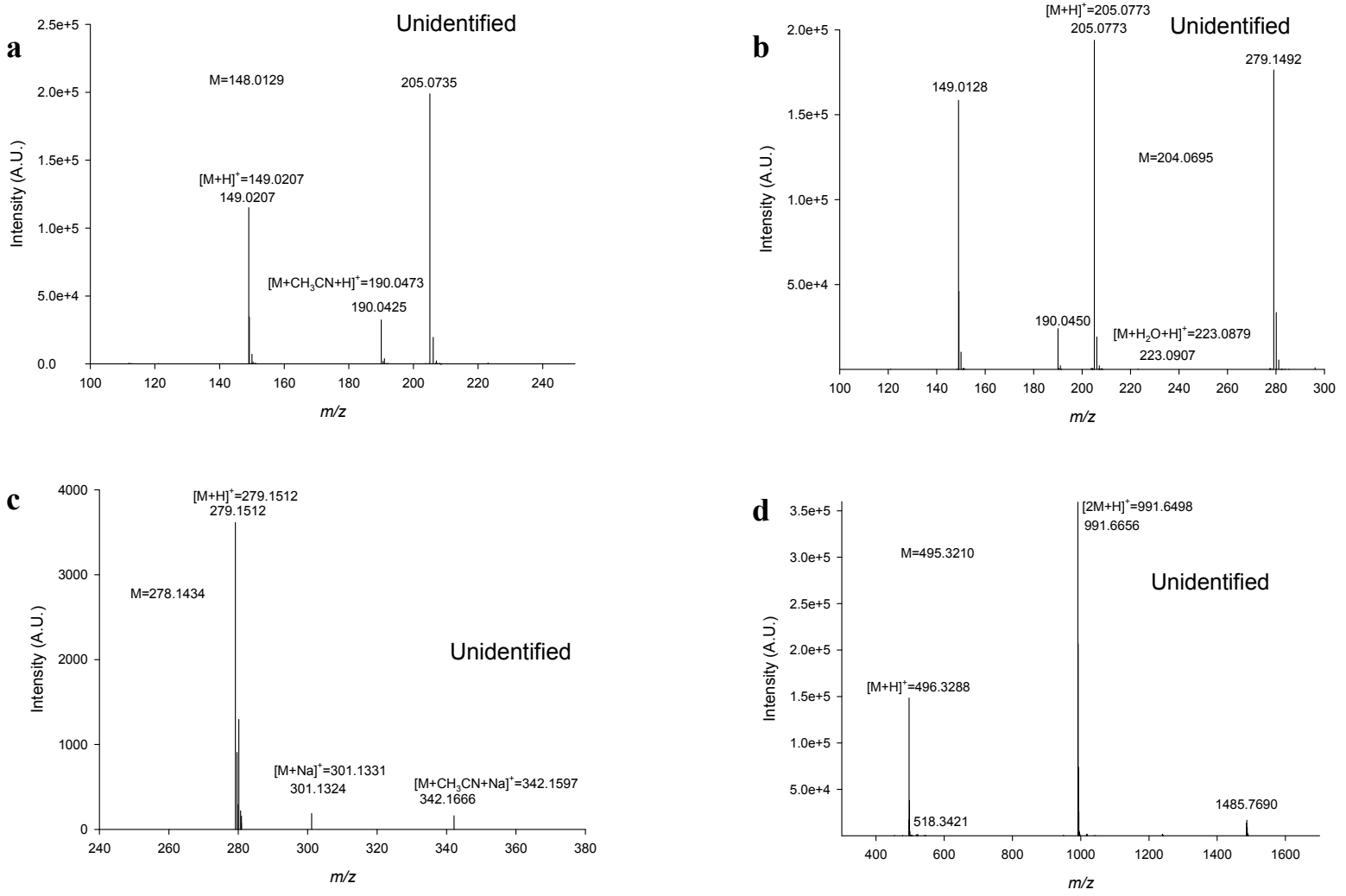

Figure B.3, cont'd. Mass spectra for SVM-RFE-selected features from multimode dataset detected in +pESI.

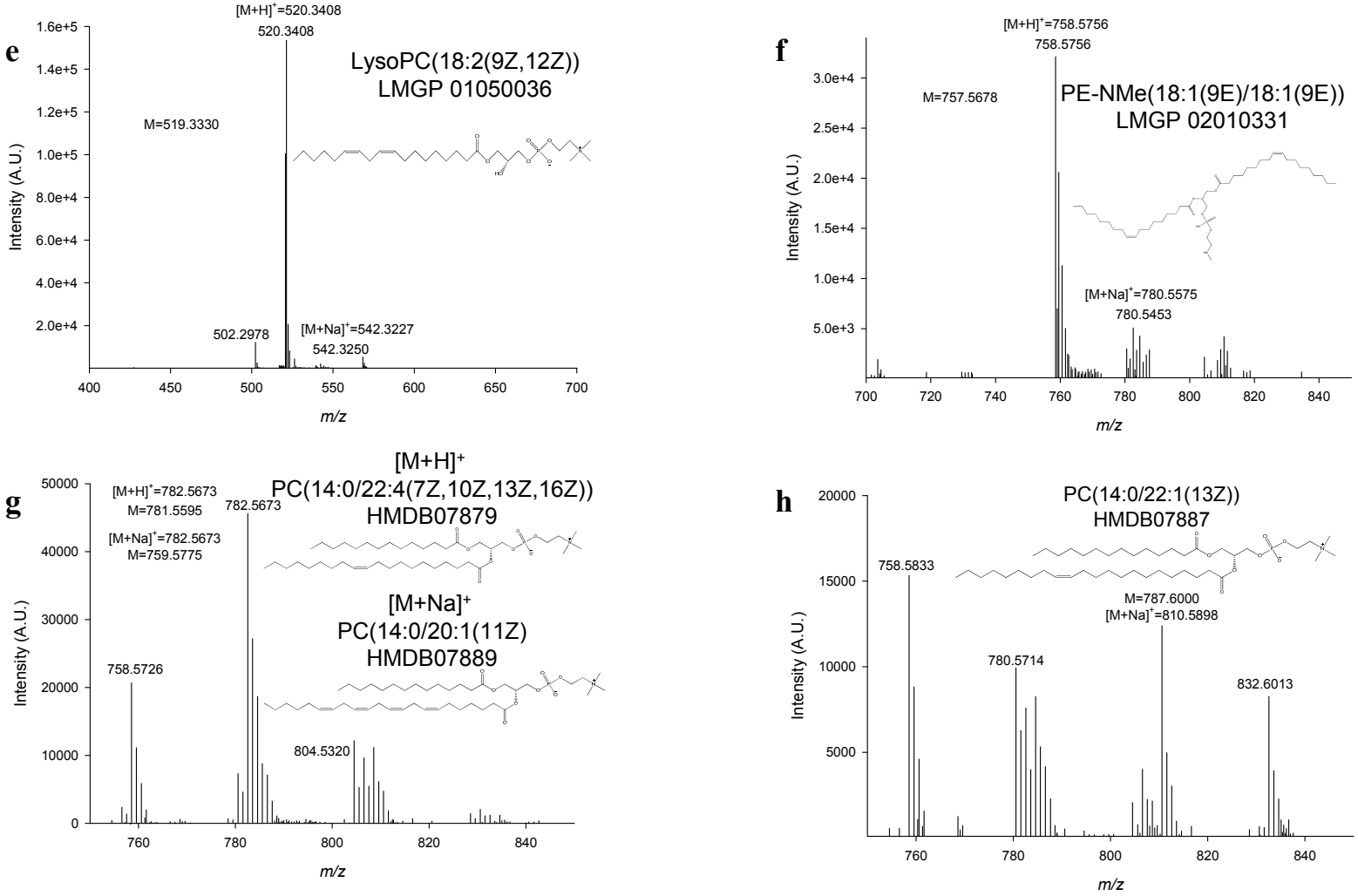

Figure B.3, cont'd. Mass spectra for SVM-RFE-selected features from multimode dataset detected in +pESI.

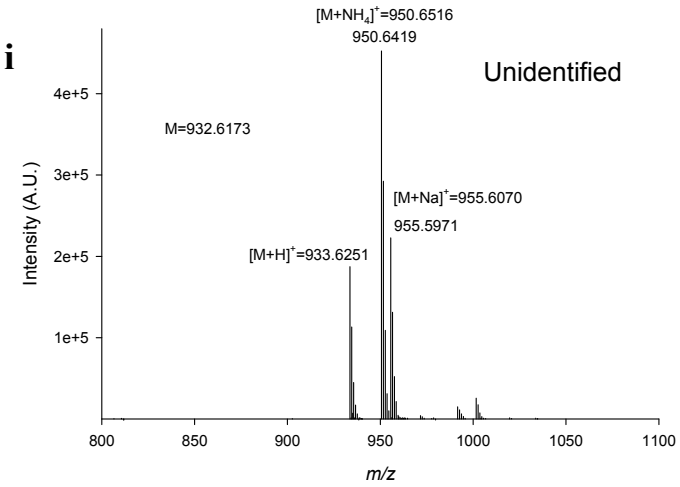

Table B.5. Tentative identifications for SVM-RFE-selected features from multimode dataset detected in -pESI. Matches to identified compounds were made using accurate mass measurements and isotope cluster matching. For species which could not be matched against metabolite databases, the top-five matching formulae (according to score) are listed (for features matching fewer than five formulae, all formulae are shown).[A]

Neutral Mass (Da)	Species Investigated	RT (min)	Estimated Formulae (in order of decreasing score)	Accuracy (ppm)	Score (%)	Name	Source	Spectra
256.2398	$[M-H]^-$	104.6898	$C_{16}H_{32}O_2$	1.7	96.3	16 carboxylic acid isomers (e.g. palmitic acid)	see footnote (B)	B.4 (a)
274.1710	$[M-H]^-$	39.2953	$C_{14}H_{27}O_3P$, $C_{13}H_{28}N_2P_2$, $C_{16}H_{22}N_2O_2$, $C_{10}H_{23}N_6OP$, $C_{13}H_{26}N_2O_2S$	1.8-14.3	99.0-95.2			B.4 (b)
280.2446	$[M-H]^-$	133.2433	$C_{15}H_{38}P_2$, $C_{15}H_{36}O_2S$, $C_{11}H_{32}N_6S$	0.9-13.2	93.7-91.4			B.4 (c)
280.2460	$[M-H]^-$	98.8490	$C_{15}H_{38}P_2$, $C_{15}H_{36}O_2S$	4.1-8.6	95.0-94.4			B.4 (d)
282.2154 [C]	$[M-H]^-$	139.6953	$C_{17}H_{30}O_3$	14.5	99.3	12-hydroxy-8E,10E-heptadecadienoic acid	MID 35560	B.4 (e)
284.2701 [D]	$[M-H]^-$	123.8672	$C_{18}H_{36}O_2$	5.0	96.1	12 carboxylic acid isomers (e.g. stearic acid)	see footnote (E)	B.4 (f)
340.2489	$[M-H]^-$	130.1342	$C_{20}H_{38}P_2$, $C_{20}H_{37}O_2P$, $C_{22}H_{32}N_2O$, $C_{17}H_{32}N_4O_3$, $C_{16}H_{33}N_6P$	4.3-12.4	98.1-95.4			B.4 (g)
354.1676	$[M-H]^-$	42.4019	$C_{14}H_{22}N_6O_5$	6.9	95.4	6 peptide isomers (e.g. GlnHisAla)	see footnote (F)	B.4 (h)
368.1652 [G]	$[M-H]^-$	85.4803	$C_{19}H_{28}O_5S$	1.4	93.1	2 isomers (e.g. DHEA Sulfate)	see footnote (H)	B.4 (i)
384.2831 [I]	$[M+CH_3COO]^-$	90.7391	$C_{26}H_{40}S$, $C_{23}H_{44}S_2$, $C_{21}H_{40}N_2O_2S$, $C_{29}H_{36}$, $C_{18}H_{44}N_2O_2S_2$	3.4-13.9	94.0-85.9			B.4 (j)
398.2982 [I]	$[M+HCOO]^-$	90.7391	$C_{27}H_{42}S$, $C_{24}H_{46}S_2$, $C_{22}H_{42}N_2O_2S$, $C_{25}H_{38}N_2O_2$, $C_{19}H_{46}N_2O_2S_2$	3.8-14	94.0-86.9			B.4 (j)
433.3256 [J]	$[M+HCOO]^-$	91.9683	$C_{26}H_{43}NO_4$	14.8	98.8	Lithocholic acid glycine conjugate	HMDB 00698 [K]	B.4 (k)
444.3037 [I]	$[M-H]^-$	90.7391	$C_{24}H_{40}N_6S$, $C_{28}H_{45}PS$, $C_{28}H_{44}O_2S$, $C_{25}H_{49}PS_2$, $C_{25}H_{48}O_2S_2$	0.45-13.0	94.1-91.9			B.4 (j)

Table B.5, cont'd. Tentative identifications for SVM-RFE-selected features from multimode dataset detected in -pESI.

Neutral Mass (Da)	Species Investigated	RT (min)	Estimated Formulae (in order of decreasing score)	Accuracy (ppm)	Score (%)	Name	Source	Spectra
479.3310 [J]	$[M-H]^-$	91.9683	$C_{24}H_{50}NO_6P$	13.7	96.6	8 glycerophosphocholine isomers (e.g. PC(P-16:0/0:0))	see footnote (L)	B.4 (k)
481.2835	[M-H]-	106.0719	$C_{22}H_{44}NO_8P$	6.3	90.4	10 glycerophosphocholine isomers (e.g. PC(10:0/4:0))	see footnote (M)	B.4 (l)
481.3047	$[M-H]^-$	116.2758	$C_{12}H_{35}N_{17}O_4$, $C_{12}H_{36}N_{17}O_2P$, $C_{17}H_{50}N_5O_4P_3$, $C_{16}H_{39}N_{11}O_6$, $C_{17}H_{51}N_5O_2P_4$	2.2-14.9	95.1-93.4			B.4 (m)
499.9613	$[M-H]^-$	166.3375	$C_{21}H_8O_{13}S$, $C_{21}H_9O_{11}PS$, $C_{20}H_{10}N_2O_8P_2S$, $C_{19}H_{22}P_6S_2$, $C_{18}H_4N_4O_{12}S$	22.0-14.5	96.6-96.1			B.4 (n)
505.2842	$[M-H]^-$	100.0856	$C_{22}H_{47}N_5P_4$, $C_{22}H_{46}N_5O_2P_3$, $C_{17}H_{31}N_{17}O_2$, $C_{20}H_{36}N_{13}OP$, $C_{19}H_{41}N_9O_3P_2$	0.9-12.1	99.5-97.9			B.4 (o)
505.3308 [N]	$[M+CH_3COO]^-$	147.7737	$C_{28}H_{49}N_3OP_2$, $C_{29}H_{49}NO_2P_2$, $C_{27}H_{39}N_9O$, $C_{29}H_{48}NO_4P$, $C_{25}H_{44}N_7O_2P$	2.5-13.8	94.0-92.6			B.4 (s)
507.3131	$[M-H]^-$	112.7721	$C_{28}H_{45}NO_7$, $C_{28}H_{46}NO_5P$, $C_{26}H_{46}N_5OPS$, $C_{27}H_{45}N_3O_4S$, $C_{26}H_{37}N_9O_2$	0.1-12.8	97.3-96.2			B.4 (p)
509.3156	$[M-H]^-$	121.2736	$C_{24}H_{48}NO_8P$	7.6	91.8	6 glycerophospholipid isomers (e.g.PE(9:0/10:0))	see footnote (O)	B.4 (q)
519.3459 [N]	$[M+HCOO]^-$	147.7737	$C_{26}H_{46}N_7O_2P$, $C_{27}H_{57}NP_4$, $C_{29}H_{51}N_3OP_2$, $C_{26}H_{45}N_7O_4$, $C_{27}H_{45}N_5O_5$	1.7-14.2	93.3-92.8			B.4 (s)
529.2699	$[M-H]^-$	105.7854	$C_{26}H_{43}NO_8S$	1.9	82.7	3 carboxylic acid isomers (e.g. glycoursodeoxycholic acid 3-sulfate)	see footnote (P)	B.4 (r)
563.3363 [N]	$[M-H]^-$	147.7737	$C_{26}H_{47}N_9OP_2$, $C_{24}H_{37}N_{17}$, $C_{28}H_{57}NO_2P_4$, $C_{25}H_{37}N_{15}O$, $C_{27}H_{46}N_7O_4P$	2.7-10.2	94.0-93.0			B.4 (s)

Table B.5, cont'd. Tentative identifications for SVM-RFE-selected features from multimode dataset detected in -pESI.

Neutral Mass (Da)	Species Investigated	RT (min)	Estimated Formulae (in order of decreasing score)	Accuracy (ppm)	Score (%)	Name	Source	Spectra
683.5089 [Q]	$[M+CH_3COO]^-$	140.4283	$C_{37}H_{66}N_9OP$, $C_{39}H_{77}NP_4$, $C_{39}H_{76}NO_2P_3$, $C_{34}H_{62}N_{13}P$, $C_{38}H_{66}N_7O_2P$	0.1-14.7	88.7-87.9			B.4 (t)
697.5246 [Q]	$[M+HCOO]^-$	140.4283	$C_{35}H_{64}N_{13}P$, $C_{40}H_{79}NP_4$, $C_{34}H_{63}N_{15}O$, $C_{36}H_{74}N_7P_3$, $C_{35}H_{63}N_{13}O_2$	2.7-14.5	88.6-88.1			B.4 (t)
743.5300 [Q]	$[M-H]^-$	140.4283	$C_{37}H_{77}N_7P_4$, $C_{35}H_{66}N_{15}OP$, $C_{36}H_{76}N_9OP_3$, $C_{38}H_{87}NP_6$, $C_{37}H_{76}N_7O_2P_3$	1.6-14.7	88.7-88.2			B.4 (t)
757.5457 [Q]	$[M-CH_3]^-$	140.4283	$C_{39}H_{89}NP_6$, $C_{37}H_{78}N_9OP_3$, $C_{38}H_{79}N_7P_4$, $C_{39}H_{88}NO_2P_5$, $C_{32}H_{63}N_{21}O$	4.8-14.5	88.8-88.2			B.4 (t)

(A) For species having multiple isomers the following nomenclature is given: # isomers found including **name of isomer** *[source (cross-listed source, if any)]*.

(B) 16 isomers found including **palmitic acid** *[LMFA 01010001 (HMDB 00220)],* **isopalmitic acid** *[LMFA 01020010],* **2,6-dimethyl-tetradecanoic acid** *[LMFA 01020038],* **2,8-dimethyl-tetradecanoic acid** *[LMFA 01020039],* **3-methyl-pentadecanoic acid** *[LMFA 01020164],* **2-propyl-tridecanoic acid** *[LMFA 01020165],* **2-hexyl-decanoic acid** *[LMFA 01020166],* **3-ethyl-3-methyl-tridecanoic acid** *[LMFA 01020167],* **2-heptyl-nonanoic acid** *[LMFA 01020168],* **6-ethyl-tetradecanoic acid** *[LMFA 01020169],* **2,4-dimethyl-tetradecanoic acid** *[LMFA 01020170],* **3,5-dimethyl-tetradecanoic acid** *[LMFA 01020171],* **4-hexyl-decanoic acid** *[LMFA 01020172],* **2-ethyl-2-butyl-decanoic acid** *[LMFA 01020173],* **13-methyl-pentadecanoic acid** *[LMFA 01020192],* **4,8,12-trimethyl-tridecanoic acid** *[LMFA 01020249]*.

(C) Adduct analysis yielded multiple possible ion species for this feature. Only 1 species could be tentatively identified.

(D) Adduct analysis yielded multiple possible ion species for this feature. Only 1 species could be tentatively identified.

Table B.5, cont'd. Tentative identifications for SVM-RFE-selected features from multimode dataset detected in -pESI.

(E) 12 isomers found including **stearic acid** [HMDB 00827 (LMFA 01010018, MID 189, MMCD cq_00998)], **10-methyl-heptadecanoic acid** [MID 4292 (LMFA 01020013)], **(+)-isostearic acid** [MID 4293 (LMFA 01020014)], **2,6-dimethyl-hexadecanoic acid** [MID 4324 (LMFA 01020042)], **4,8-dimethyl-hexadecanoic acid** [MID 4325 (LMFA 01020043)], **2,14-dimethyl-hexadecanoic acid** [MID 4326 (LMFA 01020044)], **4,14-dimethyl-hexadecanoic acid** [MID 4327 (LMFA 01020045)], **6,14-dimethyl-hexadecanoic acid** [MID 4328 (LMFA 01020046)], **lambda isostearic acid** [MID 4493 (LMFA 01020093)], **neostearic acid** [MID 4620 (LMFA 01020094)], **11,15-dimethyl-hexadecanoic acid** [MID 34604 (LMFA 01020175)], **15-methyl-heptadecanoic acid** [MID 34632 (LMFA 01020205)].

(F) 6 isomers found including **Gln His Ala** [MID 23091], **Gln Ala His** [MID 22217], **Ala His Gln** [MID 21229], **Ala Gln His** [MID 16023], **His Gln Ala** [MID 20595], **His Ala Gln** [MID 18707].

(G) Adduct analysis yielded multiple possible ion species for this feature. Only 1 species could be tentatively identified.

(H) 2 isomers found including **DHEA sulfate** [HMDB 01032 (LMST 05020010)], **testosterone sulfate** [HMDB 02833].

(I) Adduct analysis yielded multiple possible ion species for this feature. All are listed as none could be matched against the databases.

(J) Adduct analysis yielded multiple possible ion species for this feature. Only species that could be tentatively identified are listed.

(K) Cross-listed as MMCD cq-10750 and MID 5666.

(L) 8 isomers found including **PC(P-16:0/0:0)** [HMDB 10407 (LMGP 01070006)], **PC(O-16:1/0:0)** [LMGP 01050100, 01050101, 01050102, 01050103, 01050104, 01070004, 01070005].

(M) 10 isomers found including **PC(10:0/4:0)** [LMGP 01010403], **PC(12:0/2:0)** [LMGP 01010443], **PC(6:0/8:0)** [LMGP 01011233, 01011234], **PC(7:0/7:0)** [LMGP 01011238, 01011239, 01011240], **PC(8:0/6:0)** [LMGP 01011248, 01011249], **PC(9:0/5:0)** [LMGP 01011269].

(N) Adduct analysis yielded multiple possible ion species for this feature. All are listed as none could be matched against the databases.

(O) 6 isomers found including **PE(9:0/10:0)[U]** [MID 40490 (LMGP 02010091)], **PE(10:0/9:0)[U]** [MID 40669 (LMGP 02010272)], **PC(14:0/2:0)** [LMGP 01010504], **PC(8:0/8:0)** [LMGP 01011251, 01011252, 01011253].

Table B.5, cont'd. Tentative identifications for SVM-RFE-selected features from multimode dataset detected in -pESI.

(P) 3 isomers found including glycoursodeoxycholic acid 3-sulfate *[HMDB 02409 (MMCD cq_17361, MID 6670)],* glycochendeoxycholic acid 7-sulfate *[HMDB 02496 (MMCD cq_17159, MID 6692)],* glycochendeoxycholate-3-sulfate *[HMDB 02497 (MMCD cq_17507, MID 6702)]*.

(Q) Adduct analysis yielded multiple possible ion species for this feature. All are listed as none could be matched against the databases.

Figure B.4. Mass spectra for SVM-RFE-selected features from multimode dataset detected in -pESI (structure and name of 1st isomer listed is included as inset in spectra for those features that were matched to compounds).

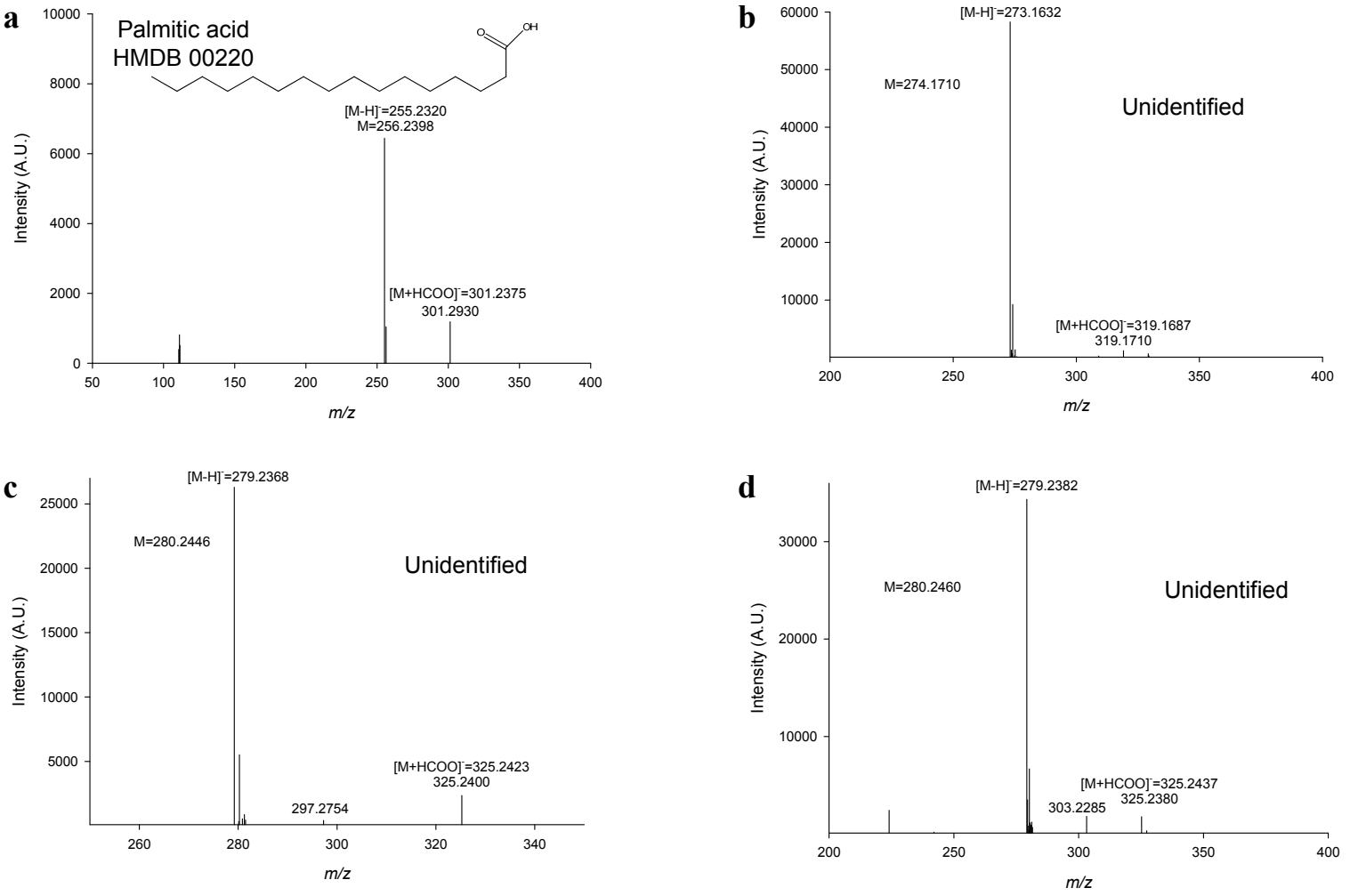

Figure B.4, cont'd. Mass spectra for SVM-RFE-selected features from multimode dataset detected in -pESI.

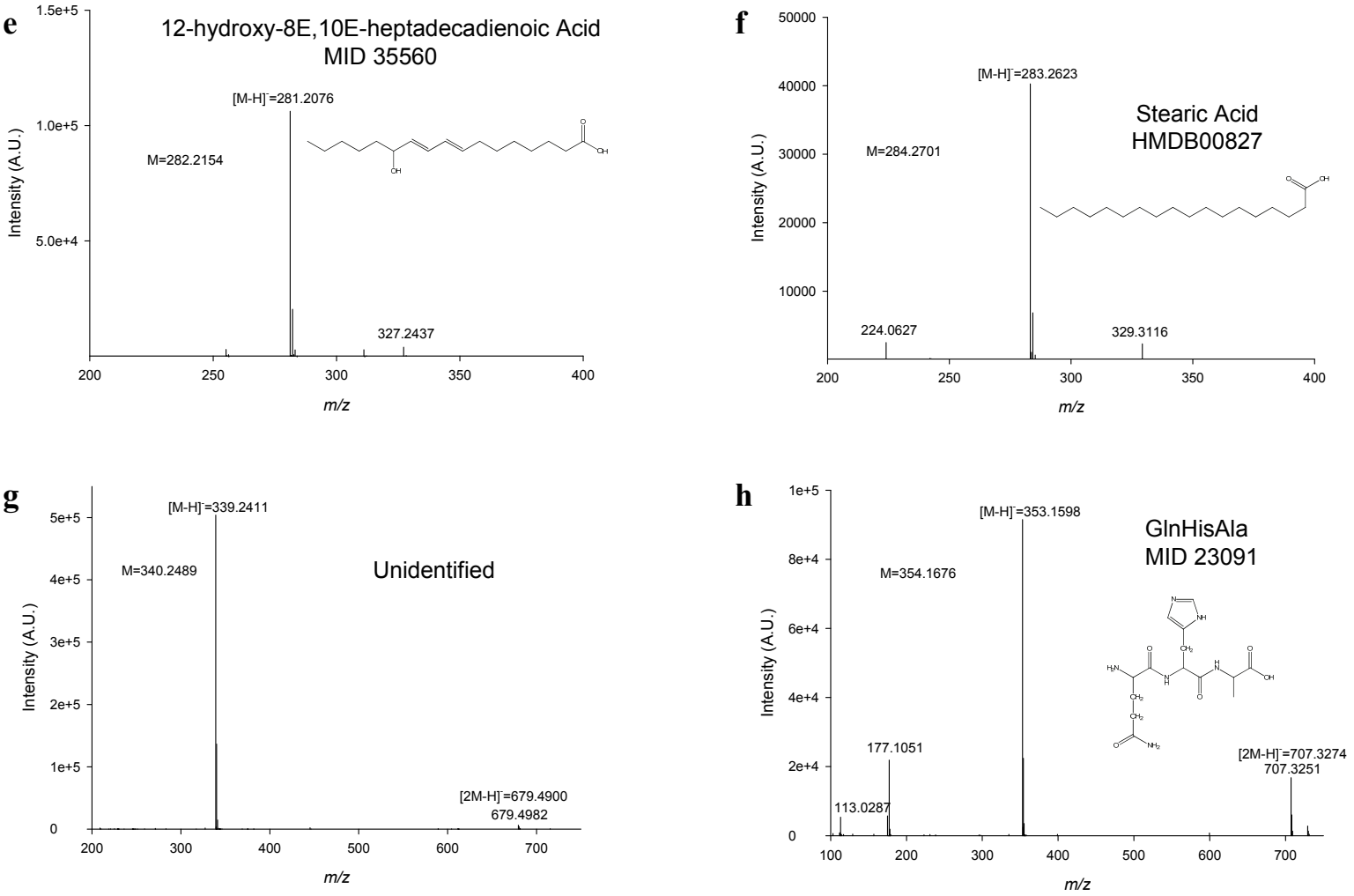

Figure B.4, cont'd. Mass spectra for SVM-RFE-selected features from multimode dataset detected in -pESI.

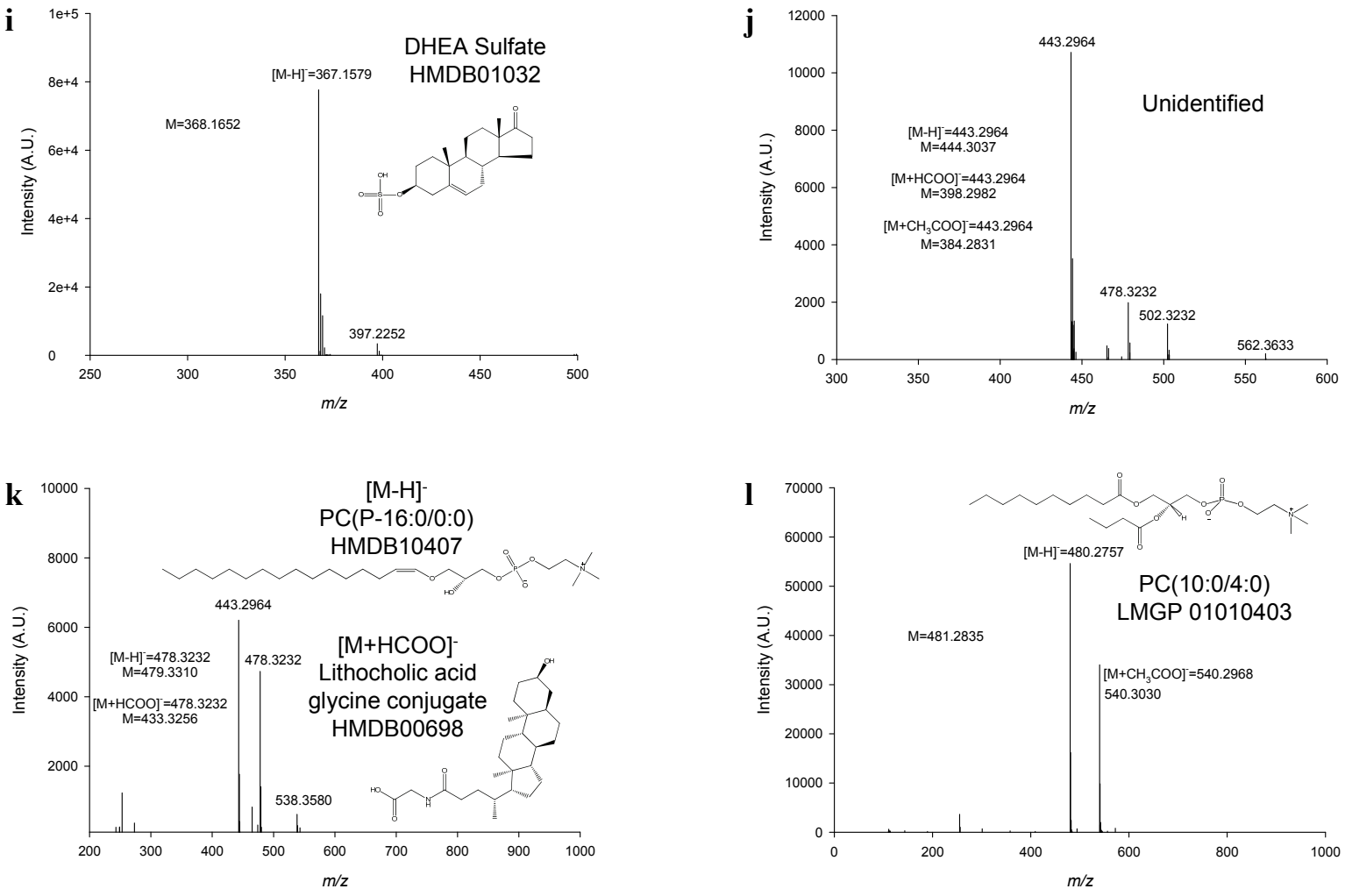

Figure B.4, cont'd. Mass spectra for SVM-RFE-selected features from multimode dataset detected in -pESI.

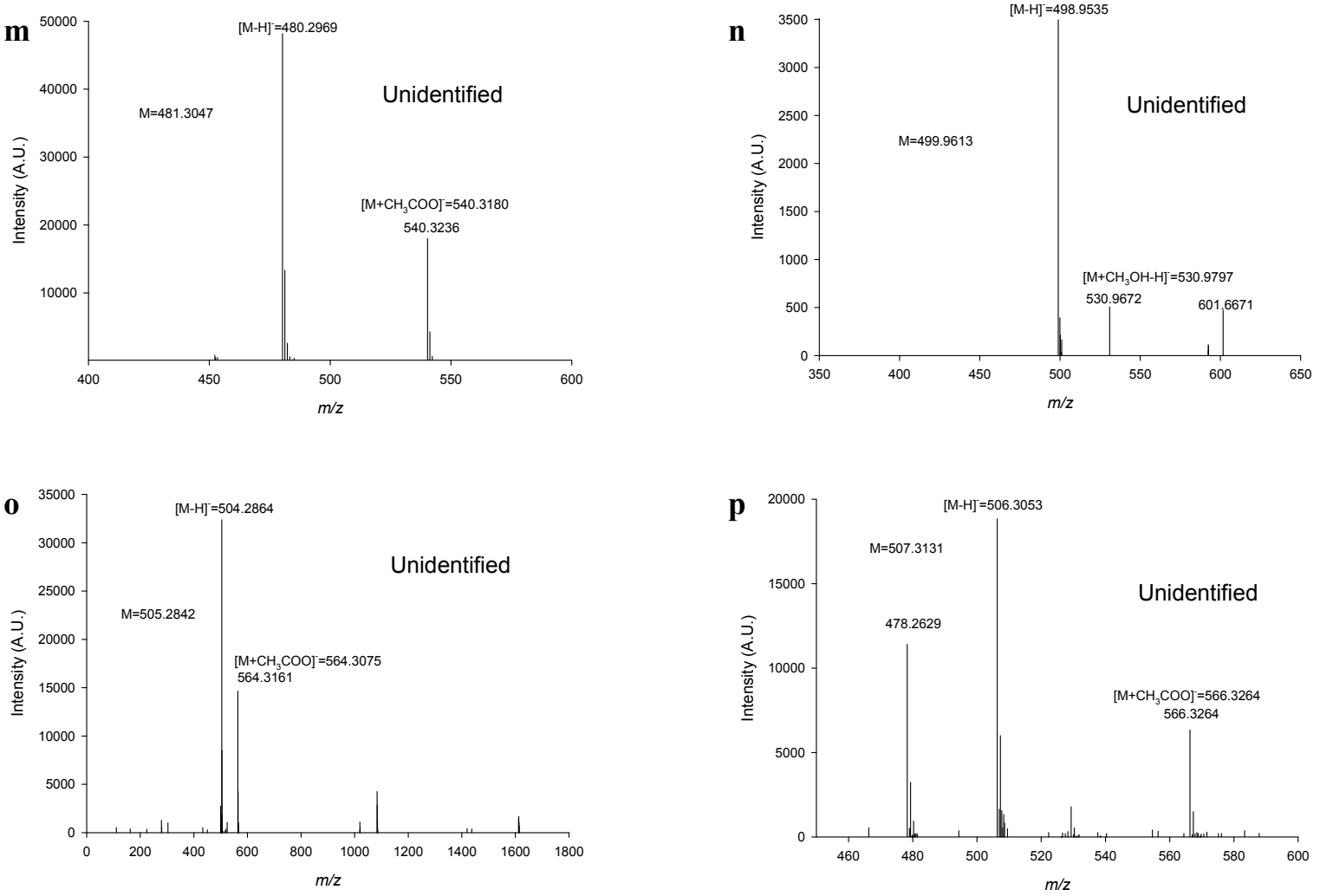

Figure B.4, cont'd. Mass spectra for SVM-RFE-selected features from multimode dataset detected in -pESI.

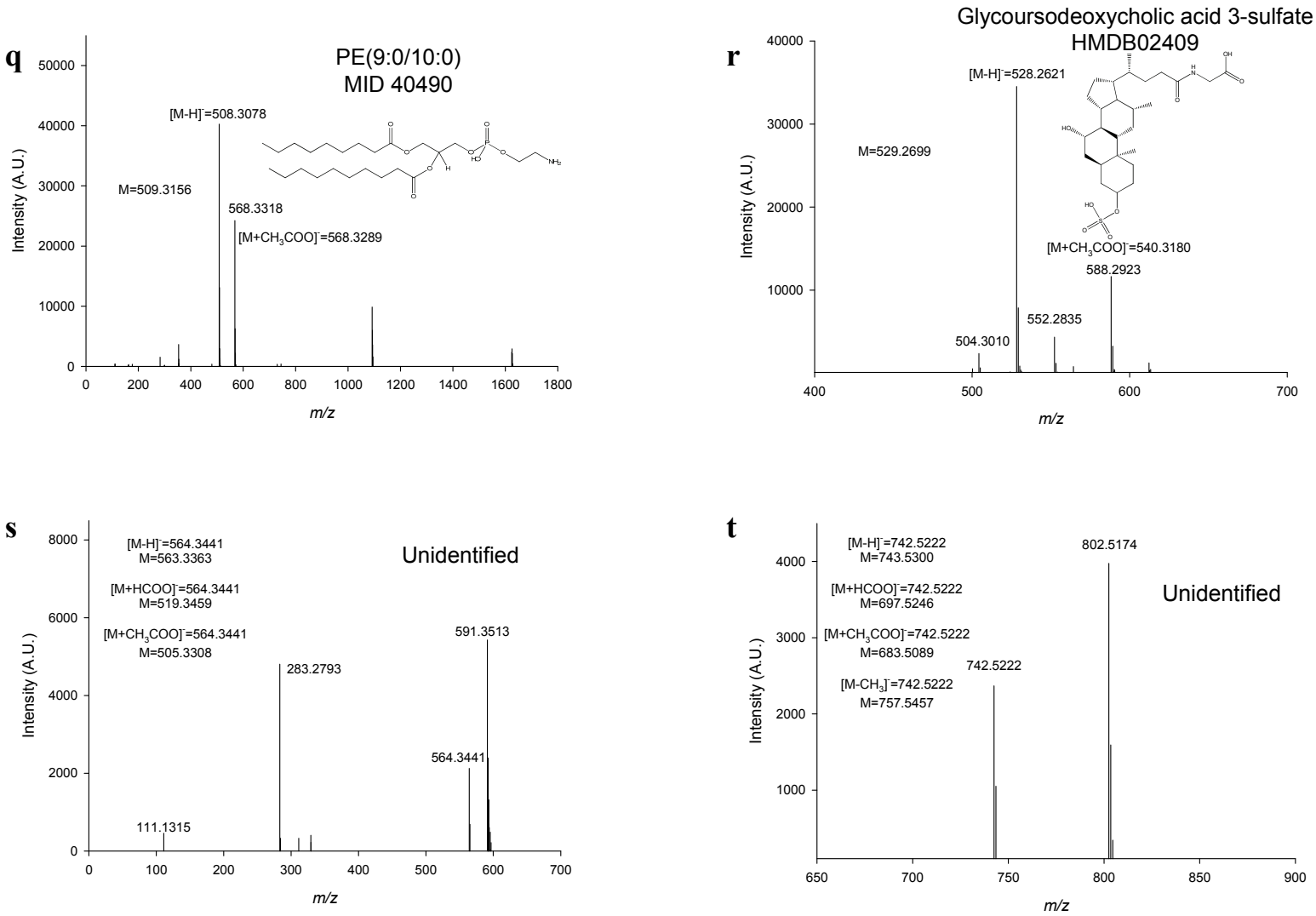

B.7. Conclusions

The results presented here demonstrate that LC-MS-based serum metabolomic experiments combined with state-of-the-art machine learning methods have the potential to generate metabolic profiles of ovarian cancer with possible application to the problem of developing accurate, effective diagnostic assays for disease. Using SVM-RFE, a model was built having a prediction accuracy of 80.6% with sensitivity and selectivity results of 83.8% and 77.1%, respectively. Adduct analysis of the 45 features selected by this model yielded 29 chemical formulae to search against human metabolite databases. This search led to the identification of 171 possible isomeric matches for these formulae and includes compounds such as glycerophospholipids, peptides, fatty acids, and hormones. These promising findings provide justification for continued investigation of this issue. However, future studies should include examination of a larger sample set, which will likely improve the figures of merit for the model, and the use of more sophisticated analytical tools such as UPLC and accurate mass MS/MS analyses. Inclusion of these tools will provide improved throughput and utility, and will also enable generation of fragmentation data that can aid in identification of these metabolites by allowing for differentiation between isomers.

REFERENCES

(1) Curie, E. *Madame Curie: A Biography*; Da Capo Press: [S.l.], **2001**.

(2) Busch, K. L.; Cooks, R. G. **(1982)**. "Mass Spectrometry of Large, Fragile, and Involatile Molecules", *Science*, 218(4569), pp. 247-254.

(3) Vestal, M. L. **(2001)**. "Methods of Ion Generation", *Chemical Reviews*, 101(2), pp. 361-375.

(4) Dempster, A. J. **(1918)**. "A New Method of Positive Ray Analysis", *Physical Review*, 11(4), pp. 316-324.

(5) Munson, M. S. B.; Field, F. H. **(1966)**. "Chemical Ionization Mass Spectrometry", *Journal of the American Chemical Society*, 88(12), pp. 2621-2630.

(6) Ives, H. E. **(1923)**. "Positive Rays in Alkali Metal Vapor Thermionic Tubes", *Physical Review*, 21(3), pp. 385.

(7) Kingdon, K. H.; Langmuir, I. **(1923)**. "Thermionic Phenomena Due to Alkali Vapors", *Physical Review*, 21(3), pp. 380.

(8) Woodcock, K. S. **(1931)**. "The Emission of Negative Ions Under the Bombardment of Positive Ions", *Physical Review*, 38(9), pp. 1696-1703.

(9) Dempster, A. J. **(1936)**. "Ion Sources for Mass Spectroscopy", *Review of Scientific Instruments*, 7(1), pp. 46-49.

(10) Inghram, M. G.; Gomer, R. **(1954)**. "Mass Spectrometric Analysis of Ions from the Field Microscope", *Journal of Chemical Physics*, 22(7), pp. 1279-1280.

(11) Lossing, F. P.; Tanaka, I. **(1956)**. "Photoionization as a Source of Ions for Mass Spectrometry", *Journal of Chemical Physics*, 25(5), pp. 1031-1034.

(12) Hurzeler, H.; Inghram, M. G.; Morrison, J. D. **(1958)**. "Photon Impact Studies of Molecules Using a Mass Spectrometer", *Journal of Chemical Physics*, 28(1), pp. 76.

(13) Beckey, H. D. **(1969)**. "Field Desorption Mass Spectrometry: A Technique for the Study of Thermally Unstable Substances of Low Volatility", *International Journal of Mass Spectrometry and Ion Physics*, 2(6), pp. 500-506.

(14) Coburn, J. W.; Kay, E. **(1971)**. "A New Technique for the Elemental Analysis of Thin Surface Layers of Solids", *Applied Physics Letters*, 19(9), pp. 350-352.

(15) Evans, C. A.; Hendrick, C. D. **(1972)**. "Electrohydrodynamic Ion-Source for Mass-Spectrometry of Liquids", *Review of Scientific Instruments*, 43(10), pp. 1527-1530.

(16) Torgerson, D. F.; Skowronski, R. P.; Macfarlane, R. D. **(1974)**. "New Approach to the Mass Spectroscopy of Non-Volatile Compounds", *Biochemical and Biophysical Research Communications*, 60(2), pp. 616-621.

(17) Barber, M.; Bordoli, R. S.; Sedgwick, R. D.; Tyler, A. N.; Whalley, E. T. **(1981)**. "Fast Atom Bombardment Mass Spectrometry of Bradykinin and Related Oligopeptides", *Biological Mass Spectrometry*, 8(8), pp. 337-342.

(18) Barber, M.; Green, B. N. **(1987)**. "The Analysis of Small Proteins in the Molecular Weight Range 10-24 kDa by Magnetic Sector Mass Spectrometry", *Rapid Communications in Mass Spectrometry*, 1(5), pp. 80-83.

(19) Becker, J. S.; Dietze, H. J. **(1998)**. "Inorganic Trace Analysis by Mass Spectrometry", *Spectrochimica Acta B: Atomic Spectroscopy*, 53(11), pp. 1475-1506.

(20) Beske, H. E.; Gijbels, R.; Hurrle, A.; Jochum, K. P. **(1981)**. "Review and Evaluation of Spark Source-Mass Spectrometry as an Analytical Method", *Fresenius Zeitschrift Fur Analytische Chemie*, 309(4), pp. 329-341.

(21) Callahan, J. H.; Hool, K.; Reynolds, J. D.; Cook, K. D. **(1987)**. "Mass-Transport Effects in Electrohydrodynamic Mass-Spectrometry", *International Journal of Mass Spectrometry and Ion Processes*, 75(3), pp. 291-317.

(22) Gross, J. H. *Mass Spectrometry: A Textbook*; Springer: Berlin, **2004**.

(23) Jonsson, G.; Hedin, A.; Hakansson, P.; Sundqvist, B. U. R.; Bennich, H.; Roepstorff, P. **(1989)**. "Compensation for Non-Normal Ejection of Large Molecular Ions in Plasma-Desorption Mass Spectrometry", *Rapid Communications in Mass Spectrometry*, 3(6), pp. 190-191.

(24) Lebedev, A. T.; Zaikin, V. G. **(2008)**. "Organic Mass Spectrometry at the Beginning of the 21st Century", *Journal of Analytical Chemistry*, 63(12), pp. 1128-1154.

(25) Northway, M. J.; Jayne, J. T.; Toohey, D. W.; Canagaratna, M. R.; Trimborn, A.; Akiyama, K. I.; Shimono, A.; Jimenez, J. L.; DeCarlo, P. F.; Wilson, K. R.; Worsnop, D. R. **(2007)**. "Demonstration of a VUV Lamp Photoionization Source for Improved Organic Speciation in an Aerosol Mass Spectrometer", *Aerosol Science and Technology*, 41(9), pp. 828-839.

(26) Garrison, B. J.; Delcorte, A.; Zhigilei, L. V.; Itina, T. E.; Krantzman, K. D.; Yingling, Y. G.; McQuaw, C. M.; Smiley, E. J.; Winograd, N. **(2003)**. "Big Molecule Ejection - SIMS vs. MALDI", *Applied Surface Science*, 203-204(1), pp. 69-71.

(27) Karas, M.; Hillenkamp, F. **(1988)**. "Laser Desorption Ionization of Proteins with Molecular Masses Exceeding 10,000 Daltons", *Analytical Chemistry*, 60(20), pp. 2299-2301.

(28) Tanaka, K.; Waki, H.; Ido, Y.; Akita, S.; Yoshida, Y.; Yoshida, T. **(1988)**. "Protein and Polymer Analyses up to *m/z* 100 000 by Laser Ionization Time-of-Flight Mass Spectrometry", *Rapid Communications in Mass Spectrometry*, 2(8), pp. 151-153.

(29) Dole, M.; Mack, L. L.; Hines, R. L.; Mobley, R. C.; Ferguson, L. D.; Alice, M. B. **(1968)**. "Molecular Beam of Macroions", *Journal of Chemical Physics*, 49(5), pp. 2240-2249.

(30) Yamashita, M.; Fenn, J. B. **(1984)**. "Electrospray Ion Source. Another Variation on the Free-Jet Theme", *Journal of Physical Chemistry*, 88(20), pp. 4451-4459.

(31) Fenn, J. B.; Mann, M.; Meng, C. K.; Wong, S. F.; Whitehouse, C. M. **(1989)**. "Electrospray Ionization for Mass Spectrometry of Large Biomolecules", *Science*, 246(4926), pp. 64-71.

(32) Caprioli, R. M.; Fan, T.; Cottrell, J. S. **(1986)**. "Continuous-Flow Sample Probe for Fast-Atom-Bombardment Mass-Spectrometry", *Analytical Chemistry*, 58(14), pp. 2949-2954.

(33) Cotter, R. J. **(1988)**. "Plasma Desorption Mass Spectrometry: Coming of Age", *Analytical Chemistry*, 60(13), pp. 781A-793A.

(34) Laiko, V. V.; Baldwin, M. A.; Burlingame, A. L. **(2000)**. "Atmospheric Pressure Matrix-Assisted Laser Desorption/Ionization Mass Spectrometry", *Analytical Chemistry*, 72(4), pp. 652-657.

(35) Cooks, R. G.; Ouyang, Z.; Takats, Z.; Wiseman, J. M. **(2006)**. "Ambient Mass Spectrometry", *Science*, 311(5767), pp. 1566-1570.

(36) Harris, G. A.; Nyadong, L.; Fernández, F. M. **(2008)**. "Recent Developments in Ambient Ionization Techniques for Analytical Mass Spectrometry", *Analyst*, 133(10), pp. 1297-1301.

(37) Takats, Z.; Wiseman, J. M.; Gologan, B.; Cooks, R. G. **(2004)**. "Mass Spectrometry Sampling under Ambient Conditions with Desorption Electrospray Ionization", *Science*, 306(5695), pp. 471-473.

(38) Cody, R.; Laramee, J.; Durst, H. **(2005)**. "Versatile New Ion Source for the Analysis of Materials in Open Air under Ambient Conditions", *Analytical Chemistry*, 77(8), pp. 2297-2302.

(39) Covey, T. R.; Lee, E. D.; Bruins, A. P.; Henion, J. D. **(1986)**. "Liquid Chromatography/Mass Spectrometry", *Analytical Chemistry*, 58(14), pp. 1451A-1461A.

(40) Thomson, B. A. **(1998)**. "Atmospheric Pressure Ionization and Liquid Chromatography/Mass Spectrometry-Together at Last", *Journal of the American Society for Mass Spectrometry*, 9(3), pp. 187-193.

(41) Horning, E. C.; Carroll, D. I.; Dzidic, I.; Haegele, K. D.; Horning, M. G.; Stillwell, R. N. **(1974)**. "Liquid Chromatograph-Mass Spectrometer-Computer Analytical Systems: A Continuous-Flow System Based on Atmospheric Pressure Ionization Mass Spectrometry", *Journal of Chromatography*, 99(1), pp. 13-21.

(42) Horning, E. C.; Carroll, D. I.; Dzidic, I.; Haegele, K. D.; Horning, M. G.; Stillwell, R. N. **(1974)**. "Atmospheric Pressure Ionization (API) Mass Spectrometry. Solvent-Mediated Ionization of Samples Introduced in Solution and in a Liquid Chromatograph Effluent Stream", *Journal of Chromatographic Science*, 12(11), pp. 725-729.

(43) Thomson, B. A.; Iribarne, J. V. **(1979)**. "Field Induced Ion Evaporation from Liquid Surfaces at Atmospheric Pressure", *Journal of Chemical Physics*, 71(11), pp. 4451-4463.

(44) Thomson, B. A.; Danylewych-May, L. In *31st Annual Conference on Mass Spectrometry and Allied Topics*: Boston, **1983**.

(45) Willoughby, R. C.; Browner, R. F. **(1984)**. "Monodisperse Aerosol Generation Interface for Combining Liquid-Chromatography with Mass-Spectroscopy", *Analytical Chemistry*, 56(14), pp. 2626-2631.

(46) Blakley, C. R.; Vestal, M. L. **(1983)**. "Thermospray Interface for Liquid Chromatography/Mass Spectrometry", *Analytical Chemistry*, 55(4), pp. 750-754.

(47) Whitehouse, C. M.; Dreyer, R. N.; Yamashita, M.; Fenn, J. B. **(1985)**. "Electrospray Interface for Liquid Chromatographs and Mass Spectrometers", *Analytical Chemistry*, 57(3), pp. 675-679.

(48) Aleksandrov, M. L.; Baram, G. I.; Gall, L. M.; Krasnov, N. V.; Kusner, Y. S.; Mirgorodskaya, O. A.; Nikolaiev, V. I.; Shkurov, W. V. **(1985)**. "Formation of Beams of Quasi-Molecular Ions of Peptides from Solutions", *Bioorganicheskaya Khimiya*, 11(5), pp. 700-704.

(49) Gaskell, S. **(1997)**. "Electrospray: Principles and Practice", *Journal of Mass Spectrometry*, 32(7), pp. 677-688.

(50) Gomez, A.; Tang, K. Q. **(1994)**. "Charge and Fission of Droplets in Electrostatic Sprays", *Physics of Fluids*, 6(1), pp. 404-414.

(51) Bruins, A. P.; Covey, T. R.; Henion, J. D. **(1987)**. "Ion Spray Interface for Combined Liquid Chromatography/Atmospheric Pressure Ionization Mass Spectrometry", *Analytical Chemistry*, 59(22), pp. 2642-2646.

(52) Iribarne, J. V.; Thomson, B. A. **(1976)**. "On the Evaporation of Small Ions from Charged Droplets", *Journal of Chemical Physics*, 64(6), pp. 2287-2294.

(53) Cole, R. B. **(2000)**. "Some Tenets Pertaining to Electrospray Ionization Mass Spectrometry", *Journal of Mass Spectrometry*, 35(7), pp. 763-772.

(54) Zhou, S. L.; Prebyl, B. S.; Cook, K. D. **(2002)**. "Profiling pH Changes in the Electrospray Plume", *Analytical Chemistry*, 74(19), pp. 4885-4888.

(55) Manier, M. L.; Cornett, D. S.; Hachey, D. L.; Caprioli, R. M. **(2008)**. "Identification of Dimethyidioctadecylammonium Ion (*m/z* 550.6) and Related Species (*m/z* 522.6, 494.6) as a Source of Contamination in Mass Spectrometry", *Journal of the American Society for Mass Spectrometry*, 19(5), pp. 666-670.

(56) Chowdhury, S. K.; Katta, V.; Chait, B. T. **(1990)**. "Probing Conformational Changes in Proteins by Mass Spectrometry", *Journal of the American Chemical Society*, 112(24), pp. 9012-9013.

(57) Iavarone, A. T.; Jurchen, J. C.; Williams, E. R. **(2000)**. "Effects of Solvent on the Maximum Charge State and Charge State Distribution of Protein Ions Produced by Electrospray Ionization", *Journal of the American Society for Mass Spectrometry*, 11(11), pp. 976-985.

(58) Chowdhury, S. K.; Chait, B. T. **(1991)**. "Method for the Electrospray Ionization of Highly Conductive Aqueous Solutions", *Analytical Chemistry*, 63(15), pp. 1660-1664.

(59) Napoli, K. L. **(2006)**. "Organic Solvents Compromise Performance of Internal Standard (Ascomycin) in Proficiency Testing of Mass Spectrometry-Based Assays for Tacrolimus", *Clinical Chemistry*, 52(4), pp. 765-766.

(60) Constantopoulos, T. L.; Jackson, G. S.; Enke, C. G. **(1999)**. "Effects of Salt Concentration on Analyte Response Using Electrospray Ionization Mass Spectrometry", *Journal of the American Society for Mass Spectrometry*, 10(7), pp. 625-634.

(61) Tang, K. Q.; Lin, Y. H.; Matson, D. W.; Kim, T.; Smith, R. D. **(2001)**. "Generation of Multiple Electrosprays Using Microfabricated Emitter Arrays for Improved Mass Spectrometric Sensitivity", *Analytical Chemistry*, 73(8), pp. 1658-1663.

(62) Tang, K.; Page, J. S.; Smith, R. D. **(2004)**. "Charge Competition and the Linear Dynamic Range of Detection in Electrospray Ionization Mass Spectrometry", *Journal of the American Society for Mass Spectrometry*, 15(10), pp. 1416-1423.

(63) Kebarle, P.; Peschke, M. **(2000)**. "On the Mechanisms by Which the Charged Droplets Produced by Electrospray Lead to Gas Phase Ions", *Analytica Chimica Acta*, 406(1), pp. 11-35.

(64) Amad, M. H.; Cech, N. B.; Jackson, G. S.; Enke, C. G. **(2000)**. "Importance of Gas-Phase Proton Affinities in Determining the Electrospray Ionization Response for Analytes and Solvents", *Journal of Mass Spectrometry*, 35(7), pp. 784-789.

(65) Constantopoulos, T. L.; Jackson, G. S.; Enke, C. G. **(2000)**. "Challenges in Achieving a Fundamental Model for ESI", *Analytica Chimica Acta*, 406(1), pp. 37-52.

(66) Emmett, M. R.; Caprioli, R. M. **(1994)**. "Micro-Electrospray Mass-Spectrometry - Ultra-High-Sensitivity Analysis of Peptides and Proteins", *Journal of the American Society for Mass Spectrometry*, 5(7), pp. 605-613.

(67) Wilm, M. S.; Mann, M. **(1994)**. "Electrospray and Taylor-Cone Theory, Doles Beam of Macromolecules at Last", *International Journal of Mass Spectrometry*, 136(2-3), pp. 167-180.

(68) Wilm, M.; Mann, M. **(1996)**. "Analytical Properties of the Nanoelectrospray Ion Source", *Analytical Chemistry*, 68(1), pp. 1-8.

(69) Wilm, M.; Shevchenko, A.; Houthaeve, T.; Breit, S.; Schweigerer, L.; Fotsis, T.; Mann, M. **(1996)**. "Femtomole Sequencing of Proteins from Polyacrylamide Gels by Nano-Electrospray Mass Spectrometry", *Nature*, 379(6564), pp. 466-469.

(70) Banks, J. F., Jr.; Shen, S.; Whitehouse, C. M.; Fenn, J. B. **(1994)**. "Ultrasonically Assisted Electrospray Ionization for LC/MS Determination of Nucleosides from a Transfer RNA Digest", *Analytical Chemistry*, 66(3), pp. 406-414.

(71) Banks, J. F.; Quinn, J. P.; Whitehouse, C. M. **(1994)**. "LC/ESI-MS Determination of Proteins Using Conventional Liquid Chromatography and Ultrasonically Assisted Electrospray", *Analytical Chemistry*, 66(21), pp. 3688-3695.

(72) Barnidge, D. R.; Nilsson, S.; Markides, K. E. **(1999)**. "A Design for Low-Flow Sheathless Electrospray Emitters", *Analytical Chemistry*, 71(19), pp. 4115-4118.

(73) Schultz, G. A.; Corso, T. N.; Prosser, S. J.; Zhang, S. **(2000)**. "A Fully Integrated Monolithic Microchip Electrospray Device for Mass Spectrometry", *Analytical Chemistry*, 72(17), pp. 4058-4063.

(74) Berggren, W. T.; Westphall, M. S.; Smith, L. M. **(2002)**. "Single-Pulse Nanoelectrospray Ionization", *Analytical Chemistry*, 74(14), pp. 3443-3448.

(75) Weinberger, S. R.; Boschetti, E.; Santambien, P.; Brenac, V. **(2002)**. "Surface-Enhanced Laser Desorption-Ionization Retentate Chromatography Mass Spectrometry (SELDI-RC-MS): A New Method for Rapid Development of Process Chromatography Conditions", *Journal of Chromatography B, Analytical Technologies in the Biomedical and Life Sciences*, 782(1-2), pp. 307-316.

(76) Aderogba, S.; Meacham, J. M.; Degertekin, F. L.; Fedorov, A. G.; Fernández, F. M. **(2005)**. "Nanoelectrospray Ion Generation for High-Throughput Mass Spectrometry Using a Micromachined Ultrasonic Ejector Array", *Applied Physics Letters*, 86(20), pp. 203110/203111-203110/203113.

(77) Wood, T. D.; Moy, M. A.; Dolan, A. R.; Bigwarfe, P. M.; White, T. P.; Smith, D. R.; Higbee, D. J. **(2003)**. "Miniaturization of Electrospray Ionization Mass Spectrometry", *Applied Spectroscopy Reviews*, 38(2), pp. 187-244.

(78) Limbach, P. A.; Meng, Z. J. **(2002)**. "Integrating Micromachined Devices with Modern Mass Spectrometry", *Analyst*, 127(6), pp. 693-700.

(79) Lazar, I. M.; Grym, J.; Foret, F. **(2006)**. "Microfabricated Devices: A New Sample Introduction Approach to Mass Spectrometry", *Mass Spectrometry Reviews*, 25(4), pp. 573-594.

(80) Li, J.; Thibault, P.; Bings, N. H.; Skinner, C. D.; Wang, C.; Colyer, C.; Harrison, J. **(1999)**. "Integration of Microfabricated Devices to Capillary Electrophoresis-Electrospray Mass Spectrometry Using a Low Dead Volume Connection: Application to Rapid Analyses of Proteolytic Digests", *Analytical Chemistry*, 71(15), pp. 3036-3045.

(81) Zhang, B.; Liu, H.; Karger, B. L.; Foret, F. **(1999)**. "Microfabricated Devices for Capillary Electrophoresis-Electrospray Mass Spectrometry", *Analytical Chemistry*, 71(15), pp. 3258-3264.

(82) Bings, N. C.; Wang, C.; Skinner, C. D.; Colyer, C. L.; Thibault, P.; Harrison, D. J. **(1999)**. "Microfluidic Devices Connected to Fused-Silica Capillaries with Minimal Dead Volume", *Analytical Chemistry*, 71(15), pp. 3292-3296.

(83) Lazar, I. M.; Ramsey, R. S.; Sundberg, S.; Ramsey, J. M. **(1999)**. "Subattomole-Sensitivity Microchip Nanoelectrospray Source with Time-of-Flight Mass Spectrometry Detection", *Analytical Chemistry*, 71(17), pp. 3627-3631.

(84) Li, J. J.; Kelly, J. F.; Chemushevich, I.; Harrison, D. J.; Thibault, P. **(2000)**. "Separation and Identification of Peptides from Gel-Isolated Membrane Proteins Using a Microfabricated Device for Combined Capillary Electrophoresis/Nanoelectrospray Mass Spectrometry", *Analytical Chemistry*, 72(3), pp. 599-609.

(85) Zhang, B. L.; Foret, F.; Karger, B. L. **(2000)**. "A Microdevice with Integrated Liquid Junction for Facile Peptide and Protein Analysis by Capillary Electrophoresis/Electrospray Mass Spectrometry", *Analytical Chemistry*, 72(5), pp. 1015-1022.

(86) Deng, Y. Z.; Henion, J.; Li, J. J.; Thibault, P.; Wang, C.; Harrison, D. J. **(2001)**. "Chip-Based Capillary Electrophoresis/Mass Spectrometry Determination of Carnitines in Human Urine", *Analytical Chemistry*, 73(3), pp. 639-646.

(87) Meng, Z. J.; Qi, S. Z.; Soper, S. A.; Limbach, P. A. **(2001)**. "Interfacing a Polymer-Based Micromachined Device to a Nanoelectrospray Ionization Fourier Transform Ion Cyclotron Resonance Mass Spectrometer", *Analytical Chemistry*, 73(6), pp. 1286-1291.

(88) Lazar, I. M.; Ramsey, R. S.; Ramsey, J. M. **(2001)**. "On-chip Proteolytic Digestion and Analysis Using 'Wrong-Way-Round' Electrospray Time-of-Flight Mass Spectrometry", *Analytical Chemistry*, 73(8), pp. 1733-1739.

(89) Zhang, B.; Foret, F.; Karger, B. **(2001)**. "High-Throughput Microfabricated CE/ESI-MS: Automated Sampling from a Microwell Plate", *Analytical Chemistry*, 73(11), pp. 2675-2681.

(90) Ivanov, A.; Zang, L.; Karger, B. L. **(2003)**. "Low Attomole ESI-MS and MS/MS Analysis of Protein Digests Using 20-μm i.d. Polystyrene-Divinylbenzene Monolithic Capillary Columns", *Analytical Chemistry*, 75(20), pp. 5306-5316.

(91) Shinohara, H.; Suzuki, T.; Kitagawa, F.; Mizuno, J.; Otsuka, K.; Shoji, S. **(2008)**. "Polymer Microchip Integrated with Nano-Electrospray Tip for Electrophoresis-Mass Spectrometry", *Sensors and Actuators B: Chemical*, B132(2), pp. 368-373.

(92) Ramsey, R. S.; Ramsey, J. M. **(1997)**. "Generating Electrospray from Microchip Devices Using Electroosmotic Pumping", *Analytical Chemistry*, 69(13), pp. 1174-1178.

(93) Xue, Q.; Foret, F.; Dunayevskiy, Y. M.; Zavracky, P. M.; McGruer, N. E.; Karger, B. L. **(1997)**. "Multichannel Microchip Electrospray Mass Spectrometry", *Analytical Chemistry*, 69(3), pp. 426-430.

(94) Xue, Q. F.; Dunayevskiy, Y. M.; Foret, F.; Karger, B. L. **(1997)**. "Integrated Multichannel Microchip Electrospray Ionization Mass Spectrometry: Analysis of Peptides from on-Chip Tryptic Digestion of Melittin", *Rapid Communications in Mass Spectrometry*, 11(12), pp. 1253-1256.

(95) Liu, H. H.; Felten, C.; Xue, Q. F.; Zhang, B. L.; Jedrzejewski, P.; Karger, B. L.; Foret, F. **(2000)**. "Development of Multichannel Devices with an Array of Electrospray Tips for High-Throughput Mass Spectrometry", *Analytical Chemistry*, 72(14), pp. 3303-3310.

(96) Huikko, K.; Ostman, P.; Grigoras, K.; Tuomikoski, S.; Tiainen, V. M.; Soininen, A.; Puolanne, K.; Manz, A.; Franssila, S.; Kostiainen, R.; Kotiaho, T. **(2003)**. "Poly(Dimethylsiloxane) Electrospray Devices Fabricated with Diamond-Like Carbon-Poly(Dimethylsiloxane) Coated Su-8 Masters", *Lab on a Chip*, 3(2), pp. 67-72.

(97) Le Gac, S.; Arscott, S.; Cren-Olive, C.; Rolando, C. **(2003)**. "Two-Dimensional Microfabricated Sources for Nanoelectrospray", *Journal of Mass Spectrometry*, 38(12), pp. 1259-1264.

(98) Svedberg, M.; Veszelei, M.; Axelsson, J.; Vangbo, M.; Nikolajeff, F. **(2004)**. "Poly(Dimethylsiloxane) Microchip: Microchannel with Integrated Open Electrospray Tip", *Lab on a Chip*, 4(4), pp. 322-327.

(99) Yang, Y.; Kameoka, J.; Wachs, T.; Henion, J. D.; Craighead, H. G. **(2004)**. "Quantitative Mass Spectrometric Determination of Methylphenidate Concentration in Urine Using an Electrospray Ionization Source Integrated with a Polymer Microchip", *Analytical Chemistry*, 76(9), pp. 2568-2574.

(100) Lozano, P.; Martinez-Sanchez, M.; Lopez-Urdiales, J. M. **(2004)**. "Electrospray Emission from Nonwetting Flat Dielectric Surfaces", *Journal of Colloid and Interface Science*, 276(2), pp. 392-399.

(101) Le Gac, S.; Rolando, C.; Arscott, S. **(2006)**. "An Open Design Microfabricated Nib-Like Nanoelectrospray Emitter Tip on a Conducting Silicon Substrate for the Application of the Ionization Voltage", *Journal of the American Society for Mass Spectrometry*, 17(1), pp. 75-80.

(102) Bedair, M. F.; Oleschuk, R. D. **(2006)**. "Fabrication of Porous Polymer Monoliths in Polymeric Microfluidic Chips as an Electrospray Emitter for Direct Coupling to Mass Spectrometry", *Analytical Chemistry*, 78(4), pp. 1130-1138.

(103) Dayon, L.; Abonnenc, M.; Prudent, M.; Lion, N.; Girault, H. H. **(2006)**. "Multitrack Electrospray Chips", *Journal of Mass Spectrometry*, 41(11), pp. 1484-1490.

(104) Kim, W.; Guo, M.; Yang, P.; Wang, D. **(2007)**. "Microfabricated Monolithic Multinozzle Emitters for Nanoelectrospray Mass Spectrometry", *Analytical Chemistry*, 79(10), pp. 3703-3707.

(105) Sikanen, T.; Tuomikoski, S.; Ketola, R. A.; Kostiainen, R.; Franssila, S.; Kotiaho, T. **(2008)**. "Analytical Characterization of Microfabricated Su-8 Emitters for Electrospray Ionization Mass Spectrometry", *Journal of Mass Spectrometry*, 43(6), pp. 726-735.

(106) Licklider, L.; Wang, X. Q.; Desai, A.; Tai, Y. C.; Lee, T. D. **(2000)**. "A Micromachined Chip-Based Electrospray Source for Mass Spectrometry", *Analytical Chemistry*, 72(2), pp. 367-375.

(107) Kim, J. S.; Knapp, D. R. **(2001)**. "Microfabricated PDMS Multichannel Emitter for Electrospray Ionization Mass Spectrometry", *Journal of the American Society for Mass Spectrometry*, 12(4), pp. 463-469.

(108) Gobry, V.; van Oostrum, J.; Martinelli, M.; Rohner, T. C.; Reymond, F.; Rossier, J. S.; Girault, H. H. **(2002)**. "Microfabricated Polymer Injector for Direct Mass Spectrometry Coupling", *Proteomics*, 2(4), pp. 405-412.

(109) Griss, P.; Melin, J.; Sjodahl, J.; Roeraade, J.; Stemme, G. **(2002)**. "Development of Micromachined Hollow Tips for Protein Analysis Based on Nanoelectrospray Ionization Mass Spectrometry", *Journal of Micromechanics and Microengineering*, 12 pp. 682-687.

(110) Sjodahl, J.; Melin, J.; Griss, P.; Emmer, A.; Stemme, G.; Roeraade, J. **(2003)**. "Characterization of Micromachined Hollow Tips for Two-Dimensional Nanoelectrospray Mass Spectrometry", *Rapid Communications in Mass Spectrometry*, 17(4), pp. 337-341.

(111) Svedberg, M.; Pettersson, A.; Nilsson, S.; Bergquist, J.; Nyholm, L.; Nikolajeff, F.; Markides, K. **(2003)**. "Sheathless Electrospray from Polymer Microchips", *Analytical Chemistry*, 75(15), pp. 3934-3940.

(112) Le Gac, S.; Arscott, S.; Rolando, C. **(2003)**. "A Planar Microfabricated Nanoelectrospray Emitter Tip Based on a Capillary Slot", *Electrophoresis*, 24(21), pp. 3640-3647.

(113) Zhang, S.; Van Pelt, C. K.; Henion, J. D. **(2003)**. "Automated Chip-Based Nanoelectrospray-Mass Spectrometry for Rapid Identification of Proteins Separated by Two-Dimensional Gel Electrophoresis", *Electrophoresis*, 24(21), pp. 3620-3632.

(114) Schilling, M.; Nigge, W.; Rudzinski, A.; Neyer, A.; Hergenroder, R. **(2004)**. "A New On-chip ESI Nozzle for Coupling of MS with Microfluidic Devices", *Lab on a Chip*, 4(3), pp. 220-224.

(115) Muck, A.; Svatos, A. **(2004)**. "Atmospheric Molded Poly(Methylmethacrylate) Microchip Emitters for Sheathless Electrospray", *Rapid Communications in Mass Spectrometry*, 18(13), pp. 1459-1464.

(116) Arscott, S.; Le Gac, S.; Rolando, C. **(2005)**. "A Polysilicon Nanoelectrospray-Mass Spectrometry Source Based on a Microfluidic Capillary Slot", *Sensors and Actuators B-Chemical*, 106(2), pp. 741-749.

(117) Zamfir, A. D.; Lion, N.; Vukelic, Z.; Bindila, L.; Rossier, J.; Girault, H. H.; Peter-Katalinic, J. **(2005)**. "Thin Chip Microsprayer System Coupled to Quadrupole Time-of-Flight Mass Spectrometer for Glycoconjugate Analysis", *Lab on a Chip*, 5(3), pp. 298-307.

(118) Corkery, L. J.; Pang, H.; Schneider, B. B.; Covey, T. R.; Siu, K. W. M. **(2005)**. "Automated Nanospray Using Chip-Based Emitters for the Quantitative Analysis of Pharmaceutical Compounds", *Journal of the American Society for Mass Spectrometry*, 16(3), pp. 363-369.

(119) Yin, N. F.; Killeen, K.; Brennen, R.; Sobek, D.; Werlich, M.; van de Goor, T. V. **(2005)**. "Microfluidic Chip for Peptide Analysis with an Integrated HPLC Column, Sample Enrichment Column, and Nanoelectrospray Tip", *Analytical Chemistry*, 77(2), pp. 527-533.

(120) Fortier, M. H.; Bonneil, E.; Goodley, P.; Thibault, P. **(2005)**. "Integrated Microfluidic Device for Mass Spectrometry-Based Proteomics and Its Application to Biomarker Discovery Programs", *Analytical Chemistry*, 77(6), pp. 1631-1640.

(121) Ghitun, M.; Bonneil, E.; Fortier, M. H.; Yin, H. F.; Killeen, K.; Thibault, P. **(2006)**. "Integrated Microfluidic Devices with Enhanced Separation Performance: Application to Phosphoproteome Analyses of Differentiated Cell Model Systems", *Journal of Separation Science*, 29(11), pp. 1539-1549.

(122) Mery, E.; Ricoul, F.; Sarrut, N.; Constantin, O.; Delapierre, G.; Garin, J.; Vinet, F. **(2008)**. "A Silicon Microfluidic Chip Integrating an Ordered Micropillar Array Separation Column and a Nano-Electrospray Emitter for LC/MS Analysis of Peptides", *Sensors and Actuators, B: Chemical*, B134(2), pp. 438-446.

(123) Kelly, R. T.; Tang, K. Q.; Irimia, D.; Toner, M.; Smith, R. D. **(2008)**. "Elastomeric Microchip Electrospray Emitter for Stable Cone-Jet Mode Operation in the Nanoflow Regime", *Analytical Chemistry*, 80(10), pp. 3824-3831.

(124) Percin, G.; Levin, L.; Khuri-Yakub, B. T. **(1997)**. "Piezoelectrically Actuated Droplet Ejector", *Review of Scientific Instruments*, 68(12), pp. 4561-4563.

(125) Percin, G.; Lundgren, T. S.; Khuri-Yakub, B. T. **(1998)**. "Controlled Ink-Jet Printing and Deposition of Organic Polymers and Solid Particles", *Applied Physics Letters*, 73(16), pp. 2375-2377.

(126) Shiea, J.; Chang, D. Y.; Lin, C. H.; Jiang, S. J. **(2001)**. "Generating Multiply Charged Protein Ions by Ultrasonic Nebulization/Multiple Channel-Electrospray Ionization Mass Spectrometry", *Analytical Chemistry*, 73(20), pp. 4983-4987.

(127) He, L.; Murray, K. K. **(1999)**. "337 nm Matrix-Assisted Laser Desorption/Ionization of Single Aerosol Particles", *Journal of Mass Spectrometry*, 34(9), pp. 909-914.

(128) Dixon, R. B.; Sampson, J. S.; Muddiman, D. C. **(2009)**. "Generation of Multiply Charged Peptides and Proteins by Radio Frequency Acoustic Desorption and Ionization for Mass Spectrometric Detection", *Journal of the American Society for Mass Spectrometry*, 20(4), pp. 597-600.

(129) Fedorov, A. G.; Degertekin, F. L. *Electrospray Systems and Methods*, 7,208,727, 04/24/2007

(130) Meacham, J. M.; Ejimofor, C.; Kumar, S.; Degertekin, F. L.; Fedorov, A. G. **(2004)**. "Micromachined Ultrasonic Droplet Generator Based on a Liquid Horn Structure", *Review of Scientific Instruments*, 75(5), pp. 1347-1352.

(131) Meacham, J.; Varady, M.; Degertekin, F.; Fedorov, A. **(2005)**. "Droplet Formation and Ejection from a Micromachined Ultrasonic Droplet Generator: Visualization and Scaling", *Physics of Fluids*, 17(10), pp. 100605-100601/100605-100608.

(132) Meacham, J. M. **(2006)** *A Micromachined Ultrasonic Droplet Generator: Design, Fabrication, Visualization, and Modeling*, George W. Woodruff School of Mechanical Engineering, Georgia Institute of Technology, Atlanta, GA, USA.

(133) Hampton, C. Y.; Forbes, T. P.; Varady, M. J.; Meacham, J. M.; Fedorov, A. G.; Degertekin, F. L.; Fernández, F. M. **(2007)**. "Analytical Performance of a Venturi-Assisted Array of Micromachined Ultrasonic Electrosprays Coupled to Ion Trap Mass Spectrometry for the Analysis of Peptides and Proteins", *Analytical Chemistry*, 79(21), pp. 8154-8161.

(134) Forbes, T. P.; Degertekin, F. L.; Fedorov, A. G. **(2007)**. "Multiplexed Operation of a Micromachined Ultrasonic Droplet Ejector Array", *Review of Scientific Instruments*, 78(10), pp. 104101.

(135) Hampton, C. Y.; Silvestri, C. J.; Forbes, T. P.; Varady, M. J.; Meacham, J. M.; Fedorov, A. G.; Degertekin, F. L.; Fernández, F. M. **(2008)**. "Comparison of the Internal Energy Deposition of Venturi-Assisted Electrospray Ionization and a Venturi-Assisted Array of Micromachined Ultrasonic Electrosprays (AMUSE)", *Journal of the American Society for Mass Spectrometry*, 19(9), pp. 1320-1329.

(136) Cotter, R. J. **(1999)**. "The New Time-of-Flight Mass Spectrometry", *Analytical Chemistry*, 71(13), pp. 445A-451A.

(137) Schwartz, J. C.; Senko, M. W.; Syka, J. E. P. **(2002)**. "A Two-Dimensional Quadrupole Ion Trap Mass Spectrometer", *Journal of the American Society for Mass Spectrometry*, 13(6), pp. 659-669.

(138) Hardman, M.; Makarov, A. A. **(2003)**. "Interfacing the Orbitrap Mass Analyzer to an Electrospray Ion Source", *Analytical Chemistry*, 75(7), pp. 1699-1705.

(139) Hu, Q. Z.; Noll, R. J.; Li, H.; Makarov, A.; Hardman, M.; Cooks, R. G. **(2005)**. "The Orbitrap: A New Mass Spectrometer", *Journal of Mass Spectrometry*, 40(4), pp. 430-443.

(140) Syka, J. E. P.; Marto, J. A.; Bai, D. L.; Horning, S.; Senko, M. W.; Schwartz, J. C.; Beatrix, U.; Garcia, B.; Busby, S.; Muratore, T.; Shabanowitz, J.; Hunt, D. F. **(2004)**. "Novel Linear Quadrupole Ion Trap/FT Mass Spectrometer: Performance Characterization and Use in the Comparative Analysis of Histone H3 Post-Translational Modifications", *Journal of Proteome Research*, 3(3), pp. 621-626.

(141) Makarov, A.; Denisov, E.; Kholomeev, A.; Balschun, W.; Lange, O.; Strupat, K.; Horning, S. **(2006)**. "Performance Evaluation of a Hybrid Linear Ion Trap/Orbitrap Mass Spectrometer", *Analytical Chemistry*, 78(7), pp. 2113-2120.

(142) Pringle, S. D.; Giles, K.; Wildgoose, J. L.; Williams, J. P.; Slade, S. E.; Thalassinos, K.; Bateman, R. H.; Bowers, M. T.; Scrivens, J. H. **(2007)**. "An Investigation of the Mobility Separation of Some Peptide and Protein Ions Using a New Hybrid Quadrupole/Travelling Wave IMS/oa-TOF Instrument", *International Journal of Mass Spectrometry*, 261(1), pp. 1-12.

(143) Chen, H.; Talaty, N. N.; Takats, Z.; Cooks, R. G. **(2005)**. "Desorption Electrospray Ionization Mass Spectrometry for High-Throughput Analysis of Pharmaceutical Samples in the Ambient Environment", *Analytical Chemistry*, 77(21), pp. 6915-6927.

(144) Haddad, R.; Sparrapan, R.; Eberlin, M. N. **(2006)**. "Desorption Sonic Spray Ionization for (High) Voltage-Free Ambient Mass Spectrometry", *Rapid Communications in Mass Spectrometry*, 20(19), pp. 2901-2905.

(145) Shieh, I. F.; Lee, C. Y.; Shiea, J. **(2005)**. "Eliminating the Interferences from Tris Buffer and Sds in Protein Analysis by Fused-Droplet Electrospray Ionization Mass Spectrometry", *Journal of Proteome Research*, 4(2), pp. 606-612.

(146) Shiea, J.; Huang, M. Z.; HSu, H. J.; Lee, C. Y.; Yuan, C. H.; Beech, I.; Sunner, J. **(2005)**. "Electrospray-Assisted Laser Desorption/Ionization Mass Spectrometry for Direct Ambient Analysis of Solids", *Rapid Communications in Mass Spectrometry*, 19(24), pp. 3701-3704.

(147) Sampson, J. S.; Hawkridge, A. M.; Muddiman, D. C. **(2006)**. "Generation and Detection of Multiply-Charged Peptides and Proteins by Matrix-Assisted Laser Desorption Electrospray Ionization (MALDESI) Fourier Transform Ion Cyclotron Resonance Mass Spectrometry", *Journal of the American Society for Mass Spectrometry*, 17(12), pp. 1712-1716.

(148) Nemes, P.; Vertes, A. **(2007)**. "Laser Ablation Electrospray Ionization for Atmospheric Pressure, in Vivo, and Imaging Mass Spectrometry", *Analytical Chemistry*, 79(21), pp. 8098-8106.

(149) Rezenom, Y. H.; Dong, J.; Murray, K. K. **(2008)**. "Infrared Laser-Assisted Desorption Electrospray Ionization Mass Spectrometry", *Analyst*, 133(2), pp. 226-232.

(150) Coon, J. J.; McHale, K. J.; Harrison, W. W. **(2002)**. "Atmospheric Pressure Laser Desorption/Chemical Ionization Mass Spectrometry: A New Ionization Method Based on Existing Themes", *Rapid Communications in Mass Spectrometry*, 16(7), pp. 681-685.

(151) Cheng, S. C.; Cheng, T. L.; Chang, H. C.; Shiea, J. **(2009)**. "Using Laser-Induced Acoustic Desorption/Electrospray Ionization Mass Spectrometry to Characterize Small Organic and Large Biological Compounds in the Solid State and in Solution Under Ambient Conditions", *Analytical Chemistry*, 81(3), pp. 868-874.

(152) Chen, H.; Zheng, O. Y.; Cooks, R. G. **(2006)**. "Thermal Production and Reactions of Organic Ions at Atmospheric Pressure", *Angewandte Chemie, International Edition*, 45(22), pp. 3656-3660.

(153) McEwen, C. N.; McKay, R. G.; Larsen, B. S. **(2005)**. "Analysis of Solids, Liquids, and Biological Tissues Using Solids Probe Introduction at Atmospheric Pressure on Commercial LC/MS Instruments", *Analytical Chemistry*, 77(23), pp. 7826-7831.

(154) Takats, Z.; Cotte-Rodriguez, I.; Talaty, N.; Chen, H. W.; Cooks, R. G. **(2005)**. "Direct, Trace Level Detection of Explosives on Ambient Surfaces by Desorption Electrospray Ionization Mass Spectrometry", *Chemical Communications*, 2005(15), pp. 1950-1952.

(155) Luosujarvi, L.; Arvola, V.; Haapala, M.; Pol, J.; Saarela, V.; Franssila, S.; Kostiainen, R.; Kotiaho, T.; Kauppila, T. J. **(2008)**. "Desorption Atmospheric Pressure Photoionization-Mass Spectrometry in Drug Analysis", *European Journal of Pharmaceutical Sciences*, 34(1), pp. S29-S29.

(156) Ratcliffe, L. V.; Rutten, F. J. M.; Barrett, D. A.; Whitmore, T.; Seymour, D.; Greenwood, C.; Aranda-Gonzalvo, Y.; Robinson, S.; McCoustrat, M. **(2007)**. "Surface Analysis Under Ambient Conditions Using Plasma-Assisted Desorption/Ionization Mass Spectrometry", *Analytical Chemistry*, 79(16), pp. 6094-6101.

(157) Harper, J. D.; Charipar, N. A.; Mulligan, C. C.; Zhang, X. R.; Cooks, R. G.; Ouyang, Z. **(2008)**. "Low-Temperature Plasma Probe for Ambient Desorption Ionization", *Analytical Chemistry*, 80(23), pp. 9097-9104.

(158) Chen, H.; Venter, A.; Cooks, R. G. **(2006)**. "Extractive Electrospray Ionization for Direct Analysis of Undiluted Urine, Milk and Other Complex Mixtures without Sample Preparation", *Chemical Communications*, 2006(19), pp. 2042-2044.

(159) Chen, H. W.; Zenobi, R. **(2007)**. "Direct Analysis of Living Objects by Extractive Electrospray Mass Ionization Spectrometry", *Chimia*, 61(12), pp. 843-843.

(160) Chen, H.; Wortmann, A.; Zenobi, R. **(2007)**. "Neutral Desorption Sampling Coupled to Extractive Electrospray Ionization Mass Spectrometry for Rapid Differentiation of Biosamples by Metabolomic Fingerprinting", *Journal of Mass Spectrometry*, 42(9), pp. 1123-1135.

(161) Na, N.; Zhao, M.; Zhang, S.; Yang, C. L.; Zhang, X. **(2007)**. "Development of a Dielectric Barrier Discharge Ion Source for Ambient Mass Spectrometry", *Journal of the American Society for Mass Spectrometry*, 18(10), pp. 1859-1862.

(162) Schilling, G. D.; Shelley, J. T.; Broekaert, J. A. C.; Sperline, R. P.; Denton, M. B.; Barinaga, C. J.; Koppenaal, D. W.; Hieftje, G. M. **(2009)**. "Use of an Ambient Ionization Flowing Atmospheric-Pressure Afterglow Source for Elemental Analysis through Hydride Generation", *Journal of Analytical Atomic Spectrometry*, 24(1), pp. 34-40.

(163) Zhu, L.; Gamez, G.; Chen, H. W.; Chingin, K.; Zenobi, R. **(2009)**. "Rapid Detection of Melamine in Untreated Milk and Wheat Gluten by Ultrasound-Assisted Extractive Electrospray Ionization Mass Spectrometry (EESI-MS)", *Chemical Communications*, (5), pp. 559-561.

(164) Venter, A.; Sojka, P. E.; Cooks, R. G. **(2006)**, "Kinematic Investigation of Charged Droplets for Mechanistic Considerations of Desorption Electrospray Ionization (DESI)" *54th ASMS Conference on Mass Spectrometry* Seattle, WA

(165) Venter, A.; Sojka, P. E.; Cooks, R. G. **(2006)**. "Droplet Dynamics and Ionization Mechanisms in Desorption Electrospray Ionization Mass Spectrometry", *Analytical Chemistry*, 78(24), pp. 8549-8555.

(166) Costa, A. B.; Cooks, R. G. **(2007)**. "Simulation of Atmospheric Transport and Droplet–Thin Film Collisions in Desorption Electrospray Ionization", *Chemical Communications*, 2007(38), pp. 3915-3917.

(167) Wiseman, J. M.; Takats, Z.; Gologan, B.; Davisson, V. J.; Cooks, R. G. **(2005)**. "Direct Characterization of Enzyme-Substrate Complexes by Using Electrosonic Spray Ionization Mass Spectrometry", *Angewandte Chemie, International Edition*, 44(6), pp. 913-916.

(168) Yang, P. X.; Cooks, R. G.; Ouyang, Z.; Hawkridge, A. M.; Muddiman, D. C. **(2005)**. "Gentle Protein Ionization Assisted by High-Velocity Gas Flow", *Analytical Chemistry*, 77(19), pp. 6174-6183.

(169) Cotte-Rodriguez, I.; Takats, Z.; Talaty, N.; Chen, H.; Cooks, R. G. **(2005)**. "Desorption Electrospray Ionization of Explosives on Surfaces: Sensitivity and Selectivity Enhancement by Reactive Desorption Electrospray Ionization", *Analytical Chemistry*, 77(21), pp. 6755-6764.

(170) Cotte-Rodriguez, I.; Chen, H.; Cooks, R. G. **(2006)**. "Rapid Trace Detection of Triacetone Triperoxide (TATP) by Complexation Reactions During Desorption Electrospray Ionization", *Chemical Communications*, 2006(9), pp. 953-955.

(171) Nyadong, L.; Green, M.; De Jesus, V.; Newton, P. N.; Fernández, F. M. **(2007)**. "Reactive Desorption Electrospray Ionization Linear Ion Trap Mass Spectrometry of Latest-Generation Counterfeit Antimalarials via Non-Covalent Complex Formation", *Analytical Chemistry*, 79(5), pp. 2150-2157.

(172) Lee, C. C.; Chang, D. Y.; Jeng, J.; Shiea, J. **(2002)**. "Generating Multiply Charged Protein Ions via Two-Step Electrospray Ionization Mass Spectrometry", *Journal of Mass Spectrometry*, 37(1), pp. 115-117.

(173) Cody, R. B. **(2009)**. "Observation of Molecular Ions and Analysis of Nonpolar Compounds with the Direct Analysis in Real Time Ion Source", *Analytical Chemistry*, 81(3), pp. 1101-1107.

(174) Song, L.; Dykstra, A. B.; Yao, H.; Bartmess, J. E. **(2009)**. "Ionization Mechanisms of Negative Ion-Direct Analysis in Real Time: A Comparative Study with Negative Ion-Atmospheric Pressure Photoionization", *Journal of the American Society for Mass Spectrometry*, 20(1), pp. 42-50.

(175) McEwen, C. N.; Gutteridge, S. **(2007)**. "Analysis of the Inhibition of the Ergosterol Pathway in Fungi Using the Atmospheric Solids Analysis Probe (ASAP) Method", *Journal of the American Society for Mass Spectrometry*, 18(7), pp. 1274-1278.

(176) Williams, J. P.; Patel, V. J.; Holland, R.; Scrivens, J. H. **(2006)**. "The Use of Recently Described Ionisation Techniques for the Rapid Analysis of Some Common Drugs and Samples of Biological Origin", *Rapid Communications in Mass Spectrometry*, 20(9), pp. 1447-1456.

(177) Chen, H.; Zheng, J.; Zhang, X.; Luo, M.; Wang, Z.; Qiao, X. **(2007)**. "Surface Desorption Atmospheric Pressure Chemical Ionization Mass Spectrometry for Direct Ambient Sample Analysis without Toxic Chemical Contamination", *Journal of Mass Spectrometry*, 42(8), pp. 1045-1056.

(178) Luosujarvi, L.; Arvola, V.; Haapala, M.; Pol, J.; Saarela, V.; Franssila, S.; Kotiaho, T.; Kostiainen, R.; Kauppila, T. J. **(2008)**. "Desorption and Ionization Mechanisms in Desorption Atmospheric Pressure Photoionization", *Analytical Chemistry*, 80(19), pp. 7460-7466.

(179) Huang, G.; Ouyang, Z.; Cooks, R. G. **(2009)**. "High-Throughput Trace Melamine Analysis in Complex Mixtures", *Chemical Communications*, (5), pp. 556-558.

(180) Andrade, F. J.; Wetzel, W. C.; Chan, G. C. Y.; Webb, M. R.; Gamez, G.; Ray, S. J.; Hieftje, G. M. **(2006)**. "A New, Versatile, Direct-Current Helium Atmospheric-Pressure Glow Discharge", *Journal of Analytical Atomic Spectrometry*, 21(11), pp. 1175-1184.

(181) Andrade, F. J.; Shelley, J. T.; Wetzel, W. C.; Webb, M. R.; Gamez, G.; Ray, S. J.; Hieftje, G. M. **(2008)**. "Atmospheric Pressure Chemical Ionization Source. 2. Desorption-Ionization for the Direct Analysis of Solid Compounds", *Analytical Chemistry*, 80(8), pp. 2654-2663.

(182) Andrade, F. J.; Shelley, J. T.; Wetzel, W. C.; Webb, M. R.; Gamez, G.; Ray, S. J.; Hieftje, G. M. **(2008)**. "Atmospheric Pressure Chemical Ionization Source. 1. Ionization of Compounds in the Gas Phase", *Analytical Chemistry*, 80(8), pp. 2646-2653.

(183) Newton, P. N.; Hampton, C. Y.; Alter Hall, K.; Teerwarakulpana, T.; Prakongpan, S.; Ruangveerayuth, R.; White, N.; Day, N. P. J.; Tudino, M. B.; Mancuso, N.; Fernández, F. M. **(2008)**. "Characterization of 'Yaa Chud' Medicine on the Thailand-Myanmar Border: Selecting for Drug-Resistant Malaria and Threatening Public Health", *American Journal of Tropical Medicine and Hygiene*, 79(5), pp. 662-669.

(184) Fernández, F. M.; Cody, R. B.; Green, M.; Hampton, C. Y.; McGready, R.; Sengaloundeth, S.; White, N. J.; Newton, P. N. **(2006)**. "Characterization of Solid Counterfeit Drug Samples by Desorption Electrospray Ionization and Direct-Analysis-in-Real-Time Coupled to Time-of-Flight Mass Spectrometry", *ChemMedChem*, 1(7), pp. 702-705.

(185) Newton, P. N.; McGready, R.; Fernández, F. M.; Green, M. D.; Sunjio, M.; Bruneton, C.; Phanouvong, S.; Millet, P.; Whitty, C. J. M.; Talisuna, A. O.; Proux, S.; Christophel, E. M.; Malenga, G.; Singhasivanon, P.; Bojang, K.; Kaur, H.; Palmer , K.; Day, N. P. J.; Greenwood, B. M.; Nosten, F.; White, N. J. **(2006)**. "Manslaughter by Fake Artesunate in Asia - Will Africa Be Next?" *PLoS Medicine*, 3(6), pp. e197.

(186) Newton, P. N.; Green, M.; Fernández, F. M.; Day, N. P. J.; White, N. J. **(2006)**. "Counterfeit Anti-Infective Drugs", *Lancet Infectious Diseases*, 6(9), pp. 602-612.

(187) Fernández, F. M.; Newton, P. N.; Green, M. **(2008)**. "Prevalence and Detection of Counterfeit Pharmaceuticals: A Mini Review." *Industrial & Engineering Chemistry Research*, 47(3), pp. 585-590.

(188) Newton, P. N.; Fernández, F. M.; Plancon-Lecadre, A.; Mildenhall, D.; Green, M. D.; Ziyong, L.; Christophel, E. M.; Phanouvong, S.; Howells, S.; MacIntosh, E.; Laurin, P.; Blum, N.; Hampton, C. Y.; Faure, K.; Nyadong, L.; Soong, C. W. R.; Santoso, B.; Zhiguang, W.; Newton, J.; Palmer , K. **(2008)**. "An Epidemiological Collaborative Investigation into the Criminal Fake Artesunate Trade in South East Asia", *PLoS Medicine*, 5(2), pp. e32.

(189) Fernández, F. M.; Hampton, C. Y.; Nyadong, L.; Navare, A.; Kwasnik, M. "Liquid Chromatography and Ambient Ionization Time-of-Flight Mass Spectrometry for the Analysis of Genuine and Counterfeit Pharmaceuticals", In *LC/TOF-MS for Accurate Mass Analysis: Principles, Tools, and Applications for Accurate Mass Analysis*; Ferrer, I., Thurman, E. M., Eds.; Wiley: Hoboken, NJ, **2009**; Vol. 173, pp 113-132.

(190) Jones, R. W.; Cody, R. B.; McClelland, J. F. **(2006)**. "Differentiating Writing Inks Using Direct Analysis in Real Time Mass Spectrometry", *Journal of Forensic Sciences*, 51(4), pp. 915-918.

(191) Morlock, G.; Schwack, W. **(2006)**. "Determination of Isopropylthioxanthone (ITX) in Milk, Yoghurt and Fat by HPTLC-FLD, HPTLC-ESI/MS and HPTLC-DART/MS", *Analytical and Bioanalytical Chemistry*, 385(3), pp. 586-595.

(192) Pierce, C. Y.; Barr, J. R.; Cody, R. B.; Massung, R.; Woolfitt, A.; Moura, H.; Thompson, H. A.; Fernández, F. M. **(2007)**. "Ambient Generation of Fatty Acid Methyl Ester Ions from Bacterial Whole Cells by Direct Analysis in Real Time (DART) Mass Spectrometry", *Chemical Communications*, 2007(8), pp. 807-809.

(193) Banerjee, S.; Madhusudanan, K. P.; Khanuja, S. P.; Chattopadhyay, S. K. **(2008)**. "Analysis of Cell Cultures of *Taxus Wallichiana* Using Direct Analysis in Real Time Mass Spectrometric Technique", *Biomedical Chromatography*, 22(3), pp. 250-253.

(194) Haefliger, O. P.; Jeckelmann, N. **(2007)**. "Direct Mass Spectrometric Analysis of Flavors and Fragrances in Real Applications Using DART", *Rapid Communications in Mass Spectrometry*, 21(8), pp. 1361-1366.

(195) Morlock, G.; Ueda, Y. **(2007)**. "New Coupling of Planar Chromatography with Direct Analysis in Real Time Mass Spectrometry", *Journal of Chromatography A*, 1143(1-2), pp. 243-251.

(196) Yu, S.; Crawford, E.; Tice, J.; Musselman, B.; Wu, J. T. **(2009)**. "Bioanalysis without Sample Cleanup or Chromatography: The Evaluation and Initial Implementation of Direct Analysis in Real Time Ionization Mass Spectrometry for the Quantification of Drugs in Biological Matrixes", *Analytical Chemistry*, 81(1), pp. 193-202.

(197) Nielen, M. W. F.; Marvin, H. J. P. "Challenges in Chemical Food Contaminants and Residue Analysis", In *Comprehensive Analytical Chemistry: Food Contaminants and Residue Analysis, 51*; Pico, Y., Ed.; Oxford: Elsevier, Wilson and Wilson's, **2008**; Vol. 51, pp 1-27.

(198) Schurek, J.; Vaclavik, L.; Hooijerink, H.; Lacina, O.; Poustka, J.; Sharman, M.; Caldow, M.; Nielen, M. W. F.; Hajslova, J. **(2008)**. "Control of Stobilurin Fungicides in Wheat Using Direct Analysis in Real Time Accurate Time-of-Flight and Desorption Electrospray Ionization Linear Ion Trap Mass Spectrometry", *Analytical Chemistry*, 80(24), pp. 9567-9575.

(199) Yew, J. Y.; Cody, R. B.; Kravitz, E. A. **(2008)**. "Cuticular Hydrocarbon Analysis of an Awake Behaving Fly Using Direct Analysis in Real Time Time-of-Flight Mass Spectrometry", *Proceedings of the National Academy of Sciences*, 105(20), pp. 7135-7140.

(200) Ionsense.
http://www.ionsense.com/applications.php

(201) van Agtmael, M. A.; Eggelte, T. A.; van Boxtel, C. J. **(1999)**. "Artemisinin Drugs in the Treatment of Malaria: From Medicinal Herb to Registered Medication", *Trends in Pharmacological Sciences*, 20(5), pp. 199-205.

(202) Newton, P. N.; Dondorp, A.; Green, M.; Mayxay, M.; White, N. J. **(2003)**. "Counterfeit Artesunate Antimalarials in Southeast Asia", *Lancet*, 362(9378), pp. 169.

(203) Dondorp, A. M.; Newton, P. N.; Mayxay, M.; Van Damme, W.; Smithuis, F. M.; Yeung, S.; Petit, A.; Lynam, A. J.; Johnson, A.; Hien, T. T.; McGready, R.; Farrar, J. J.; Looareesuwan, S.; Day, N. P. J.; Green, M. D.; White, N. J. **(2004)**. "Fake Antimalarials in Southeast Asia Are a Major Impediment to Malaria Control: Multinational Cross-Sectional Survey on the Prevalence of Fake Antimalarials", *Tropical Medicine & International Health*, 9(12), pp. 1241-1246.

(204) Aldhous, P. **(2005)**. "Murder by Medicine", *Nature*, 434(7030), pp. 132-136.

(205) Aldhous, P.; Akunyili, D. **(2005)**. "News Feature - in the Line of Fire", *Nature*, 434(7030), pp. 134.

(206) Cockburn, R.; Newton, P. N.; Agyarko, E. K.; Akunyili, D.; White, N. J. **(2005)**. "The Global Threat of Counterfeit Drugs: Why Industry and Governments Must Communicate the Dangers", *PLoS Medicine*, 2(4), pp. e100.

(207) Zook, D. R.; Bruins, A. P. **(1997)**. "On Cluster Ions, Ion Transmission, and Linear Dynamic Range Limitations in Electrospray (Ionspray) Mass Spectrometry", *International Journal of Mass Spectrometry and Ion Processes*, 162(1-3), pp. 129-147.

(208) El-Faramawy, A.; Siu, K. W. M.; Thomson, B. A. **(2005)**. "Efficiency of Nano-Electrospray Ionization", *Journal of the American Society for Mass Spectrometry*, 16(10), pp. 1702-1707.

(209) Berkout, V. D.; Kryuchkov, S. I.; Doroshenko, V. M. **(2007)**. "Modeling of Ion Processes in Atmospheric Pressure Matrix-Assisted Laser Desorption/Ionisation", *Rapid Communications in Mass Spectrometry*, 21(13), pp. 2046-2050.

(210) Zhou, L.; Yue, B.; Dearden, D. V.; Lee, E. D.; Rockwood, A. L.; Lee, M. L. **(2003)**. "Incorporation of a Venturi Device in Electrospray Ionization", *Analytical Chemistry*, 75(21), pp. 5978-5983.

(211) Prior, D. C.; Price, J.; Bruce, J. E. *Sample Inlet Tube for Ion Source*, 6,455,846, 09/24/2002

(212) Wu, S.; Zhang, K.; Kaiser, N. K.; Bruce, J. E. **(2006)**. "Incorporation of a Flared Inlet Capillary Tube on a Fourier Transform Ion Cyclotron Resonance Mass Spectrometer", *Journal of the American Society for Mass Spectrometry*, 17(6), pp. 772-779.

(213) Dixon, R. B.; Muddiman, D. C. **(2007)**. "Quantitative Comparison of a Flared and a Standard Heated Metal Capillary Inlet with a Voltage-Assisted Air Amplifier on an Electrospray Ionization Linear Ion Trap Mass Spectrometer", *Rapid Communications in Mass Spectrometry*, 21(19), pp. 3207-3212.

(214) Him, T.; Tolmachev, A. V.; Harkewicz, R.; Prior, D. C.; Anderson, G.; Udseth, H. R.; Smith, R. D.; Bailey, T. H.; Rakov, S.; Futrell, J. H. **(2000)**. "Design and Implementation of a New Electrodynamic Ion Funnel", *Analytical Chemistry*, 72(10), pp. 2247-2255.

(215) Shaffer, S. A.; Tang, K. Q.; Anderson, G. A.; Prior, D. C.; Udseth, H. R.; Smith, R. D. **(1997)**. "A Novel Ion Funnel for Focusing Ions at Elevated Pressure Using Electrospray Ionization Mass Spectrometry", *Rapid Communications in Mass Spectrometry*, 11(16), pp. 1813-1817.

(216) Hawkridge, A. M.; Zhou, L.; Lee, M. L.; Muddiman, D. C. **(2004)**. "Analytical Performance of a Venturi Device Integrated into an Electrospray Ionization Fourier Transform Ion Cyclotron Resonance Mass Spectrometer for Analysis of Nucleic Acids", *Analytical Chemistry*, 76(14), pp. 4118-4122.

(217) Dixon, R. B.; Muddiman, D. C.; Hawkridge, A. M.; Fedorov, A. G. **(2007)**. "Probing the Mechanisms of an Air Amplifier Using a LTQ-FT-ICR-MS and Fluorescence Spectroscopy", *Journal of the American Society for Mass Spectrometry*, 18(11), pp. 1909-1913.

(218) Valaskovic, G. A.; Kelleher, N. L.; Little, D. P.; Aaserud, D. J.; Mclafferty, F. W. **(1995)**. "Attomole-Sensitivity Electrospray Source for Large-Molecule Mass-Spectrometry", *Analytical Chemistry*, 67(20), pp. 3802-3805.

(219) Brauer Airmovers. http://www.brauer.co.uk/php/airmoverindex.php?csvfile=airmoverindex.csv&indexprimary=airmover&indextitle=Airmovers

(220) Graham, J. F.; Griffiths, K.; Kovar, M.; Norton, P. R.; Ogini, F.; Warren, O. L. **(1999)**. "Surface Derivatization of Nanoscale Tungsten Probes for Interfacial Force Microscopy", *Journal of Vacuum Science and Technology A*, 17(4), pp. 2240-2245.

(221) Grandori, R. **(2001)**. "Detecting Equilibrium Cytochrome C Folding Intermediates by Electrospray Ionization Mass Spectrometry: Two Partially Folded Forms Populate the Molten-Globule State", *Protein Science*, 11(3), pp. 453-458.

(222) Vekey, K. **(1996)**. "Internal Energy Effects in Mass Spectrometry", *Journal of Mass Spectrometry*, 31(5), pp. 445-463.

(223) MS Number 248144, National Institute of Standards and Technology Mass Spectrometry Data Center, U.S. Secretary of Commerce. http://webbook.nist.gov/cgi/cbook.cgi?ID=C50555&Units=SI&Mask=200#Mass-Spec

(224) Luo, G.; Marginean, I.; Vertes, A. **(2002)**. "Internal Energy of Ions Generated by Matrix-Assisted Laser Desorption/Ionization", *Analytical Chemistry*, 74(24), pp. 6185-6190.

(225) Vertes, A.; Luo, G.; Ye, L.; Chen, Y.; Marginean, I. **(2004)**. "Laser Pulse Length Dependence of Internal Energy Transfer in UV-MALDI-MS", *Applied Physics A*, 79(4-6), pp. 823-825.

(226) Gabelica, V.; De Pauw, E. **(2005)**. "Internal Energy and Fragmentation of Ions Produced in Electrospray Sources", *Mass Spectrometry Reviews*, 24(4), pp. 566-587.

(227) Touboul, D.; Jecklin, M. C.; Zenobi, R. **(2008)**. "Ion Internal Energy Distributions Validate the Charge Residue Model for Small Molecule Ion Formation by Spray Methods", *Rapid Communications in Mass Spectrometry*, 22(7), pp. 1062-1068.

(228) Hirabayashi, A.; Sakairi, M.; Koizumi, H. **(1995)**. "Sonic Spray Mass-Spectrometry", *Analytical Chemistry*, 67(17), pp. 2878-2882.

(229) Takats, Z.; Wiseman, J. M.; Gologan, B.; Cooks, R. G. **(2004)**. "Electrosonic Spray Ionization. A Gentle Technique for Generating Folded Proteins and Protein Complexes in the Gas Phase and for Studying Ion-Molecule Reactions at Atmospheric Pressure", *Analytical Chemistry*, 76(14), pp. 4050-4058.

(230) Sakamoto, S.; Fujita, M.; Yamaguchi, K. **(2000)**. "Characterization of Self-Assembling Nano-Sized Structures by Means of Coldspray Ionization Mass Spectrometry", *Tetrahedron*, 56 pp. 955-964.

(231) Takats, Z.; Nanita, S. C.; Cooks, R. G.; Schlosser, G.; Vekey, K. **(2003)**. "Amino Acid Clusters Formed by Sonic Spray Ionization", *Analytical Chemistry*, 75(6), pp. 1514-1523.

(232) Hirabayashi, A.; Hirabayashi, Y.; Sakairi, M.; Koizumi, H. **(1996)**. "Multiply-Charged Ion Formation by Sonic Spray", *Rapid Communications in Mass Spectrometry*, 10(13), pp. 1703-1705.

(233) Konig, S.; Kollas, O.; Dreisewerd, K. **(2007)**. "Generation of Highly Charged Peptide and Protein Ions by Atmospheric Pressure Matrix-Assisted Infrared Laser Desorption/Ionization Ion Trap Mass Spectrometry", *Analytical Chemistry*, 79(14), pp. 5484-5488.

(234) Nishimura, S.; Nagahori, N.; Takaya, K.; Tachibana, Y.; Miura, N.; Monde, K. **(2005)**. "Direct Observation of Sugar-Protein, Sugar-Sugar, and Sugar-Water Complexes by Cold-Spray Ionization Time-of-Flight Mass Spectrometry", *Angewandte Chemie, International Edition*, 44(4), pp. 571-575.

(235) Sakamoto, S.; Yamaguchi, K. **(2003)**. "Low Tm DNA Duplexes Observed by Cold-Spray Ionization Mass Spectrometry", *Tetrahedron Letters*, 44(16), pp. 3341-3344.

(236) Konn, D. O.; Murrell, J.; Despeyroux, D.; Gaskell, S. J. **(2005)**. "Comparison of the Effects of Ionization Mechanism, Analyte Concentration, and Ion 'Cool-Times' on the Internal Energy of Peptide Ions Produced by Electrospray and Atmospheric Pressure Matrix-Assisted Laser Desorption Ionization", *Journal of the American Society for Mass Spectrometry*, 16(5), pp. 743-751.

(237) Dodd, E. E. **(1953)**. "The Statistics of Liquid Spray and Dust Electrification by the Hopper and Laby Method", *Journal of Applied Physics*, 24(1), pp. 73-80.

(238) Guo, N.; Zhang, R.; Song, F.; He, J.; Xia, B.; Albiz, Z. **(2009)**. "Characterization of Acid-Induced Protein Conformational Changes and Noncovalent Complexes in Solution by Using Coldspray Ionization Mass Spectrometry", *Journal of the American Society for Mass Spectrometry*, 20(5), pp. 845-851.

(239) Kambara, H.; Kanomata, I. **(1976)**. "Collisional Dissociation in Atmospheric Pressure Ionization Mass Spectrometry", *Mass Spectroscopy*, 24(4), pp. 271-282.

(240) Hunt, D. F.; Henderson, R. A.; Shabanowitz, J.; Sakaguchi, K.; Michel, H.; Sevilir, N.; Cox, A. L.; Appella, E.; Engelhard, V. H. **(1992)**. "Characterization of Peptides Bound to the Class I MHC Molecules HLA-A2.1 by Mass Spectrometry", *Science*, 255(5049), pp. 1261-1263.

(241) Juraschek, R.; Dulcks, T.; Karas, M. **(1999)**. "Nanoelectrospray - More Than Just a Minimized-Flow Electrospray Ionization Source", *Journal of the American Society for Mass Spectrometry*, 10(4), pp. 300-308.

(242) Schmidt, A.; Bahr, U.; Karas, M. **(2001)**. "Influence of Pressure in the First Pumping Stage on Analyte Desolvation and Fragmentation in Nano-ESI MS", *Analytical Chemistry*, 73(24), pp. 6040-6046.

(243) Smith, R. D.; Loo, J. A.; Barinaga, C. J.; Edmonds, C. G.; Udseth, H. R. **(1990)**. "Collisional Activation and Collision-Activated Dissociation of Large Multiply Charged Polypeptides and Proteins Produced by Electrospray Ionization", *Journal of the American Society for Mass Spectrometry*, 1(1), pp. 53-65.

(244) Schneider, B. B.; Baranov, V. I.; Javaheri, H.; Covey, T. R. **(2003)**. "Particle Discriminator Interface for Nanoflow ESI-MS", *Journal of the American Society for Mass Spectrometry*, 14(11), pp. 1236-1246.

(245) Smith, R. D.; Olivares, J. A.; Nguyen, N. T.; Udseth, H. R. **(1988)**. "Capillary Zone Electrophoresis - Mass Spectrometry Using an Electrospray Ionization Interface", *Analytical Chemistry*, 60(5), pp. 436-441.

(246) Chowdhury, S. K.; Katta, V.; Chait, B. T. **(1990)**. "An Electrospray-Ionization Mass-Spectrometer with New Features", *Rapid Communications in Mass Spectrometry*, 4(3), pp. 81-87.

(247) Gabelica, V.; De Pauw, E. D.; Karas, M. **(2004)**. "Influence of the Capillary Temperature and the Source Pressure on the Internal Energy Distribution of Electrosprayed Ions", *International Journal of Mass Spectrometry*, 231(2-3), pp. 189-195.

(248) Voyksner, R. D.; Pack, T. **(1991)**. "Investigation of Collisional-Activation Decomposition Process and Spectra in the Transport Region of an Electrospray Single-Quadrupole Mass-Spectrometer", *Rapid Communications in Mass Spectrometry*, 5(6), pp. 263-268.

(249) Collette, C.; De Pauw, E. **(1998)**. "Calibration of the Internal Energy Distribution of Ions Produced by Electrospray", *Rapid Communications in Mass Spectrometry*, 12(4), pp. 165-170.

(250) Hoxha, A.; Collette, C.; De Pauw, E.; Leyh, B. **(2001)**. "Mechanism of Collisional Heating in Electrospray Mass Spectrometry: Ion Trajectory Calculations", *Journal of Physical Chemistry A*, 105(31), pp. 7326-7333.

(251) Drahos, L.; Heeren, R. M. A.; Collette, C.; De Pauw, E.; Vekey, K. **(1999)**. "Thermal Energy Distribution Observed in Electrospray Ionization", *Journal of Mass Spectrometry*, 34(12), pp. 1373-1379.

(252) Kenttämaa, H. I.; Cooks, R. G. **(1985)**. "Internal Energy-Distributions Acquired through Collisional Activation at Low and High-Energies", *International Journal of Mass Spectrometry and Ion Processes*, 64(1), pp. 79-83.

(253) Collette, C.; Drahos, L.; De Pauw, E.; Vekey, K. **(1998)**. "Comparison of the Internal Energy Distributions of Ions Produced by Different Electrospray Sources", *Rapid Communications in Mass Spectrometry*, 12(22), pp. 1673-1678.

(254) Naban-Maillet, J.; Lesage, D.; Bossee, A.; Gimbert, Y.; Sztaray, J.; Vekey, K.; Tabet, J. C. **(2005)**. "Internal Energy Distribution in Electrospray Ionization", *Journal of Mass Spectrometry*, 40(1), pp. 1-8.

(255) Nefliu, M.; Smith, J. N.; Venter, A.; Cooks, R. G. **(2008)**. "Internal Energy Distributions in Desorption Electrospray Ionization (DESI)", *Journal of the American Society for Mass Spectrometry*, 19(3), pp. 420-427.

(256) Katritzky, A. R.; Watson, C. H.; Dega-Szafran, Z.; Eyler, J. R. **(1990)**. "Collisionally-Activated Dissociation of N-Alkylpyridinium Cations to Pyridine and Alkyl Cations in the Gas Phase", *Journal of the American Chemical Society*, 112(7), pp. 2471-2478.

(257) Fenn, J. B. **(1993)**. "Ion Formation from Charged Droplets - Roles of Geometry, Energy, and Time", *Journal of the American Society for Mass Spectrometry*, 4(7), pp. 524-535.

(258) Verheijen, H. J. J.; Prins, M. W. J. **(1999)**. "Reversibly Electrowetting and Trapping of Charge: Model and Experiments", *Langmuir*, 15(20), pp. 6616-6620.

(259) Fisenko, S. P.; Wang, W. N.; Lenggoro, I. W.; Okyuama, K. **(2006)**. "Evaporative Cooling of Micron-Sized Droplets in a Low-Pressure Aerosol Reactor", *Chemical Engineering Science*, 61(18), pp. 6029-6034.

(260) Arpino, P. J.; Guiochon, G. **(1979)**. "LC-MS Coupling", *Analytical Chemistry*, 51(7), pp. 682A-701A.

(261) Karger, B. L.; Vouros, P. **(1985)**. "A Chromatographic Perspective of High-Performance Liquid-Chromatography Mass-Spectrometry", *Journal of Chromatography*, 323(1), pp. 13-32.

(262) Li, Z.; Ortega-Vilain, A. C.; Patil, G. S.; Chu, D. L.; Foreman, J. E.; Eveleth, D. D.; Powers, J. C. **(1996)**. "Novel Peptidyl Alpha-Keto Amide Inhibitors of Calpains and Other Cysteine Proteases", *Journal of Medicinal Chemistry*, 39(20), pp. 4089-4098.

(263) Wang, M. S.; Davis, A. A.; Culver, D. G.; Wang, Q.; Powers, J. C.; Glass, J. D. **(2004)**. "Calpain Inhibition Protects Against Taxol-Induced Sensory Neuropathy", *Brain*, 127(Pt 3), pp. 671-679.

(264) Krasnoslobodtsev, A. V.; Smirnov, S. N. **(2002)**. "Effect of Water on Silanization of Silica by Trimethoxysilanes", *Langmuir*, 18(8), pp. 3181-3184.

(265) Schlosser, A.; Volkmer-Engert, R. **(2003)**. "Volatile Polydimethylcyclosiloxanes in the Ambient Laboratory Air Identified as Source of Extreme Background Signals in Nanoelectrospray Mass Spectrometry", *Journal of Mass Spectrometry*, 38(5), pp. 523-525.

(266) Carrara, V. I.; Sirilak, S.; Thonglairuam, J.; Rojanawatsirivet, C.; Proux, S.; Gilbos, V.; Brockman, A.; Ashley, E. A.; McGready, R.; Krudsood, S.; Leemingsawat, S.; Looareesuwan, S.; Singhasivanon, P.; White, N.; Nosten, F. **(2006)**. "Deployment of Early Diagnosis and Mefloquine-Artesunate Treatment of *Falciparum* Malaria in Thailand: The Tak Malaria Initiative", *PLoS Medicine*, 3(6), pp. e183.

(267) Nosten, F.; van Vugt, M.; Price, R.; Luxemburger, C.; Thway, K. L.; Brockman, A.; McGready, R.; ter Kuile, F.; Looareesuwan, S.; White, N. J. **(2000)**. "Effects of Artesunate-Mefloquine Combination on Incidence of *Plasmodium Falciparum* Malaria and Mefloquine Resistance in Western Thailand: A Prospective Study", *Lancet*, 356(9226), pp. 297-302.

(268) Price, R. N.; Nosten, F. **(2001)**. "Drug Resistant *Falciparum* Malaria: Clinical Consequences and Strategies for Prevention", *Drug Resistance Updates*, 4(3), pp. 187-196.

(269) White, N. J. **(1999)**. "Antimalarial Drug Resistance and Combination Chemotherapy", *Philosophical Transactions of the Royal Society of London, B.*, 354(1384), pp. 739-749.

(270) White, N. J. **(2004)**. "Antimalarial Drug Resistance", *Journal of Clinical Investigation*, 113(8), pp. 1084-1092.

(271) Jaidee, S.; Limpananon, J.; Wittayanartpaisal, S. **(1980)**. "Drug Utilization of Yaa-Chud in Thailand", *Thai Journal of Pharmaceutical Sciences*, 5 pp. 219-220.

(272) Kamolratanakul, P.; Dhanamun, B.; Thaithong, S. **(1992)**. "Human Behavior in Relation to Selection of Malaria Treatment", *The Southeast Asian Journal of Tropical Medicine & Public Health*, 23(2), pp. 189-194.

(273) Wiwat, C.; Silapa-archa, W.; Temsirilerkhul, R.; Chiowatana, J. **(1982)**. "Rural Self-Medication in Malaria Infection", *Thai Journal of Pharmaceutical Sciences*, 7 pp. 14-29.

(274) Foster, S. D. **(1991)**. "Pricing, Distribution, and Use of Antimalarial Drugs", *Bulletin of the World Health Organisation*, 69(3), pp. 349-363.

(275) Amin, A. A.; Hughes, D. A.; Marsh, V.; Abuya, T. O.; Kokwaro, G. O.; Winstanley, P. A.; Ochola, S. A.; Snow, R. W. **(2004)**. "The Difference between Effectiveness and Efficacy of Antimalarial Drugs in Kenya", *Tropical Medicine & International Health*, 9(9), pp. 967-974.

(276) Basco, L. K. **(2004)**. "Molecular Epidemiology of Malaria in Cameroon. XIX. Quality of Antimalarial Drugs Used for Self-Medication", *American Journal of Tropical Medicine and Hygiene*, 70(3), pp. 245-250.

(277) Weston, D. J.; Bateman, R.; Wilson, I. D.; Wood, T. R.; Creaser, C. S. **(2005)**. "Direct Analysis of Pharmaceutical Drug Formulations Using Ion Mobility Spectrometry/Quadrupole-Time-of-Flight Mass Spectrometry Combined with Desorption Electrospray Ionization", *Analytical Chemistry*, 77(23), pp. 7572-7580.

(278) Penning, F. M. **(1927)**. "Ionization by Metastable Atoms", *Naturwissenschaften*, 15(40), pp. 818.

(279) Harris, G. A.; Fernández, F. M. **(2009)**. "Simulations and Experimental Investigation of Atmospheric Transport in an Ambient Metastable-Induced Chemical Ionization Source", *Analytical Chemistry*, 81(1), pp. 322-329.

(280) WHO, *WHO Model List of Essential Medicines*, World Health Organisation, Geneva, **2006**.

(281) Wendlandt, W. W.; Zief, M. **(1958)**. "Thermal Decomposition of Antibiotics", *Nature*, 182(4636), pp. 665-666.

(282) Hirsch, R.; Ternes, T. A.; Haberer, K.; Mehlich, A.; Ballwanz, F.; Kratz, K. L. **(1998)**. "Determination of Antibiotics in Different Water Compartments via Liquid Chromatography Electrospray Tandem Mass Spectrometry", *Journal of Chromatography A*, 815(2), pp. 213-223.

(283) Chernushevich, I. V.; Loboda, A. V.; Thomson, B. A. **(2001)**. "An Introduction to Quadrupole-Time-of-Flight Mass Spectrometry", *Journal of Mass Spectrometry*, 36(8), pp. 849-865.

(284) Beers, M. H.; Porter, R. S.; Jones, T. V.; Kaplan, J. L.; Berwits, M. *The Merck Manual of Diagnosis and Therapy*, *18th ed.*; Merck Research Laboratories: Whitehouse Station, NJ, USA, **2006**.

(285) Yaa Chud Compilation. http://web.chemistry.gatech.edu/%7Efernandez/Fernandez_Website/Yaa%20chud%20Compilation%202007.pdf

(286) Anon. *British National Formulary*, *53rd ed.*; BMJ Publishing Group & RPS Publishing: London, UK, **2007**.

(287) Roper, C.; Pearce, R.; Nair, S.; Sharp, B.; Nosten, F.; Anderson, T. **(2004)**. "Intercontinental Spread of Pyrimethamine-Resistant Malaria", *Science*, 305(5687), pp. 1124.

(288) Anon. **(2007)**. "Resistance to Artemisinin Derivatives Along the Thai-Cambodian Border", *Weekly Epidemiological Record*, 82(41), pp. 360.

(289) Bousema, J. T.; Gouagna, L. C.; Meutstege, A. M.; Okech, B. E.; Akim, N. I.; Githure, J. I.; Beier, J. C.; Sauerwein, R. W. **(2003)**. "Treatment Failure of Pyrimethamine-Sulphadoxine and Induction of *Plasmodium Falciparum* Gametocytaemia in Children in Western Kenya", *Tropical Medicine & International Health*, 8(5), pp. 427-430.

(290) Malaria. http://www.who.int/mediacentre/factsheets/fs094/en/index.html. Accessed 10 August 2007.

(291) Newton, P. N.; Proux, S.; Green, M.; Smithuis, F. M.; Rozendaal, J.; Prakongpan, S.; Chotivanich, K.; Mayxay, M.; Looareesuwan, S.; Farrar, J. J. **(2001)**. "Fake Artesunate in Southeast Asia", *Lancet*, 357(9272), pp. 1948-1950.

(292) Yang, Q.; Shi, W.; Li, R.; Gan, J. **(1982)**. "The Antimalarial and Toxic Effect of Artesunate on Animal Models", *Journal of Traditional Chinese Medicine*, 2(2), pp. 99-103.

(293) Saving Lives, Buying Time: Economics of Malaria Drugs in an Age of Resistance. http://www.nap.edu/books/0309092183/html/. Accessed 5 August 2007.

(294) Deisingh, A. K. **(2005)**. "Pharmaceutical Counterfeiting", *Analyst*, 130(3), pp. 271-279.

(295) World Malaria Report. http://www.rbmm.who.int/wmr2005/html/1-2.htm. Accessed 22 July 2007.

(296) Rozendaal, J. **(2000)**. "Fake Antimalarials Circulating in Cambodia", *Bulletin of the Mekon Malaria Forum*, 7 pp. 62-68.

(297) Alter Hall, K.; Newton, P. N.; Green, M. D.; De Veij, M.; Vandenabeele, P.; Pizzanelli, D.; Mayxay, M.; Dondorp, A.; White, N. J.; Fernández, F. M. **(2006)**. "Characterization of Counterfeit Artesunate Antimalarial Tablets from SE Asia", *American Journal of Tropical Medicine and Hygiene*, 75(5), pp. 804-811.

(298) Lon, C. T.; Tsuyuoka, R.; Phanouvong, S.; Nivanna, N.; Socheat, D.; Sokhan, C.; Blum, N.; Christophel, E. M.; Smine, A. **(2006)**. "Counterfeit and Substandard Antimalarial Drugs in Cambodia", *Transactions of the Royal Society of Tropical Medicine & Hygiene*, 100(11), pp. 1019-1024.

(299) Table Recording Act Producers - Artepal Project. http://www.artepal.org/index.php?option=com_docman&task=doc_download&gid=13&Itemid=60. Accessed 5 August 2007.

(300) Green, M. D.; Dwight, L. M.; Wirtz, r. A.; White, N. J. **(2000)**. "A Colorimetric Field Method to Assess the Authenticity of Drugs Sold as the Antimalarial Artesunate", *Journal of Pharmaceutical and Biomedical Analysis*, 24(1), pp. 65-70.

(301) Green, M. D.; Nettey, H.; Villalva Rojas, O.; Pamanivong, C.; Khounsaknalath, L.; Grande Ortiz, M.; Newton, P. N.; Fernández, F. M.; Vongsack, L.; Manolin, O. **(2007)**. "Use of Refractometry and Colorimetry as Field Methods to Rapidly Assess Antimalarial Drug Quality", *Journal of Pharmaceutical and Biomedical Analysis*, 43(1), pp. 105-110.

(302) Hoefs, J. *Stable Isotope Geochemistry*; Springer-Verlag: New York, **1996**.

(303) Gergov, M.; Ojanpera, I.; Vuori, E. **(2003)**. "Simultaneous Screening for 238 Drugs in Blood by Liquid Chromatography-Ion Spray Tandem Mass Spectrometry with Multiple-Reaction Monitoring", *Journal of Chromatography B: Analytical, Technological, Biomedical and Life Sciences*, 795(1), pp. 41-53.

(304) Heywood, V. H. *Flowering Plants of the World*; Oxford, **1978**.

(305) Wolff, J. C.; Thomson, L. A.; Eckers, C. **(2003)**. "Identification of the 'Wrong' Active Pharmaceutical Ingredient in a Counterfeit Halfan (TM) Drug Product Using Accurate Mass Tandem Mass Spectrometry and Liquid Chromatography/Mass Spectrometry", *Rapid Communications in Mass Spectrometry*, 17(3), pp. 215-221.

(306) Rivier, L. **(2003)**. "Criteria for the Identification of Compounds by Liquid Chromatography-Mass Spectrometry and Liquid Chromatography-Multiple Mass Spectrometry in Forensic Toxicology and Doping Analysis", *Analytica Chimica Acta*, 492(1-2), pp. 69-82.

(307) Hernandez, F.; Ibanez, M.; Sancho, J. V.; Pozo, O. J. **(2004)**. "Comparison of Different Mass Spectrometric Techniques Combined with Liquid Chromatography for Confirmation of Pesticides in Environmental Water Based on the Use of Identification Points", *Analytical Chemistry*, 76(15), pp. 4349-4357.

(308) Hedenmalm, K.; Spigset, O. **(2002)**. "Agranulocytosis and Other Blood Dyscrasias Associated with Dipyrone (Metamizole)", *European Journal of Clinical Pharmacology*, 58(4), pp. 265-274.

(309) United Nations, (1988) United Nations Convention against Illicit Traffic in Narcotic Drugs and Psychotropic Substances. www.unodc.org/pdf/convention_1988_en.pdf. Accessed 11 August 2007.

(310) Manisali, I.; Chen, D. D. Y.; Schneider, B. B. **(2006)**. "Electrospray Ionization Source Geometry for Mass Spectrometry: Past, Present, and Future", *Trends in Analytical Chemistry*, 25(3), pp. 243-256.

(311) Lenard, P. **(1892)**. "Ueber Die Electricitat Der Wasserfalle", *Wiedemann's Annalen*, 46 pp. 584-686.

(312) Chapman, S. **(1934)**. "The Charges on Droplets Produced by the Spraying of Liquids as Revealed by the Millikan Oil Drop Method", *Physics*, 5(6), pp. 150-152.

(313) Chapman, S. **(1937)**. "Carrier Mobility Spectra of Spray Electrified Liquids", *Physical Review*, 52(3), pp. 184-190.

(314) Hines, R. L. **(1966)**. "Electrostatic Atomization and Spray Painting", *Journal of Applied Physics*, 37(7), pp. 2730-2736.

(315) Kantrowitz, A.; Grey, J. **(1951)**. "A High Intensity Source for the Molecular Beam .1. Theoretical", *Review of Scientific Instruments*, 22(5), pp. 328-332.

(316) Mylchreest, I. C.; Hail, M. E. *Electrospray Ion Source with Reduced Neutral Noise and Method*, 5171990, 05/17/1991

(317) Henion, J. D.; Covey, T. R.; Bruins, A. P. *Ion Spray Apparatus and Method*, 4861988, 08/29/1989

(318) Bertsch, J. L.; Fischer, S. M.; Henry, K. D.; Wong, E. M. *Ionization Chamber and Mass Spectrometry System Containing an Asymmetric Electrode*, 5838003, 11/17/1998

(319) Niessen, W. M. A. **(1998)**. "Advances in Instrumentation in Liquid Chromatography Mass Spectrometry and Related Liquid-Introduction Techniques", *Journal of Chromatography A*, 794(1-2), pp. 407-435.

(320) Cech, N. B.; Enke, C. G. **(2001)**. "Practical Implications of Some Recent Studies in Electrospray Ionization Fundamentals", *Mass Spectrometry Reviews*, 20(6), pp. 362-387.

(321) Shelley, J. T.; Wiley, J. S.; Chan, G. C.; Schilling, G. D.; Ray, S. J.; Hieftje, G. M. **(2009)**. "Characterization of Direct-Current Atmospheric-Pressure Discharges Useful for Ambient Desorption/Ionization Mass Spectrometry", *Journal of the American Society for Mass Spectrometry*, 20(5), pp. 837-844.

(322) Steiner, R. R.; Larson, R. L. **(2009)**. "Validation of the Direct Analysis in Real Time Source for Use in Forensic Drug Screening", *Journal of Forensic Sciences*, 54(3), pp. 617-622.

(323) Bartus, R. T.; Hayward, N. J.; Elliott, P. J.; Sawyer, S. D.; Baker, K. L.; Dean, R. L.; Akiyama, A.; Straub, J. A.; Harbeson, S. L.; Li, Z. **(1994)**. "Calpain Inhibitor AK295 Protects Neurons from Focal Brain Ischemia. Effects of Postocclusion Intra-Arterial Administration", *Stroke*, 25(11), pp. 2265-2270.

(324) Saatman, K. E.; Murai, H.; Bartus, R. T.; Smith, D. H.; Hayward, N. J.; Perri, B. R.; McIntosh, T. K. **(1996)**. "Calpain Inhibitor AK295 Attenuates Motor and Cognitive Deficits Following Experimental Brain Injury in the Rat", *Proceedings of the National Academy of Sciences*, 93(8), pp. 3428-3433.

(325) Ovat, A.; Li, Z. Z.; Hampton, C. Y.; Asress, S. A.; Fernández, F. M.; Glass, J. D.; Powers, J. C. **(2009)**. "Peptidyl α-Ketoamides with Nucleotide Bases and Dimethylaminoalkyl Substituents as Calpain Inhibitors", *Journal of Medicinal Chemistry*, In Preparation.

(326) American Cancer Society **(2009)**, Key Statistics About Ovarian Cancer. http://www.cancer.org/docroot/cri/content/cri_2_4_1x_what_are_the_key_statistics_for_ovarian_cancer_33.asp

(327) Odunsi, K.; Wollman, R. M.; Ambrosone, C. B.; Hutson, A.; McCann, S. E.; Tammela, J.; Geisler, J. P.; Miller, G.; Sellers, T.; Cliby, W.; Qian, F.; Keitz, B.; Intengan, M.; LeleJ, S.; Alderfer, A. L. **(2005)**. "Detection of Epithelial Ovarian Cancer Using ^{1}H-NMR-Based Metabonomics", *International Journal of Cancer*, 113(5), pp. 782-788.

(328) An, H. J.; Miyamoto, S.; Lancaster, K. S.; Kirmiz, C.; Li, B.; Lam, K. S.; Leiserowitz, G. S.; Lebrilla, C. B. **(2006)**. "Profiling of Glycans in Serum for the Discovery of Potential Biomarkers for Ovarian Cancer", *Journal of Proteome Research*, 5(7), pp. 1626-1635.

(329) Petricoin, E. F.; Ardekani, A. M.; Hitt, B. A.; Levine, P. J.; Fusaro, V. A.; Steinberg, S. M.; Mills, G. B.; Simone, C.; Fishman, D. A.; Kohn, E. C.; Liotta, L. A. **(2002)**. "Use of Proteomic Patterns in Serum to Identify Ovarian Cancer", *Lancet*, 359(9306), pp. 572-577.

(330) Mueller, W. K.; Handschu.R; Wade, M. E. **(1971)**. "Serum Haptoglobin in Patients with Ovarian Malignancies", *Obstetrics and Gynecology*, 38(3), pp. 427-435.

(331) Williams, T. I.; Toups, K. L.; Saggese, D. A.; Kalli, K. R.; Cliby, W. A.; Muddiman, D. C. **(2007)**. "Epithelial Ovarian Cancer: Disease Etiology, Treatment, Detection, and Investigational Gene, Metabolite, and Protein Biomarkers", *Journal of Proteome Research*, 6(8), pp. 2936-2962.

(332) Nicholson, J. K.; Lindon, J. C.; Holmes, E. **(1999)**. "Metabonomics: Understanding the Metabolic Response of Living Systems to Pathophysiological Stimuli via Multivariate Statistical Analysis of Biological NMR Spectroscopic Data", *Xenobiotica*, 29(11), pp. 1181-1189.

(333) Fiehn, O.; Kind, T. "Metabolite Profiling in Blood Plasma", In *Metabolomics: Methods and Protocols*; Weckwerth, W., Ed.; Humana Press: Totowa, NJ, **2006**.

(334) Xu, Y.; Shen, Z. Z.; Wiper, D. W.; Wu, M. Z.; Morton, R. E.; Elson, P.; Kennedy, A. W.; Belinson, J.; Markman, M.; Casey, G. **(1998)**. "Lysophosphatidic Acid as a Potential Biomarker for Ovarian and Other Gynecologic Cancers", *JAMA, the Journal of the American Medical Association*, 280(8), pp. 719-723.

(335) Baker, D. L.; Morrison, P.; Miller, B.; Riely, C. A.; Tolley, B.; Westermann, A. M.; Bonfrer, J. M. G.; Bais, E.; Moolenaar, W. H.; Tigyi, G. **(2002)**. "Plasma Lysophosphatidic Acid Concentration and Ovarian Cancer", *JAMA, the Journal of the American Medical Association*, 287(23), pp. 3081-3082.

(336) Sutphen, R.; Xu, Y.; Wilbanks, G. D.; Fiorica, J.; Grendys, E. C.; LaPolla, J. P.; Arango, H.; Hoffman, M. S.; Martino, M.; Wakeley, K.; Griffin, D.; Blanco, R. W.; Cantor, A. B.; Xiao, Y. J.; Krischer, J. P. **(2004)**. "Lysophospholipids Are Potential Biomarkers of Ovarian Cancer", *Cancer Epidemiology, Biomarkers and Prevention*, 13(7), pp. 1185-1191.

(337) Schwartz, P. E.; Chambers, S. K.; Chambers, J. T.; Gutmann, J.; Katopodis, N.; Foemmel, R. **(1987)**. "Circulating Tumor-Markers in the Monitoring of Gynecologic Malignancies", *Cancer*, 60(3), pp. 353-361.

(338) Vardi, J. R.; Tadros, G. H.; Malhotra, C.; Charney, T.; Shebes, M.; Foemmel, R. **(1989)**. "Lipid Associated Sialic-Acid in Plasma in Patients with Advanced-Carcinoma of the Ovaries", *Surgery, Gynecology and Obstetrics*, 168(4), pp. 296-301.

(339) Vardi, J. R.; Tadros, G. H.; Foemmel, R.; Shebes, M. **(1989)**. "Plasma Lipid-Associated Sialic-Acid and Serum CA-125 as Indicators of Disease Status with Advanced Ovarian-Cancer", *Obstetrics and Gynecology*, 74(3), pp. 379-383.

(340) Petru, E.; Sevin, B. U.; Averette, H. E.; Koechli, O. R.; Perras, J. P.; Hilsenbeck, S. **(1990)**. "Comparison of 3 Tumor-Markers CA-125, Lipid-Associated Sialic-Acid (LSA), and Nb 70k - in Monitoring Ovarian-Cancer", *Gynecologic Oncology*, 38(2), pp. 181-186.

(341) Schutter, E. M. J.; Visser, J. J.; Vankamp, G. J.; Mensdorffpouilly, S.; Vandijk, W.; Hilgers, J.; Kenemans, P. **(1992)**. "The Utility of Lipid-Associated Sialic-Acid (LASA or LSA) as a Serum Marker for Malignancy - a Review of the Literature", *Tumour Biology*, 13(3), pp. 121-132.

(342) Want, E. J.; Nordstrom, A.; Morita, H.; Siuzdak, G. **(2007)**. "From Exogenous to Endogenous: The Inevitable Imprint of Mass Spectrometry in Metabolomics", *Journal of Proteome Research*, 6(2), pp. 459-468.

(343) Frahm, J. L.; Howard, B. E.; Heber, S.; Muddiman, D. C. **(2006)**. "Accessible Proteomics Space and Its Implications for Peak Capacity for Zero-, One- and Two-Dimensional Separations Coupled with FT-ICR and TOF Mass Spectrometry", *Journal of Mass Spectrometry*, 41(3), pp. 281-288.

(344) Rui, Z.; Jian-Guo, J.; Yuan-Peng, T.; Hai, P.; Bing-Gen, R. **(2003)**. "Use of Serological Proteomic Methods to Find Biomarkers Associated with Breast Cancer", *Proteomics*, 3(4), pp. 433-439.

(345) Ahmed, N.; Oliva, K. T.; Barker, G.; Hoffmann, P.; Reeve, S.; Smith, I. A.; Quinn, M. A.; Rice, G. E. **(2005)**. "Proteomic Tracking of Serum Protein Isoforms as Screening Biomarkers of Ovarian Cancer", *Proteomics*, 5(17), pp. 4625-4636.

(346) Wulfkuhle, J. D.; McLean, K. C.; Paweletz, C. P.; Sgroi, D. C.; Trock, B. J.; Steeg, P. S.; Petricoin, E. F., 3rd **(2001)**. "New Approaches to Proteomic Analysis of Breast Cancer", *Proteomics*, 1(10), pp. 1205-1215.

(347) Li, J.; Zhang, Z.; Rosenzweig, J.; Wang, Y. Y.; Chan, D. W. **(2002)**. "Proteomics and Bioinformatics Approaches for Identification of Serum Biomarkers to Detect Breast Cancer", *Clinical Chemistry*, 48(8), pp. 1296-1304.

(348) Wulfkuhle, J. D.; Paweletz, C. P.; Steeg, P. S.; Petricoin, E. F., 3rd; Liotta, L. **(2003)**. "Proteomic Approaches to the Diagnosis, Treatment, and Monitoring of Cancer", *Adv Exp Med Biol*, 532 pp. 59-68.

(349) Conrads, T. P.; Fusaro, V. A.; Ross, S.; Johann, D.; Rajapakse, V.; Hitt, B. A.; Steinberg, S. M.; Kohn, E. C.; Fishman, D. A.; Whiteley, G.; Barrett, J. C.; Liotta, L. A.; Petricoin, E. F.; Veenstra, T. D. **(2004)**. "High-Resolution Serum Proteomic Features for Ovarian Cancer Detection", *Endocrine-Related Cancer*, 11(2), pp. 163-178.

(350) Lenz, E. M.; Wilson, I. D. **(2007)**. "Analytical Strategies in Metabonomics", *Journal of Proteome Research*, 6(2), pp. 443-458.

(351) Trygg, J.; Holmes, E.; Lundstedt, T. **(2007)**. "Chemometrics in Metabonomics", *Journal of Proteome Research*, 6(2), pp. 469-479.

(352) Denkert, C.; Budczies, J.; Kind, T.; Weichert, W.; Tablack, P.; Sehouli, J.; Niesporek, S.; Könsgen, D.; Dietel, M.; Fiehn, O. **(2006)**. "Mass Spectrometry–Based Metabolic Profiling Reveals Different Metabolite Patterns in Invasive Ovarian Carcinomas and Ovarian Borderline Tumors", *Cancer Research*, 66(22), pp. 10795-10804.

(353) Roy, S. M.; Anderle, M.; Lin, H.; Becker, C. H. **(2004)**. "Differential Expression Profiling of Serum Proteins and Metabolites for Biomarker Discovery", *International Journal of Mass Spectrometry*, 238(2), pp. 163-171.

(354) Wilsona, I. D.; Plumbb, R.; Grangerb, J.; Majorc, H.; Williamsa, R.; Lenza, E. M. **(2005)**. "HPLC-MS-Based Methods for the Study of Metabonomics", *Journal of Chromatography B*, 817(1), pp. 67-76.

(355) Patterson, A. D.; Li, H.; Eichler, G. S.; Krausz, K. W.; Weinstein, J. N.; Formace, A. J.; Gonzalez, F. J.; Idle, J. R. **(2008)**. "UPLC-ESI-TOFMS-Based Metabolomics and Gene Expression Dynamics Inspector Self-Organizing Metabolomic Maps as Tools for Understanding the Cellular Response to Ionizing Radiation", *Analytical Chemistry*, 80(3), pp. 665-674.

(356) Ding, J.; Sorensen, C. M.; Zhang, Q. B.; Jiang, H. L.; Jaitly, N.; Livesay, E. A.; Shen, Y. F.; Smith, R. D.; Metz, T. O. **(2007)**. "Capillary LC Coupled with High-Mass Measurement Accuracy Mass Spectrometry for Metabolic Profiling", *Analytical Chemistry*, 79(16), pp. 6081-6093.

(357) Stoll, D. R.; Wang, X. L.; Carr, P. W. **(2008)**. "Comparison of the Practical Resolving Power of One- and Two-Dimensional High-Performance Liquid Chromatography Analysis of Metabolomic Samples", *Analytical Chemistry*, 80(1), pp. 268-278.

(358) Dwivedi, P.; Wu, P.; Klopsch, S. J.; Puzon, G. J.; Xun, L.; Hill, H. H. **(2008)**. "Metabolic Profiling by Ion Mobility Mass Spectrometry (IMMS)", *Metabolomics*, 4(1), pp. 63-80.

(359) Wold, S. **(1976)**. "Pattern-Recognition by Means of Disjoint Principal Components Models", *Pattern Recognition*, 8(3), pp. 127-139.

(360) Wold, S.; Esbensen, K.; Geladi, P. **(1987)**. "Principal Component Analysis", *Chemometrics and Intelligent Laboratory Systems*, 2(1-3), pp. 37-52.

(361) Bangalore, A. S.; Shaffer, R. E.; Small, G. W.; Arnold, M. A. **(1996)**. "Genetic Algorithm-Based Method for Selecting Wavelengths and Model Size for Use with Partial Least-Squares Regression: Application to Near-Infrared Spectroscopy", *Analytical Chemistry*, 68(23), pp. 4200-4212.

(362) Hasegawa, K.; Funatsu, K. **(2000)**. "Partial Least Squares Modeling and Genetic Algorithm Optimization in Quantitative Structure-Activity Relationships", *SAR and QSAR in Environmental Research*, 11(3-4), pp. 189-209.

(363) Leardi, R. "Genetic Algorithm-PLS as a Tool for Wavelength Selection in Spectral Data Sets", In *Nature-Inspired Methods in Chemometrics: Genetic Algorithms and Artificial Neural Networks*; Elsevier: Amsterdam, The Netherlands, **2003**; Vol. 23, pp 169-196.

(364) Durand, A.; Devos, O.; Ruckebusch, C.; Huvenne, J. P. **(2007)**. "Genetic Algorithm Optimization Combined with Partial Least Squares Regression and Mutual Information Variable Selection Procedures in Near-Infrared Quantitative Analysis of Cotton-Viscose Textiles", *Analytica Chimica Acta*, 595(1-2), pp. 72-79.

(365) Guyon, I.; Weston, J.; Barnhill, S.; Vapnik, V. **(2002)**. "Gene Selection for Cancer Classification Using Support Vector Machines", *Machine Learning*, 46(1-3), pp. 389-422.

(366) Vapnik, V. *The Nature of Statistical Learning Theory*; Springer, **2000**.

(367) Li, L.; Tang, H.; Wu, Z.; Gong, J.; Gruidl, M.; Zou, J.; Tockman, M.; Clark, R. A. **(2004)**. "Data Mining Techniques for Cancer Detection Using Serum Proteomic Profiling", *Artificial Intelligence in Medicine*, 32(2), pp. 71-83.

(368) Rajapakse, J. C.; Duan, K. B.; Yeo, W. K. **(2005)**. "Proteomic Cancer Classification with Mass Spectrometry Data", *American Journal of Pharmacogenomics*, 5(5), pp. 281-292.

(369) Yu, J. S.; Ongarello, S.; Fiedler, R.; Chen, X. W.; Toffolo, G.; Cobelli, C.; Trajanoski, Z. **(2005)**. "Ovarian Cancer Identification Based on Dimensionality Reduction for High-Throughput Mass Spectrometry Data", *Bioinformatics*, 21(10), pp. 2200-2209.

(370) MZmine 0.60.
http://mzmine.sourceforge.net

(371) Seven Golden Rules.
http://fiehnlab.ucdavis.edu/projects/Seven_Golden_Rules

(372) Metlin, Scripps Center for Mass Spectrometry.
http://metlin.scripps.edu/metabo_batch.php

(373) KEGG, Kyoto Encyclopedia of Genes and Genomes.
http://www.genome.jp/kegg/ligand.html

(374) HMDB, Human Metabolome Database.
http://www.hmdb.ca/search/spectra?type=ms_search

(375) MMCD, Madison Metabolomics Consortium Database.
http://mmcd.nmrfam.wisc.edu/

(376) Lipid Maps.
http://www.lipidmaps.org/data/structure/LMSDSearch.php?Mode=SetupTextOntologySearch

LIST OF PUBLICATIONS

CHAPTER 2

Hampton CY, Forbes TB, Varady MJ, Meacham JM, Fedorov AG, Degertekin FL, Fernández FM, "Analytical Performance of a Venturi-assisted Array of Micromachined Ultrasonic Electrosprays (AMUSE) Coupled to Ion Trap Mass Spectrometry for the Analysis of Peptides and Proteins", *Anal. Chem.*, **2007**, 79, 8154-8161.

CHAPTER 3

Hampton CY, Silvestri CJ, Forbes TP, Varady MJ, Meacham JM, Degertekin FL, Fedorov AG, Fernández FM, "Comparison of the Internal Energy Deposition of Venturi-Assisted Electrospray Ionization and a Venturi-Assisted Array of Micromachined UltraSonic Electrosprays (AMUSE)", *J. Am. Soc. Mass Spectrom.*, **2008**, 19(9), 1320-1329.

CHAPTER 4

Hampton CY, Forbes TP, Varady MJ, Degertekin FL, Fedorov AG, Fernández FM, "Characterization of a New Array-Format Ionization Source for LC-MS", *Rapid Commun. Mass Spectrom.*, **2009**, Publication Contingent Upon Results.

CHAPTER 5

Newton PN, Hampton CY, Alter-Hall K, Teerwarakulpana T, Prakongpan S, Ruangveerayuth R, White NJ, Day NPJ, Tudino MB, Mancuso N, Fernández FM, "Characterisation of 'Yaa Chud' Medicine on the Thailand-Myanmar Border: Selecting for Drug-resistant Malaria and Threatening Public Health", *Am. J. Trop. Med. Hyg.,* **2008**, 79, 662-669.

Fernández FM, Hampton CY, Nyadong L, Navare A, Kwasnik M, "Liquid Chromatography and Ambient Ionization Time-of-flight Mass Spectrometry for the Analysis of Genuine and Counterfeit Pharmaceuticals", in **LC/TOF-MS for Accurate Mass Analysis: Principles and Applications**, ed. by I. Ferrer and E.M. Thurman, Wiley: **2009**.

CHAPTER 6

Fernández FM, Cody RB, Newton PN, Green MD, Hampton CY, White NJ, "Characterization of Solid Drug Samples by Direct-analysis-in-real-time/Time-of-flight Mass Spectrometry", *ChemMedChem*, **2006**, 1(7), 702-705.

Newton PN, Fernández FM, Plancon-Lecadre A, Mildenhall D, Green MD, Laurin P, Blum N, Hampton CY, Faure K, Nyadong L, Soong CWR, Santoso B, Zhiguang W, Newton J, Palmer K, "A collaborative epidemiological investigation into the criminal fake artesunate trade in South East Asia", *PLoS Med.*, **2008**, 5(2), e32.

Sengaloundeth S, Green MD, Fernández FM, Manolin O, Phommayong K, Insixiengmay V, Hampton CY, Nyadong L, Mildenhall D, Hostetler D, Khounsaknalath L, Vongsack L, Phompida S, Vanisaveth V, Syhakhang L, Newton PN, "A stratified random survey of the proportion of poor quality oral artesunate sold at medicine outlets in the Lao PDR – implications for therapeutic failure and drug resistance", *Malaria J.,* **2009**, Submitted.

CHAPTER 7

Harris GA, Hostetler DM, Hampton CY, Fernández FM. "Comparison of the Internal Energy Deposition of Direct Analysis in Real Time and Electrospray Ionization Time-of-Flight Mass Spectrometry", *J. Am. Soc. Mass Spectrom.,* **2009**, In Preparation.

APPENDIX A

Ovat A, Li ZZ, Hampton CY, Asress SA, Fernández FM, Glass JD, Powers JC. "Peptidyl α-Ketoamides with Nucleotide Bases and Dimethylaminoalkyl Substituents as Calpain Inhibitors: Novel Inhibitors", *J. Med. Chem.*, **2009**, Submitted.

APPENDIX B

Guan W, Zhou M, Hampton CY, Gray A, McDonald JF, Fernández FM, "A Comprehensive Comparison of Support Vector Machine Classifiers of Ovarian Cancer Metabolomic Data", *BMC Bioinformatics*, **2009**, Accepted.

VITA

CHRISTINA YOUNG HAMPTON

Christina Young Hampton was born in Seoul, South Korea. She attended public schools in Korea, Japan, and Texas before moving to Washington State where she received her high school diploma. She received an A.A.S. from Pierce Community College in Lakewood, WA in 2001 and transferred to Western Washington University in Bellingham, WA where she received a B.S. in Chemistry in 2003. In 2004, she moved to Atlanta to pursue a doctorate in analytical chemistry from the Georgia Institute of Technology. When she is not working on her research (rarely happens), Ms. Hampton enjoys reading, watching movies, making kimchi, and tinkering with broken equipment to learn how it works.